Contributions to Libration Orbit Mission Design using Hyperbolic Invariant Manifolds

Elisabet Canalias Vila

Departament de Matemàtica Aplicada 1 – Universitat Politècnica de Catalunya

Programa de Doctorat en Ciència i Tecnologia Aeroespacial

Memòria per aspirar al grau de Doctor
per la Universitat Politècnica de Catalunya

Certifico que aquesta tesi ha estat realitzada per l'Elisabet Canalias Vila i
dirigida per mi.

Barcelona, 11 de maig del 2007.

Josep Joaquim Masdemont Soler

Al meu avi, una de les persones de qui més coses he après.

Contents

Abstract

This doctoral thesis lies within the framework of astrodynamics. In particular, it deals with mission design near libration point orbits. The starting point of the studies contained in the present dissertation is dynamical systems theory, which provides an accurate description of the dynamics governing libration regions. However, this work is aimed at real applications, and therefore it makes use of this theoretical description as a means to provide solutions to problems that have been identified in mission design.

The restricted three body problem (RTBP) is a well known model to study the motion of an infinitesimal mass under the gravitational attraction of two massive bodies. Its 5 equilibrium points have been thoroughly studied since the last century. The results contained in the present dissertation refer to two of these equilibrium points: L_1 and L_2, which lie on both sides of the smallest of the massive bodies of the system and are the ones on which more practical interest has been focused in the last decades (for missions such as SOHO, Genesis, Hershel-Planck...). Instability is a basic property of the aforementioned equilibrium points, which is inherited by the orbits surrounding them and accounts for the existence of stable and unstable directions at each point of these orbits. The union of these directions or, more precisely, of the asymptotic orbits arising from the periodic and quasi-periodic motions around L_1 and L_2, forms an invariant object either approaching (stable directions) or leaving (unstable directions) the vicinity of libration points. These invariant objects are the hyperbolic manifolds of libration point orbits. A proper knowledge and description of such manifolds is extremely useful for mission design, as they are the key to understanding the dynamics of the system.

The first problem that has been tackled in our work is the eclipse avoidance in Lissajous orbits. Generically, a spatial probe placed in an orbit around the solar libration point L_2 is affected by occultations due to the shadow of the Earth, unless eclipse avoidance maneuvers are planned. If the orbit surrounds L_1, eclipses due to the strong solar electromagnetic influence occur. On the other hand, Lissajous-type orbits are a kind of libration motion resulting from the combination of two perpendicular oscillations. Their main advantage over other kinds of orbits, such as the elongated Halo orbits, is that the amplitudes of each one of the oscillations can be chosen independently, and this fact makes them suitable for certain mission requirements. This work uses the linear approximation to the analytical description of Lissajous orbits in order to compute the so-called non escape direction which allows for transfers between different orbits by changing either the amplitudes or the phases (or both at the same time) while avoiding the unstable part of the movement.

Furthermore, another interesting problem in space mission design is the rendez-vous, understood in our work as the strategy to make two different satellites meet at a certain orbit or to approach each other to a given small distance. The tools developed for eclipse avoidance in Lissajous orbits also allow us to plan simple rendez-vous strategies, which can be used either for preliminary mission analysis or as a contingency plan.

On the other hand, there exist low cost channels between the libration points L_1 and L_2 of a given system, like the ones used in the Genesis mission. These channels provide a natural way of transfering between the libration regions and they can be found by intersecting stable and unstable manifolds of orbits around L_1 and L_2. Remember that stable manifolds tend to an invariant object in forwards time. Unstable manifolds do so backwards in time. Therefore, when an intersection

is found between a stable manifold and an unstable one, it provides a path that goes away from a libration orbit and approaches another one. Connections between planar Lyapunov orbits, which are planar periodic motions around L_1 and L_2 are studied in this dissertation, being specifically computed for the Sun-Earth and Earth-Moon systems.

Moreover, the idea of intersecting stable and unstable manifolds in order to find low cost connecting trajectories can also be applied in the search for low cost paths from the lunar libration regions to the solar libration orbits. It is well known that the stable manifolds of orbits around libration points of the Earth-Moon problem do not come close enough to the Earth as to provide a direct transfer to the Moon. On the contrary, stable and unstable manifolds of some libration orbits around L_2 in the Sun-Earth problem do come to a close approach with the Earth. Therefore, if a natural path between the solar libration orbits and the lunar ones could be found, this would result in a cheap way of reaching the Moon. And the other way round, a path from the lunar libration regions to the solar ones would allow for the placement of a gateway station at the vicinity of a lunar libration point aimed at providing services to solar libration missions, for instance. This is the idea that drives the last part of the dissertation. With the goal of joining the lunar libration orbits and the solar ones by using invariant manifolds, the four body problem Sun-Earth-Moon- spacecraft is decoupled in two restricted three body problems. Then, we can search for intersections between manifolds of libration orbits belonging to both problems. At first, connecting trajectories from the planar Lyapunov orbits around L_2 in the Earth-Moon system to planar Lyapunov orbits around the solar L_2 point are computed. Afterwards, the search is conducted in the 3-dimensional case, between Lissajous type orbits around the aforementioned libration points of both problems. The computation of connecting trajectories in the spatial case is much more complicated, as the dimension of the state space in which we look for intersections increases with respect to the planar case. However, a method for finding and classifying such trajectories is detailed in this work. Furthermore, realistic JPL ephemeris trajectories are obtained by means of a multiple shooting procedure applied on the connecting trajectories found in the coupled RTBPs model. Finally, a method for refining the aforementioned trajectories in JPL coordinates to zero cost connecting trajectories, when possible, is presented and provides free realistic transfers from Earth-Moon to Sun-Earth which are ready to be used in mission design.

Agraïments

No és possible donar les gràcies explícitament a tothom que ha aportat algun granet de sorra a la realització d'aquesta tesi, que no per petit és menys important. Espero que qui s'hagi de donar per al.ludit em perdoni aquesta manca de referència directa.

A qui sí que és possible donar les gràcies és al meu director de tesi, el Dr. Josep J. Masdemont. No podria haver tingut un director millor. Gràcies per fer en tot moment que les coses semblin senzilles.

Per altra banda, si he pogut acabar aquesta tesi és en gran mesura gràcies a una beca de tipus FPU del Ministeri d'Educació, adscrita al departament de Matemàtica Aplicada 1 de la Universitat Politècnica de Catalunya. Voldria agrair a aquest departament els mitjans que ha posat a la meva disposició, sobretot el cluster d'ordinadors Eixam, sense els quals la realització d'aquest treball i la seva difusió en congressos internacionals no hagués estat possible. Sense oblidar-me de les persones del departament, que sovint m'han fet els migdies més agradables dinant al cafè, i en especial els meus companys de despatx, amb qui he compartit les penes i les alegries d'aquesta feina de precari.

En un apartat més personal, agraeixo de tot cor als meus pares la seva absoluta dedicació a nosaltres. No només han acceptat perfectament el fet de tenir una filla que es passa mitja vida estudiant o treballant, o fent no se sap ben bé el què davant una pantalleta, sinó que han hagut d'aguantar sovint les meves cabòries i m'han encoratjat sempre a seguir endavant, amb una actitud que em demostra que lluny de molestar-los, aquesta dedicació meva els omple d'orgull. És per això i moltes altres coses que jo també estic tan orgullosa d'ells. I tu, Judit, recorda que la meva felicitat passa sempre, necessàriament, per veure't a tu contenta.

Finalment, no hi pot faltar un record pels meus amics. A tots els que saben que són importants per mi. Tant si els veig sovint com no; tant si viuen a prop meu com en un altre racó d'Europa. En especial a les persones que són els pilars fonamentals de la meva vida, encara que segurament a partir d'ara sempre que sigui a prop d'una estaré lluny de l'altra. També tinc ganes de donar les gràcies a la persona amb qui he compartit la millor part d'aquests últims anys; ell sap que un trosset de la tesi és ben seu.

Preface

This doctoral dissertation is structured in chapters. The first and second chapters provide a general insight into the Restricted Three Body Problem, the libration point orbits, as well as the state of the art in several aspects of mission design near libration points. These initial chapters are aimed at motivating the working topics contained in the present dissertation, while introducing concepts and relevant references to previous works. Thus, they do not contain new results.

The new contributions of the thesis are contained in chapters 3, 4 and 5.

Chapter 3 deals with non-escape maneuvers in Lissajous type orbits. A strategy for eclipse avoidance, a method for transferring between different Lissajous orbits and a rendez-vous methodology are presented using this kind of impulsive maneuvers.

In chapter 4, a complete methodology for the computation of connecting trajectories between planar periodic orbits around L_1 and L_2 libration points of a given RTBP is presented. This methodology is applied to the Sun-Earth and Earth-Moon RTBPs and the resulting families of connecting trajectories are included in the final part of the aforementioned chapter.

Moreover, in chapter 5 similar ideas as in chapter 4 are applied in the search for connecting trajectories, but for joining libration regions belonging to two different problems: Sun-Earth and Earth-Moon. In particular, trajectories between planar Lyapunov orbits of the solar and lunar libration regions are computed in the first part of the chapter. In the second part of it, a method for computing connecting trajectories between Lissajous orbits belonging to the aforementioned problems is introduced. A database containing a sample of these connecting trajectories in the coupled RTBPs is attached to the dissertation in the form of a DVD. In the last part of the chapter, a methodology which has been developed in order to refine the connecting trajectories between Lissajous orbits to realistic JPL ephemeris coordinates, as well as slowly reducing the maneuver in the coupling point until zero cost transfers are obtained, is presented.

The dissertation ends by pointing at some possible directions for future work.

Finally, two appendices are added to the present work. Appendix A contains information on how to use the database of the attached DVD. Appendix B contains the translation of the abstract to Catalan.

Chapter 1

Motivation and State of the Art

In the last 25 years, we have attended the breakthrough of the use of libration orbits in space mission design. Nowadays, anyone involved in space related topics is, at least, familiar with the words *Lagrange point orbit* or *libration region*. We even dare to affirm that the vast majority of mission analysts would be able to list some past, present or future missions having such orbits as nominal paths.

In 1978, the ISEE-3 (the third Sun-Earth explorer spacecraft) was launched to pursue studies of the Sun-Earth interactions in a first step of what is now known as Space Weather. After a direct transfer to the vicinity of the Sun-Earth L_1 Lagrange point, ISEE-3 was inserted into a nearly periodic halo orbit. When some revolutions were completed in this location, the spacecraft visited the vicinity of L_2 point to study the magneto tail of the Earth. Finally, and after making use of a double lunar swing-by the spacecraft was renamed as the International Cometary Explorer (ICE) and had a close encounter with comet Giacobini-Zinner ([67], [18]). This early libration mission is already an example of the huge advantages that dynamical systems theory applied to libration regions provide for space exploration ([73], [21], [41]): adaptability, sophistication and fuel budget savings. Consequently, interest in the Lagrange libration points has continued to increase and to provide more challenging scientific applications, partly reflected in missions such as the well known SOHO ([11], [37]) or Genesis ([42], [3]).

In short, libration points, also known as Lagrange points, are the equilibrium solutions of the Restricted Three Body Problem (RTBP), which is a model for the motion of a particle of very small mass under the gravitational attraction of two massive bodies (primaries) that follow Keplerian orbits around their centre of masses. For space missions, the particle is the spacecraft and the two big masses can be either the Sun and a planet or the Earth and the Moon, for instance[1]. There exist 5 equilibrium solutions to the system of differential equations of motion of the RTBP, which are called L_i, with i from 1 to 5. Up to now, practical interest has been mainly focused on L_1 and L_2, which are the ones closest to the small primary ([12], [32]).

The object of this chapter is to provide an insight into the characteristics of the L_1 and L_2 regions, which make them suitable for space exploration, as well as into mission analysis topics and problems arising in the aforementioned regions. Furthermore, some relevant studies or techniques that have been developed to tackle these problems will also be mentioned. In this way, we will be ready to motivate and understand the different parts that the present dissertation deals with.

---

[1]This model will be technically described in chapter 2.

Note on the bibliography and references

Phase	Topic	References
Transfer to libration regions	From Earth to libration regions Transfers between libration orbits Low-thrust, ballistic captures	[23], [43], [7], [82], [75], [84] [24], [40], [56] [77], [2], [51], [59], [80]
In the vicinity of libration points	Dynamical description, orbit types Station keeping strategies Eclipse avoidance	[30], [48], [64], [35], [36], [85] [81], [5], [60], [38], [4] [15], [31], [45], [6] [8], [62], [39]
Beyond libration regions	4-body models Interplanetary travel Gateway lunar station	[22], [17], [83]. [68] [55], [74], [19] [52], [54]

Table 1.1: Some references concerning different stages of mission design near libration points

A large amount of researchers, university groups and space related scientists have carried out studies concerning the description of the vicinity of the points L_1 and L_2 and their possible uses in mission design. These studies range from the pure analytical description to the precise numerical implementation. It is not the object of this section to provide an exhaustive collection of bibliography, but to set a general frame of reference in order to be able to introduce the work developed in this doctoral dissertation in a natural and understandable way. To this aim, some references are included in table 1, covering several aspects of libration orbit mission design.

In addition to these references concerning particular topics, it is worth mentioning here the works which have been used as basic references. First of all, the works by H. Poincaré and V. Szebehely ([63], [81]) laid down the basis on which to start constructing a dynamical systems study of the libration regions of the Restricted Three Body problem. Furthermore, the work summarised in [32], [33] and [34], among others by the same group of researchers, combines rigorous analytical studies and efficient numerical implementations for a wide range of problems arising in libration regions and it has to be regarded as an essential tool for understanding the present dissertation. Finally, valuable help on numerical computations can be found, for instance, in [71], [79] and [72].

Characteristics and applications of libration regions

Which are the reasons for the aforementioned suitability of solar libration regions for mission design purposes?

First of all, solar libration regions are easy and inexpensive to reach from Earth. In the restricted three body problem, there are always manifolds approaching the smallest of the primaries. Therefore, for the Sun-Earth case, some manifolds can give a ride to the spacecrafts from a parking LEO orbit to the desired libration motion ([57]). Moreover, once in the libration regions, a good observation site of the Sun and other celestial bodies and space objects is pro-

vided ([14], [10]). The Earth-Sun-libration point relative geometry is almost constant, due to the fact that the libration points rotate with the Sun-Earth axis. In addition, the communication system design is simple and cheap (as long as eclipses are avoided), due to this overall constant geometry and the proximity between the Earth and L_1 and L_2. On the other hand, the thermal stability existing in the libration regions, specially around L_2, makes them the perfect locations for non-cryogenic missions and highly precise visible light telescopes.

Lunar libration regions have also received some attention in the last decades and are nowadays starting to be considered in spatial mission design, even for manned spacecraft. The lunar L_2 point was proposed, for instance, to hold a constant communication link between the Earth and the hidden part of the Moon ([6], [15]). Moreover, lunar regions can provide ballistic low cost captures such as the one used for the Japanese Hiten mission ([1]).

Finally, an ambitious idea, which foresees a net of low cost paths between any pair of given locations in the solar system was born some years ago. These paths would be computed using the invariant manifolds of libration orbits of different restricted three body problems, and intersecting them in an adequate way. Cheap trajectories from the Earth and return, and between L_1 and L_2 were studied for missions such as Genesis ([53]). The idea is to extend the asymptotic connections existing in the 3-body problems to different n-body problems, obtained by coupling RTBPs. Some studies have already been performed for the Sun-Earth-Moon-spacecraft 4 body problem and for tours of the Jupiter moons (JIMO). However, this is a field to which lots of efforts are bound to be devoted in the years to come.

Some mission design aspects

The first question that one has to solve when trying to design a libration point missions is how to get to the libration orbit. Transfers from Low Earth Orbits to the corresponding libration region have to be planned taking into account the capabilities of current launchers. There are two different approaches to the transfer problem: direct shooting methods and invariant manifolds methods. The first one, direct shooting, uses forward and backward propagators (from the origin and arriving orbit respectively) and tries to match the obtained trajectories in such a way that they satisfy given boundary conditions and/or minimise the total fuel. Invariant manifold techniques, on the other hand, take advantage of the hyperbolic character of the libration orbits and of the fact that solar libration manifolds approach the Earth, in order to plan cheap and close to natural transfers. A generalisation of the stable manifold of the desired arriving orbit can be taken and the intersecting points of this generalisation and the LEO orbit can be computed. At each point, a Δv will be needed for the matching in position and velocities. This Δv mainly depends on the base point of the nominal libration orbit from which the trajectory arises and can be therefore minimised by moving this point. Note that for the return trajectories, the same techniques can be used just by switching from stable to unstable manifolds, or from forward to backward propagators. For the lunar libration regions, however, a direct transfer from the Earth using invariant manifolds is not possible, as the manifolds of the Earth-Moon problem do not approach the Earth. Therefore, for these cases other techniques have to be planned, such as the composition of the use of solar libration points as steps on the way (Shoot the Moon, [52]) or lunar ballistic captures ([2]). In any case, transfer strategies should also be accompanied by trajectory correcting maneuvers, aimed at correcting the drifts caused by inaccuracies in the injection phase

([29]).

Once in the libration region, the transfer problem may not be completely solved. For instance, if the suitable stable manifold providing the transfer from the Earth to the libration region does not belong to the final nominal orbit. For these cases, transfers between different libration orbits have been thoroughly studied ([28], [40], [75]). In addition, another related problem is travelling from one libration point to the other one. In this direction, studies concerning the so-called heteroclinic connections, which act as natural channels between different libration regions, have been developed ([27]).

There is still something else to be taken into account concerning the injection of the space probe in the nominal trajectory: the point in the orbit where we actually want to insert the satellite. A similar problem, for missions using more than one satellite, consists of making the satellites meet or adopt a particular relative geometry at a given point of the orbit. This can be summarised as the rendez-vous problem ([46], [58]). Two different ways of looking at the rendez-vous problem could be from the Earth, planning the launches and intermediate trajectory maneuvers so as to make the satellites reach the orbit at similar points and times, or from the libration orbit, letting the satellites reach the orbit independently and then planning maneuvers to make them approach each other. The second approach can also be used as contingency plan, when the launches aimed at making the satellites be injected close to each other fail in some way.

Furthermore, if one knows how to reach the desired orbit and even travel from one libration orbit to the other one, it is the time to worry about how close to the nominal orbit the spacecraft will stay. Several perturbations, due to the hyperbolic character of libration regions and other perturbing forces, will cause the actual trajectory to deviate from the nominal path. For this reason, station keeping strategies have to be planned. Different approaches have been used to plan station keeping maneuvers ([31], [70]). We can cite for instance the so-called Target mode approach, which is aimed at planning maneuvers which minimise the weighted deviations at some given future positions, or the Floquet mode approach, which makes use of the knowledge of the hyperbolic unstable terms, responsible for the short term drifts from the nominal orbit, in order to plan maneuvers which reduce these instabilities to zero.

Libration regions may well be adequate locations for space probes, but there is still an important handicap which has to be dealt with, which are eclipses. These phenomena, understood for instance as regions where the spacecraft suffers from an occultation which either interrupts its power source or its availability to communicate with the ground station, have to be avoided. Passive eclipse avoidance strategies consist of using orbits which do not suffer from eclipses which can affect the mission performance (either big orbits which do not cross the eclipse zone, such as halo orbits or short mission lifetimes and adequate injection conditions which allow for the mission to be finished when the first eclipse occurs...). On the other hand, active eclipse avoidance strategies taking advantage of the orbital characteristics can also be planned ([62], [8]).

Motivation and short presentation of the dissertation parts

A summary of some relevant works and mission design concepts for libration regions has been presented in the above sections. In this context, the work contained in the present doctoral dissertation can be roughly divided in three parts, each one dealing with a particular problem of libration mission design and using slightly different dynamical systems ideas and techniques.

The first part is motivated by the eclipse avoidance problem in libration regions. Traditionally, big Halo orbits which don't cross the exclusion zone have been used as nominal paths in order to avoid the problem of occultations (in solar L_2) or excessive electromagnetic flow (in solar L_1). However, the in plane and out of plane amplitudes of a Halo orbit have to satisfy a stiff relation, which may not be always desirable or adequate for mission purposes. On the contrary, Lissajous libration point orbits are quasi periodic motions which allow for a high degree of freedom in their amplitude choice. Nevertheless, Lissajous orbits usually cross the exclusion zone if no maneuvers are planned. To this aim, a design tool called Effective Phases Plane (EPP), which is useful for describing the motion on Lissajous orbits and also proves to be a useful tool for mission design, has been developed. In fact, not only does the EPP provide a simple geometrical solution to the eclipse avoidance problem, but it also has a straightforward application to the rendez-vous problem.

Secondly, a study of homoclinic and heteroclinic connections between planar Lyapunov orbits in the Sun-Earth and Earth-Moon problems is presented. These connections provide cheap channels between L_1 and L_2 regions, which can be used for cost effective transportation in libration regions. Moreover, they can be found by intersecting hyperbolic invariant manifolds of different orbits (one stable manifold integrated backwards with an unstable manifold integrated forwards). The analytic approximations taken for the Lyapunov orbits and manifolds in this case contain high order terms, assuring a precise description of the libration region dynamics in the frame of the restricted three body problems involved. Furthermore, the numerical tools developed for this part of the work were also used in the studies that followed, concerning transfers between different RTBPs coupled in an adequate way.

Finally, the last chapter of the present doctoral dissertation is devoted to finding connecting trajectories between the solar and the lunar L_2 libration regions. This work is both a generalisation of the aforementioned search for asymptotic homoclinic and heteroclinic trajectories and a first step in the construction of a net of low cost paths in the Solar System. Furthermore, being able to join the solar and lunar libration regions is a very important fact which is bound to be essential in the future plans for human lunar exploration. For instance, a gateway station could be placed in a lunar libration region in order to provide services to solar libration point missions. On the other hand, these solar-lunar connections can also be simply regarded as a cheap means of reaching the Moon using invariant manifolds. Studies of possible transfer trajectories from the L_2 region of the Earth-Moon system to the L_2 region of the Sun-Earth region have been performed by coupling the Sun Earth and Earth Moon RTBPs in two different cases: using the planar RTBPs, transfer trajectories between planar Lyapunov orbits around both problems have been found; on the other hand, using the 3 dimensional RTBPs, transfer trajectories between Lissajous orbits have been studied. Moreover, the last part of the dissertation deals with the refinement of these coupled RTBP trajectories to realistic models of motion (JPL ephemeris).

Chapter 2

Introduction

2.1 The restricted three body problem

Consider the motion of an infinitesimal particle, m, under the gravitational attraction of two point like big masses, called primaries: m_1 and m_2. In our work, the infinitesimal particle (m) will be a spacecraft affected by the Sun and a planet or by the Earth and the Moon, which are the so called primaries $(m_1$ and $m_2)$. Let the attraction of the infinitesimal particle on the primaries be neglected, so the primaries describe Keplerian orbits around their common centre of mass. The study of the motion of m under the gravitational effects of the primaries is known as restricted three body problem or RTBP. Moreover, we assume that the primaries are moving in circles around their centre of mass. Therefore, the model we use is the Circular Restricted Three Body Problem (CRTBP). The word circular, however, is often omitted.

For the sake of simplicity, let us take units of mass, length and time such that the sum of the masses of the primaries, the gravitational constant and the period of the primaries is equal to 1, 1 and 2π respectively. With these units, the distance between the primaries is also 1. We denote by μ the mass of the smallest primary, and therefore, $1-\mu$ stands for the mass of the big one.

Furthermore, the use of a synodic or non-inertial coordinate system, centred at the centre of mass of the primaries and rotating along with the axis joining them is convenient, and frequently found in the literature ([81], [61]). The orientation of this axis, the x axis, is given by the direction that goes from the smallest to the biggest primary. The z axis has the direction given by the angular motion of the primaries and, finally, the y axis is chosen orthogonal to the previous ones to have a positively oriented coordinate system. The convenience of this reference frame becomes clear when one realizes that the primaries remain fixed for all times, t. The small primary of mass μ is located at $(\mu-1,0,0)$ and the primary of mass $1-\mu$ at $(\mu,0,0)$.

The equations of motion of the third particle in the RTBP, using Newton's laws and the coordinates and units explained above are (see [81]),

$$\left.\begin{array}{rcl} \ddot{X} - 2\,\dot{Y} & = & \frac{\partial\Omega}{\partial X} \\ \ddot{Y} + 2\,\dot{X} & = & \frac{\partial\Omega}{\partial Y} \\ \ddot{Z} & = & \frac{\partial\Omega}{\partial Z} \end{array}\right\} \tag{2.1}$$

where $\Omega(X,Y,Z) = \frac{1}{2}(X^2 + Y^2) + \frac{1-\mu}{r_1} + \frac{\mu}{r_2} + \frac{1}{2}\mu(1-\mu)$, and r_1, r_2 denote the distances from

the spacecraft to the primaries m_1 and m_2 respectively: $r_1^2 = (X - \mu)^2 + Y^2 + Z^2$, and $r_2^2 = (X + 1 - \mu)^2 + Y^2 + Z^2$.

Equilibrium points of the RTBP: particular solutions

The equilibrium points of a system of ordinary differential equations are the ones where the field associated with the system is zero. That is to say,

$$\dot{X} = \ddot{X} = 0, \quad \dot{Y} = \ddot{Y} = 0, \quad \dot{Z} = \ddot{Z} = 0.$$

If the infinitesimal particle was placed on one of this points, with no velocity and no acceleration, it would remain at rest forever. Therefore, equilibrium points are considered to be special solutions of the RTBP, as computing them implies finding a solution for all possible moments of time t.

Let (X,Y,Z) be an equilibrium point of the restricted three body problem. Then, it has to satisfy that the right hand side terms of equations 2.1 are zero. That is,

$$\frac{\partial \Omega}{\partial X} = 0, \quad \frac{\partial \Omega}{\partial Y} = 0, \quad \frac{\partial \Omega}{\partial Z} = 0.$$

In more detail,

$$\left.\begin{array}{rcl} \frac{\partial \Omega}{\partial X} & = & X - \frac{1-\mu}{r_1^3}(X - \mu) - \frac{\mu}{r_2^3}(X + 1 - \mu) = 0 \\ \frac{\partial \Omega}{\partial Y} & = & Y - \frac{1-\mu}{r_1^3}Y - \frac{\mu}{r_2^3}Y = 0 \\ \frac{\partial \Omega}{\partial Z} & = & -\frac{1-\mu}{r_1^3}Z - \frac{\mu}{r_2^3}Z = 0 \end{array}\right\} \qquad (2.2)$$

The third equation in (2.2) is trivially satisfied iff Z=0, because $-\frac{1-\mu}{r_1^3} - \frac{\mu}{r_2^3}$ is clearly negative. Therefore, all equilibrium points are contained in the plane of relative motion of the primaries. On the other hand, $Y = 0$ is a solution of the second equation in (2.2). Then, let us firstly study the equilibrium points contained in the axis joining the primaries, $Y = Z = 0$.

By studying the function $\frac{\partial \Omega}{\partial X}$, one finds that it is continuous for X different from the position of both primaries. Furthermore, it undergoes changes of sign near the primaries: it has negative sign at $-\infty$ and positive sign for $X = -1 + \mu - \epsilon$, for ϵ sufficiently small. It has negative sign again for $X = -1 + \mu + \epsilon$ but positive sign for $X = \mu - \epsilon$. Finally, the sign changes one more time from negative at $X = \mu + \epsilon$ to positive at ∞. Therefore, three different crossings of the X axis occur.

Let the distance from the small primary and the equilibrium point between this mass and $-\infty$ be represented by γ. Then, $X + 1 - \mu = -\gamma$ and $X - \mu = -1 - \gamma$. Therefore, after clearing the fractions, the first equation of (2.2) can be written,

$$\gamma^5 + (3 - \mu)\gamma^4 + (3 - 2\mu)\gamma^3 - \mu\gamma^2 - 2\mu\gamma - \mu = 0.$$

This quintic equation has one real solution which can be written as a power series of $\left(\frac{\mu}{3}\right)^{1/3}$ and provides the position of the so-called L_2 point:

$$\gamma = \left(\frac{\mu}{3}\right)^{\frac{1}{3}} + \frac{1}{3}\left(\frac{\mu}{3}\right)^{\frac{2}{3}} + \frac{1}{9}\left(\frac{\mu}{3}\right)^{\frac{3}{3}} + \dots$$

Similarly, let γ represent the distance between the small primary and the equilibrium point found between the m_1 and m_2. In this case, $X + 1 - \mu = \gamma$ and $X - \mu = -1 + \gamma$. Then, the quintic equation to be solved is,

$$\gamma^5 - (3 - \mu)\gamma^4 + (3 + 2\mu)\gamma^3 - \mu\gamma^2 + 2\mu\gamma - \mu = 0,$$

whose real solution can also be expressed in powers of $\left(\frac{\mu}{3}\right)^{1/3}$ and represents the position of the so-called L$_1$ point:

$$\gamma = \left(\frac{\mu}{3}\right)^{\frac{1}{3}} - \frac{1}{3}\left(\frac{\mu}{3}\right)^{\frac{2}{3}} - \frac{1}{9}\left(\frac{\mu}{3}\right)^{\frac{3}{3}} + \ldots$$

Finally, let $1 - \gamma$ be the distance between the big primary and ∞. Then we have $X - \mu = 1 + \gamma$. The equation to be solved is now,

$$\gamma^5 - (7 + \mu)\gamma^4 + (19 + 6\mu)\gamma^3 - (24 + 13\mu)\gamma^2 + (12 + 14\mu)\gamma - 7\mu = 0.$$

The real solution of this quintic can be written in powers of μ. This equilibrium point, found in the opposite side of the big primary with respect to the small primary, is usually called L$_3$:

$$\gamma = \frac{7}{12}\mu + \frac{237^2}{12^4}\mu^3 + \ldots$$

Now, all solutions of (2.2) with $Y = 0$ have already been found. Let us look for the ones with $Y \neq 0$. Since Y is not zero, we can divide the second equation by it and we obtain:

$$1 - \frac{1 - \mu}{r_1^3} - \frac{\mu}{r_2^3} = 0$$

Multiply this equation by $(X - \mu)$ and subtract the resulting equation from the first one. Then, do the same with $(X + 1 - \mu)$. Therefore, equations (2.2) reduce to,

$$\left.\begin{array}{rcl} 1 - \frac{1}{r_1^3} & = & 0 \\ -1 + \frac{1}{r_2^3} & = & 0 \\ z & = & 0 \end{array}\right\} \tag{2.3}$$

whose only real solutions are $r_1 = r_2 = 1$. So, the two equilibrium points which do not belong to the X axis are the points forming equilateral triangles with the primaries, one with $Y > 0$ and the other one with $Y < 0$.

The three equilibrium points which lay in the x-axis, are known as Euler points L$_1$, L$_2$ and L$_3$. The other two, are known as Lagrange points or L$_4$ and L$_5$[1]. The five equilibrium points, as well as the position of the primaries in the synodic reference frame are represented in figure 2.1.

---

[1]However, all five L$_i$ are commonly referred in the literature as Lagrangian points. They are also usually called libration points.
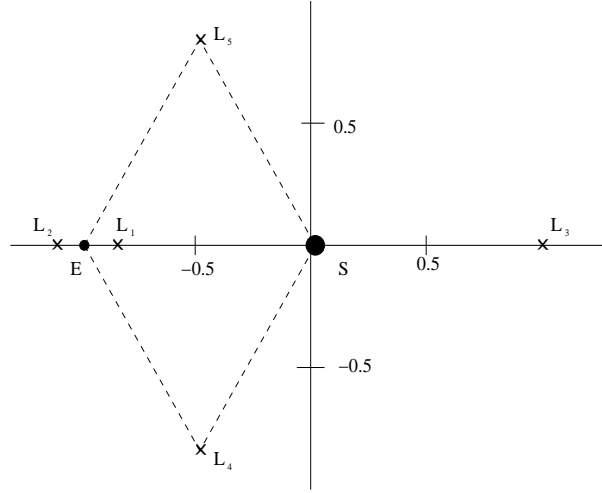
Figure 2.1: The five equilibrium points of the RTBP.

Hamiltonian character of the RTBP

The RTBP is a Hamiltonian system. Taking the momenta $p_x = \dot{X} - Y$, $p_y = \dot{Y} + X$ and $p_z = \dot{Z}$, the corresponding Hamiltonian function is given by,

$$H = \frac{1}{2}(p_x^2 + p_y^2 + p_z^2) + Yp_z - Xp_y - \frac{1-\mu}{((X-\mu)^2 + Y^2 + Z^2)^{1/2}} - \frac{\mu}{((X-\mu+1)^2 + Y^2 + Z^2)^{1/2}}$$

The Hamiltonian equations of the system are,

$$\left.\begin{array}{rcl}
\dot{X} &=& p_x + Y \\
\dot{Y} &=& p_y - X \\
\dot{Z} &=& p_z \\
\dot{p}_x &=& p_y - \frac{(1-\mu)}{r_1^3}(X-\mu) - \frac{\mu}{r_2^3}(X-\mu+1) \\
\dot{p}_y &=& -p_x - \frac{(1-\mu)}{r_1^3}Y - \frac{\mu}{r_2^3}Y \\
\dot{p}_z &=& -\frac{(1-\mu)}{r_1^3}Z - \frac{\mu}{r_2^3}Z
\end{array}\right\} \tag{2.4}$$

Furthermore, at least one first integral of the motion exists for the RTBP (i.e. a quantity which remains constant on the solutions) represented by this Hamiltonian function. However, we will use it in an almost equivalent form, known as Jacobi constant or energy level, defined as:

$$\mathcal{C}(X,Y,Z,\dot{X},\dot{Y},\dot{Z}) = 2\Omega(X,Y,Z) - (\dot{X}^2 + \dot{Y}^2 + \dot{Z}^2), \tag{2.5}$$

with $\Omega(X,Y,Z)$ as in (2.1). It can be proved that $\mathcal{C}(X,Y,Z,\dot{X},\dot{Y},\dot{Z}) = -2H(X,Y,Z,\dot{X},\dot{Y},\dot{Z})$.

Zero velocity curves

It yields from equation (2.5) that for a given value of the Jacobi constant, $\mathcal{C}^*$, the motion is only possible in the points of the state space such that

$$\mathcal{C}(X,Y,Z,\dot{X},\dot{Y},\dot{Z}) - 2\Omega(X,Y,Z) < 0.$$

Figure 2.2: Zero velocity curves and forbidden regions. From left to right: $\mathcal{C} < \mathcal{C}_{L_2}$, $\mathcal{C}_{L_2} < \mathcal{C} < \mathcal{C}_{L_1}$ and $\mathcal{C} > \mathcal{C}_{L_1}$.

Otherwise, $v^2 = \dot{X}^2 + \dot{Y}^2 + \dot{Z}^2$ would be negative, and this does not correspond to a real motion.

Consequently, the equality $\mathcal{C} = 2\Omega(X, Y, Z)$ is satisfied by the points on the so-called zero velocity surfaces, which divide $\mathbb{R}^3$ in a zone where the RTBP motion is possible and, on the other hand, a forbi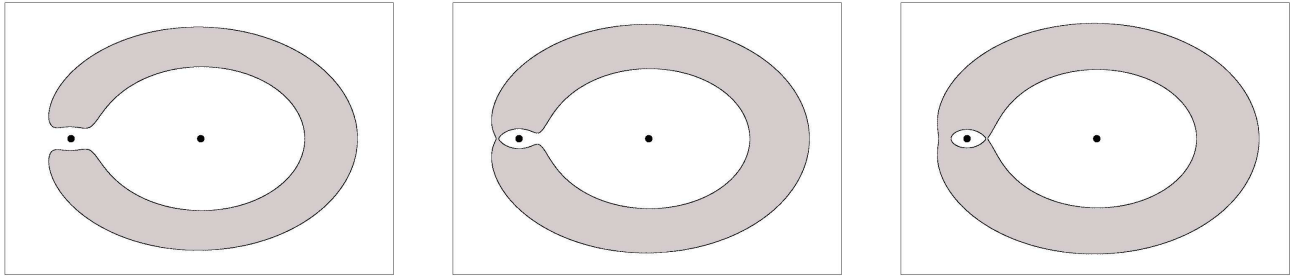dden region, whose xy projection is shown in figure 2.2. In this figure, the grey zones represent the region where motion is not possible.

It can be observed from the first picture on the left in figure 2.2 that for some values of the Jacobi constant, the zero velocity surfaces allow for the existence of trajectories going from the region of the big primary (in the centre of the 'corona') to the region of the small primary (on the left, between the zero velocity curves) and escaping afterwards to the outer region. On the other hand, when the L_2 side is closed (second picture in figure 2.2) no transit is allowed between the interior region, containing the primaries, and the outer region. Furthermore, when the zero velocity surfaces close both in L_1 and L_2, the movement takes place only around the primaries with no possible transfers from one to the other (i.e. approximately 2-body motions around each one of the primaries). We will usually work in energy levels corresponding to $\mathcal{C} < \mathcal{C}_{L_2}$, as these are the cases in which the movement around L_1 and L_2, as well as the transfers from one to the other take place.

2.2   The phase space around the libration points

2.2.1   Stability of the L_i points

We know from basic dynamical systems theory that given a linear system of differential equations, $\dot{x} = Bx$, with B a constant matrix of real coefficients:

   i. The system is asymptotically stable $\Leftrightarrow$ all eigenvalues of B have negative real part.

  ii. If the system is stable, all eigenvalues of B have non positive real part.

 iii. Conversely, if all eigenvalues of B have non positive real part, and the ones with 0 real part are simple (multiplicity 1), then the system is stable.

When a linear system is also Hamiltonian, then its matrix B has to be infinitesimal symplectic. That is, $B^T J + JB = 0$, where J=$\begin{pmatrix} 0 & I \\ -I & 0 \end{pmatrix}$ and I is the identity matrix.

The eigenvalues of a infinitesimal symplectic matrix have to satisfy:

iv. If λ is eigenvalue of B $\Rightarrow$ $-\lambda$, $\bar{\lambda}$ and $-\bar{\lambda}$ are also eigenvalues of B ($\bar{\lambda} = \overline{a + ib} = a - ib$, is the complex conjugate).

v. If 0 is eigenvalue of B, then it has to have an even multiplicity.

Consequently, for a linear Hamiltonian system, the stability conditions are:

- The system is never asymptotically stable. If it existed an eigenvalue λ, with $Re(\lambda) < 0$, then it would exist $\lambda' = -\lambda$ with $Re(\lambda') > 0$ (see iv.). So, condition i. can never be fulfilled for a Hamiltonian system.

- If the system is stable, then all eigenvalues of B are pure imaginary ($Re(\lambda) = 0$). This case is called elliptic stability.

- If all eigenvalues of B are pure imaginary (no real part) and simple, then the system is stable.

The RTBP is a Hamiltonian system. However, it is not linear. Therefore, in order to study the stability of its equilibrium points, it is convenient to linealize the system around them. Let x_0 be one of the five equilibrium points of the RTBP. Then the Hamiltonian system of equation (2.4) can be written $\dot{x} = X_H(x)$ and its linearised form around x_0 is,

$$\dot{x} = DX_H(x_0)(x - x_0).$$

$DX_H(x_0) = JD^2H(x_0)$, where $D^2H(x_0)$ is the matrix of second derivatives of the Hamiltonian function 2.4. The eigenvalues of $DX_H(x_0)$ are called characteristic exponents of X_H in x_0, and are the ones we have to compute in order to study the stability properties of the system around the aforementioned equilibrium points:

- If there exists a characteristic exponent λ with $Re(\lambda) > 0$, then we can already affirm that x_0 is unstable. Therefore, for x_0 to be stable it is necessary that all characteristic exponents are pure imaginary (elliptic points).

- Unfortunately, for a non-linear Hamiltonian system, one cannot affirm that being all characteristic exponents pure imaginary and simple, stability is guaranteed. However, if this is the case, then there exists a symplectic change of coordinates such that the Hamiltonian function can be cast into:

$$H = \frac{1}{2}\sum_{j=1}^{n} \omega_j(q_j^2 + p_j^2) + H_3 + H_4 + \dots$$

where, w_j are the imaginary part of the characteristic exponents but with a well determined sign. w_j are then called characteristic frequencies. (H_3 and H_4 stand for third and fourth order terms of the Hamiltonian function after the change of coordinates respectively).

  – If $w_j > 0 \; \forall j$ or $\omega_j < 0 \; \forall j$, we can affirm that the system is stable around x_0 (Dirichlet theorem).

  – On the contrary, if there exist negative and positive characteristic frequencies, nothing can be affirmed concerning stability. Other studies have to be performed (for $n = 2$, KAM theory assures stability under certain conditions, for $n \geq 3$ the notion of 'effective stability' is defined and proved).

For the particular case of the Lagrangian and Eulerian points of the RTBP we have that:

- The collinear equilibrium points L_1, L_2 and L_3 are unstable. In particular, for all values of $\mu \leq 0.5$, they have a couple of real characteristic exponents (λ and $-\lambda$) and two couples of pure imaginary characteristic exponents ($\pm \omega_1 \mathrm{i}$ and $\pm \omega_2 \mathrm{i}$). That is to say that the linear phase space around these points is of the type saddle×centre×centre. This is a property we will use in order to find the central manifold (4 dimensional, arising from the centre× centre part) and the stable and unstable manifolds (hyperbolic manifolds corresponding to the saddle part).

- On the contrary, the characteristic exponents of L_4 and L_5 points are pure imaginary for μ small enough ($\mu < \frac{1}{2}\left(1 - \sqrt{\frac{23}{27}}\right) \approx 0.0385$, critical Routh mass. Note that in celestial mechanics, the value of the critical Routh mass is rather big, as μ is 0.012 for the Earth-Moon problem and smaller for Sun-planet cases, even for Sun-Jupiter, with $\mu = 0.0009538$.). Therefore, L_4 and L_5 are elliptic equilibrium points. Although they do not have a linear hyperbolic character, stability around these points is not straightforward, as their characteristic frequencies have varying signs. Therefore, Dirichlet theorem for stability cannot be applied. However, other studies prove their effective stability ([9]), in the sense that motions in the vicinity of these points need to be integrated for a long time span before they go away from them.

2.2.2   Types of libration orbits

From now on we are interested in the motion in the vicinity of L_1 and L_2. So we set the origin of coordinates at the libration point, and scale the variables in such a way that the distance from the smallest primary to the equilibrium point is equal to one (see [65]). In particular, the changes of coordinates that we perform are:

$$\left.\begin{array}{rcl} x & = & -\frac{1}{\gamma}(X - \mu + 1 \mp \gamma) \\ y & = & -\frac{1}{\gamma}Y \\ z & = & \frac{1}{\gamma}Z \end{array}\right\}$$

where the upper sign in the expression of x corresponds to L_1 and the lower sign to L_2, and γ is the distance from the equilibrium point to the small primary, m_2. In the new coordinates, equations (2.1) become,

$$\left.\begin{array}{rcl} \ddot{x} - 2\,\dot{y} &=& \frac{1}{\gamma^2}\frac{\partial\Omega}{\partial x} \\ \ddot{y} + 2\,\dot{x} &=& \frac{1}{\gamma^2}\frac{\partial\Omega}{\partial y} \\ \ddot{z} &=& \frac{1}{\gamma^2}\frac{\partial\Omega}{\partial z} \end{array}\right\} \tag{2.6}$$

Now, in Ω the expression for r_1 and r_2 (distances from the particle m to the primaries) is,

$$r_1^2 = (-\gamma x - 1 \pm \gamma)^2 + \gamma^2 y^2 + \gamma^2 z^2 = \gamma^2\left[\left(x - \frac{(-1\pm\gamma)}{\gamma}\right)^2 + y^2 + z^2\right],$$

$$r_2^2 = (-\gamma x \pm \gamma)^2 + \gamma^2 y^2 + \gamma^2 z^2 = \gamma^2[(x-1)^2 + y^2 + z^2],$$

where the upper sign corresponds once more to L_1 case and the lower sign to L_2.

Therefore,

$$\frac{1-\mu}{r_1} = \frac{1-\mu}{\gamma}\frac{1}{\sqrt{\left(x - \frac{(-1\pm\gamma)}{\gamma}\right)^2 + y^2 + z^2}}, \qquad \frac{\mu}{r_2} = \frac{\mu}{\gamma}\frac{1}{\sqrt{(x-1)^2 + y^2 + z^2}}. \tag{2.7}$$

The square roots in the denominator can be expanded in power series using the Legendre polynomials, $P_n(x)$, and the following property,

$$\frac{1}{\sqrt{(x-A)^2 + (y-B)^2 + (z-C)^2}} = \frac{1}{\sqrt{A^2+B^2+C^2}}\sum_{n=0}^{\infty}\left(\frac{\rho}{A^2+B^2+C^2}\right)^n P_n\left(\frac{Ax+By+Cz}{\rho\sqrt{A^2+B^2+C^2}}\right),$$

where $\rho = x^2 + y^2 + z^2$.

So, expressions in (2.7) become,

$$\frac{1-\mu}{r_1} = \frac{1-\mu}{|-1\pm\gamma|}\sum_{n=0}^{\infty}(-1)^n\left(\frac{\gamma}{|-1\pm\gamma|}\right)^n \rho^n P_n\left(\frac{x}{\rho}\right)$$

$$\frac{\mu}{r_2} = \frac{\mu}{\gamma}\sum_{n=0}^{\infty}(\pm 1)^n \rho^n P_n\left(\frac{x}{\rho}\right).$$

Consequently, we have that,

$$\frac{1}{\gamma^2}\Omega(x,y,z) = \frac{1}{2\gamma^2}[(\gamma x - (\mu - 1 \pm \gamma)^2 + \gamma^2 y^2] + \sum_{n=0}^{\infty}\frac{1}{\gamma^2}c_n \rho^n P_n\left(\frac{x}{\rho}\right)$$

with,

$$c_n = \frac{1}{\gamma^2}\left(\frac{1-\mu}{|-1\pm\gamma|}(-1)^n\left(\frac{\gamma}{|-1\pm\gamma|}\right)^n + \frac{\mu}{\gamma}(\pm 1)^n\right). \tag{2.8}$$

Remember that Legendre polynomials are defined as follows:

$$P_0 = 1, \quad P_1(x) = x \quad \text{and} \quad P_{n+1}(x) = \frac{2n+1}{n+1}xP_n(x) - \frac{n}{n+1}P_{n-1}(x).$$

We can introduce the expression of the derivatives of Ω in terms of power series in the right side of equations (2.6). However, in both L_1 and L_2, $\frac{\partial \Omega}{\partial x} = \frac{\partial \Omega}{\partial y} = \frac{\partial \Omega}{\partial z} = 0$. Consequently, neither the independent terms of the series nor the linear ones appear in equations (2.6), which can be cast into,

$$
\begin{aligned}
\ddot{x} - 2\dot{y} - (1 + 2c_2)x &= \frac{\partial}{\partial x} \sum_{n \geq 3} c_n \rho^n P_n \left(\frac{x}{\rho} \right), \\
\ddot{y} + 2\dot{x} + (c_2 - 1)y &= \frac{\partial}{\partial y} \sum_{n \geq 3} c_n \rho^n P_n \left(\frac{x}{\rho} \right), \\
\ddot{z} + c_2 z &= \frac{\partial}{\partial z} \sum_{n \geq 3} c_n \rho^n P_n \left(\frac{x}{\rho} \right).
\end{aligned}
\tag{2.9}
$$

The left side of the above equations corresponds to the linearised system of ODE's around the libration points L_1 and L_2.

Furthermore, the expansion in power series can also be introduced in the the Hamiltonian function 2.4. In this way, we obtain:

$$
H = \frac{1}{2} \left(p_x^2 + p_y^2 + p_z^2 \right) + yp_x - xp_y - \sum_{n \geq 2} c_n \rho^n P_n \left(\frac{x}{\rho} \right).
$$

In order to get a picture of the phase space in a first approximation, we look at the linear part of the system. With a linear symplectic change of coordinates (see [34]), the second order part of the Hamiltonian is set into its real normal form,

$$
H_2 = \lambda x p_x + \frac{\omega}{2}(y^2 + p_y^2) + \frac{\nu}{2}(z^2 + p_z^2),
$$

where λ, ω and ν are positive real numbers depending on c_2. H_2 implies a linear behaviour near the collinear points of the type saddle$\times$centre$\times$centre. The centre$\times$centre part accounts for the existence of two oscillating motions: one in the xy plane and the other one in the vertical direction, z. When terms of higher order are added to the solutions, the problem is no longer linear. However, these two oscillations give rise to periodic motions: the planar Lyapunov orbit (arising from the oscillation in the xy plane, and having a null vertical oscillating amplitude) and the vertical Lyapunov orbit (respectively arising from the vertical oscillation).

Furthermore, the frequencies of the oscillations vary with the amplitudes and for a suitable amplitude, both frequencies become equal. At this point the well known halo type periodic orbits appear. When the frequencies of the two oscillations (vertical and planar) are not commensurable, the motion is not periodic, but quasi periodic, resulting in the so-called Lissajous orbits (see figure 2.3). This kind of motion is found both around the vertical periodic orbit and around the halo orbits ([35], [36]). 2D tori, with two basic frequencies tending to ω and ν when the amplitudes tend to zero, are also bound to appear. The rigorous proof of the existence of these tori is problematic and similar to the KAM theorem (see [47]).

A convenient way of representing all these libration orbits, for a given energy level, consists of representing their intersections with the plane of motion of the primaries, $z = 0$. This is called the

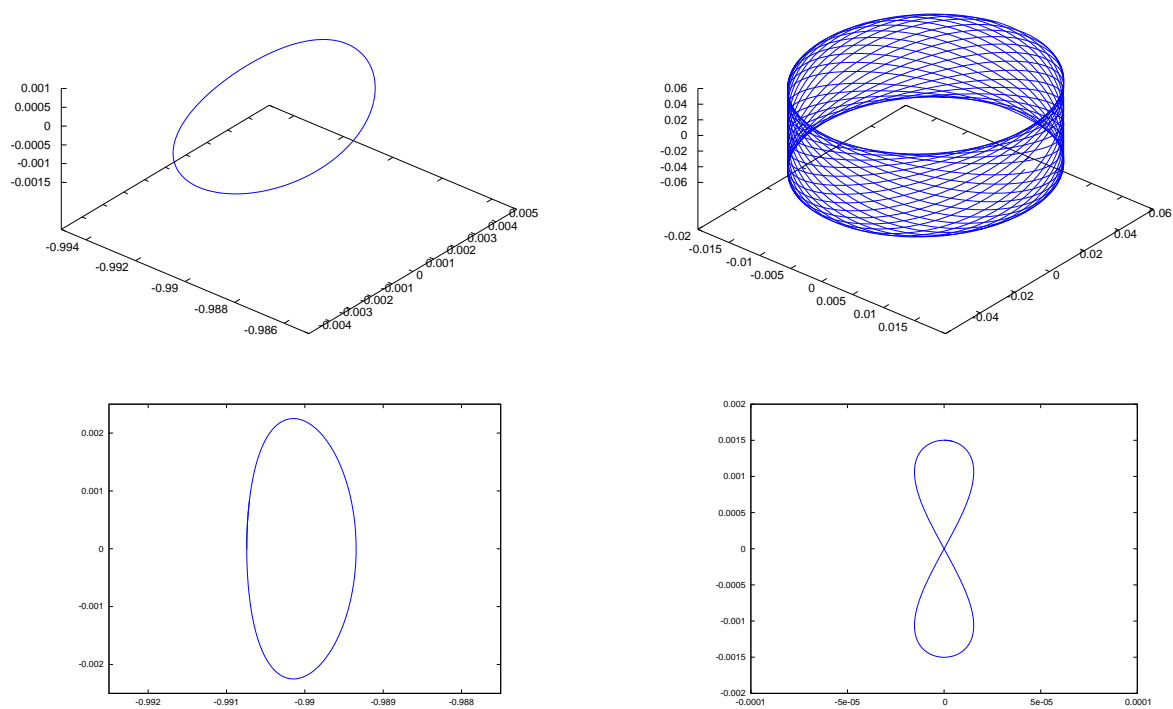Figure 2.3: Types of libration orbits. Top left: Halo orbit (xyz representation). Top right: Lissajous type orbit (xyz representation). Bottom left: planar lyapunov orbit (xy projection). Bottom right: vertical Lyapunov orbit (yz projection).

Poincaré map representation. A planar orbit will appear in it as a closed curve, a periodic orbit as a single point, and a quasi-periodic one as a set of points lying, more or less, on a curve. Figure 2.4 shows one of these representations. Near the centre of the figure one can see a fixed point. It corresponds to a vertical periodic orbit that crosses the $z = 0$ plane at just this point. This point (and so, the corresponding orbit) is surrounded by quasi-periodic motions that take place on invariant tori. The external curve of the figure is the planar Lyapunov orbit (corresponding to a given value of the Jacobi constant). Two other fixed points correspond to the two halo orbits, which are symmetrical to one another with respect to $z = 0$. They are, in turn, surrounded by invariant 2D tori. Between the 2D tori around the vertical orbit and the ones around the halo orbit there are traces of unstable manifolds, asymptotic to the planar Lyapunov orbit (see [34]).
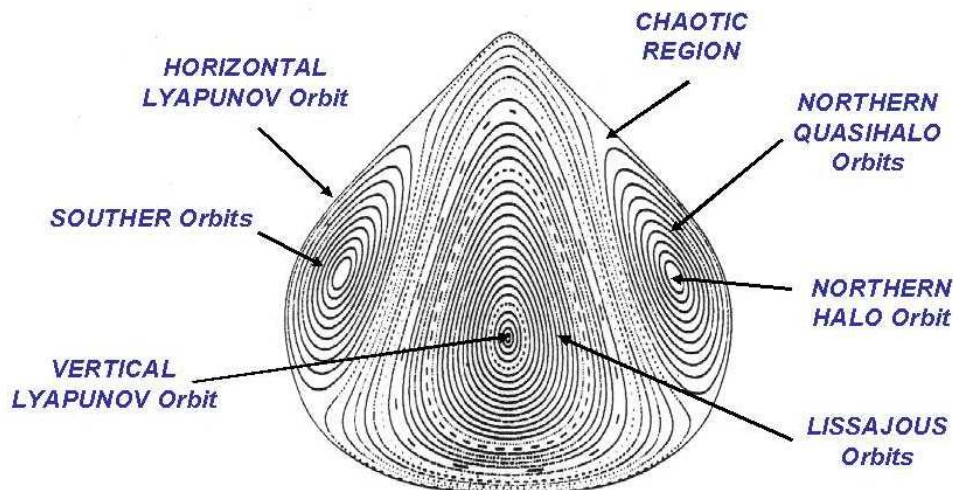
Figure 2.4: Poincaré map representation of the orbits near the libration point L_1 for the value of the Jacobi constant 3.00078515837634. The RTBP mass parameter corresponds to the Earth+Moon–Sun system.

Due to the strong unstable equilibrium that occurs near L_1 and L_2, it is not possible to perform a direct numerical simulation of the Poincaré map in order to get an idea of the phase space. Nevertheless, the centre×centre part, in all energy levels, gives rise to 4D manifolds where the dynamics have a neutral behaviour. The study of the dynamics in the central manifold can be done semi-analytically, using different methods such as the reduction to the normal form or to the center manifold (see for example [48]). In the following section we will see how libration orbits can be computed using Lindstedt-Poincaré procedures. Not only does this technique provide a semi analytical way of describing the solutions, but it also expresses them in convenient coordinates, with clear physical meaning which helps getting a geometrical insight into the problem.

2.3   Lindstedt-Poincaré procedures

The planar and vertical Lyapunov orbits, as well as the Lissajous, halo and quasi-halo orbits can be computed using Lindstedt-Poincaré procedures. In this way one obtains their expansions in convenient RTBP coordinates. Let us introduce the main ideas of the method.

The linearisation of equations (2.9) can be written,

$$\left.\begin{array}{rcl} \ddot{x} - 2\dot{y} - (1 + 2c_2)x &=& 0 \\ \ddot{y} + 2\dot{x} + (c_2 - 1)y &=& 0 \\ \ddot{z} + c_2 z &=& 0 \end{array}\right\}$$

where the value of c_2 depends on the mass parameter and the L_i we are studying (it can be computed using (2.8)). The solution of this linearised system is,

$$\left.\begin{array}{l} x(t) = A_1 e^{\lambda t} + A_2 e^{-\lambda t} + A_3 \cos \omega t + A_4 \sin \omega t \\ y(t) = cA_1 e^{\lambda t} - cA_2 e^{-\lambda t} - \kappa A_4 \cos \omega t + \kappa A_3 \sin \omega t \\ z(t) = A_5 \cos \nu t + A_6 \sin \nu t \end{array}\right\} \qquad (2.10)$$

where A_i are arbitrary constants and c, κ, ω, λ and ν are constants depending on c_2 only:

$$\omega = \sqrt{\frac{2 - c_2 + \sqrt{9c_2^2 - 8c_2}}{2}}, \quad \nu = \sqrt{c_2}, \quad c = \frac{\lambda^2 - 1 - 2c_2}{2\lambda}, \qquad (2.11)$$

$$\lambda = \sqrt{\frac{c_2 - 2 + \sqrt{9c_2^2 - 8c_2}}{2}}, \quad \kappa = \frac{-(\omega^2 + 1 + 2c_2)}{2\omega}.$$

We can see in (2.10) that A_1 and A_2 are the coefficients of the exponential part, which corresponds to the saddle component of the phase space. A_1 is called the unstable hyperbolic amplitude, because it accompanies the part corresponding to the eigenvalue which is responsible for instability. On the other hand, A_2 is the stable hyperbolic amplitude as it corresponds to an eigenvalue with negative real part.

Solutions with $A_1 = A_2 = 0$ belong to the so-called centre manifold, as they only have bounded terms (oscillating) as they only contain the part of the solution corresponding to pure imaginary eigenvalues. That is, the manifold containing the solutions of the center$\times$ center part, with no saddle components. Furthermore, it is convenient to look at the central solutions as having an amplitude and a phase in the xy plane (A_x and ϕ) as well as an amplitude and a phase in the z direction (A_z and ψ). Therefore, we use the following relations,

$$A_3 = A_x \cos \phi, \quad A_4 = -A_x \sin \phi,$$

$$A_5 = A_z \cos \psi \quad \text{and} \quad A_6 = -A_z \sin \psi.$$

Finally, the expression of the linearised solutions on the center manifold takes the form,

$$\begin{array}{rcl} x(t) &=& A_x \cos(\omega t + \phi) \\ y(t) &=& \kappa A_x \sin(\omega t + \phi) \\ z(t) &=& A_z \cos(\nu t + \psi) \end{array} \qquad (2.12)$$

where ω and ν are the planar and vertical characteristic frequencies and κ is a constant. The parameters A_x and A_z are the in-plane and out-of-plane amplitudes of the orbit and ϕ, ψ are the phases. These linear solutions are already Lissajous trajectories. When we consider the nonlinear

terms (in order to obtain solutions of the complete system), we look for formal series solutions in powers of the amplitudes A_x and A_z of the type

$$
\left\{ \begin{array}{c} x \\ y \\ z \end{array} \right\} = \sum_{i,j=1}^{\infty} \left(\sum_{|k|\leq i, |m|\leq j} \left\{ \begin{array}{c} x \\ y \\ z \end{array} \right\}_{ijkm} \left\{ \begin{array}{c} \cos \\ \sin \\ \cos \end{array} \right\} (k\theta_1 + m\theta_2) \right) A_x^i A_z^j, \qquad (2.13)
$$

where $\theta_1 = \omega_p t + \phi$ and $\theta_2 = \omega_v t + \phi$. Due to the presence of nonlinear terms, the frequencies ω_p and ω_v cannot be kept equal to ω and ν, and they must be expanded in powers of the amplitudes

$$
\omega_p = \omega + \sum_{i,j=1}^{\infty} \omega_{ij} A_x^i A_z^j, \quad \omega_v = \nu + \sum_{i,j=1}^{\infty} \nu_{ij} A_x^i A_z^j.
$$

The goal is to compute the coefficients x_{ijkm}, y_{ijkm}, z_{ijkm}, ω_{ij}, and ν_{ij} recurrently up to a finite order $N = i + j$. Identifying the coefficients of the general solution (2.13) with the ones obtained from the solution of the linear part (2.12), we see that the non zero values are $x_{1010} = 1$, $y_{1010} = \kappa$, $z_{1010} = 1$, $\omega_{00} = \omega$ and $\nu_{00} = \nu$. Inserting the linear solution (2.12) in the equations of motion, we get a remainder for each equation, which is a series in A_x and A_z beginning with terms of order $i + j = 2$. In order to get the coefficients of order two, this known order 2 terms must be equated to the unknown order 2 terms of the left hand side of the equations. The general step is similar. It assumes that the solution has been computed up to a certain order $n - 1$. Then it is substituted in the right hand side of the RTBP equations, producing terms of order n in A_x and A_z. This known order n terms must be equated with the unknown terms of order n of the left hand side.

Lissajous orbits already appear as solutions of the linearised system, halo and quasi-halo orbits don't. Therefore, modifications to the Lindstedt Poincaré technique have to be used in each particular computation. For instance, we know that halo orbits appear when the in plane and out of plane frequencies are equal. This is a 1:1 resonance that appears as a consequence of the nonlinear terms of the equations and this is why halo orbits do not appear as a solution of the linearised equations. We have to look for these 1-D tori as series expansions with a single frequency. In order to use Lindstedt-Poincaré procedures, we add a term Δz to the third equation of equation (2.9), where Δ is a frequency type series, $\Delta = \sum_{i,j=0}^{\infty} d_{ij} A_x^i A_z^j$, that must verify $\Delta = 0$. We start by looking for the librating solutions with frequency ω,

$$
\begin{array}{rcl}
x(t) & = & A_x \cos(\omega t + \phi) \\
y(t) & = & \kappa A_x \sin(\omega t + \phi) \\
z(t) & = & A_z \cos(\omega t + \psi)
\end{array}
\qquad (2.14)
$$

After this step, halo orbits are determined up to order 1, and $\Delta = 0$ is read as $d_{00} = 0$. Halo orbits depend only on one frequency or one amplitude since they are 1-D invariant tori, so we have not two independent amplitudes A_x and A_z. The relation between the amplitudes is contained in the condition $\Delta = 0$ which implicitly defines $A_x = A_x(A_z)$.

When we consider the full equations, we look for formal expansions in powers of the amplitudes A_x and A_z of the type

$$
\left\{ \begin{array}{c} x \\ y \\ z \end{array} \right\} = \sum_{i,j=1}^{\infty} \left(\sum_{|k|\leq i+j} \left\{ \begin{array}{c} x \\ y \\ z \end{array} \right\}_{ijk} \left\{ \begin{array}{c} \cos \\ \sin \\ \cos \end{array} \right\} (k\theta) \right) A_x^i A_z^j,
$$

where $\theta = \omega_p t + \phi$ and, as in the case of 2-D invariant tori, the frequency ω must be expanded as $\omega_p = \sum_{i,j=0}^{\infty} \omega_{ij} A_x^i A_z^j$. The procedure for the computation of the unknown coefficients x_{ijk}, y_{ijk}, z_{ijk}, ω_{ij} and d_{ij} is close to the one described for the Lissajous trajectories.

For an accurate description, as well as the computation of other types of orbits see [60].

2.4   JPL Solar System Ephemeris

We have described in the previous section the RTBP as a means to model the behaviour of a system consisting of two massive bodies and a small particle. This approximation is an acceptable model for the motion of the small mass for providing preliminary guesses. In addition, in the frame of the RTBP, the dynamics in the vicinity of libration points has been thoroughly studied and different kinds of orbits have been computed. However, when it comes to real mission design, more realistic models have to used, such as the JPL Solar System Ephemeris.

The JPL Solar System Ephemeris specifies the past and future positions of the Sun, Moon and nine planets in three-dimensional space. Planetary positions are generated by a computer integration fit to the best available observations of the positions of the Sun, Moon, planets and five largest asteroids. The computer integration involves step wise computation of the position of each planet as determined by the gravitation of all of the other objects in the Solar System. The planet's position is stepped both forward and backward in time from some chosen epoch. Minor adjustments are made to the masses and shapes of the Moon and planets to get best agreement with their observed position of the last 80 years or so.

Each JPL ephemeris file consists of data blocks containing the coefficients for Chebyshev polynomials that specify each of the three coordinate values and three coordinate velocity components (by numeric differentiation) for each object over the time span of the data block, generally 32 days (8 for Mercury, 16 for the Earth and 4 for the Moon). In the header of the ephemeris file, the constants assumed by the integrator are contained (such as the values of the masses of the planets or the value of the astronomical unit, AU). We use the file JPL DE403, which is based on planetary and reference data available in 1995 (see [76]), and uses the Earth mean equator and equinox of epoch 2000.0 as the reference frame, with origin at the full Solar System barycenter of that epoch.

Chapter 3

Eclipse avoidance and impulsive transfers in Lissajous orbits

3.1   Introduction

Two of the main subsystems of a space vehicle, the power source and the communication subsystem, can be seriously affected by eclipses in solar libration orbits. Around the Sun-Earth axis there exists a cylinder-like zone where solar electromagnetic radiation is specially strong. The L_1 libration point lays on the aforementioned axis and in between the two bodies. Therefore, the communication link between a satellite orbiting L_1 and the Earth can be damaged or interrupted whenever the satellites crosses this cylinder. On the other hand, the problem around L_2 is that the Earth half-shadow can produce occultations which result in the space vehicle being temporarily unable to obtain solar energy. Both problems can be modelled by placing a forbidden zone in the yz plane (around the libration point) which should not be crossed and that is called exclusion zone. Traditionally, big Halo orbits, which don't cross the exclusion zone, have been used as nominal paths in order to avoid this problem ([66], [20]). The main disadvantage of this kind of periodic motion is that the in plane and out of plane amplitudes of a Halo orbit have to satisfy a fixed relation, which may not always be optimal for mission requirements as this fact increases the complexity and cost of some hardware parts of the satellites. On the contrary, Lissajous libration point orbits are quasi periodic motions which allow for a high degree of freedom in the choice of their amplitudes. Nevertheless, Lissajous orbits cross the exclusion zone if no maneuvers are applied. This is the fact that motivates the work presented in this chapter.

A strategy for eclipse avoidance based on maneuvers which do not introduce unstable terms to the motion in the Lissajous orbit is developed. The linear approximation to the Lissajous motion is enough for the eclipse avoidance purpose ([8]) and leads to the implementation of a design tool, the Effective Phases Plane (EPP). The EPP allows for a simple geometric solution not only of the eclipse avoidance problem itself, but also of the planning of impulsive maneuvers for transfers between Lissajous orbits. Finally, the EPP has also been applied in solving the rendez-vous problem between different satellites on a Lissajous orbit, as shown in the last part of the chapter.

3.2 Linear approximation to Lissajous orbits.

Remember that the restricted three body problem, RTBP, is a simplified model for the motion of a small particle under the gravitational attraction of two massive bodies. In this work we focus on orbits around the equilibrium points known as L_1 and L_2, that are the ones closest to the small primary. Therefore, a reference system centred on the corresponding equilibrium point will be used as shown in chapter 2. In this new reference system, the form of the linearised equations is,

$$\left.\begin{array}{rcl} \ddot{x} - 2\,\dot{y} - (1 + 2c_2)\,x &=& 0 \\ \ddot{y} + 2\,\dot{x} + (c_2 - 1)\,y &=& 0 \\ \ddot{z} + c_2\,z &=& 0 \end{array}\right\} \tag{3.1}$$

where c_2 is a constant which can be written in terms of the mass parameter, μ and γ, the distance between the equilibrium point and the small primary (see again chapter 2),

$$c_2 = \frac{1}{\gamma^3}(\mu + (1-\mu)\frac{\gamma^3}{(1 \mp \gamma)^3}) \quad \text{for L}_1 \text{ (upper sign) and L}_2 \text{ (lower sign).}$$

Quasi-periodic solutions of the linear system (3.1) are characterised by an harmonic motion in the xy plane (also known as in-plane component) and an uncoupled oscillation in the z direction (also known as out-of-plane component) with a different period. The general solution is obtained by adding the hyperbolic exponential parts to this oscillation or harmonic part. The hyperbolic exponential parts have a part with positive exponent and, due to the Hamiltonian character, a part with negative exponent. Therefore, the general form of the solutions of (3.1) can be written,

$$\left.\begin{array}{l} x(t) = A_1 e^{\lambda t} + A_2 e^{-\lambda t} + A_3 \cos \omega t + A_4 \sin \omega t \\ y(t) = cA_1 e^{\lambda t} - cA_2 e^{-\lambda t} - \kappa A_4 \cos \omega t + \kappa A_3 \sin \omega t \\ z(t) = A_5 \cos \nu t + A_6 \sin \nu t \end{array}\right\} \tag{3.2}$$

where A_i are arbitrary constants and c, κ, ω, λ and ν are constants depending on c_2:

$$\omega = \sqrt{\frac{2 - c_2 + \sqrt{9c_2^2 - 8c_2}}{2}}, \quad \nu = \sqrt{c_2}, \quad c = \frac{\lambda^2 - 1 - 2c_2}{2\lambda}, \tag{3.3}$$

$$\lambda = \sqrt{\frac{c_2 - 2 + \sqrt{9c_2^2 - 8c_2}}{2}}, \quad \kappa = \frac{-(\omega^2 + 1 + 2c_2)}{2\omega}.$$

Furthermore, in this linear approximation the in-plane and out-of-plane motions are decoupled and we get the following relations between the coordinates of the trajectory and the constants $A_1, A_2, ..., A_6$, (which are in fact first integrals of the motion),

$$\begin{pmatrix} x \\ y \\ \dot{x} \\ \dot{y} \end{pmatrix} = \begin{pmatrix} e^{\lambda t} & e^{-\lambda t} & \cos \omega t & \sin \omega t \\ c\,e^{\lambda t} & -c\,e^{-\lambda t} & \kappa \sin \omega t & -\kappa \cos \omega t \\ \lambda\,e^{\lambda t} & -\lambda\,e^{-\lambda t} & -\omega \sin \omega t & \omega \cos \omega t \\ c\lambda\,e^{\lambda t} & c\lambda\,e^{-\lambda t} & \kappa\omega \cos \omega t & \kappa\omega \sin \omega t \end{pmatrix} \begin{pmatrix} A_1 \\ A_2 \\ A_3 \\ A_4 \end{pmatrix}$$

$$\begin{pmatrix} z \\ \dot{z} \end{pmatrix} = \begin{pmatrix} \cos \nu t & \sin \nu t \\ -\nu \sin \nu t & \nu \cos \nu t \end{pmatrix} \begin{pmatrix} A_5 \\ A_6 \end{pmatrix} \tag{3.4}$$

Inverting the system we get the first integrals of (3.2) in terms of a given state vector at time t, $(x(t), y(t), z(t), \dot{x}(t), \dot{y}(t), \dot{z}(t))$:

$$\begin{pmatrix} A_1 \\ A_2 \\ A_3 \\ A_4 \end{pmatrix} = \begin{pmatrix} \frac{-\kappa\omega}{2d_1}e^{-\lambda t} & \frac{\omega}{2d_2}e^{-\lambda t} & \frac{\kappa}{2d_2}e^{-\lambda t} & \frac{1}{2d_1}e^{-\lambda t} \\ \frac{-\kappa\omega}{2d_1}e^{\lambda t} & \frac{-\omega}{2d_2}e^{\lambda t} & \frac{-\kappa}{2d_2}e^{\lambda t} & \frac{1}{2d_1}e^{\lambda t} \\ \frac{c\lambda}{d_1}\cos\omega t & \frac{\lambda}{d_2}\sin\omega t & \frac{-c}{d_2}\sin\omega t & \frac{-1}{d_1}\cos\omega t \\ \frac{c\lambda}{d_1}\sin\omega t & \frac{-\lambda}{d_2}\cos\omega t & \frac{c}{d_2}\cos\omega t & -\frac{1}{d_1}\sin\omega t \end{pmatrix} \begin{pmatrix} x \\ y \\ \dot{x} \\ \dot{y} \end{pmatrix} \tag{3.5}$$

$$\begin{pmatrix} A_5 \\ A_6 \end{pmatrix} = \begin{pmatrix} \cos \nu t & \frac{-1}{\nu} \sin \nu t \\ -\sin \nu t & \frac{1}{\nu} \cos \nu t \end{pmatrix} \begin{pmatrix} z \\ \dot{z} \end{pmatrix}$$

where $d_1 = c\lambda - \kappa\omega$ and $d_2 = c\omega + \kappa\lambda$.

Finally, it is also convenient to look at the oscillatory solution of the linear part as having an amplitude and a phase,

$$\left. \begin{aligned} x(t) &= A_1 e^{\lambda t} + A_2 e^{-\lambda t} + A_x \cos(\omega t + \phi) \\ y(t) &= cA_1 e^{\lambda t} - cA_2 e^{-\lambda t} + \kappa A_x \sin(\omega t + \phi) \\ z(t) &= A_z \cos(\nu t + \psi) \end{aligned} \right\} \tag{3.6}$$

where the relations are $A_3 = A_x \cos\phi$, $A_4 = -A_x \sin\phi$, $A_5 = A_z \cos\psi$ and $A_6 = -A_z \sin\psi$.

We note that choosing, $A_1 = A_2 = 0$, we obtain a periodic motion in the xy components together with a periodic motion in z of a different period. This represents the Lissajous orbits in the linearised restricted circular three-body problem, A_x, A_z being the in-plane and out-of-plane amplitudes of the oscillations respectively. The first integrals A_1 and A_2 are directly related to the unstable and stable manifold of the linear Lissajous orbit. For instance, the relation $A_1 = 0, A_2 \neq 0$, defines a stable manifold. Any orbit verifying this condition will tend forward in time to the Lissajous orbit defined by A_x and A_z, since the term containing the A_2-component in (3.6) will die out. A similar fact happens when $A_1 \neq 0, A_2 = 0$. The term with A_1 will increase in forward time, but die out backwards in time. Therefore, solutions having $A_1 \neq 0$ go away from the oscillating or central part exponentially fast in forward time, and form the so-called unstable manifold.

3.3   Non escape maneuvers

In our analysis of the transfer we want to avoid unstable motions in forward time. As the unstable part is associated with the first integral that we call A_1, this means that we require the condition $A_1 = 0$. Using the first equation in (3.5) this is equivalent to,

$$\frac{\kappa}{d_2}\dot{x} + \frac{1}{d_1}\dot{y} = \frac{\kappa}{\omega}d_1 x - \frac{\omega}{d_2}y \tag{3.7}$$

It is important to note from this relation that given a position x, y of the spacecraft, we have an explicit formula for the set of possible velocities, $\dot{x}, \dot{y}$, for which escape is avoided.

Let us assume now that we are on a trajectory verifying the non escape condition $A_1 = 0$ (for instance on a Lissajous orbit). If we want to keep this non escape condition after performing a maneuver $(\Delta \dot{x}, \Delta \dot{y})$ we have to impose that the point after the maneuver also satisfies (3.7). Due to the linearity of the condition, as well as the fact that maneuvers do not change the instantaneous position, the condition is translated on the maneuver $(\Delta \dot{x}, \Delta \dot{y})$,

$$\frac{\kappa}{d_2} \Delta \dot{x} + \frac{1}{d_1} \Delta \dot{y} = 0.$$

So the corollary is that the maneuvers preserving $A_1 = 0$ are orthogonal to the vector $(\frac{\kappa}{d_2}, \frac{1}{d_1})$, this is, $(\Delta \dot{x}, \Delta \dot{y}) = a(\frac{1}{d_1}, \frac{-\kappa}{d_2})$ where $a \in \mathbb{R}$. This expression will be used in its equivalent form,

$$(\Delta \dot{x}, \Delta \dot{y}) = \frac{\alpha}{\sqrt{c^2 + \kappa^2}} (d_2, -\kappa d_1), \quad \alpha \in \mathbb{R} \tag{3.8}$$

where $|\alpha|$ indicates the size of the maneuver.

Note that the condition of non escape only affects components x and y of the maneuver. For the linear approximation that we are using, unstable terms represented by the constant of motion A_1 appear only in the in-plane motion. Therefore, the z components are not affected, as motion in this direction is uncoupled from the one in xy plane.

3.3.1   In plane maneuvers

We call in plane maneuvers to the maneuvers performed to the $\dot{x}$ and $\dot{y}$ components of the velocity. These maneuvers are aimed at changing either the amplitude A_x or the in plane phase, ϕ.

Changing the in-plane amplitude

Let us assume that at a given time t_m we perform a maneuver $(\Delta \dot{x}, \Delta \dot{y})$. The in-plane amplitude A_x will change from an initial value $A_x^{(i)}$ to a final one $A_x^{(f)}$ given by,

$$
\begin{aligned}
A_x^{(f)\,2} =\quad & A_3^{(f)\,2} + A_4^{(f)\,2} = \left[\frac{c\lambda}{d_1} x(t_m) \cos \omega t_m + \frac{\lambda}{d_2} y(t_m) \sin \omega t_m - \right. \\
& \left. - \frac{c}{d_2} (\dot{x}(t_m^-) + \Delta \dot{x}) \sin \omega t_m - \frac{1}{d_1} (\dot{y}(t_m^-) + \Delta \dot{y}) \cos \omega t_m \right]^2 + \left[\frac{c\lambda}{d_1} x(t_m) \sin \omega t_m - \right. \\
& \left. - \frac{\lambda}{d_2} y(t_m) \cos \omega t_m + \frac{c}{d_2} (\dot{x}(t_m^-) + \Delta \dot{x}) \cos \omega t_m - \frac{1}{d_1} (\dot{y}(t_m^-) + \Delta \dot{y}) \sin \omega t_m \right]^2 \\
=\quad & A_3^{(i)\,2} + A_4^{(i)\,2} + \left(\frac{c}{d_2} \Delta \dot{x} \sin \omega t_m + \frac{\Delta \dot{y}}{d_1} \cos \omega t_m \right)^2 + + \left(\frac{c}{d_2} \Delta \dot{x} \cos \omega t_m + \frac{\Delta \dot{y}}{d_1} \sin \omega t_m \right)^2 \\
& - 2 A_3^{(i)} \left(\frac{c}{d_2} \Delta \dot{x} \sin \omega t_m + \frac{\Delta \dot{y}}{d_1} \cos \omega t_m \right) + + 2 A_4^{(i)} \left(\frac{c}{d_2} \Delta \dot{x} \cos \omega t_m + \frac{\Delta \dot{y}}{d_1} \sin \omega t_m \right) \\
=\quad & A_x^{(i)\,2} + \frac{c^2}{d_2^2} (\Delta \dot{x})^2 + \frac{1}{d_1^2} (\Delta \dot{y})^2 - 2 A_3^{(i)} \left(\frac{c}{d_2} \Delta \dot{x} \sin \omega t_m + \frac{\Delta \dot{y}}{d_1} \cos \omega t_m \right) + \\
& + 2 A_4^{(i)} \left(\frac{c}{d_2} \Delta \dot{x} \cos \omega t_m + \frac{\Delta \dot{y}}{d_1} \sin \omega t_m \right)
\end{aligned}
$$

where $\dot{x}(t_m^-)$ has to be understood as $\lim_{t\to t_m, t<tm} \dot{x}(t)$, and analogously for $\dot{y}(t_m^-)$. These are the x and y velocities just before performing the maneuver.

We use expressions of the amplitudes A_3 and A_4 in terms of $x, y, \dot{x}, \dot{y}$ to compute the two latest terms. (From now on, t stands for t_m and $x, y, \dot{x}, \dot{y}$ are assumed to be the ones corresponding to this time):

$$A_3^{(i)}\left(\frac{c}{d_2}\Delta\dot{x}\sin\omega t_m + \frac{\Delta\dot{y}}{d_1}\cos\omega t_m\right) = \frac{c^2\lambda}{d_1 d_2}x\Delta\dot{x}\sin\omega t\cos\omega t + \frac{\lambda c}{d_2^2}y\Delta\dot{x}\sin^2\omega t -$$

$$-\frac{c^2}{d_2^2}\dot{x}\Delta\dot{x}\sin^2\omega t - \frac{c}{d_1 d_2}\dot{y}\Delta\dot{x}\sin\omega t\cos\omega t + \frac{c\lambda}{d_1^2}x\Delta\dot{y}\cos^2\omega t +$$

$$+\frac{\lambda}{d_1 d_2}y\Delta\dot{y}\sin\omega t\cos\omega t - \frac{c}{d_1 d_2}\dot{x}\Delta\dot{y}\sin\omega t\cos\omega t - \frac{1}{d_1^2}\dot{y}\Delta\dot{y}\cos^2\omega t$$

$$A_4^{(i)}\left(\frac{c}{d_2}\Delta\dot{x}\cos\omega t_m + \frac{\Delta\dot{y}}{d_1}\sin\omega t_m\right) = \frac{c^2\lambda}{d_1 d_2}x\Delta\dot{x}\sin\omega t\cos\omega t - \frac{\lambda c}{d_2^2}y\Delta\dot{x}\cos^2\omega t +$$

$$+\frac{c^2}{d_2^2}\dot{x}\Delta\dot{x}\cos^2\omega t - \frac{c}{d_1 d_2}\dot{y}\Delta\dot{x}\sin\omega t\cos\omega t - \frac{c\lambda}{d_1^2}x\Delta\dot{y}\sin^2\omega t +$$

$$+\frac{\lambda}{d_1 d_2}y\Delta\dot{y}\sin\omega t\cos\omega t - \frac{c}{d_1 d_2}\dot{x}\Delta\dot{y}\sin\omega t\cos\omega t + \frac{1}{d_1^2}\dot{y}\Delta\dot{y}\sin^2\omega t$$

$$A_x^{(f)\,2} = A_x^{(i)\,2} + \frac{c^2}{d_2^2}(\Delta\dot{x})^2 + \frac{1}{d_1^2}(\Delta\dot{y})^2 - 2\frac{c\lambda}{d_2^2}y(t_m)\Delta\dot{x} + 2\frac{c^2}{d_2^2}\dot{x}(t_m^-)\Delta\dot{x} - 2\frac{c\lambda}{d_1^2}x(t_m)\Delta\dot{y} + 2\frac{1}{d_1^2}\dot{y}(t_m^-)\Delta\dot{y}.$$

$$(3.9)$$

We note that this expression is valid in the most generic case, this is, for any maneuver $(\Delta\dot{x}, \Delta\dot{y})$. Let us assume now that the maneuver is done when the satellite is on a Lissajous orbit. In this case for $t \leq t_m$ we have,

$$x(t) = A_x^{(i)}\cos(\omega t + \phi) \qquad y(t) = \kappa A_x^{(i)}\sin(\omega t + \phi)$$
$$\dot{x}(t) = -A_x^{(i)}\omega\sin(\omega t + \phi) \qquad \dot{y}(t) = \kappa A_x^{(i)}\omega\cos(\omega t + \phi)$$

So,

$$\dot{x} = \frac{-\omega}{\kappa}y, \quad \dot{y} = \kappa\omega x \quad \text{and} A_x^{(i)\,2} = x^2 + \frac{1}{\kappa^2}y^2.$$

We use this to take $\dot{x}$ and $\dot{y}$ out from formula (3.9). Therefore, if we are on a Lissajous orbit, we have:

$$A_x^{(f)\,2} = A_x^{(i)\,2} + \frac{c^2}{d_2^2}(\Delta\dot{x})^2 + \frac{1}{d_1^2}(\Delta\dot{y})^2 - \frac{2c}{d_2}\left(\frac{c\omega}{\kappa d_2} + \frac{\lambda}{d_2}\right)y\Delta\dot{x} + \frac{2}{d_1}\left(\frac{\kappa\omega}{d_1} - \frac{c\lambda}{d_1}\right)x\Delta\dot{y} \quad (3.10)$$

However, there exist some easy to prove relations between the constants $\frac{c\omega}{\kappa d_2} + \frac{\lambda}{d_2} = \frac{1}{\kappa}$ and $\frac{\kappa\omega}{d_1} - \frac{c\lambda}{d_1} = -1$, and consequently,

$$A_x^{(f)\,2} = A_x^{(i)\,2} + \frac{c^2}{d_2^2}(\Delta\dot{x})^2 - \frac{2c}{d_2}\frac{1}{\kappa}y\Delta\dot{x} + \frac{1}{d_1^2}(\Delta\dot{y})^2 - \frac{2}{d_1}x\Delta\dot{y} = \quad (3.11)$$

$$= A_x^{(i)\,2} + \left(\frac{c}{d_2}\Delta\dot{x} - \frac{1}{\kappa}y\right)^2 - \frac{1}{\kappa^2}y^2 + \left(\frac{1}{d_1}\Delta\dot{y} - x\right)^2 - x^2.$$

Finally, using $\frac{1}{\kappa^2}y^2 + x^2 = A_x^{(i)\,2}$, we get,

$$A_x^{(f)\,2} = \left[\frac{c}{d_2}\Delta\dot{x} - \frac{1}{\kappa}y(t_m) \right]^2 + \left[\frac{1}{d_1}\Delta\dot{y} - x(t_m) \right]^2$$

which represents the final in-plane amplitude that is reached when a maneuver $(\Delta\dot{x}, \Delta\dot{y})$ is executed at time t_m in the $x(t_m), y(t_m)$ position corresponding to a Lissajous orbit. Note that we have yet to require the non escape condition to the maneuver.

Let us assume now that the maneuver at time t_m is done in order to perform a transfer from a Lissajous orbit to another one with a different in-plane amplitude, leaving the out-of-plane motion untouched. The maneuver will be aimed at reaching $A_x^{(f)}$, but keeping $A_1 = 0$. Therefore, non escape maneuvers satisfying (3.8) have to be used. The new A_2-term which appears as a consequence of the maneuver tends to vanish, since it is accompanied by the exponential decay in (3.6). The result is that the trajectory will reach the final orbit asymptotically with no more maneuvers.

If a maneuver in the non escape direction is applied, the expression for the final in-plane amplitude becomes,

$$A_x^{(f)\,2} = \left(\frac{\alpha c}{\sqrt{c^2+\kappa^2}} - \frac{1}{\kappa}y(t_m) \right)^2 + \left(\frac{\alpha\kappa}{\sqrt{c^2+\kappa^2}} + x(t_m) \right)^2 = \; = \alpha^2 + \frac{2\alpha}{\sqrt{c^2+\kappa^2}}\left[\frac{-c}{\kappa}y(t_m) + \kappa x(t_m) \right] + A_x^{(i)\,2}$$

where again, $A_x^{(i)\,2} = \frac{1}{\kappa^2}y^2 + x^2$, has been used.

At this point it is convenient to introduce a constant angle, β, defined as the slope of the vector (c, κ): $(\cos\beta, \sin\beta) = (\frac{c}{\sqrt{c^2+\kappa^2}}, \frac{\kappa}{\sqrt{c^2+\kappa^2}})$. Then, defining the function,

$$p(t) = A_x^{(i)} \sin\left(\omega t + \phi_i - \beta\right),$$

the expression for the final amplitude $A_x^{(f)}$ becomes,

$$A_x^{(f)\,2} = \alpha^2 - 2p(t_m)\alpha + A_x^{(i)\,2} \tag{3.12}$$

This means that, for a given time, the magnitude of the maneuver necessary to reach a target in-plane amplitude is given by the quadratic equation, $\alpha^2 - 2p(t_m)\alpha - (A_x^{(f)\,2} - A_x^{(i)\,2})^2$, and so, $\alpha = p(t_m) \pm \sqrt{p^2(t_m) + (A_x^{(f)\,2} - A_x^{(i)\,2})}$. Moreover, using the definition of $p(t)$, we have,

$$\alpha = A_x^{(i)} \sin\left(\omega t_m + \phi_i - \beta\right) \pm \sqrt{A_x^{(f)\,2} - A_x^{(i)\,2} \cos^2\left(\omega t_m + \phi_i - \beta\right)} \tag{3.13}$$

From this last expression, we observe that,

- If $A_x^{(f)} \geq A_x^{(i)}$, the transfer maneuver is possible at any time, as the terms inside the square root are positive.

- If $A_x^{(f)} < A_x^{(i)}$, the transfer maneuver is possible only when $\omega t_m + \phi_i - \beta \in \left[\delta, \frac{\pi}{2} + \delta\right]$ (mod π), where $\delta = \arccos\left(\frac{A_x^{(f)}}{A_x^{(i)}}\right)$. Otherwise, expression (3.13) has non real values.

Furthermore, for each fixed A_x^f, one can choose the time t_m for the transfer maneuver using two criteria:

- *Optimal maneuver time.* Select t_m in such a way that the Δv expended in changing the amplitude is a minimum. As we said in (3.8) this corresponds to the minimum of $|\alpha|$.

- *Change of the in-plane phase.* Select t_m in such a way that you arrive at the target orbit with a selected phase.

Let us comment these possibilities and their implications.

Optimal in-plane maneuvers

Let us assume that $A_x^{(f)} \neq A_x^{(i)}$. Looking for the local minima of $\alpha(t_m)$ we get that the optimal t_m are the ones that satisfy,

$$\omega t_m + \phi_i = \beta + \tfrac{\pi}{2}, \quad \text{or} \quad \omega t_m + \phi_i = \beta + \tfrac{3\pi}{2}, \quad \text{(both mod } 2\pi). \tag{3.14}$$

This corresponds to the moments when the angle $\omega t_m + \phi_i$ is orthogonal to β, or equivalently, when the satellite on a Lissajous orbit crosses the plane $cx + y = 0$. At this point the minimum fuel expenditure that is necessary for transferring from a Lissajous orbit with in plane amplitude equal to A_x^i to another one with amplitude A_x^f using non escape maneuvers occurs. The value of α in this case is, $|\alpha_{min}| = |A_x^{(f)} - A_x^{(i)}|$

Changing the in-plane phase

If we execute an in-plane maneuver at time t_m we change the in-plane amplitude from $A_x^{(i)} = \sqrt{A_3^{(i)\,2} + A_4^{(i)\,2}}$, to $A_x^{(f)} = \sqrt{A_3^{(f)\,2} + A_4^{(f)\,2}}$, which will remain constant along the new trajectory. But depending on t_m, the values of the components $A_3^{(f)}$ and $A_4^{(f)}$ will be different, giving as a result the possibility of reaching the target orbit at different phases.

Let us assume that at time t_m we perform a maneuver, $(\Delta \dot{x}, \Delta \dot{y})$. Using the equations (3.5) to compute the first integrals $A_3^{(f)}$ and $A_4^{(f)}$ in terms of $x(t_m)$, $y(t_m)$, $\dot{x}(t_m^+)$ and $\dot{y}(t_m^+)$, where $\dot{x}(t_m^+) = \dot{x}(t_m^-) + \Delta \dot{x}$, and analogously for $\dot{y}(t_m^+)$ (i.e. the velocities just after the maneuver), we obtain,

$$A_3^{(f)} = A_3^{(i)} - \frac{c}{d_2} \sin \omega t_m \Delta \dot{x} - \frac{1}{d_1} \cos \omega t_m \Delta \dot{y},$$

$$A_4^{(f)} = A_4^{(i)} + \frac{c}{d_2} \cos \omega t_m \Delta \dot{x} - \frac{1}{d_1} \sin \omega t_m \Delta \dot{y}.$$

Assuming, indeed, that the maneuver $(\Delta \dot{x}, \Delta \dot{y})$ is done in the non escape direction (3.8) and using the definition of β, these formulae can be cast into,

$$A_3^{(f)} = A_3^{(i)} - \alpha(t_m) \sin(\omega t_m - \beta), \qquad A_4^{(f)} = A_4^{(i)} + \alpha(t_m) \cos(\omega t_m - \beta), \tag{3.15}$$

where, if the maneuver is done when the satellite is on a Lissajous orbit, and the target amplitude $A_x^{(f)}$ can be effectively reached, the value of $\alpha(t_m)$ is given by (3.13).

Therefore, using that $A_3^{(f)} = A_x^{(f)} \cos\phi_f$ and $A_4^{(f)} = -A_x^{(f)} \sin\phi_f$, we get that the new phase after the in-plane maneuver is defined by,

$$\cos\phi_f = \frac{1}{A_x^{(f)}} \left(A_x^{(i)} \cos\phi_i - \alpha(t_m)\sin(\omega t_m - \beta) \right) \tag{3.16}$$

$$\sin\phi_f = \frac{1}{A_x^{(f)}} \left(A_x^{(i)} \sin\phi_i - \alpha(t_m)\cos(\omega t_m - \beta) \right)$$

In-plane phase change maneuvers maintaining the amplitude

Let us study the case where the in-plane amplitude is maintained as a particular application of the phase change maneuvers. This special case will be very useful for the design of strategies that avoid the exclusion zones.

Assume that we perform the maneuver on a Lissajous orbit,

$$x(t) = A_x^{(i)} \cos(\omega t + \phi_i), \quad y(t) = -\kappa A_x^{(i)} \sin(\omega t + \phi_i),$$

with the purpose of arriving asymptotically to another one,

$$x(t) = A_x^{(f)} \cos(\omega t + \phi_f), \quad y(t) = -\kappa A_x^{(f)} \sin(\omega t + \phi_f),$$

with $A_x^{(f)} = A_x^{(i)}$ that will be just denoted by A_x in this subsection. We want to link ϕ_f with ϕ_i depending on t_m.

In this case, according to (3.13), the non trivial maneuver at time t_m is given by,

$$\alpha(t_m) = 2A_x \sin(\omega t_m + \phi_i - \beta) = 2p(t_m).$$

Using now (3.15) and the fact that $A_3^{(i)} = A_x \cos\phi_i$, $A_4^{(i)} = -A_x \sin\phi_i$, we get the new components for the in-plane amplitude,

$$A_3^{(f)} = A_x \cos\phi_i - 2A_x \sin(\omega t_m + \phi_i - \beta)\sin(\omega t_m - \beta)$$
$$A_4^{(f)} = -A_x \sin\phi_i + 2A_x \sin(\omega t_m + \phi_i - \beta)\cos(\omega t_m - \beta).$$

And after some trigonometry the computations end up with,

$$A_3^{(f)} = A_x \cos[2(\omega t_m - \beta) + \phi_i], \quad A_4^{(f)} = A_x \sin[2(\omega t_m - \beta) + \phi_i]. \tag{3.17}$$

Comparing these expressions with their alternative ones, $A_3^{(f)} = A_x \cos\phi_f$, and $A_4^{(f)} = -A_x \sin\phi_f$, we see that the relation between the phases is $\phi_f = -2(\omega t_m - \beta) - \phi_i$ or equivalently,

$$\phi_f - \phi_i = -2(\omega t_m - \beta + \phi_i) \pmod{2\pi}. \tag{3.18}$$

It is important to note that from equation (3.18), given an initial phase ϕ_i, there is only one possible jump (modulus 2π) at each maneuvering time t_m. Or equivalently, if the desired jump in phases is known, the moment t_m at which to accomplish the change of phases can be computed from this equation.

3.3.2   Out of plane maneuvers

Let us assume that a z-maneuver is performed at a given time t_m. Using (3.5) in a similar way that for the discussion of the in-plane maneuvers, a Δv of magnitude $\Delta \dot{z}$ in the z direction changes the first integrals A_5 and A_6, according to,

$$A_5^{(f)} = A_5^{(i)} - \frac{\Delta \dot{z}}{\nu} \sin(\nu t_m), \quad A_6^{(f)} = A_6^{(i)} + \frac{\Delta \dot{z}}{\nu} \cos(\nu t_m). \tag{3.19}$$

After some algebra which uses (3.4) we get the following expression for the z-amplitude,

$$A_z^{(f)\,2} = A_5^{(f)\,2} + A_6^{(f)\,2} = A_z^{(i)\,2} + \frac{2}{\nu^2}\dot{z}(t_m^-)\Delta \dot{z} + \frac{(\Delta \dot{z})^2}{\nu^2}.$$

But according to (3.6), the motion in the z component until just before the maneuver is, $\dot{z} = -\nu A_z^{(i)} \sin(\nu t + \psi_i)$, and so,

$$A_z^{(f)\,2} = \frac{(\Delta \dot{z})^2}{\nu^2} - 2\frac{\Delta \dot{z}}{\nu}A_z^{(i)} \sin(\nu t_m + \psi_i) + A_z^{(i)\,2}. \tag{3.20}$$

We note that equations (3.19) and (3.20) are completely analogous to equations (3.15) and (3.12) of the in-plane case respectively. Essentially, the formal role of α is now played by $\Delta \dot{z}/\nu$ and the former angle, β, is now zero. Then, the discussion for the out of plane maneuvers follows a parallel way to the one we have done for the in-plane case. Therefore, the results will only be summarised here.

The formula for the required Δv analogous to (3.13) is now,

$$\frac{\Delta \dot{z}}{\nu} = A_z^{(i)} \sin(\nu t_m + \psi_i) \pm \sqrt{A_z^{(f)\,2} - A_z^{(i)\,2} \cos^2(\nu t_m + \psi_i)} \tag{3.21}$$

and the corresponding discussion is the following. If,

- $A_z^{(f)} \geq A_z^{(i)}$ the transfer maneuver is possible at any time.

- $A_z^{(f)} < A_z^{(i)}$ the transfer maneuver is possible only if the expression inside the square root is positive. More precisely, when $\nu t_m + \psi_i \in \left[\varepsilon, \frac{\pi}{2} + \varepsilon\right]$ (mod π), where $\varepsilon = \arccos\left(\frac{A_z^{(f)}}{A_z^{(i)}}\right)$.

Again, two different criteria can help in choosing the time for the maneuver: optimal cost maneuver or fixed arriving phase.

Optimal out-of-plane maneuvers

When the transfer is possible, the maneuver to change the out-of-plane amplitude from $A_z^{(i)}$ to $A_z^{(f)}$ is optimal when t_m verifies,

$$\nu t_m + \psi_i = \frac{\pi}{2}, \quad \text{or} \quad \nu t_m + \psi_i = \frac{3\pi}{2}, \quad \text{(both mod } 2\pi\text{)}. \tag{3.22}$$

In this case, the minimal $\Delta v = |\Delta \dot{z}|$ is given according to, $\Delta \dot{z} = \nu(A_z^{(i)} - A_z^{(f)})$, or $\Delta \dot{z} = \nu(A_z^{(f)} - A_z^{(i)})$, for the $\pi/2$ or $3\pi/2$ cases respectively.

Since the out-of-plane movement is governed by $z(t) = A_z^{(i)} \cos(\nu t + \psi_i)$, we note that the optimal times correspond to $z = 0$. This is when the satellite crosses the ecliptic plane, which is natural if we think in terms of energy. We remark that the ecliptic plane plays the same role for the out-of-plane maneuvers as the plane $cx + y = 0$ plays for the in-plane ones.

Changing the out-of-plane phase

Equations (3.19) give us the components of the final z-amplitude $A_z^{(f)}$. The corresponding phase, ψ_f, can be obtained from the definition, $A_5^{(f)} = A_z^{(f)} \cos \psi_f$, $A_6^{(f)} = -A_z^{(f)} \sin \psi_f$.

In this context we can also consider a maneuver in the z-component to change the out-of-plane phase without changing the amplitude. The equation which gives now the non trivial maneuver is,

$$\frac{\Delta \dot{z}}{\nu} = 2A_z \sin (\nu t_m + \psi_i), \tag{3.23}$$

and the corresponding change of phase as a function of t_m is,

$$\psi_f - \psi_i = -2(\nu t_m + \psi_i) \qquad (\text{mod } 2\pi) \tag{3.24}$$

We observe that in this case the maneuver (3.23) corresponds to inverting the z component of the velocity. Remark again that given an initial out of plane phase ψ_i, there is only one possible jump in ψ (obviously, modulus 2π) at each moment of time, t_m.

3.4   The effective phases plane (EPP)

Looking at the central part of (3.6) or equivalently, if the satellite is on a Lissajous orbit we have,

$$x(t) = A_x \cos(\omega t + \phi), \quad y(t) = \kappa A_x \sin(\omega t + \phi), \quad z(t) = A_z \cos(\nu t + \psi). \tag{3.25}$$

We note that due to the autonomous character of the original system of differential equations (3.1), we can reset $t = 0$ at any time if we recompute the A_i values of the solution (3.6) using equations (3.5). For the central part (3.25) mentioned above, due to the invariance of the amplitudes A_x and A_z it is even easier, since t can be reseted to zero at time t_0 just changing the phases ϕ and ψ by $\phi + \omega t_0$ and $\psi + \nu t_0$ respectively. This observation motivates the following definitions.

Let us define the effective phase Φ as all the epochs t and all the phases ϕ such that $\Phi(t, \phi) = \omega t + \phi$ (mod 2π). In the same way we define the effective phase Ψ as all the epochs t and all the phases ψ such that $\Psi(t, \psi) = \nu t + \psi$ (mod 2π). Even though from this definition the effective phases are a function of the time and the initial phase, (t, ϕ) or (t, ψ), taking values in subsets of $\mathbb{R} \times [0, 2\pi]$, it is more convenient to identify them by numbers Φ and Ψ in $[0, 2\pi]$.

Using equations (3.25) and taking also into account the velocities, we note that there is a biunivocal correspondence between a pair of effective phases (Φ, Ψ) and a state $(x, y, z, \dot{x}, \dot{y}, \dot{z})$ on a Lissajous orbit of given amplitudes A_x and A_z. In fact, from a dynamical systems point of view, this is a consequence that Lissajous orbits are 2D tori. Therefore, we are just using the well known action-angle variables of the tori.

The convenience of using the effective phases becomes clear since in the space (Φ, Ψ) a trajectory such as (3.25) with initial phases (ϕ_i, ψ_i), is seen as a straight line of slope ω/ν, starting at the point (ϕ_i, ψ_i), which propagates with constant velocity components ω and ν respectively in the directions Φ and Ψ. So, dynamics become much easier when studied in this representation.

As a first application of the effective phases we have that it is very easy to geometrically define the location for the optimal maneuvers in (3.14). The optimal maneuver to change the A_x

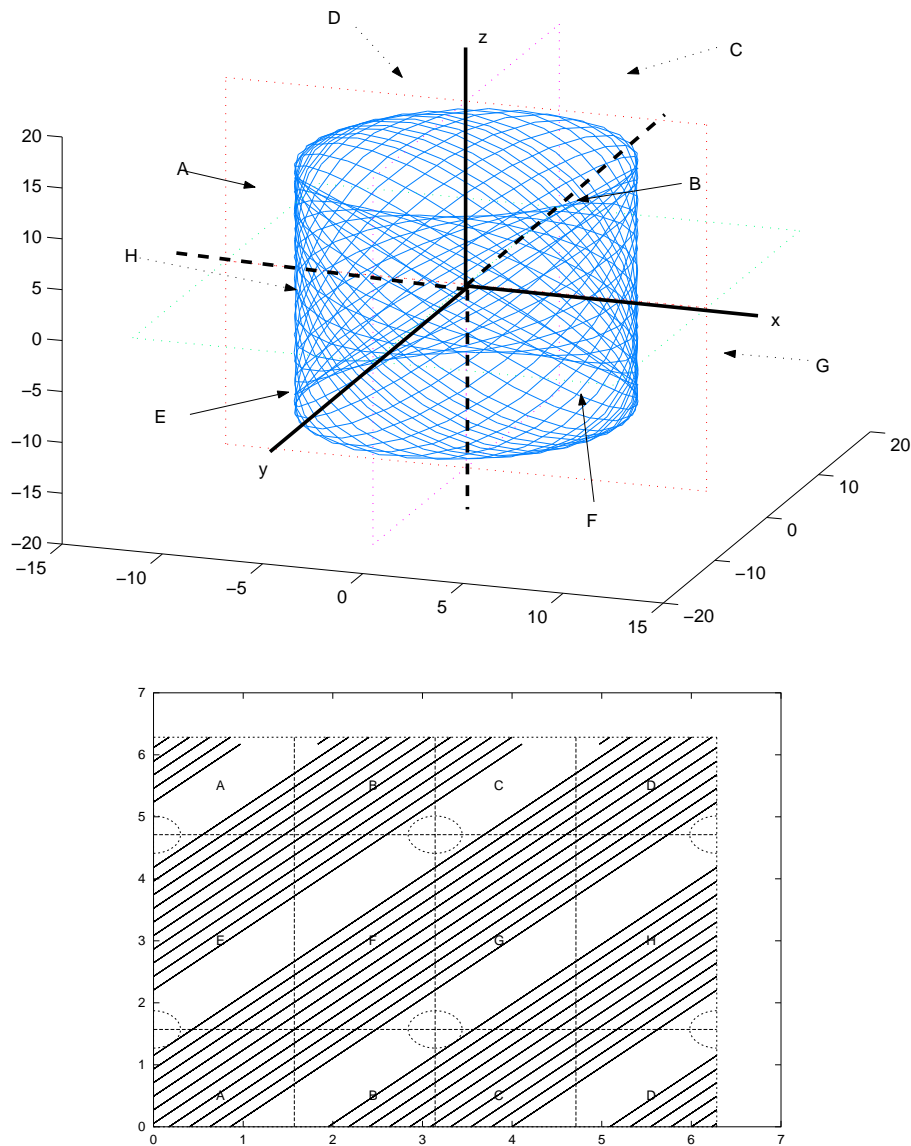Figure 3.1: Correspondence between Lissajous points (top) and the effective phases (bottom). The zones labelled with capital letters are the regions where the x, y and z coordinates have constant sign. The same labels on the EPP indicate which set of phases on the EPP leads to each zone on the orbit. The ellipse like plots in the EPP represent exclusion zones, whose crossing should be avoided.

amplitude has to be done when the trajectory in the space of effective phases crosses either the line $\Phi = \beta + \frac{\pi}{2}$ or $\Phi = \beta + \frac{3\pi}{2}$. In addition, according to (3.22), the optimal change of A_z occurs either when crossing $\Psi = \frac{\pi}{2}$ or $\Psi = \frac{3\pi}{2}$.

Actually, the space of effective phases –from now on the effective phases plane or EPP– can be used as a nice and general tool for mission design. Some of its applications are presented in the following sections.

3.5   Eclipse avoidance

Usually a technical requirement for libration point satellites is to avoid an exclusion zone. For orbits around L_1 in the Sun–Earth system, the region that has to be avoided is due to the strong electromagnetic influence of the Sun. For orbits around L_2 in the Sun–Earth system sometimes the Earth shadow has to be avoided. In both cases, since the x axis in the adapted reference system goes through the Sun and the Earth, the exclusion zone is set as a disk in the yz plane centred at the origin (as seen in figure 3.2). If the duration of the mission is long enough, the satellite will irremediable cross the exclusion zone when the nominal path follows a Lissajous orbit. The time to enter eclipse depends on the initial point of the Lissajous, as well as the amplitudes, and in the best case the time span between eclipses is about 6 years for an orbit of moderate size (see [62]).

A new eclipse avoidance strategy has been developed, based on the change of phases produced by non escape maneuvers and using single impulses. Strategies with more than one impulse could also be studied but are not the purpose of this work. Actually, one of the nicest things of single impulse strategies is their simplicity together with an affordable cost.

3.5.1   Exclusion zones

We call exclusion zone to the set of points that the satellite should not cross, as they represent the occultation or eclipse points. Assuming that the satellite is on a Lissajous orbit of amplitudes A_x and A_z, the exclusion zone appears in the yz plane as a disk of radius R (see figure 3.2),

$$y^2 + z^2 < R^2.$$

Therefore, introducing the expressions for $y(t)$ and $z(t)$ seen in (3.6), with $A_1 = A_2 = 0$, and using the definition of the effective phases, $\Phi = \omega t + \phi_i$, $\Psi = \nu t + \psi_i$, we have that the border of the disk in the effective phases plane satisfies the equation,

$$\kappa^2 A_x^2 \sin^2 \Phi + A_z^2 \cos^2 \Psi = R^2, \tag{3.26}$$

and are the ellipse like plots represented in figure 3.3.

Of course, it is necessary that the Lissajous orbit is big enough, that is $R < A_y = \kappa A_x$ and $R < A_z$ (otherwise, the orbit will suffer from a continuous eclipse!).

For the sake of simplicity, the EPP will be reduced to $[0, 2\pi] \times [0, 2\pi]$. The values $\Phi = 0$ and $\Phi = 2\pi$ are identified, as well as $\Psi = 0$ and $\Psi = 2\pi$ (i.e. we are using the well known equivalence of phases modulus 2π). Once the amplitudes A_x and A_z are fixed, each couple of phase in the EPP gives complete information of the point they represent in the state space $(x, y, z, \dot{x}, \dot{y}, \dot{z})$. In
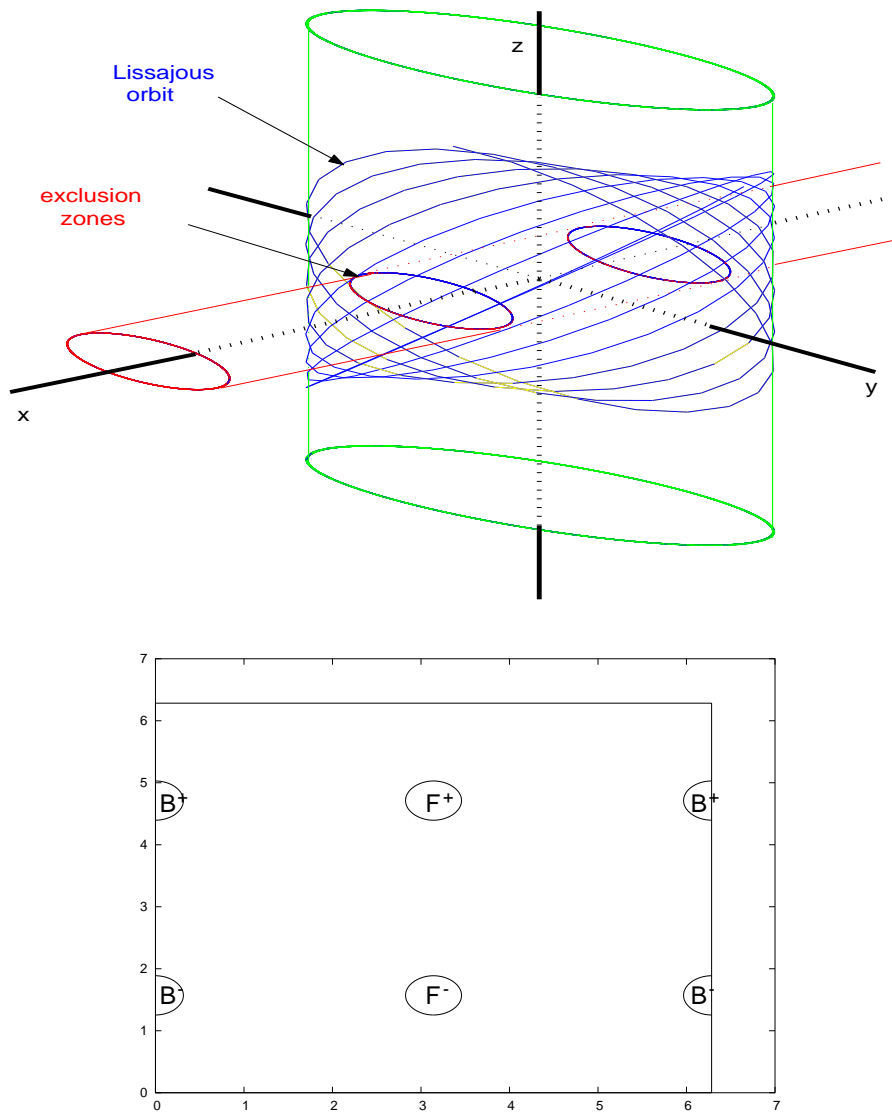
Figure 3.2: 3-D view of the exclusion disks on a real Lissajous orbit (top), and their representation on the EPP (bottom). The exclusion zone crosses the Lissajous, intersecting the orbit in the front (labelled as F in the picture at the bottom) and in the back (labelled as B). Around L_2, the ones marked with F correspond to the one closest to the Earth $(x > 0)$ and the ones with B correspond to the furthest. For the L_1 case, letters F and B must be interchanged.
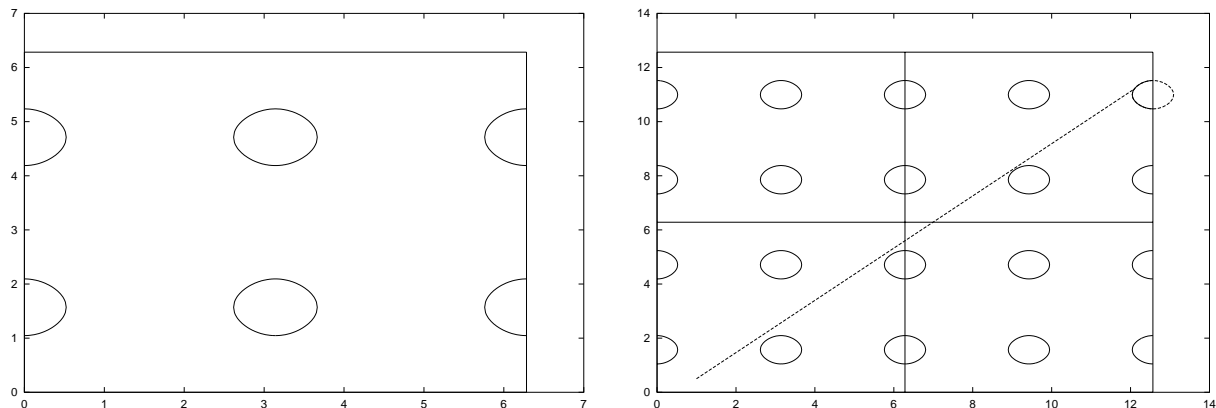
Figure 3.3: Exclusion zone in the effective phases plane (EPP) (left) and Lissajous trajectory hitting an exclusion zone (right). We remark that in the EPP a Lissajous trajectory appears as an straight line which propagates at a constant speed. We will always use the horizontal axis for Φ and the vertical one for Ψ.

	ω	ν	ν/ω	usual R (km)	angle from Earth
L_1	2.08645356	2.01521066	0.9658545	90000	$\simeq 3.5$ deg radius
L_2	2.05701420	1.98507486	0.9650272	14000	$\simeq 0.54$ deg radius

Table 3.1: Values of the frequencies and exclusion zone size for the Sun-Earth+Moon problem.

particular, when the satellite is on a Lissajous orbit, the rectangular regions in which the EPP is divided in figure 3.1 correspond to constant sign of local coordinates. More precisely, $z > 0$ in regions A,B,C,D, $y > 0$ in regions C,D,G,H and $x > 0$ in regions A,D,E,H. Consequently, the exclusion zones that lay in the middle of the EPP (near $\Phi = \pi$) represent the exclusion zone in the Lissajous orbit that is closer to the Earth, while the ones that are splitted in $\Phi = 0$ and $\Phi = 2\pi$ represent the exclusion zone in the part of the Lissajous which is further away from the Earth. Moreover, for Lissajous around L_1 closer to the Earth means further away from the Sun. Therefore, in this case, the exclusion zones that we see in the middle of the EPP lay in the back part of the Lissajous with respect to the Sun. On the contrary, for Lissajous around L_2, the exclusion zone in the middle of the EPP is at the front part of the Lissajous with respect to the Sun (see figure 3.2).

When the Lissajous trajectory cuts one of the ellipse like curves in the EPP, it means that the satellite is entering the exclusion zone. In this way, note that the computation of the time at which the eclipse will occur is reduced to looking for the intersection between the straight line representing the Lissajous and the first exclusion zone it hits (see the picture on the right in figure 3.3). Moreover, from values in table 3.1 we see that ν/ω is slightly less than 1 in both cases, for L_1 and for L_2. This means that trajectories which are tangential to an exclusion zone at its upper points collide with another exclusion zone in a short time. On the other hand, initial conditions represented by the lower tangential points are the best ones in terms of maximising the time without eclipse, with more than 6 years from departure to collision. In figure 3.4, the

time to the first eclipse is represented for each couple of initial phases, given the values of the amplitudes. It is clear from the pictures that lower tangential trajectories (represented in yellow) are the ones that provide a longest free of eclipse period.
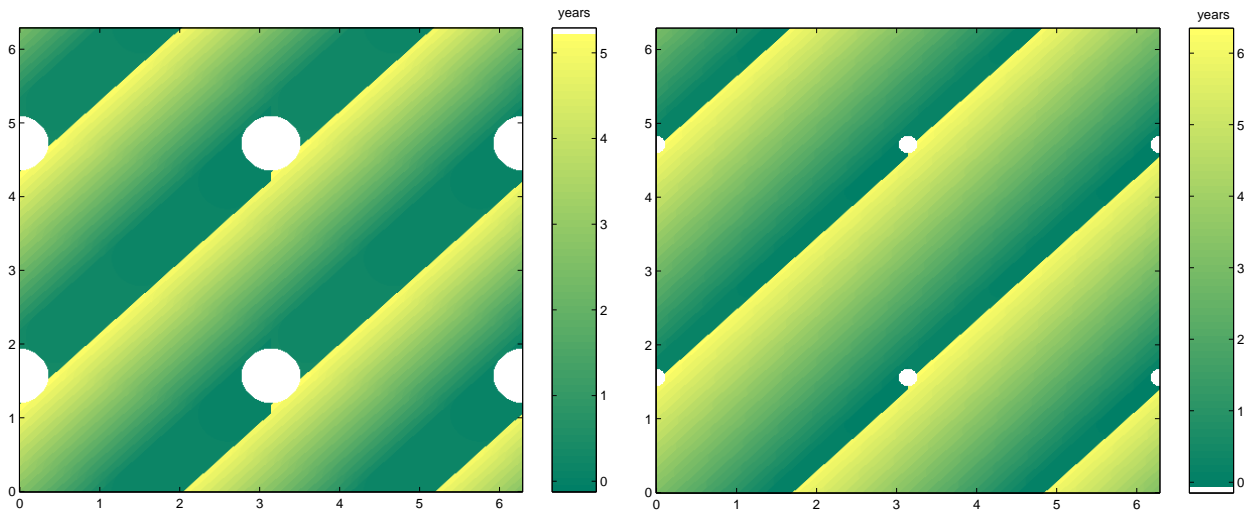
Figure 3.4: Initial phases classification according to the time when they first hit an exclusion zone. (left) L_1 case $A_y = A_z = 250000$ km, $R = 90000$ km. (right) L_2 case $A_y = A_z = 120000$ km, $R = 14000$ km.

In most of our discussion we will consider square Lissajous. This is, $A_y = A_z$ and this value will be denoted by A. In this case, the border of the exclusion zones in the EPP is given by $\sin^2 \Phi + \cos^2 \Psi = (R/A)^2$, meaning that the time without eclipse depends only on the relative size R/A of the exclusion zones. Consequently, missions with different amplitudes and different exclusion zone radius can have identical representations in the EPP if the relative size R/A is the same. This fact allows us to compute the maximum time for a mission without hitting an exclusion zone as a function only of R/A which will be considered in percentage. It is just a matter of computing the intersection time of the orbits starting at the lower tangential conditions. For all orbits and exclusion zones of moderate size, that is R/A less than 30%, the results are about 6 years and are represented in figure 3.5.

The main idea of our strategy is to perform a maneuver at an appropriate time before the satellite enters the exclusion zone, so that it returns tangentially to the exclusion zone instead of crossing it.

3.5.2   Eclipse avoidance strategy

We have seen that if we want to minimise the time without eclipse after the maneuvers, we have to use the lower tangential points or, more specifically, lower tangential trajectories as target points in our eclipse avoidance strategy. Let us explain how to reach these trajectories by means of non escape maneuvers and using the EPP.

Figure 3.5: Maximum time without entering an exclusion zone for square Lissajous as a function of the relative size of the exclusion zone R/A in percentage. Lissajous around L_1 (left), around L_2, (right).
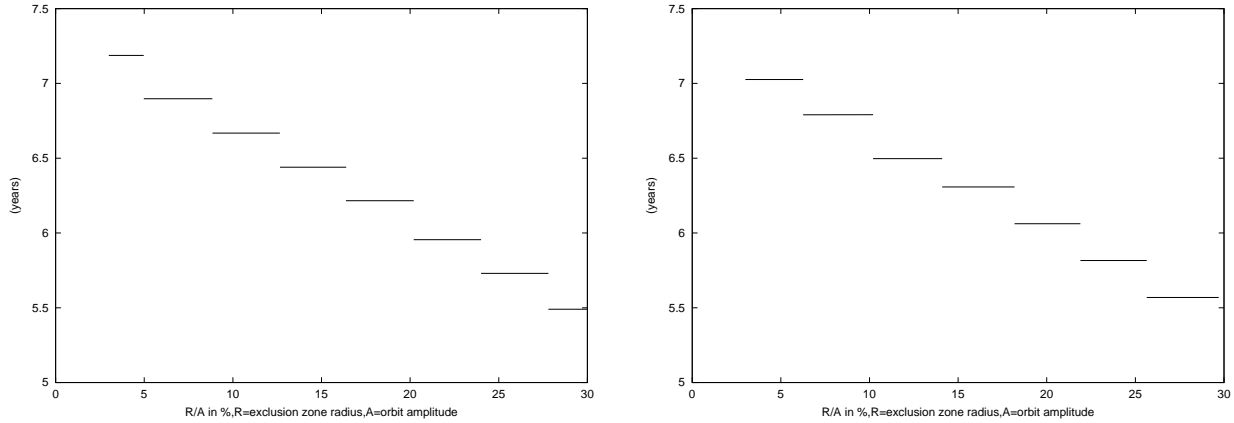
Non escape maneuvers in the EPP

Remember that maneuvers in the xy plane change the in plane phase Φ, while z-maneuvers change the out of plane phase, Ψ. When a collision with an exclusion zone occurs, the distance from the current colliding trajectory to the one being tangential to the lower part of the exclusion zone can be easily computed using the EPP. Then, the lower tangential trajectory can be reached either by using in plane or out of plane maneuvers. If xy maneuvers are used, we have to measure the distance between the trajectories horizontally, in the Φ axis of the EPP. Respectively, if z maneuvers are performed, the distance is measured vertically (in the Ψ axis).

Let $\Delta\phi$ be the jump we want to do in the ϕ direction. Equation (3.18) shows which are moments t_m that provide this change of phases. However, as the relation represented in the aforementioned equation is a congruence, there are multiple possibilities for t_m. In this work, we use t_m such that

$$\phi_i < \phi_i + \Delta\phi(t_m) < \phi_i + 2\pi. \tag{3.27}$$

On the other hand, the change of phases that is needed in the Ψ direction, $\Delta\Psi$, is computed by measuring the distance from the colliding trajectory to a trajectory that is tangential to the lowest point of the same exclusion zone with which the collision occurs. Therefore, $\Delta\psi$ is seen in the EPP as a negative jump leading to a lower value of Ψ. The time t_m yields from 3.24. In this way, the final effect on the Lissajous orbit is the same as the one obtained with xy-maneuvers (see figure 3.6). Moreover, maneuvers in the z direction are seen in the EPP as a jump which is either symmetrical with respect to the line $\Psi = \pi$ or with respect to $\Psi = 0$ (equivalently $\Psi = 2\pi$).

There is something to be taken into account concerning xy-maneuvers. Maneuvers of the type 3.8 produce a transfer from the central part of a Lissajous orbit to the stable manifold of another one, but not exactly to the central part of the other one. There is a short time span after a maneuver when the trajectory has stable hyperbolic exponentially decreasing terms, which lead to little deviations from the central Lissajous. These little deviations also result in the effective phases plane no longer being a biunivocal representation for the satellite trajectory. Let A_2 be the coefficient for these terms. For a biunivocal correspondence, we should somehow draw a 3D
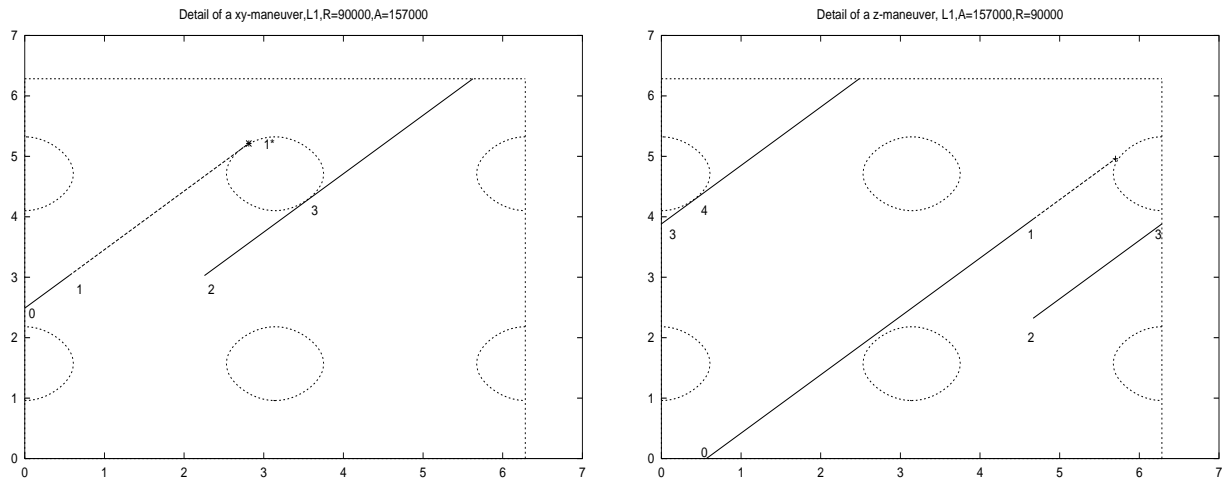
Figure 3.6: (left)Detail of a Φ-change maneuver. (right) Detail of a Ψ-change maneuver. The initial conditions correspond to the point 0 and the jump occurs from 1 to 2. Both maneuvers lead to the same lower tangential trajectory.

picture $(\phi, \psi, A_2 e^{-\lambda t})$ whose xy-section $(\phi, \psi, 0)$ corresponds to the part of the trajectory truly contained in the central part of a Lissajous orbit. These exponentially decreasing terms vanish long before we intersect a new exclusion zone. Thus, they are not important for our maneuver performance, but we have to bear them in mind for a correct approach to the linear problem as well as when representing trajectories on the Lissajous, that always have to be continuous in position coordinates. There could exist rare exceptions in which even if the trajectory in the EPP looked tangent to the exclusion zone, the satellite still had some stable manifold component producing a deviation with respect to the represented coordinates in the wrong direction and it really crossed the exclusion zone. These exceptions can be easily avoided by considering the exclusion zone slightly bigger than what is strictly necessary. In all the examples and simulations performed during the present work, there has been no need for the enlargement of the exclusion zone. Apart from this remark, in a similar way as the z-maneuvers, the xy-maneuvers appear as jumps symmetrical with respect to $\Phi = \beta$ or with respect to $\Phi = \pi + \beta$. Both types of maneuvers are computed by implementing an easy algorithm to find the suitable t_m, which using (3.18) or (3.24) obtains the required $\Delta\Phi = \phi_f - \phi_i$ or $\Delta\Psi = \psi_f - \psi_i$.

See figure 3.6 to better understand the computation of the $\Delta\phi$ and $\Delta\psi$, as well as the effect of the maneuvers on the EPP trajectory.

The tangent to tangent cycle

Our strategy for eclipse avoidance consists of choosing a pair of initial phases, following the trajectory until it is about to collide with an exclusion zone and performing a maneuver which will resettle the satellite in another trajectory, tangential to the exclusion zone.

Therefore, the steps that have to be followed are:

1. Take $(\Phi_i, \Psi_i) \in [0, 2\pi] \times [0, 2\pi]$, initial phases in the EPP, and set $t = 0$. These are the

injection phases and represent an injection point for the satellite in the Lissajous orbit. As time increases, the satellite will inevitably approach the exclusion zone and intersect it at time t_c and phases (Φ_c, Ψ_c).

2. We look for a maneuver time t_m, previous to collision $(t_m < t_c)$, such that:

   - $(\Phi(t_m) + \Delta\phi(t_m), \Psi(t_m)) = (\Phi_m^f, \Psi_m^f) \in$ LTT, if we use in plane maneuvers.
   - $(\Phi(t_m), \Psi(t_m) + \Delta\psi(t_m)) = (\Phi_m^f, \Psi_m^f) \in$ LTT, if we use out of plane maneuvers.

   LLT stands for lower tangential trajectory, which is a line in the EPP containing lower tangential phases on the border of the exclusion zone, (ϕ_{tg}, ψ_{tg}). $(\Phi(t), \Psi(t))$ are the effective phases at time t. $\Delta\phi(t)$ (respectively $\Delta\psi(t)$) represents the maneuver in the xy (respectively z) direction) at time t. After the maneuver, we set $(\Phi_i, \Psi_i) = (\Phi_m^f, \Psi_m^f)$ and $t = 0$.

3. Once we have found t_m and the maneuver has been executed, the satellite is in a tangential trajectory. This trajectory just has to be followed until a new collision occurs. Then, we proceed as in 2 and we find the suitable t_m at which a maneuver will place the satellite in a new lower tangential trajectory.

To sum up, the time to next collision is computed after each maneuver, as well as the change in the in plane or out of plane phases that is needed to avoid this collision while jumping to a lower tangential trajectory. Once the jump is computed, the moment t_m at which it has to be performed can be deduced from equations (3.18) and (3.24). After the maneuver, the satellite enjoys the longest possible period without eclipse. Nevertheless, other collisions occur, and the avoidance maneuvers are repeated when necessary, always leading to lower tangential trajectories. This is the reason for the name of the strategy: tangent to tangent cycle.

We define a cycle as the part of trajectory in the EPP comprised between two lower tangencies and having a maneuver in between. There is a technical remark to be made about closing a cycle: several slightly different patterns in the xyz representation of the trajectory can appear. This is due to the fact that the exclusion zones displayed in the EPP have different meanings (see figure 3.2). Let us assume that the cycle begins with a tangency to the exclusion zone F^+ (the exclusion zone closer to the Earth), next tangency closing the cycle in the EPP can only happen either with F^- (again the exclusion zone closer to the Earth), or with B^+ (the exclusion zone farther from Earth). In general, a cycle goes from $F^{+,-}$ (respectively from $B^{+,-}$) to $F^{-,+}$ or to $B^{+,-}$ (respectively to $B^{-,+}$ or to $F^{+,-}$). If the cycle ends with the same letter as it started (i.e. from F to F or from B to B) we say that the cycle is one-sided, otherwise we say that is two-sided. Moreover, for both cases two cycles are needed to repeat the same starting position and velocity (and so the same pattern in the xyz-coordinates), but since both maneuvers of these cycles have the same magnitude and the time span between them is the same, it is not necessary to make such distinctions for the total amount of delta-v expended and for the results we present. A given Lissajous is associated to a one sided or to a two-sided cycle depending on the size of R/A, i.e. the size of the exclusion zone in the EPP. Figures 3.7 and 3.8 give some examples of maneuvers associated to one-sided or two-sided cycles. Note that for one-sided cycles the projection of the maneuvers in the xy plane is always the same.

Figure 3.7: Examples of one-sided cycles. Top two rows, trajectories around L_1 with $A = 157000$ km, $R = 90000$ km. Bottom two rows, trajectories around L_2 with $A = 120000$ km, R=14000 km. xy-maneuvers are used in rows 1,3 and z maneuvers in rows 2 and 4. From left to right displaying the xy, yz and xz projections. The maneuvers are marked with a small box.
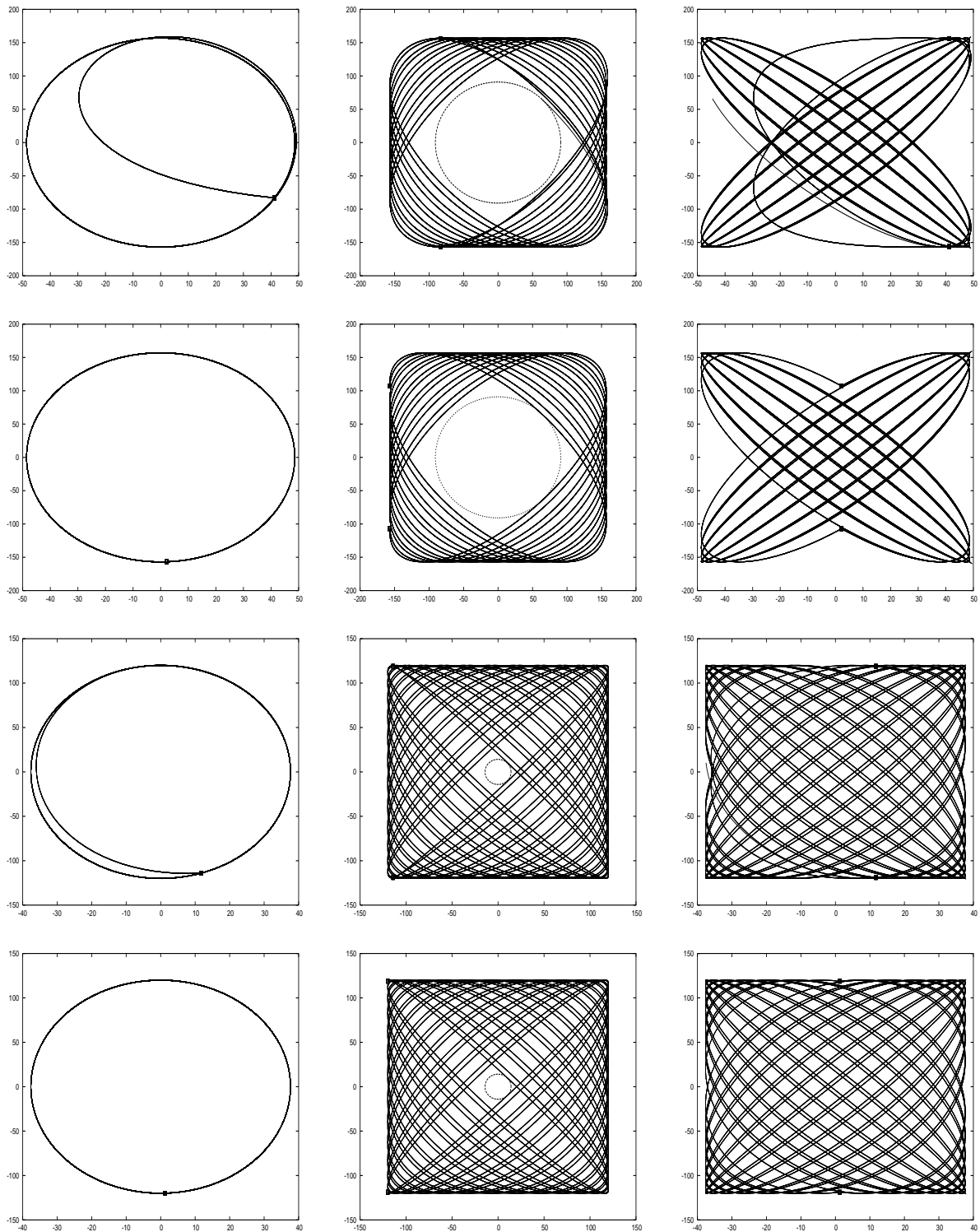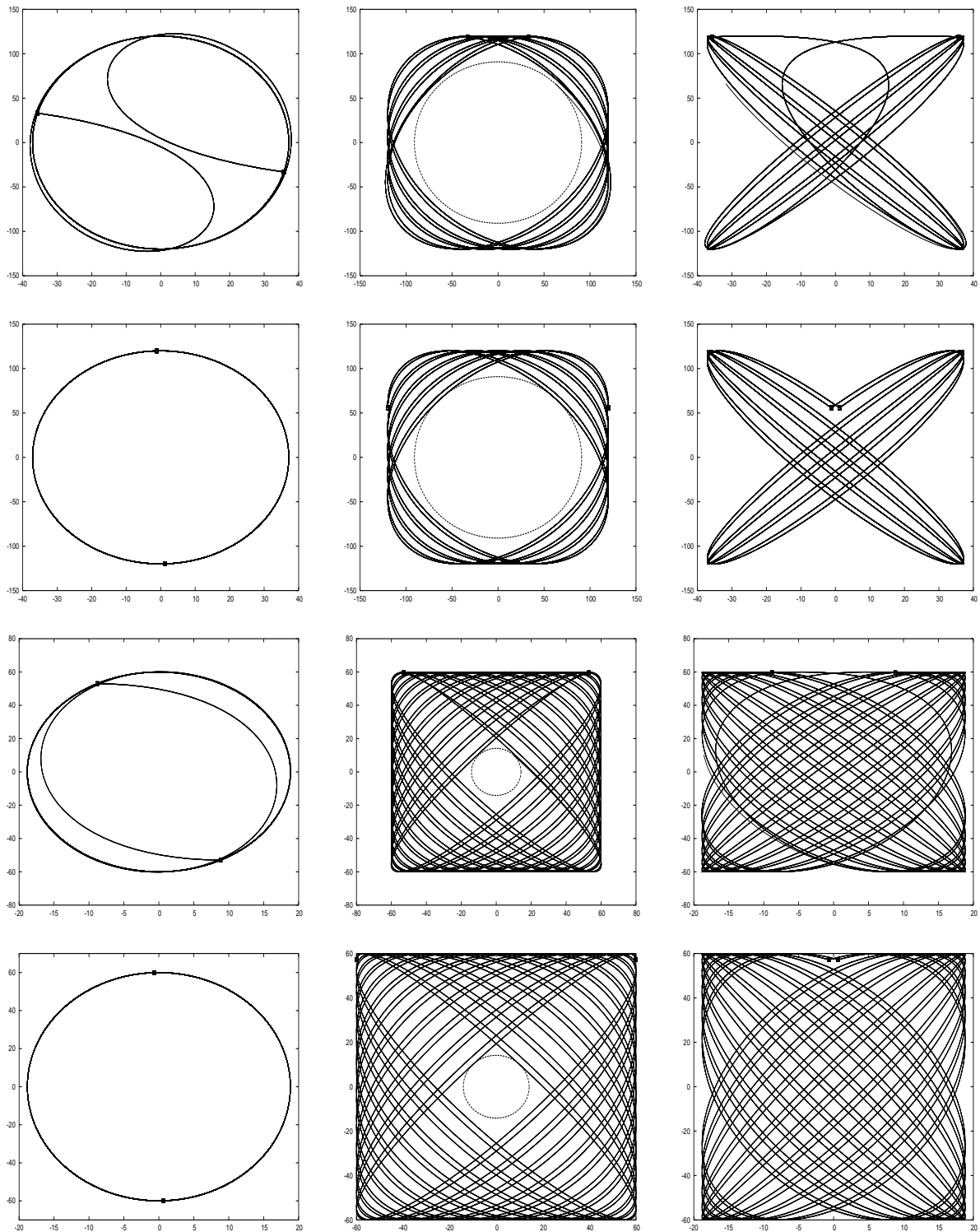
Figure 3.8: Examples of two-sided cycles. Top two rows, trajectories around L_1 with $A = 120000$ km, $R = 90000$ km. Bottom two rows, trajectories around L_2 with $A = 60000$ km, R=14000 km. xy-maneuvers are used in rows 1,3 and z maneuvers in rows 2 and 4. From left to right displaying the xy, yz and xz projections. The maneuvers are marked with a small box.

3.5.3 Results

All Lissajous orbits considered have amplitude $A = A_y = A_z$ (so-called square Lissajous). Qualitatively, the results depend only on the relative amplitude R/A. However, in terms of real cost, they also depend on A. The main result is that the xy-strategy is proportionally a little cheaper for orbits of relative size R/A less than 60%. When R/A is bigger than 60% then the z-strategy is cheaper than the xy-strategy (see figure 3.9).
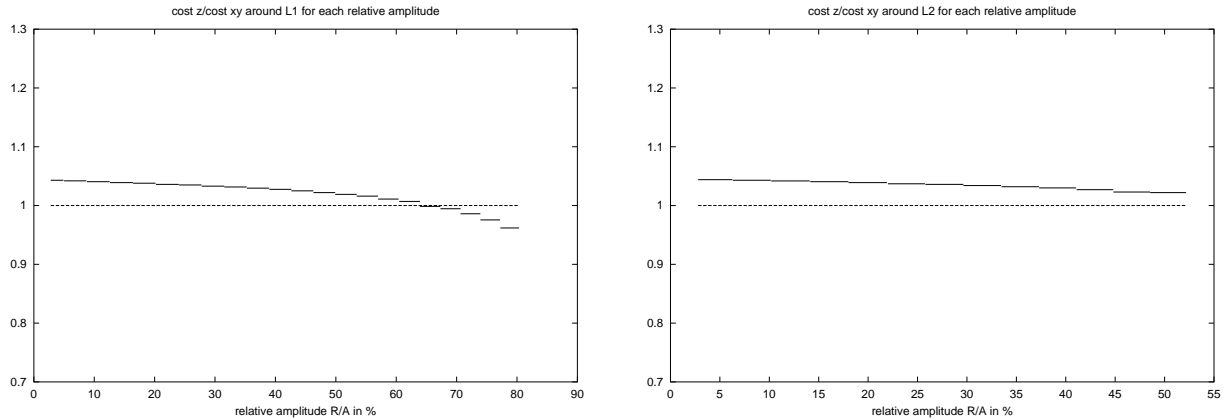
Figure 3.9: Relative cost of performing maneuvers in xy or in z, $\frac{cost_z}{cost_{xy}}$, around L_1 (left) and around L_2 (right)

Once we have fixed A and R we can apply the strategy to an arbitrary (ϕ_i, ψ_i). What we obtain is that after an adjusting initial maneuver, from the actual trajectory to a lower tangential trajectory, the satellite enters a tangent to tangent cycle of fixed period and cost per year, no matter which the initial phases are. Note that this first maneuver is different from all the others, because starting at the second maneuver, all of them jump from one lower tangential trajectory to another one. So the only thing that makes a difference in cost between a set of initial phases and another one is the cost of the first maneuver. Figure 3.10 shows the different costs of this first adjusting maneuver and the time for the second maneuver (i.e. the time at which the tangent to tangent cycle starts) for each pair of injection phases and a fixed relative amplitude, $A_R = 30\%$.

Concerning the actual costs for the eclipse avoidance strategy, these can be seen in table 3.2 for the L_1 case and in table 3.3 for the L_2 case.

Comments on the dependence of the cost on the amplitude of the Lissajous orbits.

Fixing the exclusion zone to $R = 90000$ km for the case of L_1 and to $R = 14000$ km for the case of L_2 we obtain the figures of the average cost per year with respect to the relative amplitude, shown in figure 3.11, using tables 3.2 and 3.3. It can be observed from these figures that results are essentially piecewise inversely proportional to the relative amplitude. We can clearly distinguish groups of relative amplitudes for which the proportionality constant of the cost, as well as the time without eclipse after the maneuver are the same. Each of these groups corresponds to a row in the aforementioned tables, and is represented by the corresponding segment in the figures.

R/A (%)		ACY= $K_* \times A$ (cm/s)		TWE (years)		MC= $M_* \times A$ (cm/s)	
From	To	K_{xy}	K_z	xy	z	M_{xy}	M_z
77.25	80.35	39.571	38.063	1.737	1.917	68.727	72.972
73.95	77.20	33.785	32.955	1.985	2.157	67.059	71.077
70.66	73.94	29.191	28.784	2.233	2.396	65.184	68.978
67.32	70.65	25.435	25.295	2.481	2.636	63.108	66.680
63.92	67.31	22.291	22.322	2.729	2.876	60.838	64.191
60.50	63.92	19.608	19.746	2.977	3.115	58.379	61.517
57.00	60.45	17.282	17.486	3.225	3.355	55.741	58.666
53.46	56.99	15.238	15.480	3.473	3.595	52.932	55.647
49.90	53.45	13.425	13.684	3.722	3.834	49.958	52.467
46.30	49.89	11.797	12.061	3.970	4.074	46.831	49.136
42.65	46.28	10.327	10.586	4.218	4.313	43.560	45.665
39.00	42.64	8.991	9.238	4.466	4.553	40.154	42.061
35.30	38.96	7.769	7.999	4.714	4.793	36.624	38.337
31.54	35.25	6.646	6.856	4.962	5.032	32.982	34.502
27.80	31.53	5.611	5.798	5.210	5.272	29.238	30.569
24.05	27.75	4.654	4.816	5.458	5.512	25.403	26.547
20.20	24.00	3.766	3.903	5.706	5.751	21.491	22.450
16.41	20.15	2.941	3.052	5.955	5.991	17.512	18.287
12.60	16.40	2.173	2.258	6.202	6.231	13.479	14.072
8.80	12.55	1.458	1.517	6.451	6.470	9.405	9.816
5.00	8.77	0.791	0.824	6.699	6.710	5.301	5.533
2.80	4.93	0.170	0.177	6.947	6.949	2.363	1.233

Table 3.2: Summary of results for avoiding the exclusion zone around L_1 using xy or z maneuvers. ACY= $K_* \times A$ is the average cost per year (the coefficients that appear in the table have to be multiplied by the amplitude of the Lissajous in thousands of km, and the cost per year is obtained in cm/s). TWE is the time without eclipse after each maneuver and MC= $M_* \times A$ is the cost of each maneuver in the cycle (as in the average cost per year, the coefficients have to be multiplied by the amplitude in thousands of km in order to obtain the cost in cm/s).
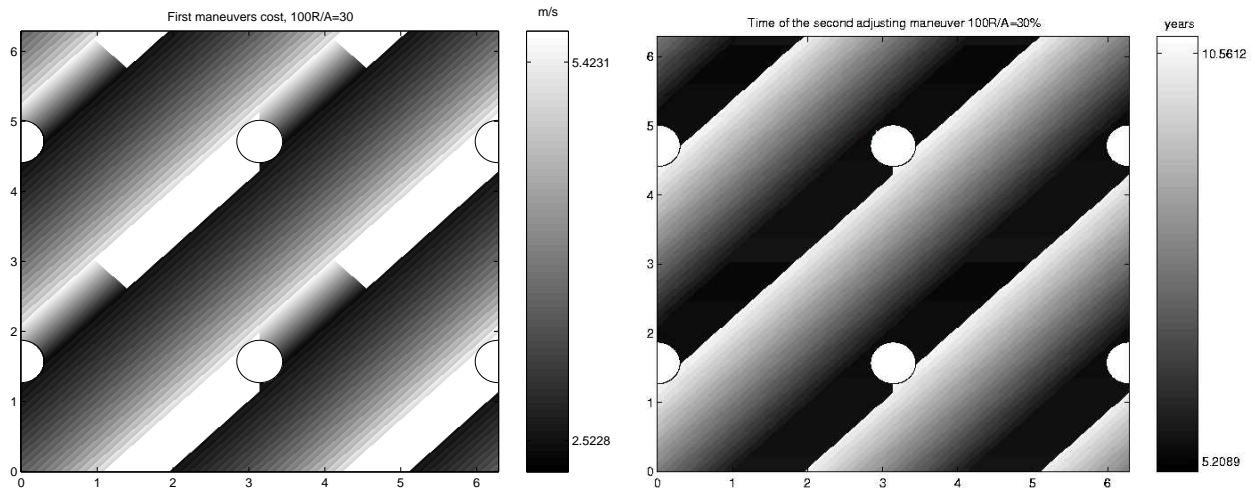
Figure 3.10: (left) First adjusting maneuvers cost representation (m/s per year). These maneuvers take the satellite from the initial trajectory to the first lower tangential trajectory. Note that the darkest zones (the cheapest) are the lower tangential trajectories, as they provide the longest time with no need for maneuvers. (right) Time when the tangent to tangent cycle starts depending on the initial phases, which represent the t=0 conditions (years) The darkest zones need eclipse avoidance maneuvers soon, as they represent upper tangential trajectories.

R/A (%)		ACY= $K_* \times A$ (cm/s)		TWE (years)		MC= $M_* \times A$ (cm/s)	
From	To	K_{xy}	K_z	xy	z	M_{xy}	M_z
48.53	52.18	12.688	12.966	3.778	3.889	47.939	50.428
44.81	48.52	11.099	11.376	4.030	4.132	44.732	47.009
41.10	44.80	9.664	9.931	4.282	4.375	41.380	43.449
37.30	41.05	8.358	8.609	4.534	4.618	37.894	39.758
33.50	37.28	7.164	7.394	4.786	4.861	34.286	35.947
29.65	33.45	6.067	6.274	5.037	5.104	30.566	32.027
25.80	29.64	5.056	5.260	5.289	5.347	26.747	28.021
22.00	25.75	4.122	4.276	5.541	5.591	22.842	23.905
18.02	21.90	3.256	3.380	5.793	5.834	18.862	19.717
14.15	18.00	2.452	2.551	6.045	6.077	14.821	15.504
10.20	14.10	1.704	1.776	6.297	6.320	10.733	11.224
6.30	10.15	1.009	1.053	6.549	6.563	6.610	6.910
2.80	6.26	0.362	0.379	6.801	6.806	2.465	2.577

Table 3.3: Summary of results for avoiding the exclusion zone for L_2 case, using xy or z maneuvers. Same comments as in table 3.2 apply here.

Figure 3.11: Average cost in m/s per year with respect to the amplitude for a fixed exclusion zone. (top) around L_1 of $R = 90000$ km. (right) around L_2 of $R = 14000$ km.
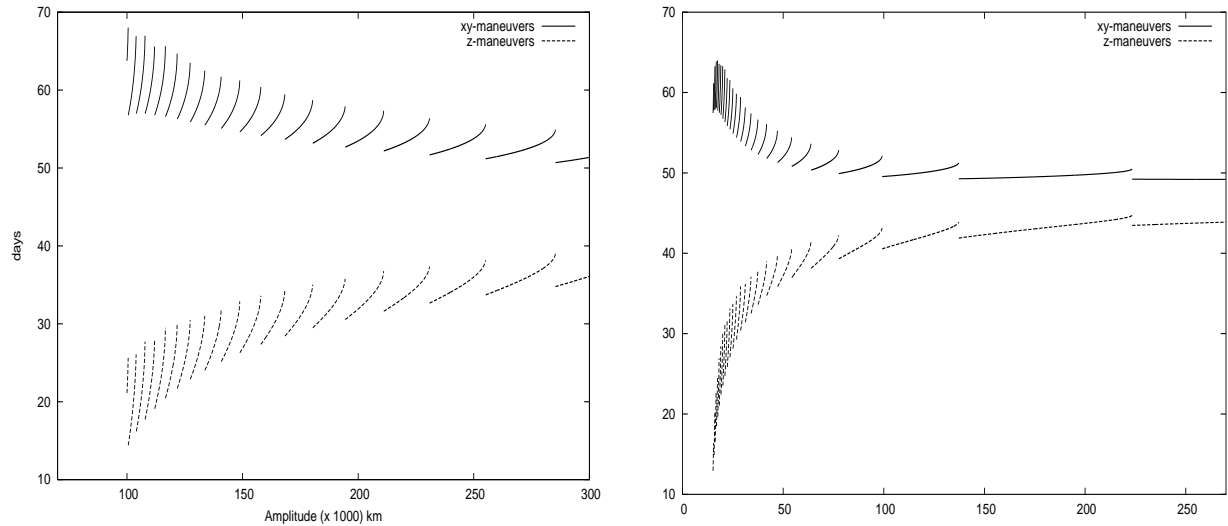
Figure 3.12: Days before collision with the exclusion zone at which a xy or z-maneuver has to be performed in order to avoid it, with respect to the amplitude of 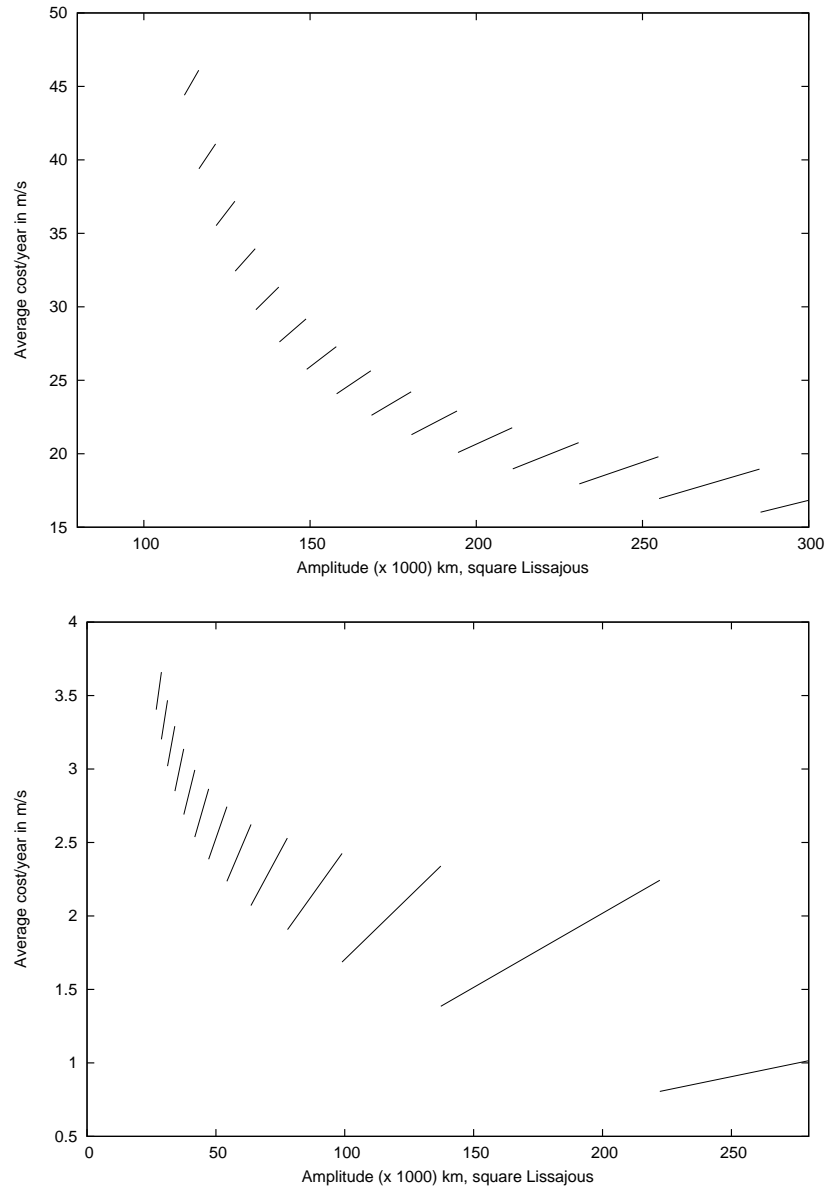the Lissajous. (left) Orbits around L_1 and exclusion zone of $R = 90000$ km. (right) Orbits around L_2 and exclusion zone of $R = 14000$ km.

Firstly, let us point out the reason for the existence of these separate groups of amplitudes. Afterwards, the behaviour of the cost inside each of the groups will be explained.

Going back to the effective phases plane representation, there is a fixed vertical ($\Delta\psi^*$) and horizontal ($\Delta\phi^*$) distance between any pair of consecutive straight lines representing a trajectory on a given Lissajous. This distance depends on the slope of the straight lines (ν/ω) and can be easily computed keeping in mind that the phases $\Phi = 0$ and $\Phi = 2\pi$ are identified, and the same for Ψ. Therefore,

$$\Delta\phi^* = 2\pi(\frac{\omega}{\nu} - 1)$$
$$\Delta\psi^* = 2\pi(1 - \frac{\nu}{\omega}) \tag{3.28}$$

If no maneuvers were ever executed, the trajectory would densely cover the torus defined by the amplitudes of the Lissajous as time tended to infinity. So the effective phases plane would also be densely covered. This fact changes when maneuvers are performed. In addition, as the maneuvers we plan make the satellite enter a cycle, only some revolutions of the Lissajous are followed. Consequently, the effective phases plane representation will only contain some straight lines, repeated cycle after cycle. We can say that the angular distance in Φ between a point of the cycle and the same point when the cycle crosses it again at a future moment in time is 2π. As we consider 2-maneuver cycles, there must exist a positive integer n for which the following identity holds:

$$2\pi = n\Delta\phi^* + \Delta\phi_1 + \Delta\phi_2 \tag{3.29}$$

where $\Delta\phi_1$ and $\Delta\phi_2$ represent the changes in the in plane phase caused by the eclipse avoidance maneuvers in a cycle. It is also satisfied in our strategy that $\Delta\phi_1 = \Delta\phi_2$. So equation (3.29) becomes,

$$2\pi = n\Delta\phi^* + 2\Delta\phi \qquad (3.30)$$

A similar deduction can be done for the Ψ case. Therefore, we have that the jumps in the EPP caused by the tangent to tangent cycle maneuvers are,

$$\Delta\phi = \pi \; + n\frac{\Delta\phi^*}{2}$$
$$\Delta\psi = \pi \; + m\frac{\Delta\psi^*}{2} \qquad (3.31)$$

with $n, \; m \in \mathbb{Z}$.

That is to say that the aforementioned jumps in the phases necessarily belong to the following sets,

$$\{\Delta\phi_n\}_{n\in Z} = \left\{ \frac{2\pi - n\Delta\phi^*}{2} \right\}_{n\in Z}$$
$$\{\Delta\psi_n\}_{n\in Z} = \left\{ \frac{2\pi - n\Delta\psi^*}{2} \right\}_{n\in Z} \qquad (3.32)$$

Furthermore, once the radius of the exclusion zone is fixed and we study the effective phases plane representation of a Lissajous trajectory, the greater the amplitude of the Lissajous we choose, the smaller the exclusion zone will seem. On the contrary, the smaller the real amplitude of the Lissajous, the greater the relative amplitude of the exclusion zones. For a given relative amplitude, there exists a n^* which satisfies that $\forall n < n^*$ the $\Delta\phi_n$ from equation (3.32) is large enough to make the satellite avoid the exclusion zone when a collision occurs. Obviously, we always use the smaller $\Delta\phi_n$ possible, that is the one associated with n^* is. However, if A_R is increased, a relative amplitude $A_R^* > A_R$ will be reached for which a greater jump will be necessary if we want to avoid the exclusion zones. Even though the variation in A_R can be done in a continuous way, we have proved that the jumps belong to a discreet set. Therefore, for $A_R^* - \epsilon$ the n^* jump may be enough, while for A_R^*, the jump associated to $n^* - 1$ will have to be used. Consequently, the fact that results shown in figure 3.11 are piecewise linear is explained by intrinsic properties of the set of possible jumps that lead to tangent to tangent cycles: each jump in the effective phases is valid for a range of relative amplitudes. As jumps belong to a discrete set, relative amplitudes are divided in groups for which a particular jump in the discrete set is valid.

On the other hand, there is something more that has to be explained concerning the average cost per year with respect to the relative amplitudes. In each group of amplitudes, the greater the A_R the cheaper the maneuvers. In order to understand this, take for instance A_{R_1} and A_{R_2} belonging to different groups, with $A_{R_1} < A_{R_2}$ and $|A_{R_1} - A_{R_2}| \ll 1$ (for example, near the critic value which separates two consecutive groups). Intuitively, we don't need to jump much more in an orbit of relative amplitude A_{R_2} than of A_{R_1} because the exclusion zones are almost of the

same relative size. However, as we have just explained, when a jump $\Delta\phi_n$ is no longer enough to avoid eclipse, jump $\Delta\phi_{n-1}$, which differs from $\Delta\phi_n$ in $\frac{\Delta\phi^*}{2}$, has to be used. For A_{R_2}, $\Delta\phi_{n-1}$ is much bigger than necessary, and therefore more expensive. On the contrary, $\Delta\phi_n$ is still enough for A_{R_1}. In general, the smallest relative amplitude of each of the groups needs maneuvers which are relatively too big for them. That is to say that a smaller jump would suffice to avoid eclipses, but not to enter a tangent to tangent cycle. Therefore, the bigger the amplitude in each of the groups, the better the jump fits the requirements and, in turn, the cheaper the strategy becomes.

3.5.4   Comments on eclipse avoidance for non-square Lissajous

When $A_y \neq A_z$, we say that the Lissajous is non-square. As a result, the exclusion zones are no longer similar to disks in the effective phases plane, but to ellipses. If A_y is greater than A_z the horizontal diameter of these disks is shorter than the vertical one, and therefore maneuvers to change the in plane phases are intuitively cheaper than the ones changing the out of plane phase. Actually, differences in the cost of executing xy-maneuvers or z-maneuvers become more significant as the difference between the two amplitudes increases. We can assert this hypothesis by applying our strategy to non-square Lissajous. Furthermore, if $A_z = \kappa A_y$ the relation between costs can be written:

$$\text{cost}_z \simeq \Upsilon\kappa \times \text{cost}_{xy} \tag{3.33}$$

where $\Upsilon \in [0.99, 1.04]$ is approximately 1. Thus when amplitudes are similar, that is $\kappa \simeq 1$, it doesn't really matter which kind of maneuvers to execute (see again figure 3.9). If for example κ is less than 1, we use z-maneuvers.
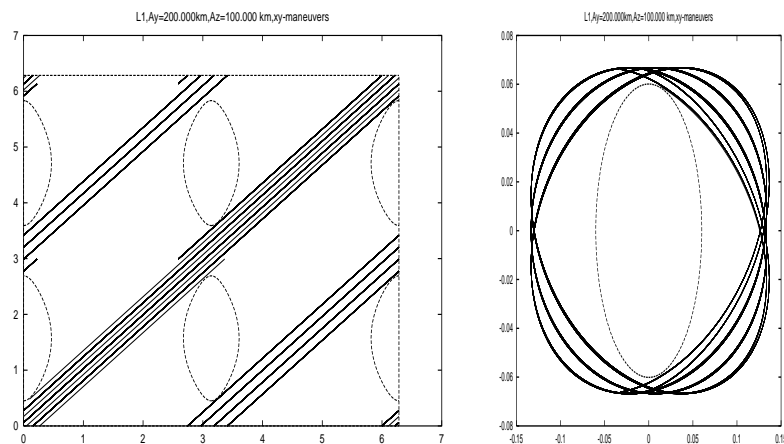
Figure 3.13: (left) Phases plane representation of a non-square Lissajous around L_1, $\kappa = 0.5$, $A_y = 200 \times 10^3$ km. Exclusion zone with a radius of 3 degrees. (right) yz-projection of the trajectory and exclusion zone.

For non-square Lissajous, the satellite also enters a cyclic trajectory, as in the case $A_y = A_z$. The time without eclipse after each maneuver coincides with the time without eclipse of one of the groups in tables 3.2 and 3.3 for xy or z maneuvers, depending on which type of maneuvers we use. This coincidence in the time without eclipse gives us the key to compute the cost of the

strategy, as it selects the group to which the current tangent to tangent cycle belongs. Then, we use the amplitude corresponding to the direction in which we are performing the maneuvers, together with the coefficient for the cost of the selected group in order to estimate the average cost per year of the strategy. In this way, there is no need to compute new tables for non-square Lissajous if we want to obtain good estimations of the cost.

3.5.5   Alternatives for short term spatial missions

The first thing to be taken into account concerning spatial missions with a short life time, for instance that last for less than 10 years, is that choosing good injection phases can lead to not having to perform any eclipse avoidance maneuver. For example, if we are interested in maintaining a satellite around L_1 avoiding the exclusion zone for about 4 or 5 years, we can study the regions in figure 3.4 for which the first collision occurs more than 5 years after the injection.

However, if for some reason this ideal phases can't be reached, or the mission is longer than the maximum possible time without eclipse, at least one maneuver to avoid the exclusion zone is required. Let us shortly present some ideas on how to choose the time for this maneuver in an efficient way.

The criterion of aiming at a lower tangential trajectory than we have developed in the previous sections is good for long term missions. It results in a low average cost per year, provides an easy way of maintaining the satellite in a cycle and maximises the time without eclipse. Nevertheless, it may not be the optimal strategy (in cost) amongst those that provide enough time without eclipse for a short mission.

On the contrary, a natural way of choosing the maneuver time, t_m, for short missions would be to find a balance between the time without eclipse and the cost of non escape maneuvers. Consider a time interval before the predicted collision time, say a year, and for each t in this interval compute:

- Cost of the non escape maneuver performed at time t, to change the in plane or the out of plane phase.

- Time until next collision if the change of phase maneuver is performed at time t. We note this time by $\tau(t)$.

If we select the moments t such that $t + \tau(t)$ is bigger than the actual mission lifetime, this problem becomes a one dimensional optimisation problem: among the suitable moments for the maneuver (in terms of time without eclipse) we select the one at which the phase change maneuver is the cheapest.

For example, let us consider a mission on a trajectory around L_2 with A=120000 km and R=14000 km, which needs 10 years without eclipse and whose injection phases are an almost exact lower tangential point. For these conditions, the first eclipse will take place 6.3 years after the injection. Therefore, we study the interval of time from 5.3 to 6.3 years, setting $t = 0$ at the injection point. The costs and next collision times for each $t \in$[5.3,6.3] are represented in figure 3.14. In this case we need that,

$$t + \tau(t) \geq 10 \text{(years)}.$$

So the suitable times and costs are those represented in the picture on the right of figure 3.14 and one of the cheapest can be selected as the maneuver time.
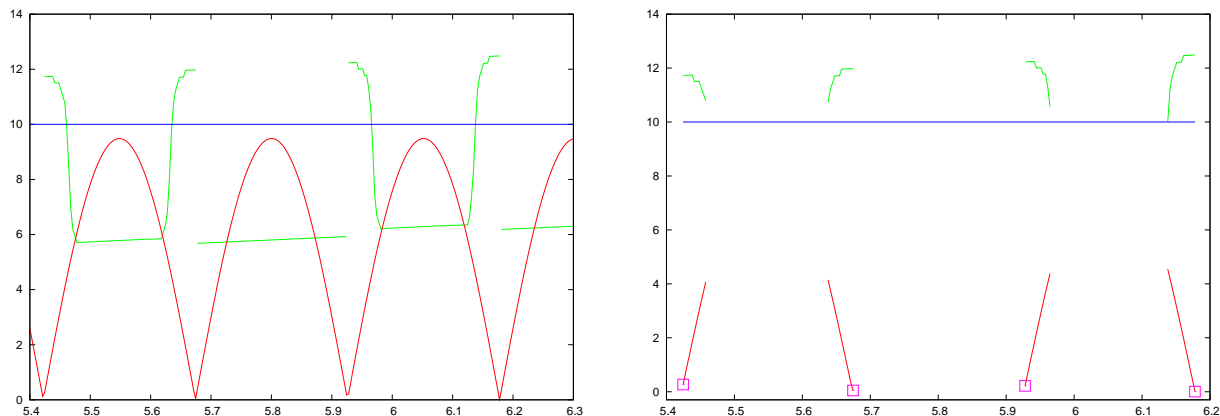

Figure 3.14: (left) x axis: Interval of possible maneuvering times before eclipse. The red curve represents the cost in m/s of the non-scape maneuver in the z direction at each moment of time. Besides, the green curve is the representation of the total time from injection ($t = 0$) to first collision with an exclusion zone, if a non-scape maneuver was performed at each moment t (i.e. $t + \tau(t)$). The horizontal line at $t = 10$ years shows which maneuvering times provide a time span which is long enough for the mission to be completed. (right) Same as the picture on the left, but containing only the times for the maneuvers which allow for more than 10 years free of eclipse time span. Among these, we would choose the points with minimum maneuver cost, which are remarked with a square and have a cost of few cm/s.

Similar strategies for short term missions have been developed previously. For instance, see the ones by Heppenheimer and Pernicka and Howell designed for trajectories around L$_1$ with a fixed duration (see [39], [62], [16]). In short, in their approach the problem is divided in three parts: segment 1, 2 and 3. In segment 1 and 3, no maneuver is executed: the fact that some parts of the Lissajous can be followed without eclipse is taken advantage of. In segment 2 an eclipse avoidance strategy is implemented. Cheap z-maneuvers to change the phases maintaining the amplitudes are planned and make the satellite describe almost circular revolutions. The way to make the Lissajous revolutions become circular is to match the xy and z periods. For this purpose, if the satellite jumps in the z direction velocity twice in each revolution, it skips a definite amount of time. This is, a change in the phases yields an alteration of the natural velocity at which the Lissajous evolves, and so it is the same as missing an interval of time (i.e. $\Delta t = \Delta\psi/\nu$).

As we have seen, phase-change maneuvers which maintain the amplitude have one degree of freedom. Either the time of the maneuver, or the phase-jump it implies can be chosen. However, once one of them is fixed, there is only one possible maneuver. Pernicka and Howell use this, as well as the knowledge of the total $\Delta\psi$ needed to balance the periods, to write a cost function and minimise the Δv expenditure in two maneuvers per revolution. As an observation, this strategy also has a geometrical interpretation in the EPP. The two maneuvers that minimise the cost per revolution are identical and result in a Ψ-jump which corresponds to half the vertical distance between two consecutive straight lines of the trajectory in the EPP. Thus, what the satellite does is to jump from one straight line to a previous one in every revolution (see figure 3.15) just

before entering the exclusion zone. The cost of each maneuver is very low and proportional to the Lissajous amplitude (assuming square-Lissajous). However, one of the main drawbacks of the strategy is that it requires a great deal of maneuvers if the mission is long; approximately 4 maneuvers each year have to be planned.

Using this strategy in the long run and measuring the amplitude, A, in thousands of km, the cost of each maneuver is $4.3 \times A$ cm/s with an average cost per year about $17.9 \times A$ cm/s with maneuvers approximately every 88 days both about L_1 and about L_2. We note that since the strategy consists in jumping upwards in the Ψ direction in the EPP, the cost only depends on the amplitude, but not on the size of the exclusion zone. Comparing these costs with the results of the tangent to tangent strategy (see tables 3.2 and 3.3) we clearly see that when the relative amplitude is not too big (less than 60%), ours strategy is cheaper, especially if the mission is long or if, at least, the maneuver to enter the cycle is not very expensive. That is, when the cost in the cycles is what rules over the cost before the cycles. When the exclusion zone is more than 2/3 of the Lissajous amplitude, it becomes difficult to jump over the exclusion zones in the EPP. Nevertheless, the Howell and Pernicka strategy is good, because it avoids the disks by performing a lot of little maneuvers, whose costs, when added, do not exceed the cost of the big maneuver that has to be performed in the tangent to tangent strategy.

3.6   Impulsive transfers between Lissajous orbits of different amplitudes

So far, we have used the non escape maneuvers as a means to plan eclipse avoidance strategies. However, remember that these maneuvers were indeed developed as a convenient way to transfer from one Lissajous orbit to another one, avoiding unstable motions. In case we are not interested in reaching the final Lissajous with particular in plane and out of plane phases, the optimum maneuvering times were computed in equations (3.14) and (3.22). By evaluating the optimal cost of the non escape maneuvers in the xy direction from (3.27), as well as z maneuvers from (3.21), we can easily compute the minimum cost of the impulsive maneuvers to perform the required transfers as a function of the initial and final amplitudes. These costs can be expressed in the following way,

$$\text{cost}_{L_1}^y = 0.37134 \, |A_y^{(f)} - A_y^{(i)}|, \qquad \text{cost}_{L_2}^y = 0.36480 \, |A_y^{(f)} - A_y^{(i)}|,$$

for changing the in plane amplitude from A_y^i to A_y^f and,

$$\text{cost}_{L_1}^z = 0.40123 \, |A_z^{(f)} - A_z^{(i)}|, \qquad \text{cost}_{L_2}^z = 0.39523 \, |A_z^{(f)} - A_z^{(i)}|,$$

for changing the out of plane amplitude, from $A_z^{(i)}$ to $A_z^{(f)}$. In the previous expressions, if amplitudes are introduced in thousands of km, the cost is obtained in m/s.

Furthermore, the cost of transferring from a square Lissajous orbit with amplitudes $A_y^{(i)} = A_z^{(i)}$, to another square Lissajous of amplitudes $A_y^{(f)} = A_z^{(f)}$ by performing separate maneuvers is obtained by adding the costs in each direction:

$$\text{cost}_{L_1} = 0.77257 \, |A^{(f)} - A^{(i)}|, \qquad \text{cost}_{L_2} = 0.76003 \, |A^{(f)} - A^{(i)}|.$$
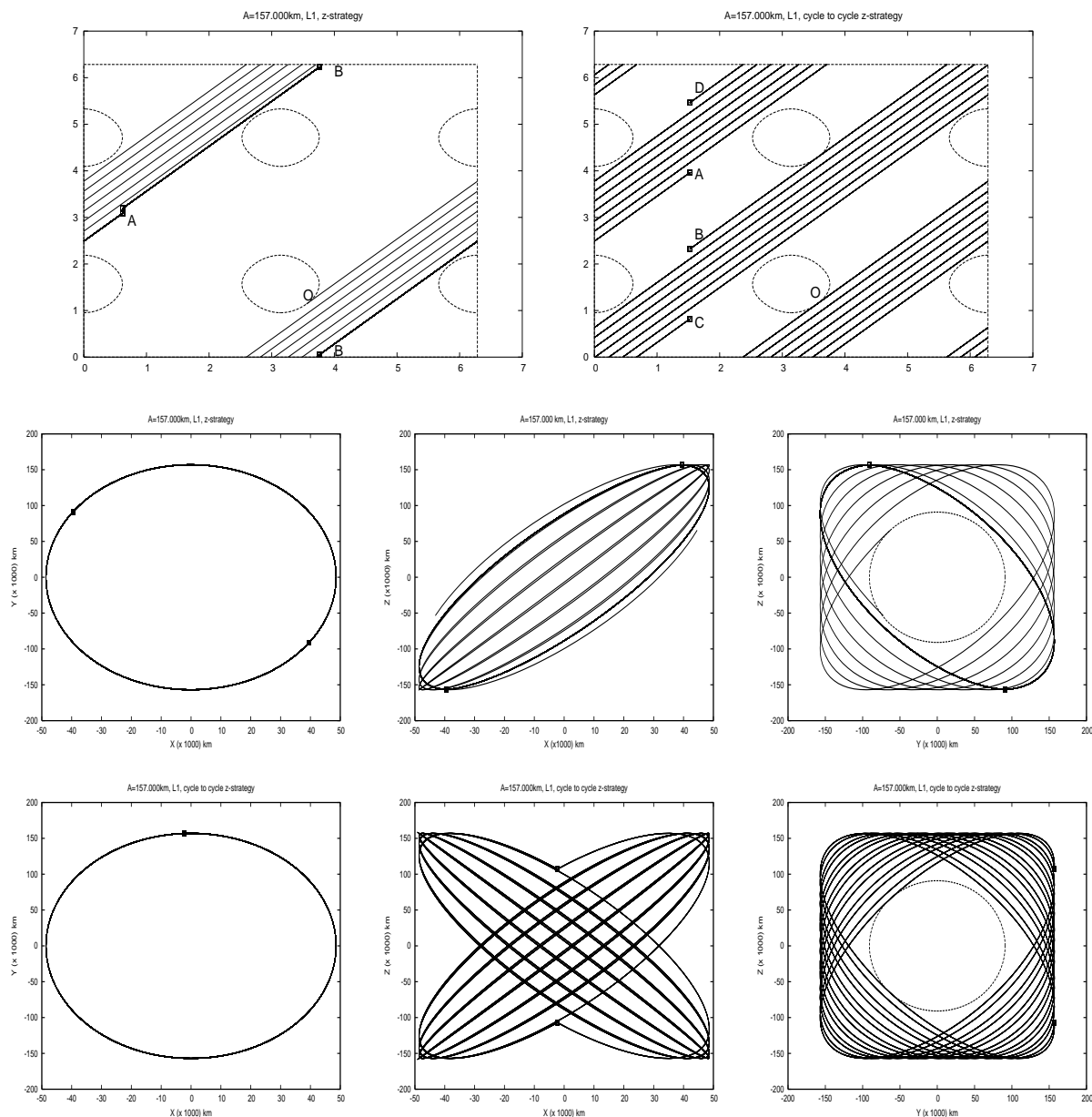
Figure 3.15: Comparison between the tangent to tangent cycle and the Pernicka and Howell strategy, for for an orbit with $A = 157000$ km and $R = 90000$ km about L_1. The first row shows the representation of both strategies in the EPP (left: Pernicka and Howell, right: tangent to tangent cycle). In the second row, the xy, xz and yz projections of the trajectory on the Lissajous are shown for the Pernicka and Howell strategy. Departing from a tangent trajectory at O, the satellite evolves till just before entering the exclusion zone, then it enters in a cycle with two z-maneuvers per revolution (four per year). The maneuvers are applied in two different places, A and B, and the jump in the Ψ direction in each place is one half of the Ψ-distance between two consecutive lines in the EPP corresponding to the same natural motion. The final cycle is seen like an ellipse about the exclusion zone. Maneuvers are stopped when the remaining time without eclipse is enough to finish the mission. In the third row, the corresponding plots using the tangent to tangent eclipse avoidance strategy with z-maneuvers are shown. Each cycle closes with a maneuver at A or C which jumps to B or D respectively. The whole pattern repeats again after two cycles. In both cases the places of the maneuvers are marked with a small box.

3.6.1   Combined maneuvers

We call combined maneuver to a maneuver executed at a given moment of time t, which is the addition of the corresponding in plane non escape maneuver and a maneuver in the z direction. That is to say, the 3 components of the velocity vector are changed at the same time.

According to the parallelogram law, the cost of a combined maneuver at time τ is always less or equal than the addition of the costs of two separate maneuvers, in the xy and z directions at the same moment of time τ,

$$C^\tau_{combined} = C^\tau_{xy+z} \leq C^\tau_{xy} + C^\tau_z,$$

and the absolute minimum of the cost of a combined maneuver is reached when the optimal times in each direction coincide.

In the EPP, the optimal times for the xy maneuvers are seen as the vertical lines $\Phi = \beta + \frac{\pi}{2}$ and $\Phi = \beta + \frac{3\pi}{2}$. Respectively, for z maneuvers, the optimal times are represented by the horizontal lines $\Psi = \frac{\pi}{2}$ and $\Psi = \frac{3\pi}{2}$. These optimal times coincide at the four intersections between the aforementioned straight lines. However, note that when this happens, the points are either inside the exclusion zone or very close to it. This fact makes them not usable as amplitude change locations, in our eclipse avoidance philosophy.

It is natural to wonder now at which moments of time a single combined maneuver would improve the results of changing the amplitudes separately. Let C_s be the sum of the minimum possible costs for a change of amplitudes from square Lissajous to square Lissajous with separate maneuvers at their optimal times. Let $C_c(\tau)$ be the cost of performing the same change in the amplitudes by executing a single combined maneuver at time τ. By an improvement we mean the moments of time when $C_c(\tau) < C_s$. When this happens, we define,

$$I(\tau) = 100 \times \frac{C_s - C_c(\tau)}{C_s},$$

the percentage of improvement of a combined maneuver over the two separate optimal maneuvers. Obviously, the maximum of this improvement $I(\tau)$ is achieved in each one of the four intersections between $\Phi = \beta + \frac{3\pi}{2}$, $\Phi = \beta + \frac{\pi}{2}$, and $\Psi = \frac{\pi}{2}$, $\Psi = \frac{3\pi}{2}$. So, the upper bounds for $I(\tau)$ computed at these intersections are,

$$\max_{L_1} I(\tau) = 29.23642\,\%, \qquad \max_{L_2} I(\tau) = 29.23266\,\%.$$

3.6.2   Increasing the size of a Lissajous orbit using a combined maneuver

As we saw in section 3.6, enlargement maneuvers can be performed at any moment of time. However, $I(\tau)$ is not positive at all points of the effective phase plane. Moreover the improvement depends on the ratio A^f/A^i.

As an example, figure 3.16 shows which are the effective phases where executing a combined maneuver leads to an improvement in cost for a 100% enlargement of a 120000 km square Lissajous around L_1. White zones are either exclusion zones, which we do not consider as valid phases, or phases where it is cheaper to make the transfer using two maneuvers. The behaviour is similar for a transfer in the vicinity of L_2 as we can see in the same figure where we represent a transfer from
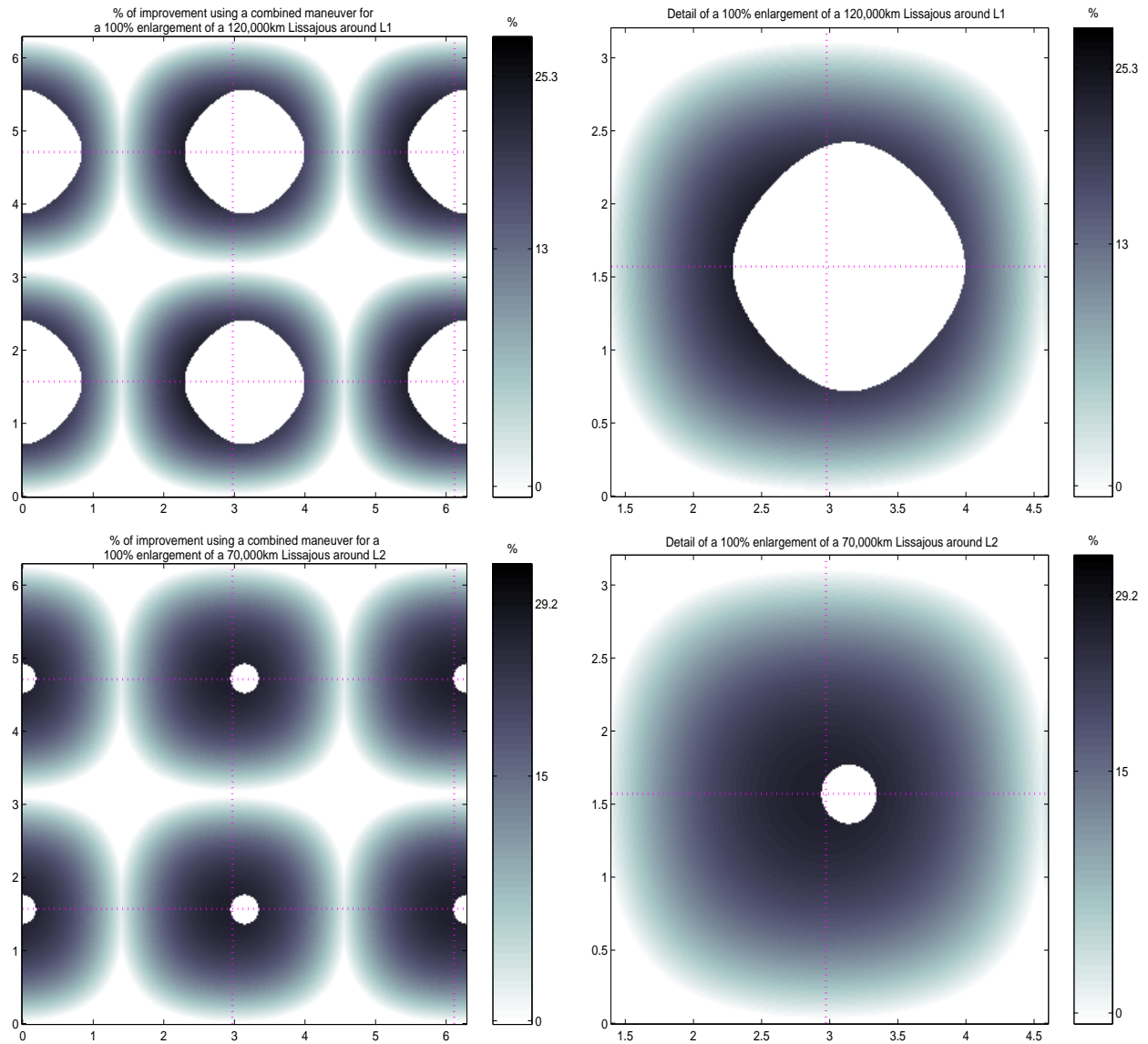
Figure 3.16: (left) $I(\tau)$ for each point (Φ_m, Ψ_m) when a combined maneuver is used to enlarge a square Lissajous orbit. (right) detail of the left figure around an exclusion zone. (top) case example around L_1 from 120000 km to 240000 km amplitude. (bottom) Case example around L_2 from 70000 km to 140000 km. Dotted lines in the figures represent the optimal places for the maneuvers to reduce the in-plane or out-of-plane amplitudes.

70000 km to 140000 km square Lissajous of amplitude (again a 100% enlargement). Note that the improvement essentially depends on the distance to the intersection between the vertical and horizontal dotted lines which correspond to the optimal places for the separate maneuvers. An example of the profile of the improvement function along the optimal coordinate lines is displayed in figure 3.17.

Other enlargements would have similar pictures, with regions surrounding the exclusion zones as the best improvement rate zones. The maximum % of improvement is around 30%, which represents a significant reduction in cost.
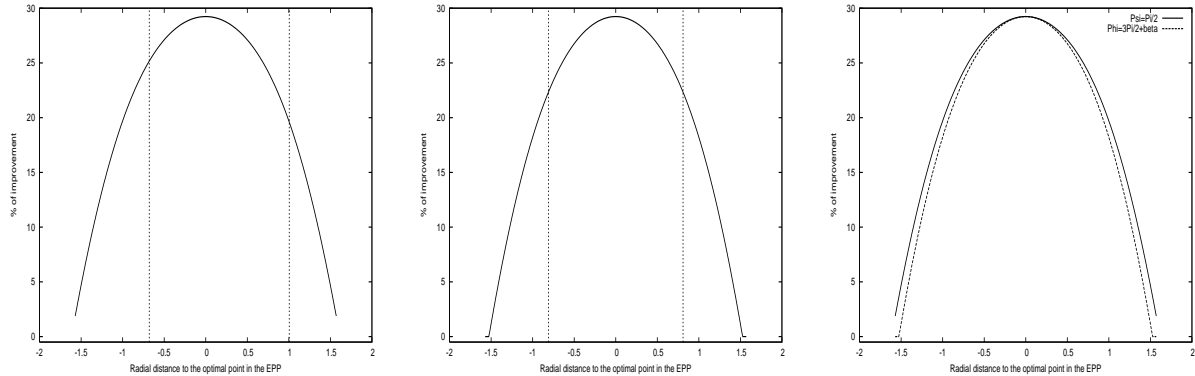
Figure 3.17: Profiles of the improvement of cost function along the lines of optimal places for in-plane or out-of-plane maneuvers. Left, along the Φ phase. Middle, along the Ψ phase and right, superposition of both plots. The zero value corresponds to the intersection point of the optimal lines and the vertical dotted lines mark the exclusion zone. The example corresponds to the enlargement maneuver of a square Lissajous around L_1 from 120000 km to 240000 km.

3.6.3   Reducing the size of a Lissajous orbit using a combined maneuver

The reduction of the amplitude of the Lissajous is constrained. According to (3.13) and (3.20) separated transfer maneuvers in the xy and z directions are only possible at some time intervals. That is, for some values of the effective phases. More precisely, for each A^f/A^i ratio, the effective phases (Φ_m, Ψ_m) for which a combined maneuver is possible are the ones that satisfy,

$$|\cos(\Psi_m)| < \frac{A^f}{A^i}, \qquad |\cos(\Phi_m - \beta)| < \frac{A^f}{A^i}, \qquad (3.34)$$

which essentially express the idea that, just by moving the velocity, one cannot jump from a pendulum oscillation with a certain amplitude to a smaller one when the pendulum is above the required small amplitude.

These pair of equations define two vertical and two horizontal strips, in whose intersection we find the possible effective phases where to perform the transfer maneuver. The more we want to reduce the Lissajous size, the thinner the strips are, and the other way round, as we see in

figure 3.18. In this figure we also observe that the permitted regions always interfere with the exclusion zones. This fact reduces even more the possible places for the maneuver, as we will never use phases inside the exclusion zones as maneuver phases.

The maximum reduction rate (MRR) defined as the maximum value of $(A^i - A^f)/A^i$ for a given pair of effective phases can also be computed using the equations (3.34). In percentage, this value is given as,

$$MRR(\Phi, \Psi) = 100 \times [1 - \max(|\cos(\Psi)|, |\cos(\Phi - \beta)|)],$$

and it is represented in figure 3.19, both around L_1 and L_2.

As it was observed for enlargement maneuvers, the zones in the EPP which produce a greater improvement in cost are those surrounding the exclusion zones. So again, either upper or lower tangential points seem to be good places to execute a combined maneuver as shown in figure 3.20. However, as the reduction rate increases, the possible effective phases for a combined maneuver become more restricted. It is even possible that for certain reduction rate and relative amplitude, all (or almost all) the effective phases where a combined maneuver is permitted are inside the exclusion zones. Therefore, it is worth commenting here how these reduction and enlargement maneuvers can be combined with eclipse avoidance strategies.

3.6.4 Eclipse avoidance in combined maneuvers to change the amplitude

Both the departure and the arrival orbit of the impulsive transfers that we have explained are Lissajous type orbits. Therefore, after the transfer, we do not have to worry about occultations anymore, as the tangent to tangent cycle can be applied to the new orbit. However, in our eclipse avoidance philosophy, it is not acceptable to have an eclipse during the transfer. Therefore, we should look for initial transfer conditions which are not only good in terms of cost but also maintain the satellite beyond distance R (radius of the exclusion zone) from the Sun-Earth x axis. That is to say we do not have to plan a new type of amplitude change transfers; we just take advantage of the ones that provide a cheap transfer without violating the exclusion zone.

Again, the EPP representation can help us in the mission design. Given initial and final amplitudes, A^i and A^f, we want to know whether there exist initial conditions for a transfer from square Lissajous with amplitude A^i to square Lissajous with amplitude A^f, such that:

a) The transfer trajectory does not violate the exclusion zone.

b) The maximum possible improvement in the total cost provided by a combined maneuver is achieved.

For the first condition, we fix an exclusion radius of 90000 km around L_1 and 14000 km around L_2. Then, given initial and final amplitudes, we compute the transfer trajectory for each pair of initial phases and the distance to the Sun-Earth x axis at each point of this trajectory. If this distance is less than the fixed radius at some point, it means that the exclusion disk is crossed during the transfer. So, the corresponding initial phases are considered to be not usable for our purposes. For instance, see figure 3.21, where the minimum distance to the x axis for the transfer
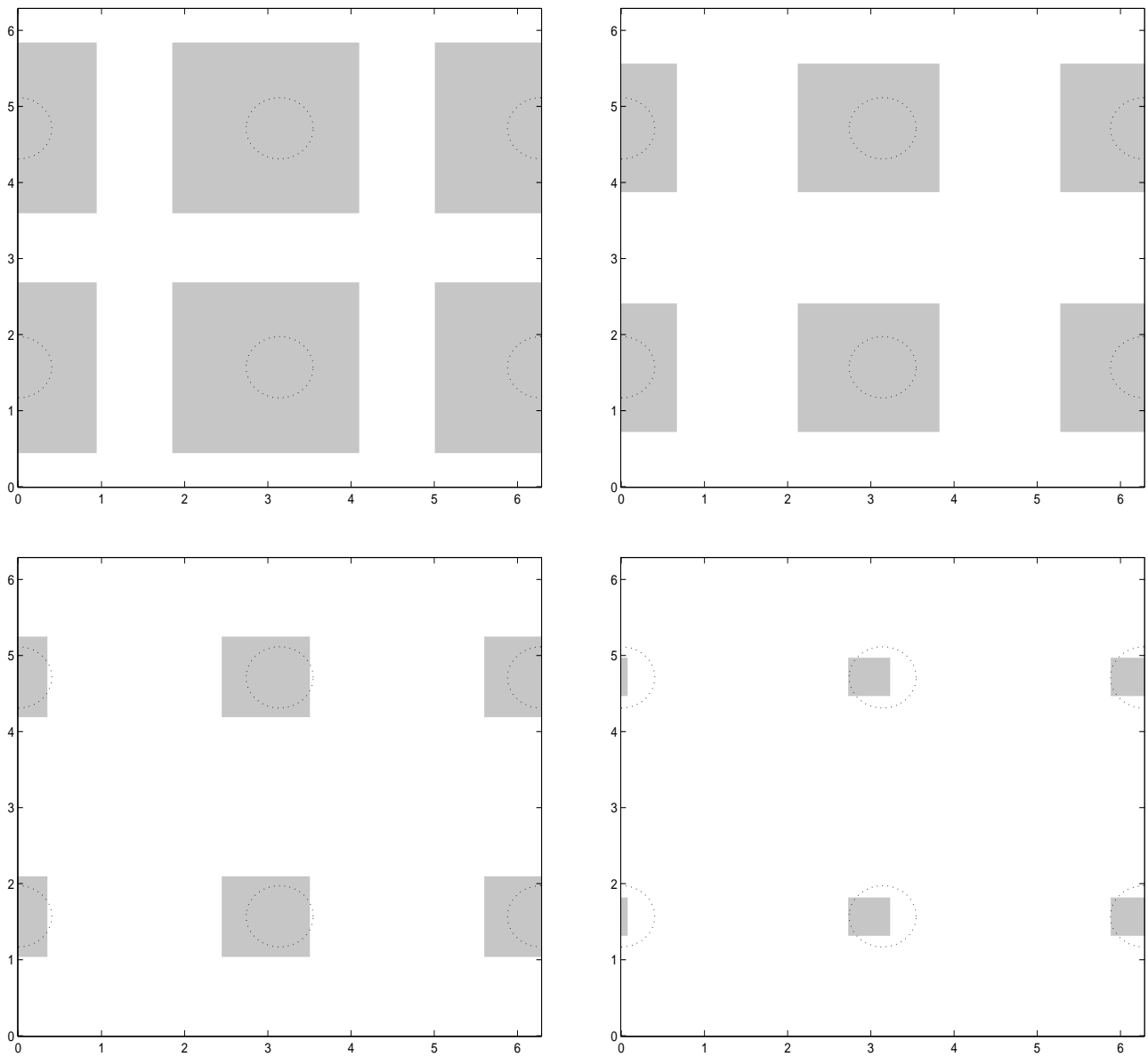
Figure 3.18: Possible (Φ_m, Ψ_m) where a combined maneuver can give a certain reduction of the Lissajous amplitude. Represented reductions $(A^i - A^f)/A^i$ of 10%, 25%, 50% and 75% from top left to bottom right.
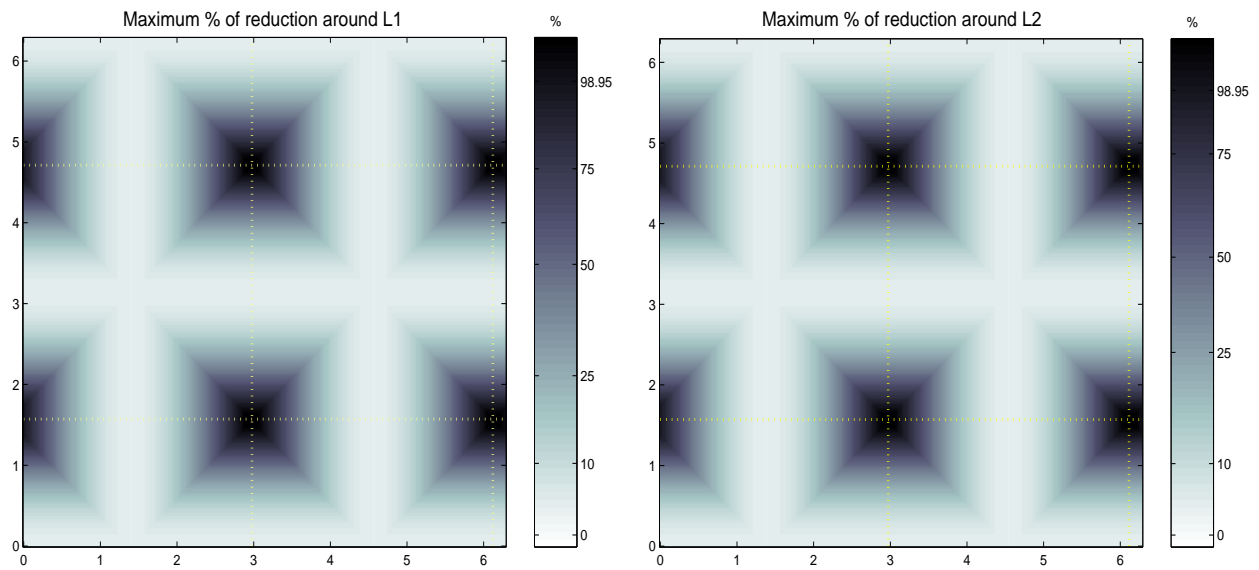
Figure 3.19: Maximum possible reduction of the amplitude using a combined maneuver, as a function of the effective phases. Right, L_1 case. Left, L_2 case.
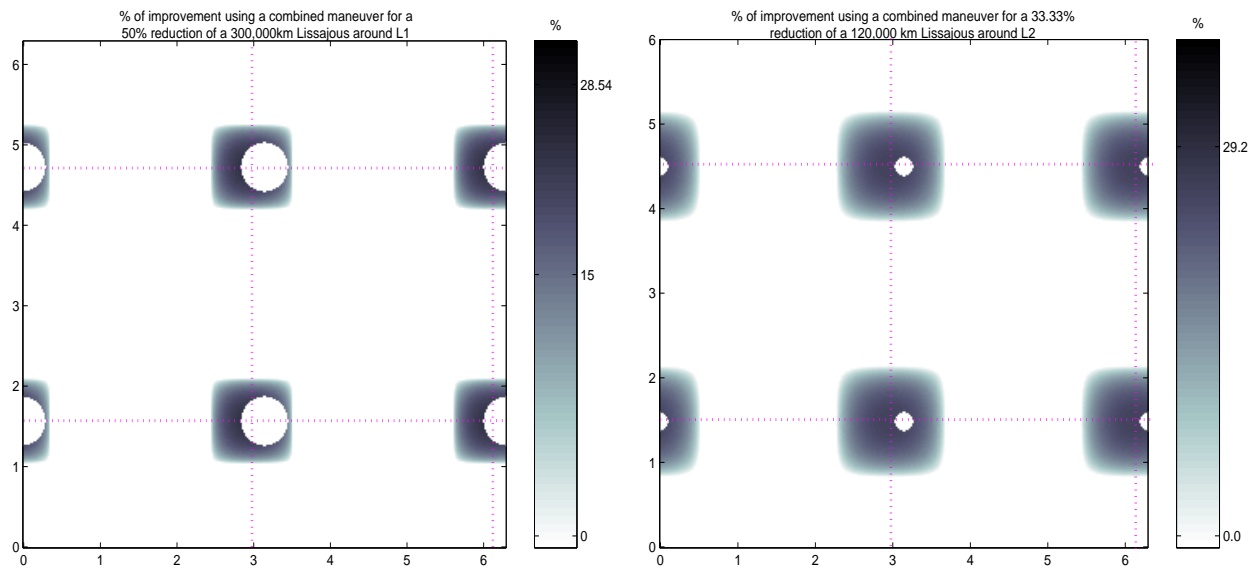
Figure 3.20: $I(\tau)$ for two examples of reduction of amplitude. Left, from 300000 km to 150000 km amplitude square Lissajous about L_1 (50% of reduction). Right, from 120000 km to 80000 km amplitude square Lissajous about L_2 (33% of reduction). The profiles of the function along the optimal coordinate lines look similar to the ones in figure 3.17 and are not displayed.

trajectory going from a square Lissajous of A_y^i=300000 km to another Lissajous of A_y^f=450000 km around L$_1$ is displayed. The white strips which are tangential to the upper part of the exclusion zones represent the points for which an eclipse occurs during the transfer.
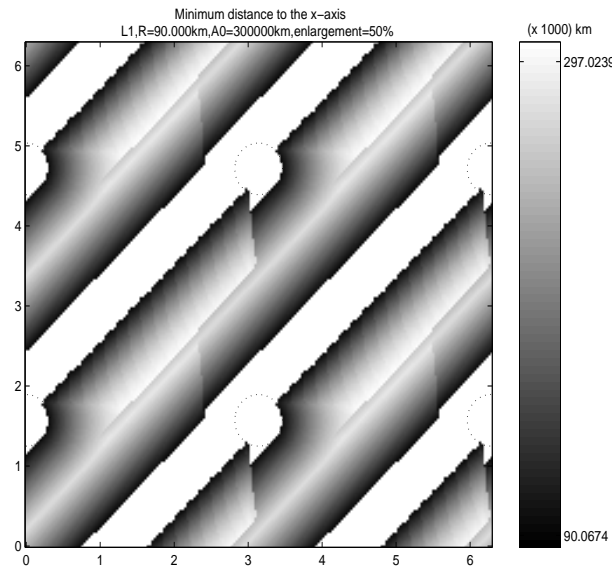
Figure 3.21: Minimum distance from the x-axis to the transfer trajectory in a 50% enlargement of a Lissajous around L_1

These studies of exclusion zone violation can be combined with the ones concerning the improvement in cost of performing a combined maneuver. That is, we reduce the search zone to the initial phases that we already know that produce a reduction of the costs when a combined maneuver is performed. Among these phases, it is just a matter of selecting the places where the maximum time without hitting the exclusion zone is enjoyed when the transfer is performed. A couple of examples are represented in figure 3.22. In these figures we represent the time without crossing the L$_2$ exclusion zone (14000 km) as a function of the effective phase where we perform the maneuver. The darkest zones are the most convenient in terms of time free of eclipse. Besides, the best improvement in cost occurs when the maneuver is executed close to the intersection of the vertical and horizontal dotted lines. Therefore, optimal places for the transfer are the darkest points which are closest to these intersections.

Furthermore, in figure 3.23 we present an example of an enlargement of a square Lissajous around L$_2$, from A^i=80000 km to A^f=120000 km. The transfer can be done by using two maneuvers at their optimal moments (figure 3.23 first row) or by choosing a couple of maneuvering phases inside the darkest zone of the picture on the right in figure 3.22, and perform the transfer using a combined maneuver. We can see how the non violation of the exclusion zone is satisfied in both cases, but the cost is reduced around 20% when a combined maneuver is used.

If a particular study for each case can't be done, points in lower tangential trajectories should be used, as they satisfy both requirements: give good improvement rates for combined maneuvers, as well as provide plenty of time without eclipse to perform the transfer.
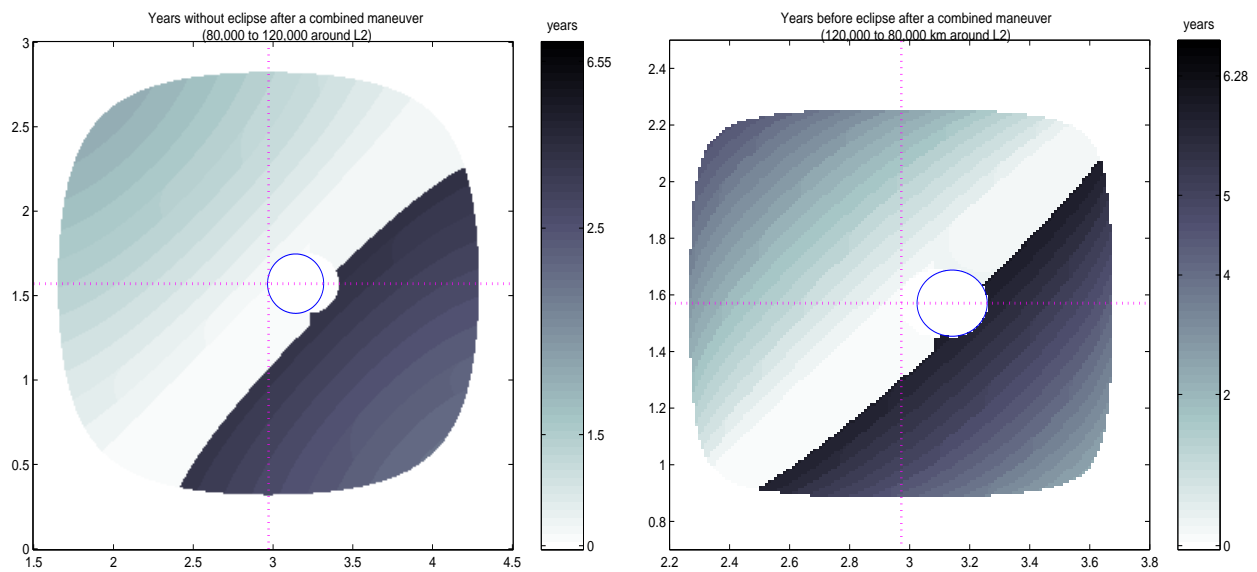
Figure 3.22: Maximum time interval without crossing the exclusion zone for a combined maneuver to change the amplitude of a square Lissajous. Both examples are details of an exclusion zone in the EPP for the L_2 case with $R = 14000$ km. Left, enlargement of the amplitude from 80000 km to 120000 km. Right, reduction from 120000 km to 80000 km. Optimal places for the transfer without crossing the exclusion zone are the darkest places closest to the intersection of the vertical and horizontal dotted lines which represent the optimal places for the separate maneuvers.
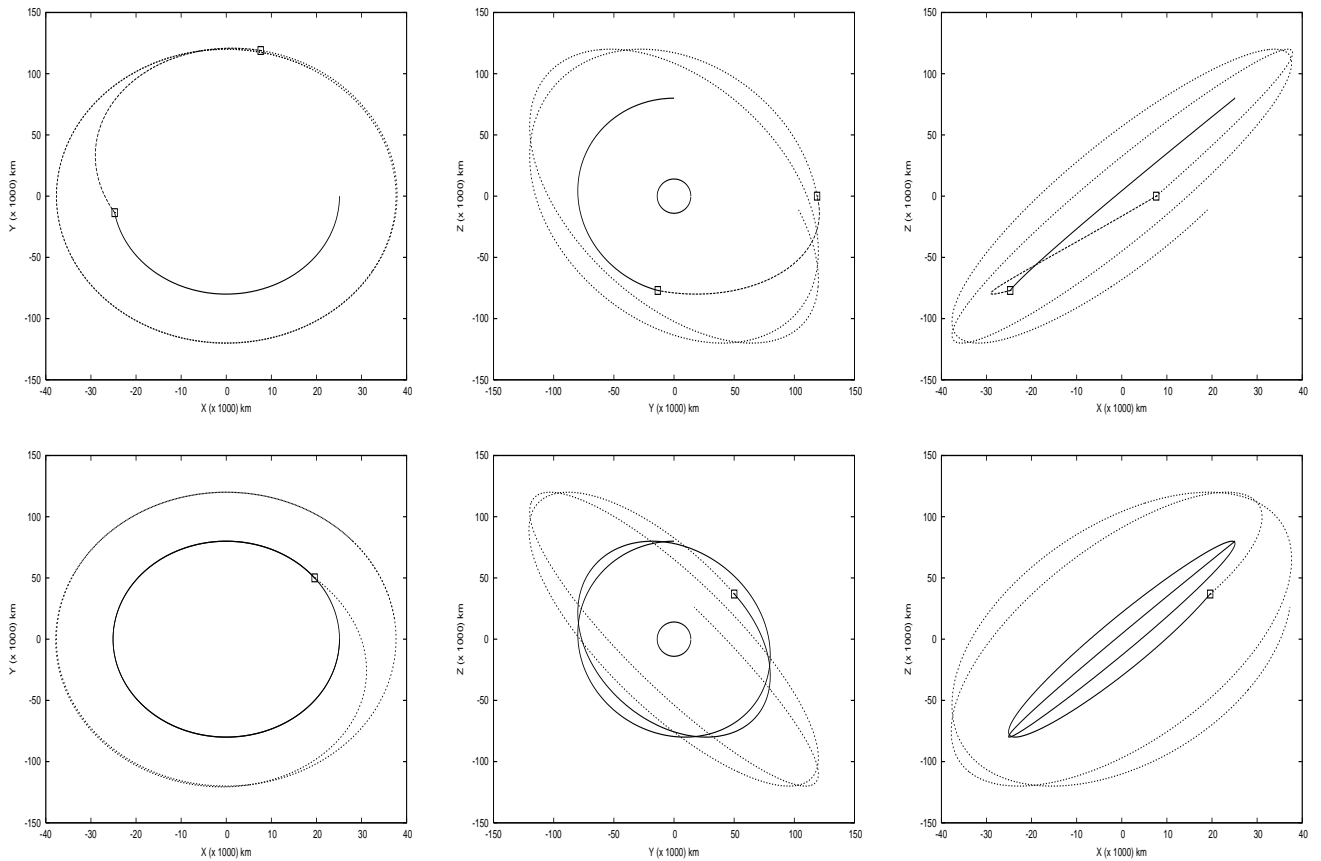
Figure 3.23: Example of a transfer from a square Lissajous about L_2 with $A = 80000$ km to $A = 120000$ km. Top, using two separate maneuvers at the optimal places with total cost 30.33 m/s. Bottom, using an optimal combined maneuver with cost 23.33 m/s. A 20.79% of improvement in the delta-v cost. Maneuvers are marked with a box.

3.7   Rendez-vous

In sections 3.5 and 3.6 the effective phases plane has been used in order to plan eclipse avoidance maneuvers and impulsive transfers between Lissajous of different sizes. These are two very important problems that may have to be faced when designing missions around libration points that use Lissajous type orbits as their nominal trajectory. Nevertheless, there is still another important topic to be addressed, which is the rendez-vous between different satellites in the same Lissajous orbit. The rendez-vous of different satellites in the frame of the restricted three body problem is a relatively unexplored area ([46]). In this section we present rendez-vous strategies developed by using the effective phases plane (EPP), which has proved, once more, to be an efficient and easy to use design tool.

3.7.1   Rendez-vous maintaining the amplitudes

Let us assume we have inserted a pair of satellites in a Lissajous orbit. The position of each one of the satellites is defined, as usual, by the hyperbolic coefficients A_1 and A_2 (equal zero); the central part amplitudes A_x and A_z (the same for both of the satellites, related to the Jacobi constant) and the phases. If the satellites are on the same Lissajous, the 4 amplitudes are the same, being $A_1 = A_2 = 0$, and so their positions only differ in the phases (in plane and/or out of plane).

We will note (ϕ_i^1, ψ_i^1) and (ϕ_i^2, ψ_i^2) the initial phases for satellites 1 and 2 respectively. Our goal is to make them meet at some other phases, at some time t_r in the future, using impulsive maneuvers with an affordable cost.

The maneuvers will be executed in the non escape direction. Remember that when amplitudes don't change, the jump in the phases that these maneuvers cause is:

$$\begin{aligned} \phi_f - \phi_i &= -2(\omega t_m + \phi_i - \beta) \\ \psi_f - \psi_i &= -2(\nu t_m + \psi_i) \end{aligned} \tag{3.35}$$

where t_m is the time for the maneuver, ϕ_i and ψ_i the phases at t=0, and β is a constant angle depending on the mass parameter. The resulting phases after the maneuver are:

$$\begin{aligned} \phi_m &= \phi_f + \omega t_m \\ \psi_m &= \psi_f + \nu t_m \end{aligned} \tag{3.36}$$

Using the definition of the effective phases,

$$(\Phi(t; \phi_i), \Psi(t; \psi_i)) = (\phi_i + \omega t, \psi_i + \nu t),$$

equations (3.35) can be rewritten as,

$$\begin{aligned} \Delta\Phi &= -2\Phi(t_m; \phi_i) + 2\beta \\ \Delta\Psi &= -2\Psi(t_m; \psi_i) \end{aligned} \tag{3.37}$$

In the linear part of the equations, the movement in the xy-plane (ecliptic or in-plane) and in the z-plane (out-of-plane) are completely uncoupled. We have seen in section 3.6 that combined maneuvers (i.e. maneuvers that simultaneously change $\dot{x}$, $\dot{y}$ and $\dot{z}$) are convenient in some cases,
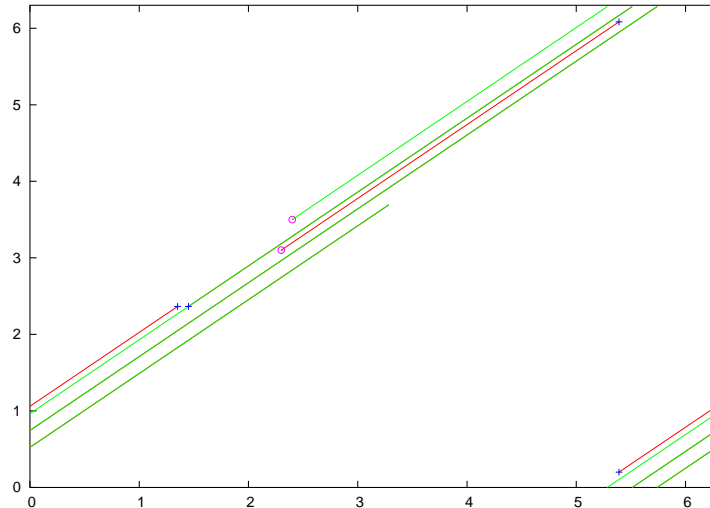
Figure 3.24: Effective phases plane representation of one satellite chasing the other.

as they have a cost which is lower than the addition of two separate maneuvers in the in plane and out of plane velocities. In this part of the work, however, separate maneuvers will be used. The reason is that there is little freedom in choosing the jump in each of the phases necessary for the rendez vous to take place. This fact implies that the time for the maneuvers is also strongly constrained (see equation (3.35)). Therefore, in plane and out of plane maneuvers will probably be performed at different times, excluding the possibility of a combined maneuver. In fact, in the cases where combined maneuvers were used for size reduction or enlargement maneuvers no attention was payed to the final arriving phases and this is not the case now.

One satellite chasing the other

An immediate solution to the problem of making two satellites meet is letting one of them follow its way unperturbed along the Lissajous, and planning maneuvers on the other one.

According to equation (3.35), there is only one possible jump in each direction at each moment of time. And the other way round, once the jump has been fixed, the time cannot be chosen. In our case, the jump in the phases is clearly determined: we want to jump from one trajectory to the other one. Therefore, the equations to be solved are,

$$\phi_i^2 = \phi_f^1 = -\phi_i^1 - 2\omega t_m^{xy} + 2\beta \pmod{2\pi}$$
$$\psi_i^2 = \psi_f^1 = -\psi_i^1 - 2\nu t_m^z \pmod{2\pi}.$$

So,

$$t_m^{xy} = \frac{\beta}{\omega} - \frac{\phi_i^2 + \phi_i^1}{2\omega} + \frac{k\pi}{\omega} \quad \text{and} \quad t_m^z = -\frac{\psi_i^2 + \psi_i^1}{2\nu} + \frac{\kappa\pi}{\nu} \tag{3.38}$$

where $k, \kappa \in \mathbb{Z}$ can be used to adjust the times to mission requirements (i.e. positive, close to each other...).

The cost of one satellite chasing the other is proportional to the initial differences in phases. The closer to 0 or to 2π that the difference $|\phi_i^1 - \phi_i^2|$ is, the cheaper the maneuvers in xy. For the z-maneuvers, the same with ψ.

Particularly, the cost of the xy-maneuvers can be measured by the size of α,

$$\alpha_{xy}(\phi_i^1, \phi_i^2) = 2A_x|\sin(\phi_i^1 + \omega t_m^{xy} - \beta)| = 2A_x\left|\sin\left(\frac{\phi_i^1 - \phi_i^2}{2}\right)\right|. \tag{3.39}$$

And by using this expression for α_{xy}, the final cost for the in plane maneuver can be computed as,

$$\text{cost}_{xy} = \alpha_{xy}(\phi_i^1, \phi_i^2)\sqrt{\frac{d_2^2 + \kappa^2 d_1^2}{c^2 + \kappa^2}},$$

where d_1, d_2, c and κ are constants depending on the mass parameter.

The cost of the z-maneuvers is,

$$\text{cost}_z(\psi_i^1, \psi_i^2) = 2A_z|\sin(\psi_i^1 + \nu t_m^z)| = 2A_z\left|\sin\left(\frac{\psi_i^1 - \psi_i^2}{2}\right)\right|. \tag{3.40}$$

So both cost_{xy} and cost_z are maximum when the differences between the initial phases are around π.
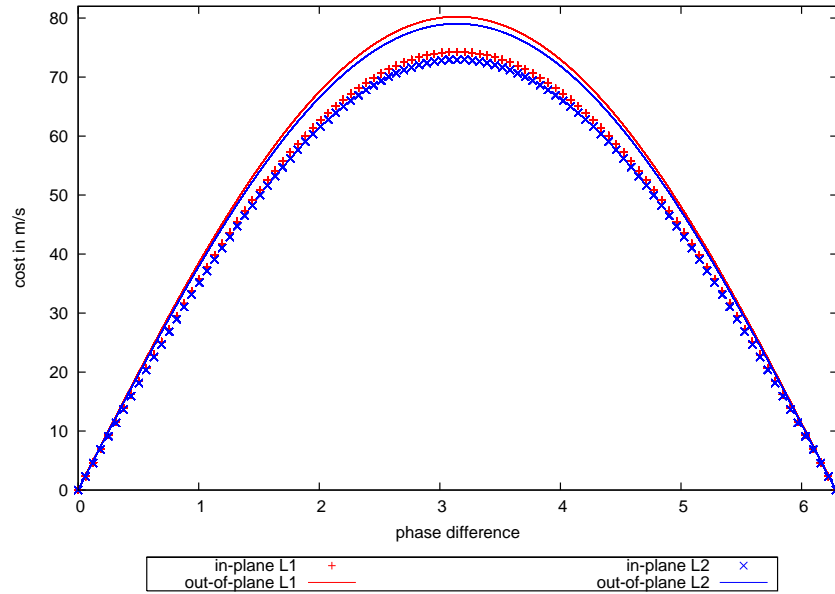
Figure 3.25: Cost of the persecution maneuvers depending on the difference between the initial phases (in red, costs for L_1 Lissajous and in blue costs for the L_2 Lissajous). The cost in m/s is proportional to the amplitude. It is shown in the figure for amplitude equal to 100000 km. Therefore, the cost for another Lissajous amplitude is easily computed by diving the costs shown in the figure by 10^5 and multiplying by the actual amplitude.

On the other hand, the time for performing the maneuvers in xy depends on $\frac{1}{2}(\phi_1 + \phi_2)$. Respectively for z maneuvers, the time depends on $\frac{1}{2}(\psi_1 + \psi_2)$ as shown in equation (3.42).
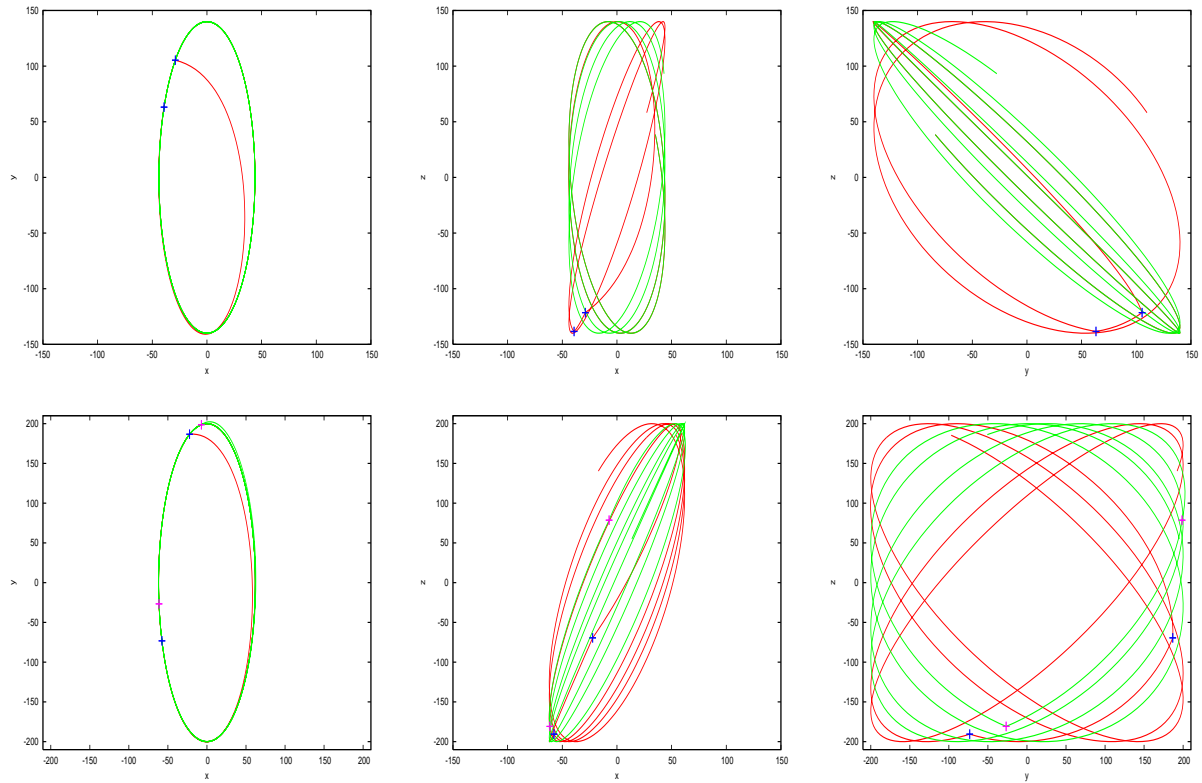
Figure 3.26: First row: xy, xz and yz projections of the one satellite following the other strategy for rendez-vous. $A_y = A_z$=140,000 km around L$_2$. Second row: xy, xz and yz projections of the four maneuvers strategy for a Lissajous around L_1, $A_y = A_z$=200,000 km.

Therefore, a natural way of representing the time between maneuvers is as a function of these semi-summations. For the xy maneuvers, there is another parameter playing a role in the computation of the time, which is β. Figure 3.27 shows the representation of the time between maneuvers depending on the initial phases of both satellites. Values on the x-axis correspond to $\phi_1 + \phi_2$, while the values on the y-axis are $\psi_1 + \psi_2$. We can see how both directions show 2π periodicity, justified by equation (3.42), (in x the base interval is $[2(\pi+\beta), 2(2\pi+\beta)]$, due to the aforementioned role of β).

To sum up, no more than 50 days will be necessary in any case between one maneuver and the other one. The worst case is when the differences in phases are around 2π (despite being cheap in Δv). The general case, with initial differences in phases being less than π, corresponds to a waiting time between maneuvers of 10 to 25 days.
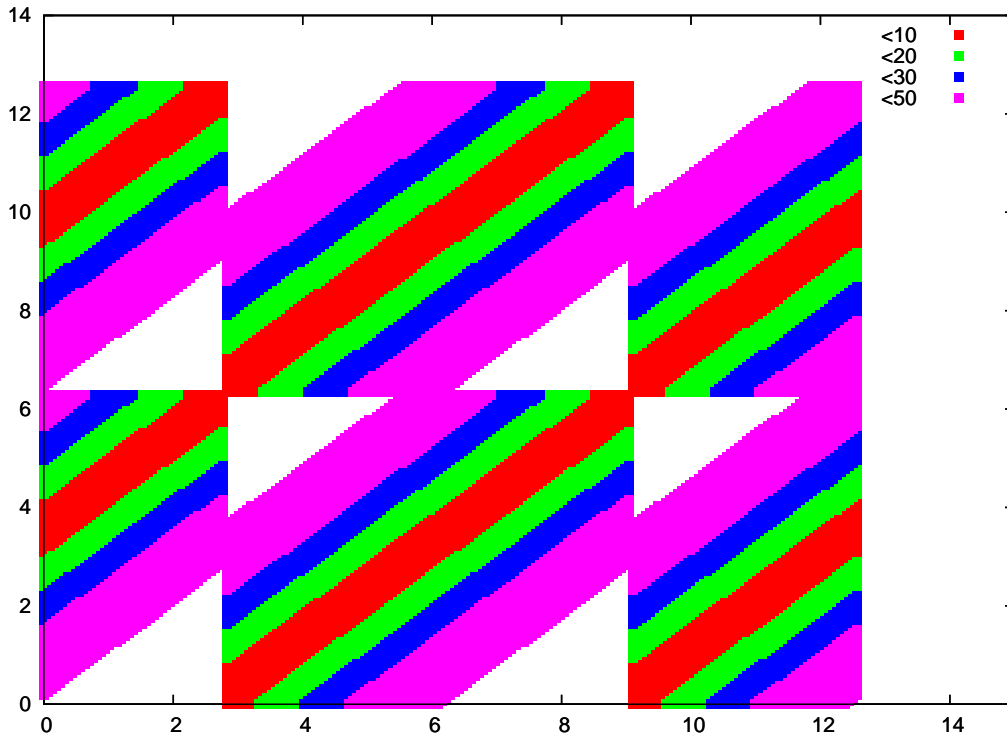
Figure 3.27: Time between maneuvers (in days) depending on $\phi_1 + \phi_2$ (x-axis) and $\psi_1 + \psi_2$ (y-axis).

Note that all the formulae used so far are symmetric with respect to the conditions (ϕ_i^1, ψ_i^1) and (ϕ_i^2, ψ_i^2). Consequently, there is absolutely no difference in choosing one satellite or the other as the one to perform the maneuvers. A combined strategy of one satellite maneuvering in one direction and the other satellite in the other direction will also lead to exactly the same results, both in terms of times and costs (switch 1 for 2 in equations (3.38), (3.39) and (3.40)). The choice may have to be made in response to some other criteria, such as the feasibility of performing maneuvers in a particular direction with each of the satellites, or the advantage of splitting the propellant load between them.

Intermediate meeting trajectory

One can think of adding a degree of freedom to the problem by executing maneuvers on both the satellites and making them meet in a trajectory which is neither the one that the first satellite follows nor the one for the second satellite. The procedure for minimising costs could take advantage of this degree of freedom in order to plan a cheaper rendez-vous. What will turn out, however, is that the new strategy will not yield a reduction in costs but more flexible time intervals for the maneuvers.

Remember once again that Lissajous orbits are seen as straight lines of constant slope ν/ω in the effective phases plane. So, what makes one trajectory different to the others in each of the straight lines of the EPP is the pair (ϕ_i, ψ_i). Performing maneuvers on both the satellites will result in the meeting taking place at a trajectory of the EPP different from the starting ones. That is, in a trajectory with different $(\bar{\phi}_i, \bar{\psi}_i)$. We refer to this new trajectory as the intermediate trajectory. When this intermediate trajectory has been chosen, the idea is to use the persecution strategy explained in section 3.7.1 twice. That is to say, making the first satellite chase the intermediate trajectory and the second one too. Given (ϕ_i^1, ψ_i^1) and (ϕ_i^2, ψ_i^2) the initial phases for the satellites, we have to determine $(\bar{\phi}_i, \bar{\psi}_i)$ in such a way that the resulting maneuvers are as cheap as possible.

Let t_{xy}^1, t_{xy}^2 be the times for the maneuvers in xy, one time for each satellite, and $t_{xy}^1 < t_{xy}^2$. The same for the z maneuvers, with times t_z^1, t_z^2 satisfying $t_z^1 < t_z^2$. For all we know about non escape maneuvers in the EPP, it is not difficult to prove that t_{xy}^2 depends on t_{xy}^1 and t_z^2 on t_z^1. The total jumps in the EPP needed for the rendez-vous are $|\phi_i^1 - \phi_i^2|$ and $|\psi_i^1 - \psi_i^2|$. When a maneuver in one of the directions is executed, part of the jump is performed. Therefore, by subtracting the part that has already been jumped from the total necessary change in phase, we obtain the jump that the second maneuver has to achieve. Due to the correspondence between times and jumps, knowing which is the necessary change in the phases leads to computing t_{xy}^2 and t_z^2. In more detail, according to equation (3.35) and with the current notation we have,

$$
\begin{aligned}
\phi_f^1 &= -\phi_i^1 - 2\omega t_{xy}^1 + 2\beta \\
\phi_f^2 &= -\phi_i^2 - 2\omega t_{xy}^2 + 2\beta \\
\psi_f^1 &= -\psi_i^1 - 2\nu t_z^1 \\
\psi_f^2 &= -\psi_i^2 - 2\nu t_z^2.
\end{aligned}
\tag{3.41}
$$

And we want the following to be true,

$$
\phi_f^1 = \phi_f^2 = \bar{\phi}_i \quad \text{and} \quad \psi_f^1 = \psi_f^2 = \bar{\psi}_i.
$$

So, equating in (3.41) we get that,

$$
t_{xy}^2 = t_{xy}^1 + \frac{(\phi_i^1 - \phi_i^2)}{2\omega} + \frac{k\pi}{\omega}
$$

$$
t_z^2 = t_z^1 + \frac{(\psi_i^1 - \psi_i^2)}{2\nu} + \frac{\kappa\pi}{\nu}.
\tag{3.42}
$$

where $k, \kappa \in \mathbb{Z}$.

To sum up, introducing an intermediate meeting trajectory $(\bar{\phi}, \bar{\psi})$ provides us with a degree of freedom in the xy direction (the time t_{xy}^1) and another one in the z direction (the time t_z^1). Once

these times have been fixed, the corresponding ones for the second satellite will also be determined. Thus, the whole strategy depends on the times for the first maneuver in each direction.

We will study the cost function in the xy direction and in the z direction of this strategy, which consists of 4 maneuvers.

Using the expressions in (3.39) and (3.40), we have that,

$$\begin{aligned}
\bar{\alpha}_{xy}(\phi_i^1, \phi_i^2) &= \alpha_{xy}(\phi_i^1, \bar{\phi}) + \alpha_{xy}(\phi_i^2, \bar{\phi}) \\
\bar{\alpha}_z(\psi_i^1, \psi_i^2) &= \alpha_z(\psi_i^1, \bar{\psi}) + \alpha_z(\psi_i^2, \bar{\psi}).
\end{aligned} \tag{3.43}$$

In fact, these expressions can be written in terms of time. Using the relations between the time for the maneuvers on satellite 1 and 2 (3.42) we have,

$$\begin{aligned}
\bar{\alpha}_{xy}(\phi_i^1, \phi_i^2, \bar{\phi}) &= 2A_x(|\sin(\phi_i^1 + \omega t_{xy}^1 - \beta)| + |\sin(\phi_i^2 + \omega t_{xy}^2 - \beta)|) = \tag{3.44} \\
&= 2A_x\left(|\sin(\phi_i^1 + \omega t_{xy}^1 - \beta)| + \left|\sin\left(\phi_i^2 + \omega\left(t_{xy}^1 + \frac{\phi_i^1 - \phi_i^2}{2\omega}\right) + k\pi - \beta\right)\right|\right) = \\
&= 2A_x(|\sin(\Phi_1 + \omega t_{xy}^1)| + |\sin(\Phi_2 + \omega t_{xy}^1)|).
\end{aligned}$$

where $\Phi_1 = \phi_i^1 - \beta$ and $\Phi_2 = -\beta + (\phi_i^1 + \phi_i^2)/2$.

As we already know, the degree of freedom is represented by the time for the maneuver on the first satellite. Particularly, the cost is equal to adding the absolute values of two sinus of the same amplitudes (A_x) and frequencies (ω), but different phases.

Analogously for the z maneuvers we have,

$$\begin{aligned}
\bar{\alpha}_z(\psi_i^1, \psi_i^2, \bar{\psi}) &= 2A_z(|\sin(\psi_i^1 + \nu t_z^1)| + |\sin(\psi_i^2 + \nu t_z^2)|) = \tag{3.45} \\
&= 2A_z\left(|\sin(\psi_i^1 + \nu t_z^1)| + \left|\sin\left(\psi_i^2 + \nu\left(t_z^1 + \frac{\psi_i^1 - \psi_i^2}{2\nu}\right) + \kappa\pi\right)\right|\right) = \\
&= 2A_z(|\sin(\Psi_1 + \nu t_z^1)| + |\sin(\Psi_2 + \nu t_z^1)|).
\end{aligned}$$

where $\Psi_1 = \psi_i^1$ and $\Psi_2 = (\psi_i^1 + \psi_i^2)/2$.

Again, the cost depends on the time for the maneuver on the first satellite.

When trying to minimise (3.44) as a function of t_{xy}^1 and (3.45) as a function of t_z^1, we get that the minimum occurs when one of the absolute values inside the summation is equal to zero. That is, when only one satellite is affected by a maneuver. So, the minimum possible cost when using the intermediate meeting trajectory coincides with the cost of the so-called one satellite chasing the other strategy.

In figure 3.28 the absolute value of two sinus, with a slight difference in the phases, and the resulting function of adding them have been represented. The addition of two sinus with different initial phase corresponds to the total cost in each direction of the intermediate meeting trajectory. Therefore, this picture shows in a graphic way what we have already stated: using this 4-maneuvers strategy doesn't yield an improvement in terms of costs. However, one can see that in the time interval going from the zero value of one of the sinus and the zero value of the other one, the cost does not vary very fast. In this interval, the cost is almost constant and equal to the absolute minimum. It slightly increases when approaching the middle of the interval, and
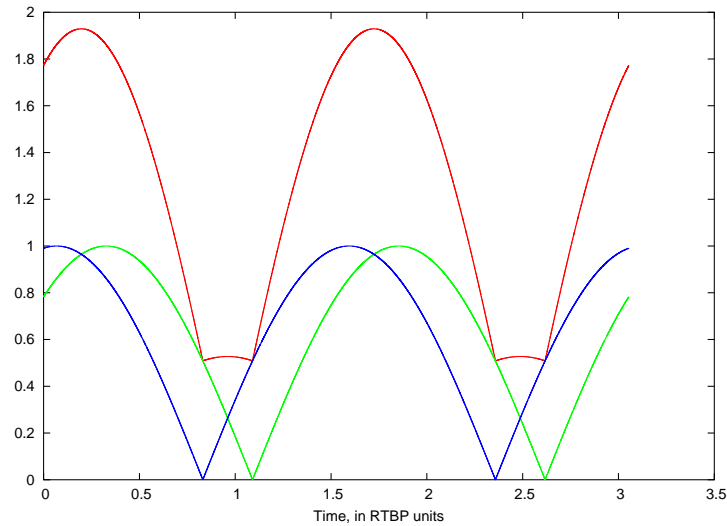
Figure 3.28: Representation of the absolute values of two sinus, with a small difference in the initial phases, and the function which results of adding them.

then decreases the same way. The local maximum reached in the middle of the aforementioned interval differs from the absolute minimum in a proportional way to the differences between the initial phases of the satellites. Again, the worst case is when the difference in phases at $t = 0$ is close to π, because the resulting local maximum in the middle of the aforementioned interval is quite different form the absolute minimum. Therefore, not all the times in the interval between two different minima are usable if we want to maintain a low cost (see figure 3.29).

The comparison between the minimum cost (i.e. strategy one satellite chasing the other) and the local maximums we have explained for the 4-maneuver strategy is depicted in figure 3.30.

From this results we can conclude that performing maneuvers on both satellites to make them meet in an intermediate trajectory is not advantageous in terms of cost, but provides the mission designer with more freedom when it comes to choosing the times for the maneuvers, with no significant increase in the cost.

3.7.2   Rendez-vous with amplitude change

Given two sets of initial conditions of the form,

$$(A_1^y, A_1^z, \phi_1, \psi_1) \quad \text{and} \quad (A_2^y, A_2^z, \phi_2, \psi_2),$$

representing the positions of two satellites on different Lissajous orbits, one can think of different forms to plan a rendez-vous using non escape maneuvers and the EPP.

To start with, amplitude reduction (or enlargement) maneuvers can be planned to make both satellites orbit the same Lissajous. Afterwards and in an independent way, one of the strategies for rendez-vous using the EPP can be applied to make them meet. Another possibility is to apply maneuvers in the non escape direction, but changing the amplitudes and the phases simultaneously in a convenient way for the rendez-vous.
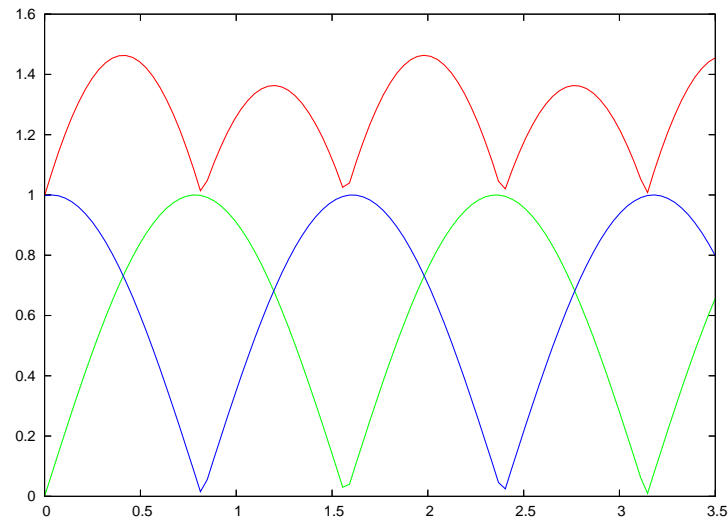
Figure 3.29: Representation of the absolute values of two sinus, with a difference in the initial phases of around π radians, as well as the function which results of adding them.
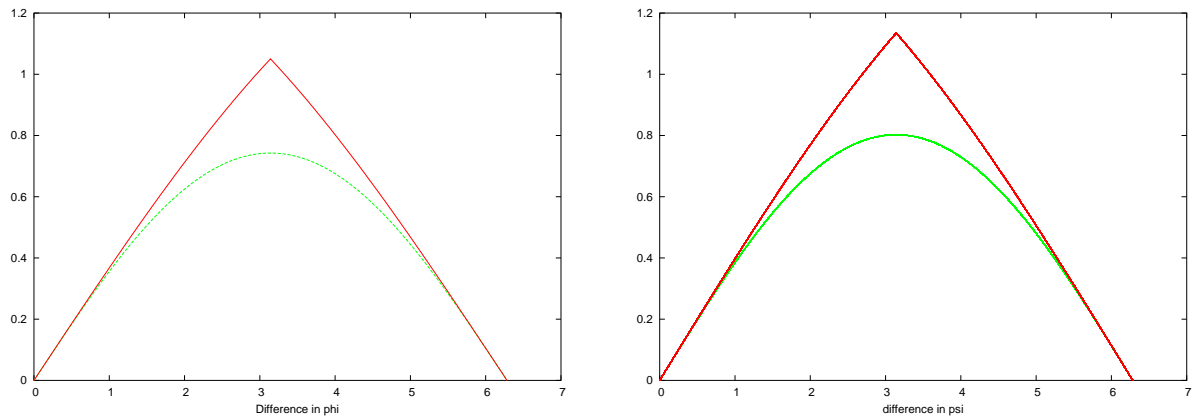
Figure 3.30: This figure shows, proportionally, the difference in cost between the absolute minimum for the rendez-vous (green) and the local maximum of the costs in the interval between two consecutive minimums in figures 3.28 and 3.29 (red), as a function of the initial difference in phases. The left picture shows this relation for the in plane phases, while the picture on the right for the out of plane phases. It is clear from these figures that in the worst case, when the initial phases differ in π radians, the local maximum is about 40% more expensive than the absolute minimum.

These two possibilities do not have to be regarded necessarily as different ways of approaching the rendez-vous problem, but rather as complementary to each other. For instance, when the satellites are in Lissajous orbits of substantially different amplitudes, an impulsive amplitude change may be considered. In case this amplitude change is done with a small % of error, the rendez-vous then has to take place between two Lissajous orbits of slightly different amplitudes. In this case, simultaneous amplitude and phase changes are perfectly suitable. Both approaches are discussed in the following sections.

Independent amplitude change and EPP rendez-vous

If we choose to apply the amplitude changes independently from the phase changes, we should start by planning the cheapest possible amplitude changes. Afterwards, once the satellites are both on the same Lissajous orbit, one of the strategies in section 3.7.1 can be applied.

The cost for the rendez-vous in phases is proportional to the amplitude. Thus, a priori, it is better to perform it in a Lissajous orbit such that,

$$A_y^f = \min(A_1^y, A_2^y) \quad , \quad A_z^f = \min(A_1^z, A_2^z). \tag{3.46}$$

However, if this choice of the final amplitudes is not allowed by mission requirements, the rendez-vous will be performed in the most favourable possible Lissajous orbit. Once the initial and final amplitudes have been chosen, optimal maneuvers for the amplitude changes can be planned (see section 3.6). Furthermore, it is easily proved that when the amplitude changes are performed at the moment of minimum cost, the phases do not change. (For instance introducing $\alpha(t_m) = A_x^{(i)} - A_x^{(f)}$ and $\omega t - \beta = \frac{\pi}{2} - \phi_i$ in equation (3.16) we get that $\cos(\phi_f)=\cos(\phi_i)$ and $\sin(\phi_f)=\sin(\phi_i)$.) Therefore, not only can amplitude and phase changes be planned independently, but also there is not a required order for the execution of the maneuvers.

Nevertheless, there is a detail which has to be taken into account concerning the rendez-vous with amplitude change. Note that amplitude change and rendez-vous maneuvers can only be executed in an independent way if the changes in the amplitude only refer to the out of plane or z amplitude. Otherwise, a maneuver in the xy non escape direction would introduce exponentially decreasing hyperbolic terms (A_2), which make equation (3.35) no longer the correct expression for the jump in the xy phases, as this equation assumes $A_1 = A_2 = 0$.

It may also be convenient for operational reasons to simultaneously change the amplitudes and the phases. It is natural, for instance, to consider the case when the satellites have been inserted into Lissajous orbits with slightly different amplitudes. A new study including maneuvers which simultaneously change amplitudes and phases will be performed in the following section.

Simultaneous amplitude change and rendez-vous

Let us define $\Delta A_x = A_x^{(f)} - A_x^{(i)}$. We will use expansions in ΔA_x up to order one. The terms $O((\Delta A_x)^2)$ are neglected, as ΔA_x is assumed to be sufficiently small.

For a given moment of time, we can look at the expression of the cost coefficient for in plane maneuvers, α, from equation (3.13) as a function of $A_x^{(f)} = \xi$,

$$\alpha(t, \xi) = A_x^{(i)} \sin\left(\omega t_m + \phi_i - \beta\right) \pm \sqrt{\xi^2 - A_x^{(i)\,2} \cos^2\left(\omega t_m + \phi_i - \beta\right)}$$

with the positive sign corresponding to the non-trivial maneuver when $\xi = A_x^{(i)}$. This is the sign we adopt, as we will look for small amplitude changes (i.e. $\xi \approx A_x^{(i)}$).

Then, we can expand $\alpha(t, x)$ in powers of ΔA_x,

$$\alpha(t, A_x^{(i)} + \Delta A_x) = \alpha(t, A_x^{(i)}) + \frac{\partial \alpha(t, \xi)}{\partial \xi}(A_x^{(i)})\Delta A_x + O((\Delta A_x)^2).$$

So,

$$\alpha(t) = 2A_x^{(i)} \sin(\omega t + \phi_i - \beta) + \frac{A_x^{(i)}}{\sqrt{(A_x^{(i)})^2 - (A_x^{(i)})^2 \cos^2(\omega t + \phi_i - \beta)}} \Delta A_x + O((\Delta A_x)^2)$$

$$\alpha(t; A_x^{(i)}, \Delta A_x) \approx 2A_x^{(i)} \sin(\omega t + \phi_i - \beta) + \frac{\Delta A_x}{\sin(\omega t + \phi_i - \beta)}. \tag{3.47}$$

If we introduce this expression of $\alpha(t; A_x^{(i)}, \Delta A_x)$ in equations (3.15), after some algebra we get,

$$\mathrm{tg}\phi_f = -\frac{A_x^{(i)} \sin(2\omega t + \phi_i - 2\beta)\sin(\omega t + \phi_i - \beta) + \Delta A_x \cos(\omega t - \beta)}{A_x^{(i)} \cos(2\omega t + \phi_i - 2\beta)\sin(\omega t + \phi_i - \beta) - \Delta A_x \sin(\omega t - \beta)}. \tag{3.48}$$

The moments t which satisfy (3.48) are the times for a xy maneuver which simultaneously changes ϕ_i to ϕ_f and $A_x^{(i)}$ to $A_x^{(f)}$. This expression can be simplified by defining $\Phi_t = \omega t - \beta$. Then, (3.48) takes the form,

$$\mathrm{tg}\phi_f = -\frac{A_x^{(i)} \sin(2\Phi_t + \phi_i)\sin(\Phi_t + \phi_i) + \Delta A_x \cos(\Phi_t)}{A_x^{(i)} \cos(2\Phi_t + \phi_i)\sin(\Phi_t + \phi_i) - \Delta A_x \sin(\Phi_t)}. \tag{3.49}$$

Note that ϕ_i, ϕ_f, $A_x^{(i)}$ and $A_x^{(f)}$ are known. The value of $A_x^{(i)}$ is the in plane amplitude of the initial Lissajous orbit. Besides, $A_x^{(f)}$ is given by the in-plane size of the Lissajous orbit on which the rendez-vous takes place. In turn, phases ϕ_i and ϕ_f correspond to the in plane phases of the satellites at the time we choose as origin ($t = 0$), being ϕ_i the phase of the satellite that jumps and ϕ_f the phase of the satellite that is chased. Moreover, one has to be careful when solving equation (3.49), as ϕ_f appears in it only through its tangent, which can lead to wrong solutions due to the fact that ϕ_f and $\phi_f + \pi$ have the same tangent but solutions using $\phi_f + \pi$ do not result in the desired rendez-vous. In addition, equation (3.49) is not numerically convenient when $\phi_f \approx \frac{\pi}{2}$ or $\phi_f \approx \frac{3\pi}{2}$ (as in these cases $\cos\phi_f < \epsilon$). We can simply use the equation for the cotangent of ϕ_f, instead of the tangent, when necessary,

$$\mathrm{cotg}\phi_f = -\frac{A_x^{(i)} \cos(2\Phi_t + \phi_i)\sin(\Phi_t + \phi_i) - \Delta A_x \sin(\Phi_t)}{A_x^{(i)} \sin(2\Phi_t + \phi_i)\sin(\Phi_t + \phi_i) + \Delta A_x \cos(\Phi_t)}.$$

On the other hand, we have seen that it is possible to perform independent phase and amplitude changes in the out-of-plane direction, in order to plan a rendez-vous. However, a power expansion method like the one used for xy maneuvers can also be developed in this case.

Let us define $\Delta A_z = A_z^{(f)} - A_z^{(i)}$. By proceeding analogously than for the xy case we have that,

$$\alpha_z(t; A_z^{(i)}, \Delta A_z) = \frac{\Delta \dot{z}}{\nu} \approx 2A_z^{(i)} \sin(\nu t + \psi_i) + \frac{\Delta A_z}{\sin(\nu t + \psi_i)}. \tag{3.50}$$

So, by using the expressions,

$$A_5^f = A_z^{(f)} \cos(\psi_f) \quad \text{and} \quad A_6^f = -A_z^{(f)} \sin(\psi_f)$$

and,

$$A_5^f = A_z^{(i)} \cos(\psi_i) - \frac{\Delta \dot{z}}{\nu} \sin(\nu t) \quad \text{and} \quad A_6^f = -A_z^{(i)} \sin(\psi_i) + \frac{\Delta \dot{z}}{\nu} \cos(\nu t),$$

we finally get that,

$$\text{tg}\,\psi_f = -\frac{A_z^{(i)} \sin(2\nu t + \psi_i) \sin(\nu t + \psi_i) + \Delta A_z^{(i)} \cos(\nu t)}{A_z^{(i)} \cos(2\nu t + \psi_i) \sin(\nu t + \psi_i) - \Delta A_z^{(i)} \sin(\nu t)}. \tag{3.51}$$

Same comments as for equation (3.48) apply here, concerning the initial and final amplitudes and phases. When ψ_f is close to $\frac{\pi}{2}$ or $\frac{3\pi}{2}$, the alternative equation for the computation of the maneuver time is the following,

$$\text{cotg}\,\psi_f = -\frac{A_z^{(i)} \cos(2\nu t + \psi_i) \sin(\nu t + \psi_i) - \Delta A_z^{(i)} \sin(\nu t)}{A_z^{(i)} \sin(2\nu t + \psi_i) \sin(\nu t + \psi_i) + \Delta A_z^{(i)}}.$$

Both equation (3.49) and equation (3.51) are transcendental equations, and therefore iterative numerical methods are needed to solve them.

Comparison between the two strategies for rendez-vous with amplitude change

The method that has been developed in the previous section for simultaneous amplitude and phase changes is valid as long as the amplitude change is small. Consequently, in terms of costs and times it is essentially the same as the rendez-vous without amplitude change, being the cost proportional to the initial amplitude and maximum when the initial phases of the satellites are opposed, i.e. $\phi_f = \phi_i + \pi$ (see figure 3.31, which shows the costs of changing from an amplitude of 100000 km to 100125 km depending on the difference in the phases at $t = 0$ and compare it to figure 3.25, which corresponds to the same phase changes but with no amplitude change).

On the other hand, given a couple of amplitudes A_1 and A_2, with $A_1 > A_2$, the optimal amplitude reduction from A_1 to A_2 has exactly the same cost as the optimal amplitude enlargement from A_2 to A_1 (because this cost is proportional to $|A_1 - A_2|$, see section 3.6). However, once in the final orbit, the smaller the amplitude the cheaper the phase change maneuvers of the EPP rendez-vous. Therefore, if the final orbit is the one with the smallest amplitude, the rendez-vous becomes globally cheaper. This is the reason why the maneuvers with negative % of amplitude change in tables 3.4 and 3.5 are always cheaper than the ones with positive %.
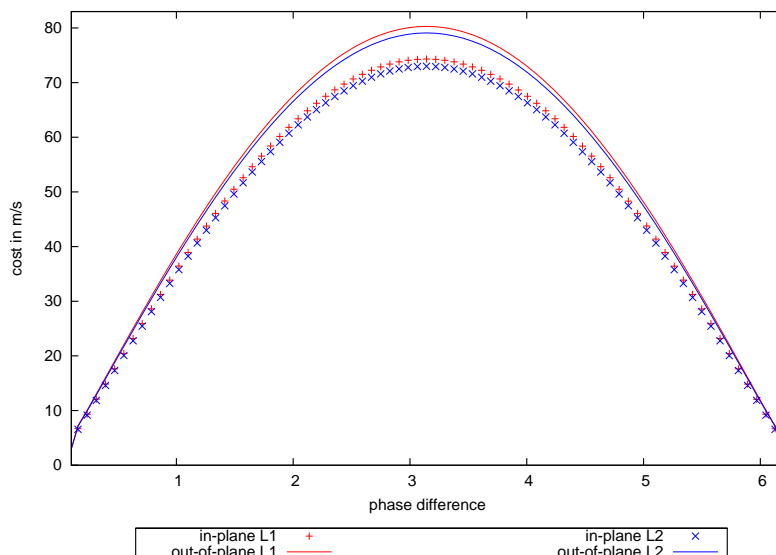
Figure 3.31: Cost of the simultaneous maneuvers of phase and amplitude change for the rendez-vous. The original orbit is a square Lissajous with amplitudes $A_y = A_z = 10^5$ km, and the amplitude change is an enlargement of the 1%. In the x axis of the figure the initial differences in phases are represented, while the y axis contains the costs of the rendez-vous in m/s.

Moreover, if the amplitudes are substantially different, independent amplitude and phase changes have to be applied. The total final cost can be computed by adding the optimal amplitude change cost (see section 3.6) and the EPP rendez-vous cost (see section 3.7.1). However, one has to take into account that when performing in-plane amplitude change maneuvers, stable hyperbolic terms may appear, placing the satellite in the stable manifold of the final Lissajous rather than on the orbit itself. Consequently, the phase change maneuver has to be planned at some time in the future when this aforementioned exponentially decreasing term will have vanished.

To sum up, when both amplitudes are very close to each other and the rendez-vous essentially requires a change in the phases, simultaneous amplitude and phase change maneuvers are advisable. Among the advantages of using the simultaneous change strategy we have the obvious simplicity of performing one maneuver instead of two maneuvers at different times, and the fact that the problems yielding from the hyperbolic stable terms that appear when changing the in-plane amplitude are avoided when performing a single maneuver. On the contrary, when the amplitudes of the Lissajous orbits are quite different, independent maneuvers have to be applied for amplitude and phase change.

As a general rule, it is better in terms of cost to use the maneuver which simultaneously changes amplitude and phase is better than performing two independent maneuvers, when both strategies are possible. However, when the Lissajous in which the rendez-vous takes place is the biggest, independent changes may be slightly cheaper for small values of $\Delta\phi$. This fact is a natural consequence of the transfer being essentially a change of amplitudes when the phase change is small. See tables 3.4 and 3.5 for examples of the cost of rendez-vous maneuvers with amplitude change.

$\Delta\phi$ (rad)	ΔA_x (%)	Independent A_x and ϕ change		Simultaneous A_x and ϕ change	
		L_1	L_2	L_1	L_2
$\frac{\pi}{3}$	-5	37.12	36.47	30.12	29.57
	-2.5	37.12	36.48	33.67	33.07
	-1	37.13	36.47	35.80	35.17
	1	37.87	37.20	38.40	37.72
	2.5	38.98	38.30	40.22	39.51
	5	40.75	40.12	43.25	42.48
π	-5	72.40	71.13	72.41	71.13
	-2.5	73.33	73.32	73.34	72.04
	-1	73.89	72.59	73.29	72.59
	1	75.38	74.05	74.64	73.32
	2.5	77.04	75.69	75.19	73.87
	5	79.83	78.43	76.11	74.78

Table 3.4: Cost (in m/s) of the rendez-vous and in-plane amplitude change maneuvers for an initial orbit of $A_x^{(i)} = 31375.5$ km (that is $A_y^{(i)} = 10^5$ km) and different % of amplitude change. The two strategies (simultaneous or separate maneuvers) are compared for two different values of the phase change, $\Delta\phi$. (The cost of the maneuvers depends on the initial amplitude in a linear way, thus costs for different $A_x^{(i)}$ can be easily computed).

$\Delta\psi$ (rad)	ΔA_z (%)	Independent A_z and ψ change		Simultaneous A_z and ψ change	
		L_1	L_2	L_1	L_2
$\frac{\pi}{3}$	-5	40.12	39.51	32.55	32.04
	-2.5	40.12	39.51	36.38	35.83
	-1	40.12	39.52	38.68	38.10
	1	40.92	40.31	41.49	40.87
	2.5	42.12	41.50	43.45	42.81
	5	44.13	43.47	46.73	47.64
π	-5	78.23	77.06	78.24	77.07
	-2.5	79.24	78.05	79.24	78.05
	-1	79.84	78.64	79.84	78.65
	1	81.45	80.23	80.64	79.44
	2.5	83.25	82.01	81.25	80.03
	5	86.26	84.98	82.25	81.02

Table 3.5: Cost (in m/s) of the rendez-vous and out-of-plane amplitude change maneuvers for an initial orbit of $A_z^{(i)} = 10^5$ km and different % of amplitude change. The two strategies (simultaneous or separate maneuvers) are compared for two different values of the phase change, $\Delta\psi$. (As for the in plane case, the cost of the maneuvers depends on the initial amplitude in a linear way, thus costs for different $A_z^{(i)}$ can be easily computed).

Chapter 4

Homoclinic and heteroclinic connections between planar Lyapunov orbits

4.1 Introduction

The introduction of invariant manifolds as a means to describe the phase space around the equilibrium points L_1 and L_2 of the restricted three body problem results in more efficient and adaptable techniques for mission analysis. Furthermore, invariant manifolds can be seen as tubes which dominate the dynamics and mass transport in the Solar System. In this context, a good knowledge of the natural transport channels that exist between the collinear points of the RTBP can help understanding and using the interactions between the celestial bodies. As an example of practical application, these natural channels have already been used in the Genesis mission, with a Δv saving of almost 100 m/s (see for instance [53], [3]).

The instability of the collinear libration point regions justifies the existence of hyperbolic invariant manifolds associated with the libration point orbits. An unstable invariant manifold can be regarded as a dynamical tube arising from the orbit and going away from it exponentially fast in forward time. On the contrary, stable manifolds approach the orbit also exponentially fast in forward time (or leave in backward time). Consequently, when an intersection between an unstable manifold and a stable one exists, it provides an asymptotic path going away from a libration orbit and approaching another one. If both manifolds belong to the same orbit, this asymptotic path is called homoclinic connection. When the intersecting manifolds belong to different orbits, the trajectories joining them are called heteroclinic connections ([27], [25], [56]).

In this chapter, a methodology aimed at finding and classifying homoclinic and heteroclinic connections in the Planar Restricted Three Body problem, which provide cheap transfers from one libration point to another, is developed. Results are presented for the Sun-Earth and Earth-Moon systems.

4.2 Methodology

We use the planar restricted three body problem to model the Earth-Moon and Sun-Earth systems. A detailed description of this model, its equations of motion and other comments such as its Hamiltonian character can be found in chapter 2. However, some ideas on the computation of the orbits and manifolds that are used in the present chapter are reviewed in the following sections.

4.2.1 Lyapunov orbits

In the planar restricted three body problem, there exists only one planar periodic motion around L_i ($i = 1, 2$) for each given energy level: the planar Lyapunov orbit. These are the orbits we use to find natural transport channels between L_1 and L_2. The use of planar Lyapunov orbits is convenient for several reasons. Obviously, the complexity of the problem is reduced when using the planar approximation, because the order of the system, as well as the dimension of the manifolds and their intersections is smaller than for the spatial problem. In addition, it is well known that planar Lyapunov orbits exist also in the 3D restricted three body problem, and they surround the rest of types of orbits in the Poincaré maps like the ones shown in chapter 2. In fact, the xy projection of hyperbolic manifolds belonging to other libration orbits (Lissajous or Halo orbits, for instance) is actually contained in the manifolds of the Lyapunov orbits of the corresponding energy level. Therefore, using these planar orbits is a natural way of studying the channels in the libration regions.

Furthermore, planar Lyapunov orbits and their hyperbolic manifolds can be computed using Lindstedt-Poincaré procedures. In this way, their expansions are obtained in convenient RTBP coordinates. As usual, we set the origin of coordinates at the libration point (L_1 or L_2) and scale the variables in such a way that the distance from the equilibrium point to the small primary is equal to one. The expansion of the equations of motion in these variables (x, y) takes the form,

$$\begin{cases} \ddot{x} - 2\,\dot{y} - (1 + 2c_2)\,x &= \dfrac{\partial}{\partial x} \sum_{n \geq 3} c_n \rho^n P_n \left(\dfrac{x}{\rho} \right), \\[2mm] \ddot{y} + 2\,\dot{x} + (c_2 - 1)\,y &= \dfrac{\partial}{\partial y} \sum_{n \geq 3} c_n \rho^n P_n \left(\dfrac{y}{\rho} \right), \end{cases} \tag{4.1}$$

where $\rho^2 = x^2 + y^2$, P_n is the Legendre polynomial of degree n, and c_n are constants which depend only on μ and the selected equilibrium point (see chapter 2, section 2.3). Note that in (4.1) the linear terms appear in the left hand side part of the equations and the nonlinear ones in the right hand side. The solution of the linear part of equations (4.1) is:

$$\begin{aligned} x_l(t) &= A_1 e^{\lambda t} + A_2 e^{-\lambda t} + A_x \cos(\omega t + \phi), \\ y_l(t) &= c A_1 e^{\lambda t} - c A_2 e^{-\lambda t} + \kappa A_x \sin(\omega t + \phi) \end{aligned} \tag{4.2}$$

where κ, c, ω and λ are constants for a given model and libration point (see equation (3.3)).

The A's are free amplitudes. A_1 and A_2 are the ones associated with the hyperbolic manifolds. If $A_1 = A_2 = 0$, we have the linear part of the Lyapunov orbit with amplitude A_x. When $A_1 = 0$ and $A_2 \neq 0$ we have orbits tending to the Lyapunov orbit of amplitude A_x when time tends to infinity (stable manifold). On the contrary when $A_x = 0$ and $A_1 \neq 0$, orbits leave the vicinity

of the Lyapunov exponentially fast in forward time (unstable manifold). When we consider also the non-linear terms of (4.1), solutions are obtained by means of formal series in powers of the amplitudes of the form:

$$\begin{array}{rcl}
x(t) & = & \sum e^{(i-j)\theta_2}[x_{ijk}^p \cos(p\theta) + \bar{x}_{ijk}^p \sin(p\theta)]A_1^i A_2^j A_x^k \\
y(t) & = & \sum e^{(i-j)\theta_2}[y_{ijk}^p \cos(p\theta) + \bar{y}_{ijk}^p \sin(p\theta)]A_1^i A_2^j A_x^k
\end{array} \tag{4.3}$$

where $\theta = \omega t + \phi$, $\theta_2 = \lambda t$ and,

$$\omega = \sum \omega_{ijk} A_1^i A_2^j A_x^k, \qquad \lambda = \sum \lambda_{ijk} A_1^i A_2^j A_x^k.$$

Summation is extended over all i, j, k and $p \in \mathbb{N}$. However, due to symmetries, many of the coefficients x_{ijk}^p, $\bar{x}_{ijk}^p$, y_{ijk}^p, $\bar{y}_{ijk}^p$, ω_{ijk}, λ_{ijk} are zero. Moreover the series are truncated at a certain (high) order (see [60] for more details).

It is important to note that the meaning of the amplitudes in the nonlinear expansions (4.3) is the same one as in the linear solutions (4.2). This fact makes Lindstedt- Poincaré set of coordinates (amplitudes and phases) suitable for our purposes, as it provides them with a clear physical meaning.

4.2.2   Fixed energy surfaces

The expression of the Jacobi constant at a given point $(x, y, \dot{x}, \dot{y})$ is,

$$\mathcal{C}(x, y, \dot{x}, \dot{y}) = -(\dot{x}^2 + \dot{y}^2) + 2\,\Omega(x, y) \tag{4.4}$$

where $\Omega(x, y) = \frac{1}{2}(x^2 + y^2) + \frac{1-\mu}{r_1} + \frac{\mu}{r_2}$ and r_1, r_2 the distances between (x, y) and the primaries, m_1 and m_2. It is easily proved that $\mathcal{C} = -2\,H$, where H is the Hamiltonian function of the RTBP, as explained in chapter 2. Therefore, the Jacobi constant is an integral of the motion in the restricted three body problem. That is to say that it remains constant on the orbits $\gamma(t) = \{(x(t), y(t), \dot{x}(t), \dot{y}(t)),\ t \in \mathbb{R}\}$, which are a solution of equations (4.1).

On the other hand, the number of degrees of freedom in the planar restricted three body problem is $n = 2$. Thus, the order of the system is $2n = 4$, which is reducible by the Jacobi constant to 3. That is to say that as $\mathcal{C}$ does not vary along the solutions, we have to study only 3 of the four coordinates of the phase-space for each orbit, obtaining the fourth one from equation (4.4).

The level surfaces of the Jacobi constant in the planar problem are called energy surfaces, three dimensional manifolds implicitly defined by equation (4.4) on which we can look for solutions of the PRTBP.

$$\mathcal{M}(\mu, \mathcal{C}_*) = \{(x, y, \dot{x}, \dot{y}) \mid \mathcal{C}(x, y, \dot{x}, \dot{y}) = \mathcal{C}_*\}$$

We use a particular range of Jacobi constants, $[\mathcal{C}_{min}, \mathcal{C}_{max}]$, which depends on the system we are modelling and on the libration point we are dealing with. As the value of $\mathcal{C}$ increases, the amplitude of the corresponding Lyapunov orbits becomes smaller, because the zero velocity curves progressively close around L_i. Actually, when the expression in equation (4.4) is evaluated exactly on a libration point, and a value of the Jacobi constant is obtained which we call $\mathcal{C}_{L_i}$, the zero velocity curves of the corresponding energy level collapse on L_i. Therefore, $\mathcal{C}_{L_i}$ corresponds to the

absolute maximum of usable values of $\mathcal{C}$. On the other hand, the values $\mathcal{C}_{min}$ that we use are found when the Lindstedt-Poincaré series no longer provide accurate results when truncated at order 15. That is, when the norm of the difference between evaluating given Lindstedt-Poincaré series at a particular moment of time and the integration of the same series over the same time span (typically one period of revolution of the primaries) is bigger than 10^{-6} in RTBP adapted units. If we wanted to work with smaller $\mathcal{C}$, we would have to use other semi analytical techniques, such as normal form expansions ([49]), or numerical continuation methods. However, for Lyapunov orbits, Lindstedt-Poincaré expansions provide good results even for amplitudes which are already too big in terms of practical interest. Therefore, the $\mathcal{C}_{min}$ that yields from the aforementioned criteria of series accuracy is enough for the purposes of this work. Consequently, only Lindstedt Poincaré expansions have been used for describing the Lyapunov orbits and their manifolds, as they are associated with coordinates that have a clear physical meaning.

To sum up, despite the fact that the range of Jacobi constants we work with may seem small, it allows the A_x amplitudes of the Lyapunov orbits to experiment a significant variation (from almost zero up to a 370×10^5km for the Sun-Earth case and 17000 km for the Earth-Moon one). See figure 4.1, where Lyapunov orbits for the usable $\mathcal{C}$ are depicted. As the Jacobi constant increases, the corresponding amplitudes decrease and the other way round. Moreover, in table 4.1 the values of the maximum and minimum Jacobi constants, as well as maximum and minimum corresponding A_x amplitudes of the Lyapunov orbits, are shown. Remember that the amplitude A_y is obtained by multiplying A_x by $\bar{k}$, which has a value of around 3.2. Therefore, the biggest possible amplitudes of the Lissajous orbits are associated with huge excursions in the y direction, which makes them rarely suitable for applications. On the other hand, the smallest amplitudes shown in the aforementioned table correspond to tiny orbits which would present operational problems such as expensive station keeping or eclipse avoidance strategies. Consequently, interest should be mainly focused on the central range of Jacobi constants and amplitudes.
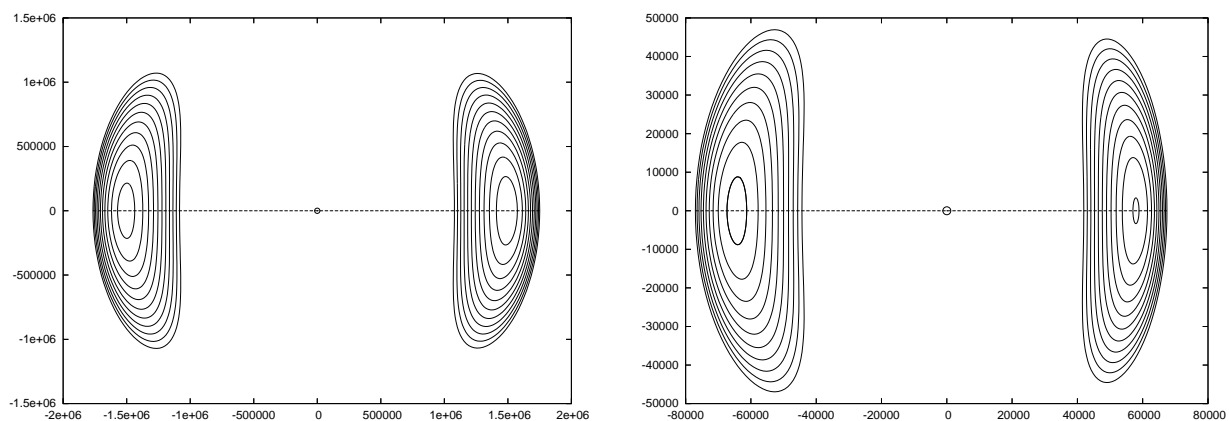
Figure 4.1: xy representation of Lyapunov orbits for the range of usable $\mathcal{C}$. Sun-Earth (left) and Earth-Moon (right) cases. The small circle in the center of the figures represents the position of the Earth and Moon respectively (not to scale).

	Sun-Earth	$\mu = 0.30404234\ 10^{-5}$	Earth-Moon	$\mu = 0.012150582$
	$\mathcal{C}_{min}$	$\mathcal{C}_{max}$	$\mathcal{C}_{min}$	$\mathcal{C}_{max}$
Homoclinic L_1	3.0007222915	3.00090098	3.149305	3.20034403
Homoclinic L_2	3.00072105	3.0008969275	3.14445	3.184163
	A_{max}	A_{min}	A_{max}	A_{min}
Homoclinic L_1	359019.1	1081.9	12661.6	100.6
Homoclinic L_2	366122.8	548.3	17258.1	50.3

Table 4.1: Range of usable Jacobi constants and corresponding A_x amplitudes (in km) of the Lyapunov orbits. The mass parameters in the Sun-Earth and Earth-Moon cases are obtained from JPL ephemeris DE403.

4.2.3   KS-Regularisation

The distance from the infinitesimal mass to both the primary bodies appears as a denominator in the RTBP equations. Therefore, when the small particle approaches one of the big primaries, the denominator tends to zero and a numerical problem of tiny denominators has to be faced. Approaching the big primary (m_1) is not a problem to be taken into account if we work in L_1 and L_2 regions. However, the distance to the small primary (namely the Earth in the Sun-Earth system and the Moon, in the Earth-Moon one) can become very small at some points, with the consequent computational problems due to this singularity. We have used a well known Regularisation method introduced by Levi-Civita (2-D) and Kustanheimo in order to overcome this drawback (see [78], [50]).

In a first step, the generalised Levi-Civita regularisation consists of introducing a new independent variable, s, to act as a fictitious time, such that $\frac{d}{dt} = \frac{1}{r}\frac{d}{ds}$ (where r is the distance to the primary which tends to be close to 0. In our case, the distance to the small primary). Therefore, as $\frac{dt}{ds} = r$, the physical time t becomes a coordinate-like variable and varies slowly in the vicinity of $r = 0$.

As for the position and velocity coordinates, the 2D Levi Civita regularisation uses the squaring technique, namely a vector $u \in \mathbb{R}^2$ such that $r = \sqrt{x^2 + y^2} = |u|^2 = u_1^2 + u_2^2$ and $x = u_1^2 - u_2^2$, $y = 2u_1 u_2$. In 3D, a vector $u \in \mathbb{R}^4$ must be introduced and the matrix,

$$L(u) = \begin{pmatrix} u_1 & -u_2 & -u_3 & u_4 \\ u_2 & u_1 & -u_4 & -u_3 \\ u_3 & u_4 & u_1 & u_2 \\ u_4 & -u_3 & u_2 & -u_1 \end{pmatrix},$$

leads to the KS transformation: $X = L(u)u$, $X = ((x_1, x_2, x_3, 0) \in \mathbb{R}^4$ Note that the upper left 2×2 matrix is indeed the original Levi-Civita matrix. In addition, X refers to the position coordinates of the infinitesimal particle in a coordinate system centred at the small primary, such that $r = \sqrt{x_1^2 + x_2^2 + x_3^2}$.

If yields from $X = L(u)u$ that,

$$
\begin{aligned}
x_1 &= u_1^2 - u_2^2 - u_3^2 + u_4^2, \\
x_2 &= 2u_1u_2 - 2u_3u_4, \\
x_3 &= 2u_1u_3 + 2u_2u_4, \\
x_4 &= 0
\end{aligned}
\tag{4.5}
$$

The inverse transformation, from X to u, is

$$
u_2^2 + u_3^2 = \frac{1}{2}(r - x_1)
\tag{4.6}
$$

$$
u_1 = \frac{x_2u_2 + x_3u_3}{r - x_1}
$$

$$
u_4 = \frac{x_3u_2 - x_2u_3}{r - x_1},
$$

if $x_1 < 0$ and,

$$
u_1^2 + u_4^2 = \frac{1}{2}(r + x_1)
\tag{4.7}
$$

$$
u_2 = \frac{x_2u_1 + x_3u_4}{r + x_1}
$$

$$
u_3 = \frac{x_3u_1 - x_2u_4}{r + x_1},
$$

if $x_1 > 0$.

In our case, if (x, y, z) are the position coordinates of the small particle in the RTBP coordinate frame centred at L_1 and normalised so that the distance from L_1 to the small primary is equal to 1, we have that,

$$
x_1 = x - 1, \quad x_2 = y, \quad x_3 = z.
$$

For the L_2 case, the only difference is $x_1 = x + 1$.

As for the velocity vectors, we apply the already defined relationship between the derivatives with respect to t and s ($\dot{x}_i = \frac{dx_i}{dt} = \frac{1}{r}\frac{dx_i}{ds} = \frac{1}{r}x_i'$) on the equations in (4.5) and we obtain,

$$
\begin{aligned}
\dot{x} &= \frac{2}{r}(u_1u_1' - u_2u_2' - u_3u_3' + u_4u_4') \\
\dot{y} &= \frac{2}{r}(u_1u_2' + u_2u_1' - u_3u_4' - u_4u_3') \\
\dot{z} &= \frac{2}{r}(u_1u_3' + u_2u_4' + u_3u_1' - u_4u_2')
\end{aligned}
\tag{4.8}
$$

Respectively, from (4.6), we get,

$$
\begin{aligned}
u_1' &= \frac{1}{2}(u_1\dot{x} + u_2\dot{y} + u_3\dot{z}) \\[4pt]
u_2' &= \frac{1}{2}(-u_2\dot{x} + u_1\dot{y} + u_4\dot{z}) \\[4pt]
u_3' &= \frac{1}{2}(-u_3\dot{x} - u_4\dot{y} + u_1\dot{z}) \\[4pt]
u_4' &= \frac{1}{2}(u_4\dot{x} - u_3\dot{y} + u_2\dot{z})
\end{aligned}
\tag{4.9}
$$

Therefore, when we are integrating a manifold, and we find a point (x, y, z) that approaches the small primary of the system to a distance which is below the permitted one (fixed to around 15000 km for the Earth-Moon system and 50000 km for the Sun-Earth one), we transform the point to u-coordinates. If x is smaller than the x coordinate of the primary, expressions in (4.6) are used for the transformation; respectively, if x is greater than the x coordinate of the primary, we use (4.7). In these expressions, four values of the u_i have to be determined from the three position coordinates (x, y, z). Consequently, we have one degree of freedom which we use for fixing $u_1 = 0$ in (4.6) (respectively $u_2 = 0$ if we use (4.7)). Note that this is not the only possibility, but it is a suitable one. Once we have computed u_i, for $i=1..4$, we can use the expressions in (4.9) to obtain u_i', $i=1..4$.

The idea now is to continue integrating the manifold, in the new coordinates, until a point is reached where the infinitesimal particle is far enough from the primary to use the usual coordinate frame again. However, in order to continue integrating the manifolds in the new coordinate system we need to know the expression of the vectorial field (i.e the system of differential equations of motion) in u coordinates. That is, we need the expression of the second derivatives of u with respect to s. After some computations, using the relation between d/ds and d/dt, we get that

$$
u'' = \frac{h}{2}u + L^T(u)BL(u)u + \frac{(uu)}{2}L^T(u)F^*,
\tag{4.10}
$$

where,

$$
F^*(x, y, z) = \left(\left(x - 1 + \frac{1}{\gamma}\right)\left(\frac{\mu - 1}{r^3} + 1\right) - \frac{\mu}{\gamma}, \ y\left(\frac{\mu - 1}{r^3} + 1\right), \ z\left(\frac{\mu - 1}{r^3}\right), \ 0 \right)^{\mathrm{T}}
$$

$$
h = \Omega(x, y) - \frac{\mu}{r} - 0.5\mathcal{C},
$$

and

$$
B = \begin{pmatrix} 0 & 2 & 0 & 0 \\ -2 & 0 & 0 & 0 \\ 0 & 0 & 0 & 0 \\ 0 & 0 & 0 & 0 \end{pmatrix}.
$$

Note that in the coordinate frame centred at L_i, $\Omega(x, y) = \frac{1}{2}((-\gamma x + \mu - 1 + \gamma)^2 + y^2\gamma^2) + \frac{1-\mu}{r_1} + \frac{\mu}{r} + 0.5\mu(1-\mu)$ (with r_1 the distance to the big primary, and r the distance to the small primary).

Moreover, the expression for F^* depends on (x, y, z), which we can compute from (u_1, u_2, u_3, u_4) at each time step.

Finally, only the equation for the time t, which is now a coordinate-like variable, has to be added to the 4 second order equations obtained from (4.10) to complete the field in the new coordinates. It is straightforward from the definition of s that

$$t' = \frac{dt}{ds} = r = u_1^2 + u_2^2 + u_3^2 + u_4^2.$$

By using this regularisation, and applying it to the integration of the RTBP vector field, we enhance the global adaptation of the model to the problem. This is to say, we are able to consider the set of solution orbits which travel close to the Earth (for the Sun-Earth case) or close to the Moon (for the Earth-Moon case). The distances at which this change of coordinates was used were of around 15000 km from the Moon center (for the Earth-Moon problem, remember that the radius of the Moon is less than 2000 km), and less than 100000 km from the Earth center for the Sun-Earth problem (radius of the Moon approximately 6700 km). These orbits, indeed, might as well be the most important in terms of practical applications for spatial missions; for instance: injection, phasing loops or reentry.

4.2.4   Homoclinic and heteroclinic phenomena

As stated in section 4.2.1, for a given energy level there is a unique planar Lyapunov orbit homeomorphic to S^1, around each libration point (L_1 and L_2). As the phase space near these points has a saddle component, there are orbits asymptotically approaching the Lyapunov in forward time (stable manifolds) and orbits leaving it as well (unstable manifold). These manifolds are two dimensional in $\mathcal{M}(\mu, \mathcal{C})$ (for details see [48]).

Assume that an intersection is found between the stable manifold associated with a Lyapunov orbit and the unstable manifold of another one. Due to the uniqueness of solutions of a system of ordinary differential equations, an intersection in the complete state space implies that the part of the trajectory belonging to the unstable manifold and the one belonging to the stable manifold are indeed the same solution. That is to say that from each intersection between the manifolds, a trajectory is obtained which asymptotically approaches a Lyapunov orbit both in forward and in backward time. Consequently, this trajectory acts as a zero cost natural transfer between Lyapunov orbits. If the aforementioned manifolds belong to the same orbit, the transfer is called homoclinic connection. On the contrary, if the manifolds are associated with different Lyapunov orbits, transfer trajectories are called heteroclinic connections. In this part of our work, connections are found between orbits laying in the same energy level of the planar RTBP. Consequently, only one periodic orbit exists around each one of the libration points. Therefore, the connections we find will only be heteroclinic when they travel from the vicinity of one of the libration points to the vicinity of the other one (from L_1 to L_2 or the other way round).

Poincaré section

Homoclinic and heteroclinic connections between planar Lyapunov orbits can be found by means of a Poincaré section. As it is well known, Poincaré sections are used to study dynamical systems

by observing their flow when crossing a given surface or plane. These crossings have a lower dimension than the complete state space. Nevertheless, they still provide useful information about the behaviour of the system.

For a given $\mathcal{M}(\mu, \mathcal{C})$, we use the following Poincaré section $\mathcal{S}$,

$$\mathcal{S} = \{(x, y, \dot{x}, \dot{y}) \in \mathcal{M}(\mu, \mathcal{C}) \mid x = -1 + \mu\}.$$

Furthermore, a positive integer, k, is chosen. Then, initial conditions which lay in the invariant stable (respectively unstable) manifolds of the corresponding Lyapunov orbit are integrated until the trajectory has crossed the section k times. After these crossings, we have the representation of the k-cut between the manifold and the section.

As we have already explained, Lyapunov planar orbits are S^1 like objects. The manifolds which arise from them are like tubes in the phase space. So, they result in curves when intersected with a transversal section, $\mathcal{S}$. We will write $W_i^{(u/s),j}$ standing for the j-th intersection of the $W^{u/s}$ (unstable or stable invariant manifold) of the Lyapunov orbit around L_i with $\mathcal{S}$. Depending on the initial phase and the Jacobi constant, some orbits escape to the exterior region (see figure 4.2) or collide with the small primary (Earth or Moon) after a certain number of cuts. If an escape or collision occurs, the structure of S^1 is broken. That is to say that not all $W_i^{(u/s),j}$ will be S^1-like objects, especially as j increases. We must mention here that in this work the word collision is used when an orbit approaches the point-mass Earth or Moon within a distance slightly bigger than their respective real radii.
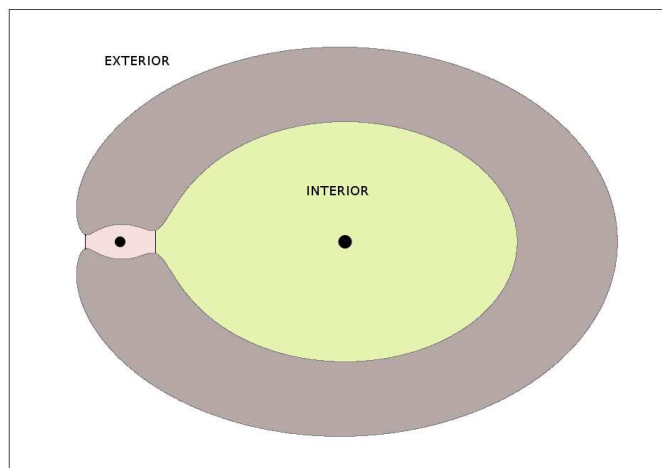
Figure 4.2: Regions defined by the zero velocity curves: In green the interior region, around the big primary. In pink, the region surrounding the small primary, connected to the interior region by L_1 and to the exterior region by L_2.

Once we have $W_i^{(u/s),j}$ on $\mathcal{S}$, it is convenient to look at it as a curve in the $(y, \dot{y})$ plane. In $\mathcal{S}$, x is fixed and $\dot{x}$ can be computed using equation (4.4). In fact, $|\dot{x}|$ is determined by the Jacobi constant, but not its sign. We need to keep in mind which is the direction of the manifolds we intersect in order to avoid problems when defining the mentioned sign across $\mathcal{S}$. Thus, a point $(y_0, \dot{y}_0)$ is enough to obtain a complete state in $\mathbb{R}^4$, for a given energy level $\mathcal{M}(\mu, \mathcal{C})$, once we know

how to choose the sign for the $\dot{x}$ component. Moreover, as the coordinates we are working with give the system an autonomous character, each point in the phase space $(x, y, \dot{x}, \dot{y})$ determines one and only one orbit or solution to equations (4.1).
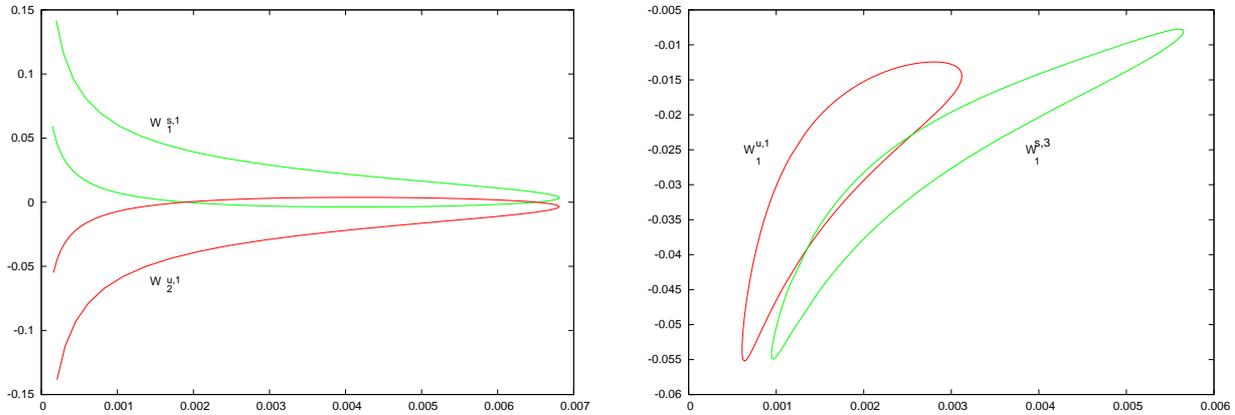
Figure 4.3: Representation of some cuts of invariant manifolds on the Poincaré section for the Sun-Earth problem. (left) $\mathcal{C} = 3.00084$, $W_1^{u,1} \cap W_2^{s,1} \neq \emptyset$, first cut with $\mathcal{S}$ of the stable manifold around the L_2 Lyapunov orbit (green) and the first cut with the same section of the unstable manifold of the Lyapunov orbit around L_1 (red). From this intersection, two heteroclinic connections are obtained. (right) $\mathcal{C} = 3.00088$ First cut on $\mathcal{S}$ of the unstable manifold of the Lyapunov orbit around L_1 (red) and third cut of the stable manifold of the same Lyapunov orbit (green), $W_1^{u,1} \cap W_1^{s,3} \neq \emptyset$. From this picture, two homoclinic connections are obtained.

Intersections on the Poincaré section

Different types of intersections between the cuts of the manifolds give rise to different types of connections:

1. Homoclinic connections around L_i, when $W_i^{u,j_1} \cap W_i^{s,j_2} \neq \emptyset$, with $i = 1$ or 2.

2. Heteroclinic connections from L_1 to L_2, when $W_1^{u,j_1} \cap W_2^{s,j_2} \neq \emptyset$.

3. Heteroclinic connections from L_2 to L_1, when $W_2^{u,j_1} \cap W_1^{s,j_2} \neq \emptyset$.

(see figure 4.3 to see how these intersections look like on $\mathcal{S}$).

If a point $(y_0, \dot{y}_0)$ belongs to one of these intersections, we can complete it by finding x_0 using the expression of $\mathcal{S}$, and $\dot{x}_0$ using the value of $\mathcal{C}$. Then, this point belongs to a trajectory which asymptotically approaches a Lyapunov orbit (as it belongs to a stable manifold) and that has left the vicinity of another Lyapunov orbit (because it also belongs to an unstable manifold). Due to the unicity of the solutions of a system of ODEs, these two trajectories on the manifolds have to be the same one. Therefore, $(x_0, y_0, \dot{x}_0, \dot{y}_0)$ represents a zero cost transfer between the Lyapunov orbits associated with the manifolds. We obtain the transfer trajectory by integrating the intersecting point forwards and backwards on the invariant stable and unstable manifolds respectively.

On the other hand, a natural way of classifying the connections consists of counting how many times they go around the small primary, the Earth or the Moon in our case. If j_1 stands for the number of cuts of the unstable manifold with $\mathcal{S}$ and j_2 the number of cuts of the stable manifold with the same section, the total number of loops is $(j_1 + j_2 - 1)/2$ for homoclinic trajectories and $(j_1 + j_2 - 2)/2$ for heteroclinic ones. This provides a parity criterion for the total number of times the Poincaré section is crossed by every connection:

$$\#\text{cuts}\ \ \text{with}\ \ \mathcal{S} = \kappa = j_1 + j_2 - 1,$$

which has to be even for homoclinic trajectories and odd for heteroclinic ones.

We use the following notation:

- Ho_i^n (n-homoclinic orbits). Homoclinic trajectory of a Lyapunov orbit around L_i, $i = 1$ or 2, with a total number of loops around the small primary m_2 equal to n (all of them travel around m_2 in the counterclockwise direction).

- He_{i_1, i_2}^n. Heteroclinic trajectory from a Lyapunov orbit around L_{i_1} to a Lyapunov orbit around L_{i_2} winding around the small primary n times. This includes all heteroclinic connections obtained as $W_{i_1}^{j_1} \cap W_{i_2}^{j_2}$ with $(j_1 + j_2 - 2)/2 = n$.

4.2.5   Details on the numerical methodology

The numerical process for finding homoclinic and heteroclinic connections can be splitted in two parts:

1. Integration of the manifolds arising from the Lyapunov orbits until they have intersected the Poincaré section a chosen number of times, resulting in the curves $\text{W}_i^{u/s,j}$.

2. Computation of the intersections between the cuts of asymptotic manifolds in the Poincaré section: $\text{W}_{i_1}^{u/s,j_1} \cap \text{W}_{i_2}^{u/s,j_2}$.

Integration of the manifolds

Lyapunov orbits are planar periodic solutions of equations (4.1) with $A_1 = A_2 = 0$, as they do not contain exponential hyperbolic terms. Their planar amplitude, A_x, depends on $\mathcal{C}$ (for each energy surface there is one and only one A_x, as there is a unique Lyapunov periodic orbit). In order to take initial conditions on the unstable (respectively stable) manifolds we set $A_1 = \epsilon$ and $A_2 = 0$ (respectively $A_1 = 0$, $A_2 = \epsilon$). ϵ is a small parameter whose sign indicates towards which branch of the manifold we integrate. Moreover, the phase θ in the aforementioned expansions can be interpreted as the parametrisation of the Lyapunov orbit (see figure 4.4).

For example, if we want to obtain the second cut of the unstable invariant manifold associated to the Lyapunov orbit around L_1 for a given value of $\mathcal{C}$, $\text{W}_1^{u,2}$, we have to set $A_1 = +\epsilon$, $A_2 = 0$ and $A_x = A_x(\mathcal{C})$. In addition, a discreetisation of θ is taken in $[0, 2\pi]$. Finally, the set of initial conditions that we integrate to the second cut with $\mathcal{S}$ is,

$$(\epsilon,\ 0,\ A_x, \theta_i),\ \ i = 1, n.$$
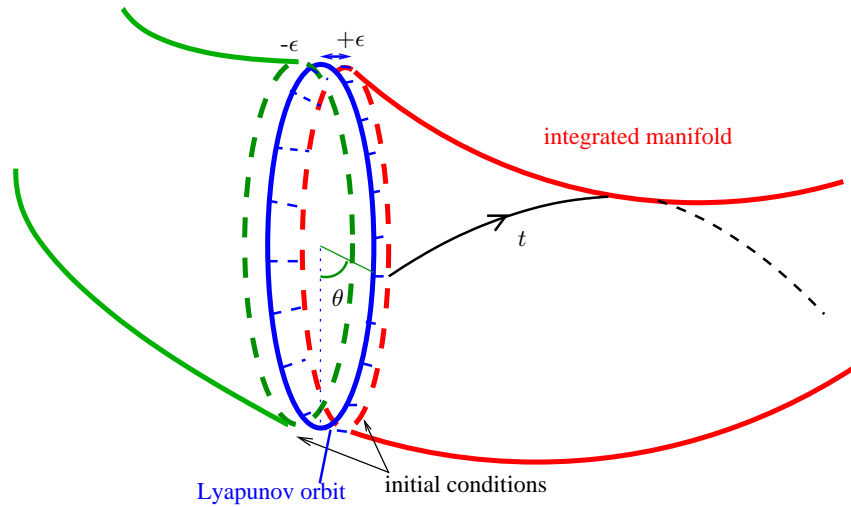
Figure 4.4: Schematic representation of a Lyapunov orbit and the hyperbolic manifolds associated to it. Depending on the sign of ϵ, the 'left' or the 'right' branch of the manifolds is integrated.

The bunch of orbits launched by these kind of initial conditions form manifold tubes like the ones schematically represented in figure 4.4. As the Poincaré section is $\{x = \mu - 1\}$, the number of cuts with the section can be easily controlled by studying the sign of $(x(t) + 1 - \mu)$. Once this expression has changed k times from positive to negative or the other way round, the k-cut is refined using for instance the Newton method on $f(t) = x(t) - 1 + \mu$.

Computation of the intersections between the cuts of asymptotic manifolds in the Poincaré section.

Given two different manifold cuts in the Poincaré section, $W_{i_1}^{u,j_1}$ and $W_{i_2}^{s,j_2}$, we think of them as smooth curves. However, we know by the discreetisation taken in the initial conditions that they are actually polygons with $n+1$ sides. Therefore, we can easily check for intersections between segments belonging to one of the manifold cuts and segments which form the sides of the other manifold cut (see figure 4.5).

When an intersection between the aforementioned segments has been detected, it is refined in the phase parameter (θ) of the Lyapunov orbits up to the required order of precision. Assume that a cut occurs between the segments whose extremes are the integrated points defined by the initial phases $(\theta_i^s, \theta_{i+1}^s)$ and $(\theta_j^u, \theta_{j+1}^u)$ on the corresponding stable and unstable manifolds. Then, we can parametrise these segments by:

$$\left. \begin{array}{rcl} \theta^s(\lambda) & = & \theta_i^s(1-\lambda) + \theta_{i+1}^s\lambda \\ \theta^u(\alpha) & = & \theta_j^u(1-\alpha) + \theta_{j+1}^u\alpha \end{array} \right\}$$

and find the values α^* and λ^* such that $\theta^s(\lambda^*) = \theta^u(\alpha^*)$. Afterwards, the initial conditions
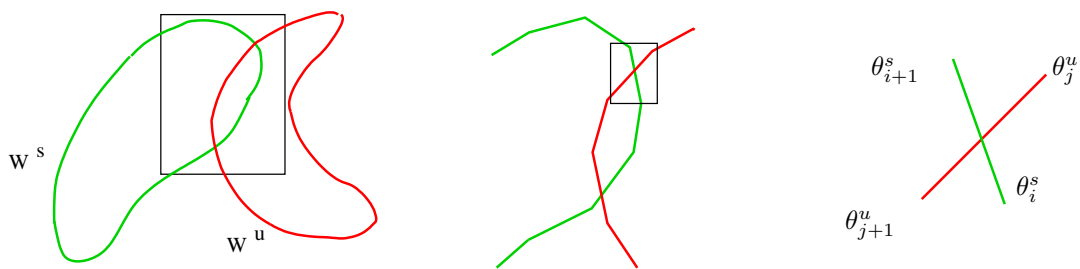
Figure 4.5: Schematic representation of the curves representing the cuts of an unstable and a stable manifold on the Poincaré section, and detail of the intersecting region. Intersections between the curves are found by comparing the segments forming them.

defined by $\theta^s(\lambda^*)$ and $\theta^u(\alpha^*)$ are integrated to the corresponding cut with the section, allowing us to obtain 4 new segments on $\mathcal{S}$:

- A couple of segments on the stable manifold cut joining the points represented by θ_i^s, $\theta^s(\lambda^*)$ and θ_{i+1}^s.

- Two more segments on the unstable manifold cut joining the points represented by θ_j^u, θ_{j+1}^u and $\theta^u(\alpha^*)$.

Note that two of these segments must contain the intersecting point between the cuts of the manifolds. So, they are compared in order to determine the new pairs of phases between which the cut occurs. Once the new intersecting segments have been detected, they are parametrised and new $\theta^s(\lambda^*)$ and $\theta^u(\lambda^*)$ are found. This process is stopped when the cut is found with the required level of accuracy.

At the end of the refining process, we store the value of the resulting phases as the representation of the connecting trajectory. The connection can then be explicitly found by integrating in forward time (respectively backward) the initial condition represented by the unstable (respectively. stable) intersecting phase until the desired number of cuts with the section is reached. In figures 4.10, 4.12, 4.13 and 4.16, some example trajectories are shown.

4.3 Families of connections: Sun-Earth and Earth-Moon systems.

Once a connection has been found using the method explained in the previous sections, we know that there are infinitely many others in its vicinity, due to the continuous dependence of the solutions with respect to the initial conditions and the asymptotic character of the manifolds. For instance, let $(\mathcal{C}, \theta^s, \theta^u)$ be the energy level and the phases on the Lyapunov orbits which are connected by a homoclinic or heteroclinic connection. Similar connections can be found either by slowly varying the initial phases on the Lyapunovs (θ^s, θ^u) or the Jacobi constant $\mathcal{C}$. In addition, a tiny modification in the initial conditions can also lead to an almost identical orbit in the phase space, which differs from the initial one in the time they spend winding around the
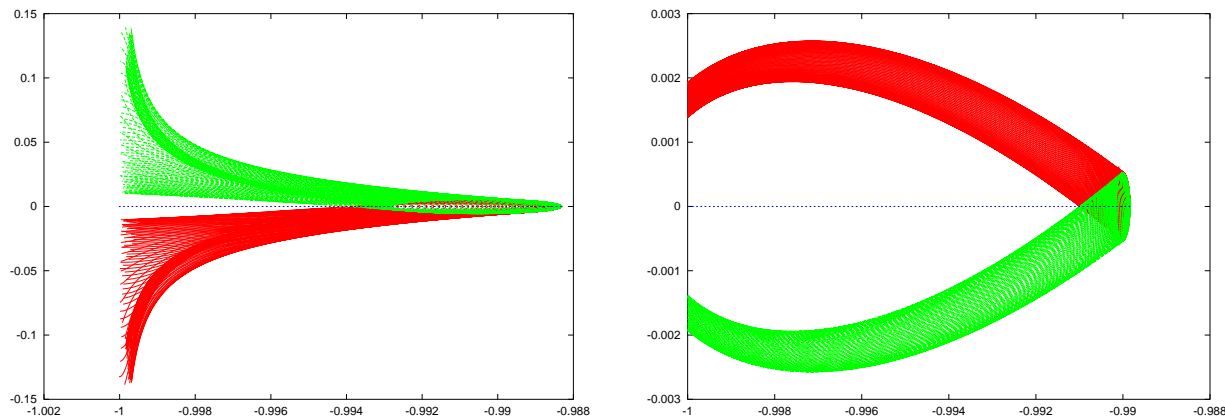
Figure 4.6: There are no 0-homoclinic orbits. The picture on the left corresponds to the smallest $\mathcal{C}$ for L_1, and shows how the $(x, \dot{x})$ projection of the stable (top) and unstable (bottom) manifolds of the Lyapunov orbit do not meet before crossing the $x = \mu - 1$ plane. On the right picture the (x, y) projection of the stable (bottom) and unstable (top) manifolds for $\mathcal{C}$=3.0009 (the biggest one used for L_1) is shown. Again, they do not intersect before crossing the Poincaré section at least once.

original Lyapunov or the final one. Obviously, the time span that an asymptotic orbit spends between leaving the original orbit and reaching the arrival one is infinite. However, for practical applications, finite times are used as we consider that trajectories reach or leave the Lyapunov orbits when in fact they are at a distance ϵ from them. This value ϵ is the one that is given to the corresponding hyperbolic amplitude, A_1 or A_2 (see figure 4.4).

Moreover, the classification that has been performed in this work aims at astrodynamical applications. Therefore, it mainly deals with simple paths, in the sense that they only wind around Lyapunov orbits in the departure and arrival parts but not during the mid-course. Furthermore, connections with a small number of loops around the small primary are usually preferred. For instance, when the intention is to move from one libration point to the other in a fast way. Nevertheless, homoclinic connections with up to 8 loops and heteroclinic connections with up to 5 loops around the small primary have been included in this study.

Finally, it is also important to note that there do not exist 0-homoclinic connections. That is, homoclinic connections go around the small primary at least once. This is a consequence of the fact that the manifolds never cross the x-axis before crossing the $x = \mu - 1$ plane (see figure 4.6). On the contrary, the simplest heteroclinic connections are found by intersecting the first cut of the manifolds from both sides, consequently having a number of loops around the small primary $n = 0$.

4.3.1   Homoclinic connecting trajectories

For all we learnt in the previous sections, we know how to find connections given two Lyapunov orbits and a number of cuts with the section. We also know that once a connection is found, there must be some others in its vicinity. So, we start by $\mathcal{C}_{min}^i$ and find the points on $\mathcal{S}$ which represent a homoclinic connection on this energy surface, for a given number of loops n. Then, we

take a value of $\mathcal{C}$ close to the first one and find the connecting trajectories corresponding to this new energy level. If we have not varied $\mathcal{C}$ too much, the new connecting trajectories are bound to be similar to the former ones, due to the continuous dependency of the solutions of the PRTBP with respect to initial conditions. That is, they cross the section at similar points. We can do the same for slowly increasing values of $\mathcal{C}$, storing the points at which the connections cross the section, until a value of the Jacobi constant is reached for which the manifolds do not intersect. When this happens, we say we have obtained the whole family of connections corresponding to a fixed number of loops, n. Afterwards, we can repeat the same procedure for a greater n.

If we represent any coordinate of the crossing points we stored versus the Jacobi constant, we can draw curves which summarise the information concerning the so called families of connecting trajectories. Each family of connections consists of several branches, depending on the number of intersecting points between the cuts of the manifolds. The generic number of intersections between two manifold cuts on a given section is 0, 2 or 4. However, for particular values of $\mathcal{C}$, tangencies occur between the cuts of the manifolds, giving rise to 3 connecting trajectories (when the tangency changes the number of cuts from 4 to 2) or to a single trajectory, when the tangency occurs at the maximum value of $\mathcal{C}$ for which the manifolds with the number of loops equal to the n that we are considering intersect (see figure 4.7).
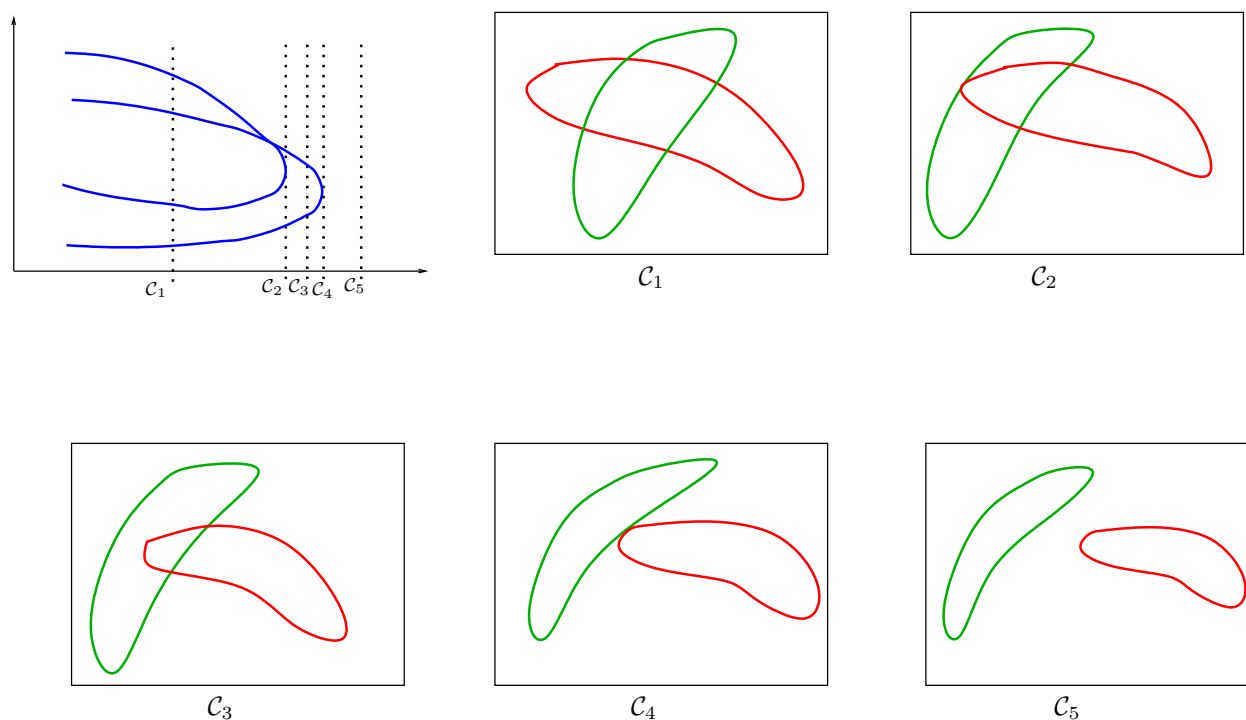
Figure 4.7: Schematic representation of how the curves representing the families of connections are obtained. In the first picture on the top left corner, a family of connections consisting of 4 branches is shown. (x axis: values of the Jacobi constant, y-axis: y coordinate of the intersecting points on $\mathcal{S}$). The vertical lines in this figure correspond to chosen values of the Jacobi constant, intersecting the family in 4, 3, 2, 1 or 0 points. Then, a qualitative representation of the cuts of the manifolds on $\mathcal{S}$ corresponding to these energy values is depicted in the figures labelled by $\mathcal{C}_i$.

Results for homoclinic connections are shown in figure 4.8, where the y-coordinate of the connecting trajectories in the Poincaré section is represented for every Jacobi constant. In these representations, the number of cuts of the manifolds W^s, W^u with $\mathcal{S}$, j_s and j_u respectively, is chosen so that $|j_s - j_u| = 1$ and $y > 0$.

Furthermore, in the aforementioned figure 4.8 each family of orbits, which corresponds to orbits with the same number of loops around the small primary, is depicted using a different line style. Each one of the families has different branches that come close to each other as $\mathcal{C}$ increases and finally meet at a bifurcation value, $\mathcal{C}_{bif}$. If we pick a $\mathcal{C}$ such that $\delta = \mathcal{C}_{bif} - \mathcal{C}$ is big, the corresponding orbits in each branch are quite different. However, as this distance δ decreases, the families approach, tending to a common limiting orbit associated with $\mathcal{C}_{bif}$. The evolution of the two branches of homoclinic connecting trajectories around L_1 in the Sun-Earth problem, Ho_1^1, which meet at a bifurcation value of the Jacobi constant equal to 3.00088389, is shown in figure 4.10.

Symmetries in the homoclinic families

In the restricted planar three body problem, if a curve $(x(t), y(t), \dot{x}(t), \dot{y}(t))$ is a solution of the equations then $(x(t), -y(t), -\dot{x}(t), \dot{y}(t))$ is also a solution.

Some asymptotic connections are a closed set with respect to this symmetry property, while some others are not. This fact motivates the following definitions:

Definition 1. γ is a *symmetric (homoclinic) orbit* if it satisfies,

$$(x, y, \dot{x}, \dot{y}) \in \gamma \Leftrightarrow (x, -y, -\dot{x}, \dot{y}) \in \gamma.$$

Definition 2. γ_1, γ_2 are *complementary orbits* (or families of orbits) if they satisfy,

$$(x, y, \dot{x}, \dot{y}) \in \gamma_1 \Leftrightarrow (x, -y, -\dot{x}, \dot{y}) \in \gamma_2.$$

We note that Lyapunov periodic orbits are symmetric. Also, all 1-homoclinic orbits are symmetric in the sense of definition 1 above. For n-homoclinic orbits, $n > 1$, we can see in figure 4.8 that there are 4 branches in each family: two of them are symmetric (definition 1), while the other two are complementary to each other (definition 2). See figure 4.11 for the classification of these branches according to their symmetry properties. Around L_2 the classification of homoclinic orbits in symmetric and complementary ones is qualitatively the same.

In figure 4.12 a representation of a symmetric 1-homoclinic trajectory and a pair of complementary 3-homoclinic ones for the Sun-Earth case are shown. Respectively, the pictures in figure 4.13 show a symmetric 2-homoclinic orbit around L_1 and a pair of 3-homoclinic complementary ones around L_2 for the Earth-Moon case.

On the other hand, the planar three body problem with $0 < \mu < \frac{1}{2}$ is not symmetric in L_1-L_2. However, as $\mu \to 0$ we have an increasing "almost-symmetry" with respect to the $x = \mu - 1$ axis. The limiting case, Hill's problem, has exact geometrical symmetry with respect to this vertical axis crossing the primary. When γ_1 is homoclinic around L_1, then its *almost-vertical-symmetric* partner, γ_2, has to be an homoclinic trajectory around L_2. To find which families are *almost-symmetric* to each other with respect to the surface of section $x = \mu - 1$ we just have to compare the two pictures in figure 4.8. If we choose a number of loops around the Earth, n,
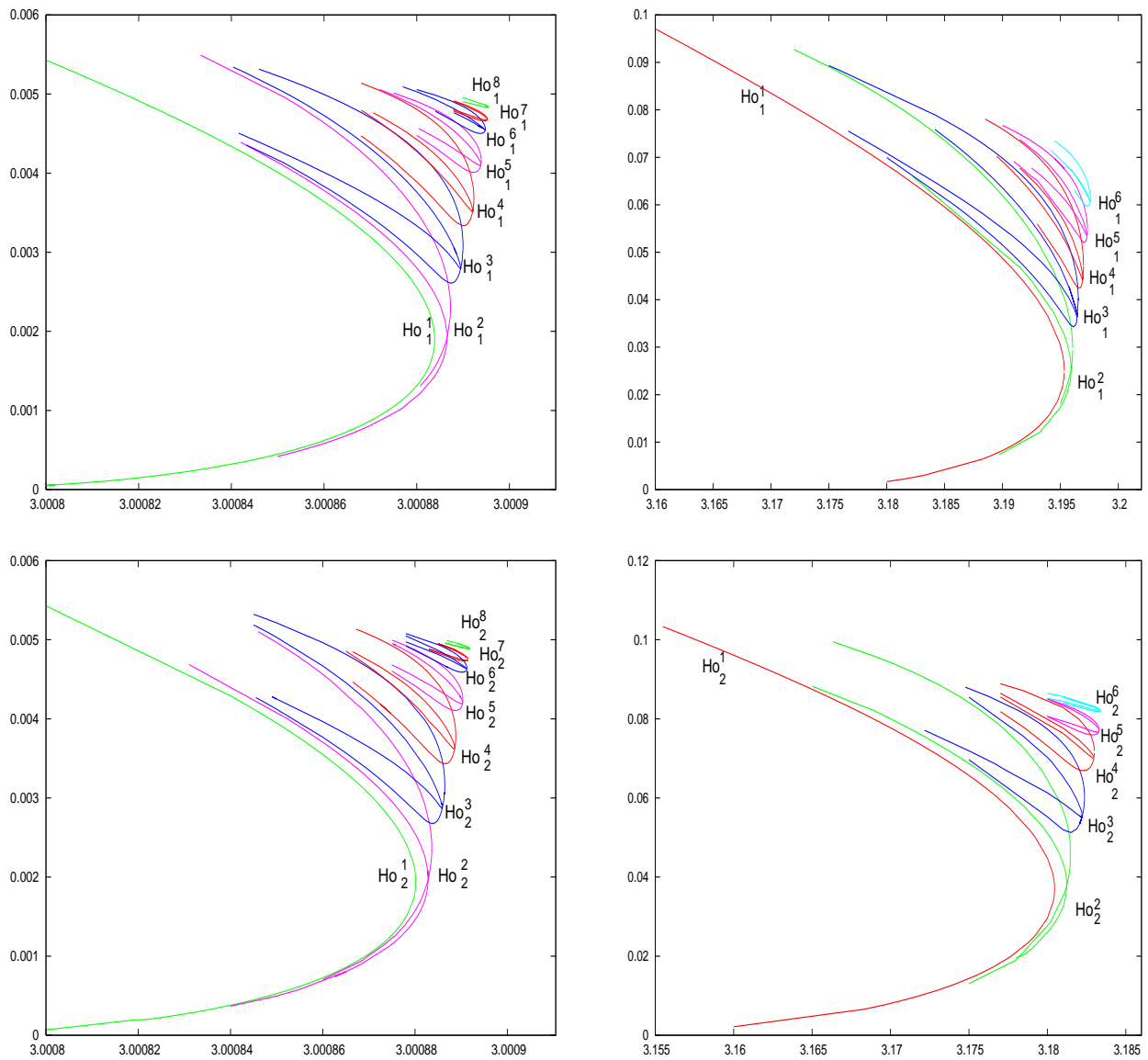
Figure 4.8: Homoclinic connections of the Lyapunov orbits. Around L_1 in the first row and around L_2 in the second one. Sun-Earth system corresponds to the left column and Earth-Moon system to the right one. The x-axis of this figures shows the range of Jacobi constants, while in the y-axis the y coordinate of the central cut of the trajectory with $\mathcal{C}$ is represented.
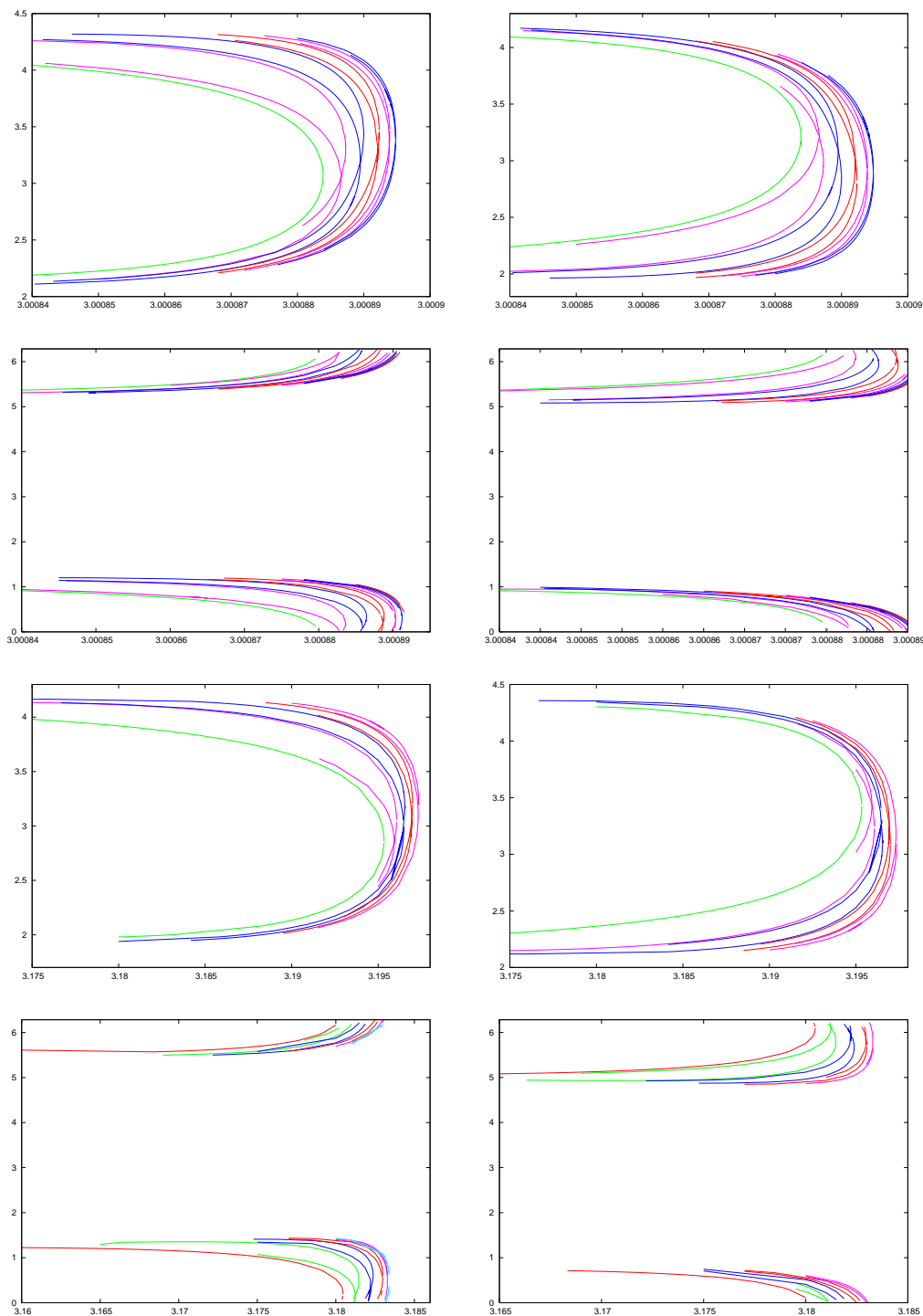
Figure 4.9: Families of homoclinic connections. The x axis of each picture contains the values of the Jacobi constant, while the y axis contains the starting (or arriving) phases on the manifolds. First and second rows correspond to homoclinic connections for the Sun-Earth case, the first one homoclinic families around L_1, the second one around L_2. Third and fourth rows correspond to homoclinic connections for the Earth-Moon case (third for L_1, fourth for L_2). In the column on the left phases on the unstable manifolds are shown (starting phases), while in the column on the right, the corresponding arriving phases (stable manifold).Note that any figure from the left is symmetric to the corresponding one on the right with respect to the horizontal axis $\theta = \pi$.
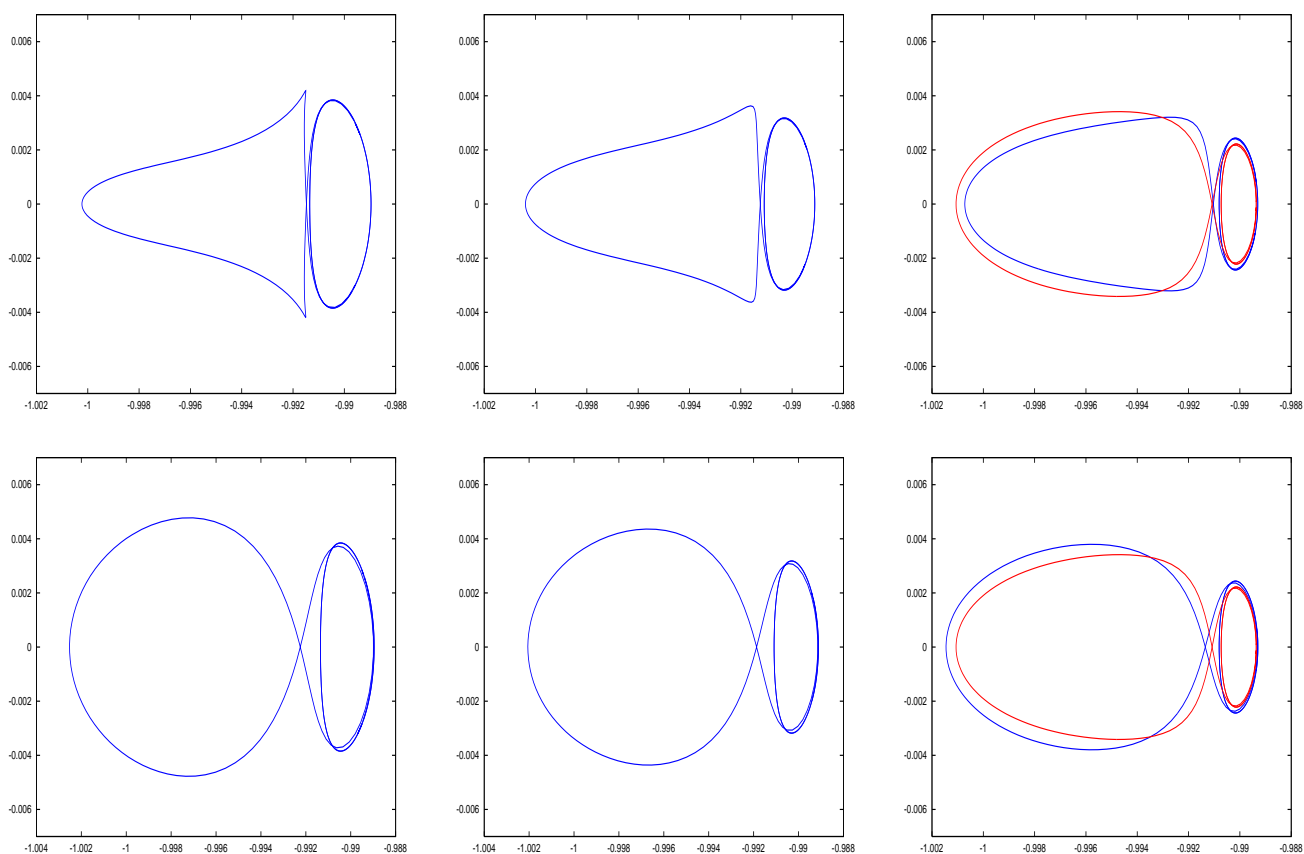
Figure 4.10: Sample trajectories belonging to a family of homoclinic orbits around L_1 for the Sun-Earth case. Each row corresponds to a branch of the Ho_1^1 family. We can see how from left to right the two branches become more similar, as $\mathcal{C}$ tends to the bifurcation value. Left, $\mathcal{C} = 3.00085$, middle $\mathcal{C} = 3.000866$ and right $\mathcal{C} = 3.0008804$. In the picture on the right, the bifurcation trajectory is also represented, in red.
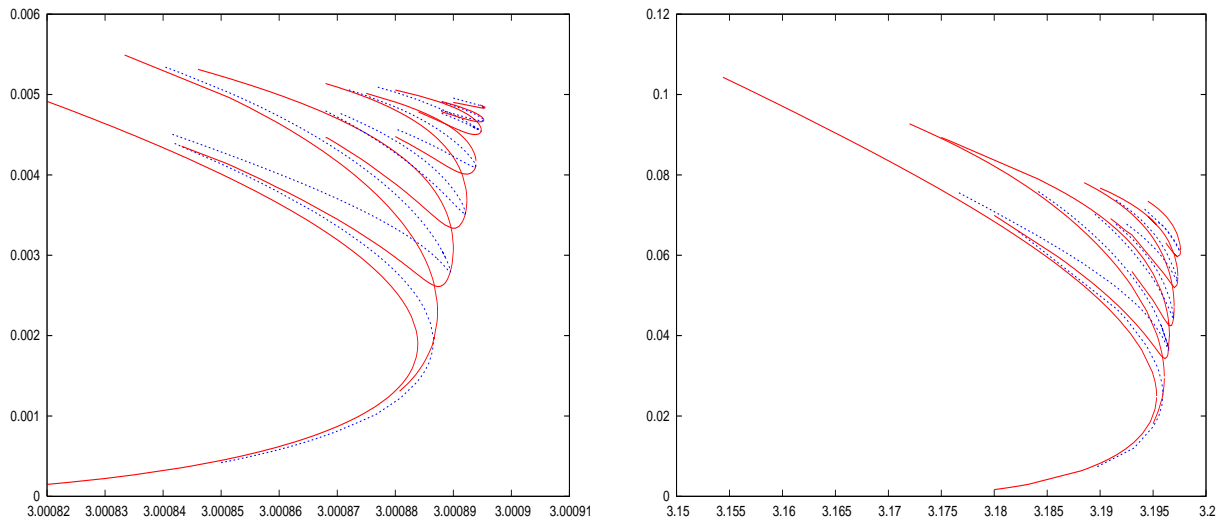
Figure 4.11: Symmetric (continuous red line) and complementary (dotted blue line) families of homoclinic trajectories. (left) Sun-Earth problem. (right) Earth-Moon problem.

and pick one of the four branches which represent n-homoclinic trajectories around L_{i_1} (two if $n = 1$) the corresponding branch of trajectories around L_{i_2} contains n-homoclinic orbits which are *vertically almost-symmetric* to the first ones. For example, see trajectories in figure 4.12. If μ is not very small vertical symmetry is lost. That is the case of the Earth-Moon mass parameter (see figure 4.13).

4.3.2   Heteroclinic connecting trajectories

If we look for intersections between hyperbolic manifolds of different periodic orbits around L_i, what we obtain is a set of heteroclinic connections instead of homoclinic orbits. Nevertheless, the procedure used for finding heteroclinic trajectories is exactly the same as the one we explained for homoclinic ones.

Obviously, the range of values of the Jacobi constant for which we can search for heteroclinic connections between Lyapunov orbits has to be the intersection between the intervals in which we have restricted our expansions for both libration points. That is $[\mathcal{C}_{min}^1, \mathcal{C}_{max}^2]$. If we proceed exactly as we did for homoclinic orbits, storing the connections for each value of $\mathcal{C}$, what we get is represented in figure 4.14. In more detail, the points of any vertical line (corresponding to a particular value of $\mathcal{C}$) which intersect one of the curves of the figure, represent heteroclinic connections between L_1 and L_2 going through the Poincaré section with the y value represented in the y-axis of picture (i.e. y-axis corresponds to the y coordinate of the connections when $x = -1 + \mu$). The figure is symmetric with respect to $y = 0$, but connections with $y > 0$ go from L_1 to L_2, while connections with $y < 0$ go from L_2 to L_1 and are symmetric to the previous ones due to RTBP symmetry which will be further explained for heteroclinic trajectories.

The bifurcation phenomena is similar, with pairs of families of connections tending to a single one at a bifurcation value of the Jacobi constant. In figure 4.16 we can observe the evolution
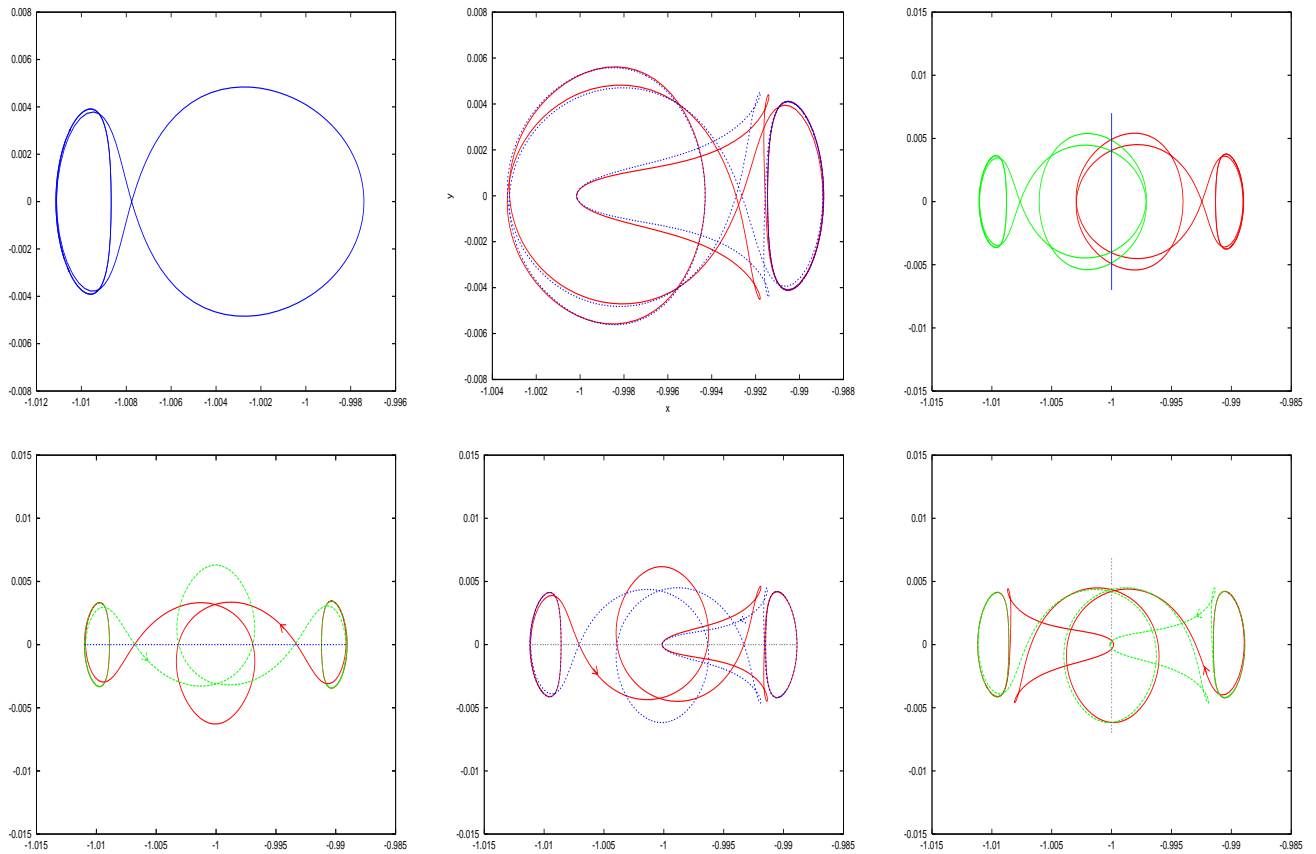
Figure 4.12: Example trajectories for the Sun-Earth case. First row: (left) Symmetric 2-homoclinic trajectory around L_1 corresponding to $\mathcal{C} = 3.00075$. (middle) Pair of complementary 3-homoclinic L_1 trajectories, Ho_1^3, $\mathcal{C} = 3.0008428$. (right) Almost symmetric 2-homoclinic orbits with respect to the vertical axis, corresponding to $\mathcal{C} = 3.00085226$. Second row: (left) Symmetric heteroclinic channel (with respect to the horizontal and vertical axis), $\mathcal{C} = 3.00086$. (middle) Symmetric heteroclinic channel (with respect to the horizontal axis) $\mathcal{C} = 3.00084$. (right) Almost-symmetric heteroclinic trajectories (with respect to the vertical axis) from L_1 to L_2, $\mathcal{C} = 3.00084$.
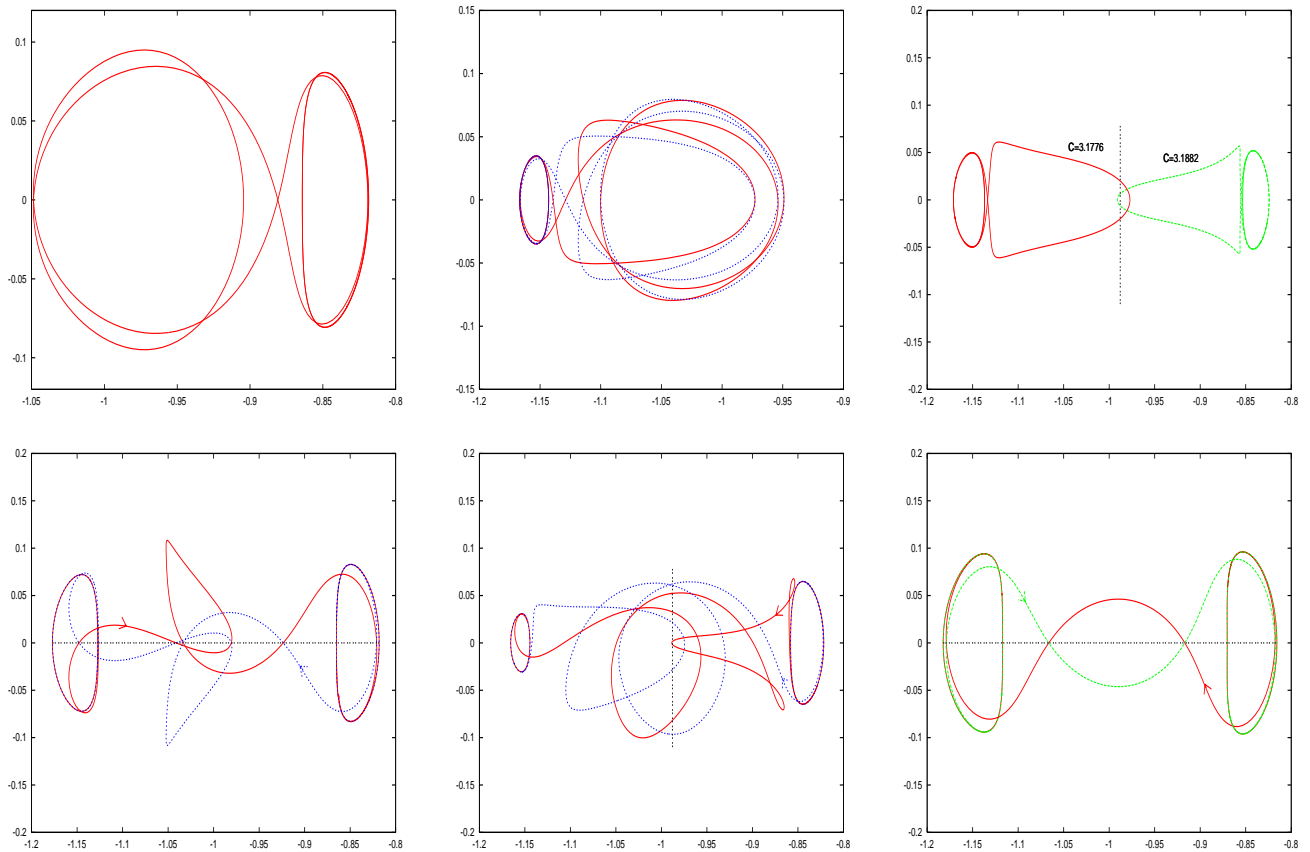
Figure 4.13: Examples for the Earth-Moon case. First row: (left) Symmetric trajectory with respect to the x axis corresponding to a 2-homoclinic orbit around L_1 with $\mathcal{C} = 3.17$. (middle) Pair of complementary (i.e. symmetric one to another with respect to x axis) L_2 3-homoclinic orbits, $\mathcal{C} = 3.181$. (right) Vertical quasi-symmetry is lost in the Earth Moon problem. Homoclinic orbits around L_1 are not quasi symmetric to homoclinic orbits around L_2 for values of the $\mathcal{C}$ that result in orbits of rather different amplitudes around both libration points. Second row: (left) Symmetric heteroclinic channel with respect to the horizontal axis corresponding to $\mathcal{C} = 3.17053333$. (middle) Another example of how the vertical quasi-symmetry is lost for values of $\mathcal{C}$ for which Lyapunov orbits from both sides have different amplitudes (in this case, $\mathcal{C} = 3.1699667$). (right) Heteroclinic channel which is symmetric with respect to the x axis and quasi-symmetric with respect to the y axis. The loss of vertical symmetry is not that obvious if $\mathcal{C}$ is small enough (in this case $\mathcal{C} = 3.161$).
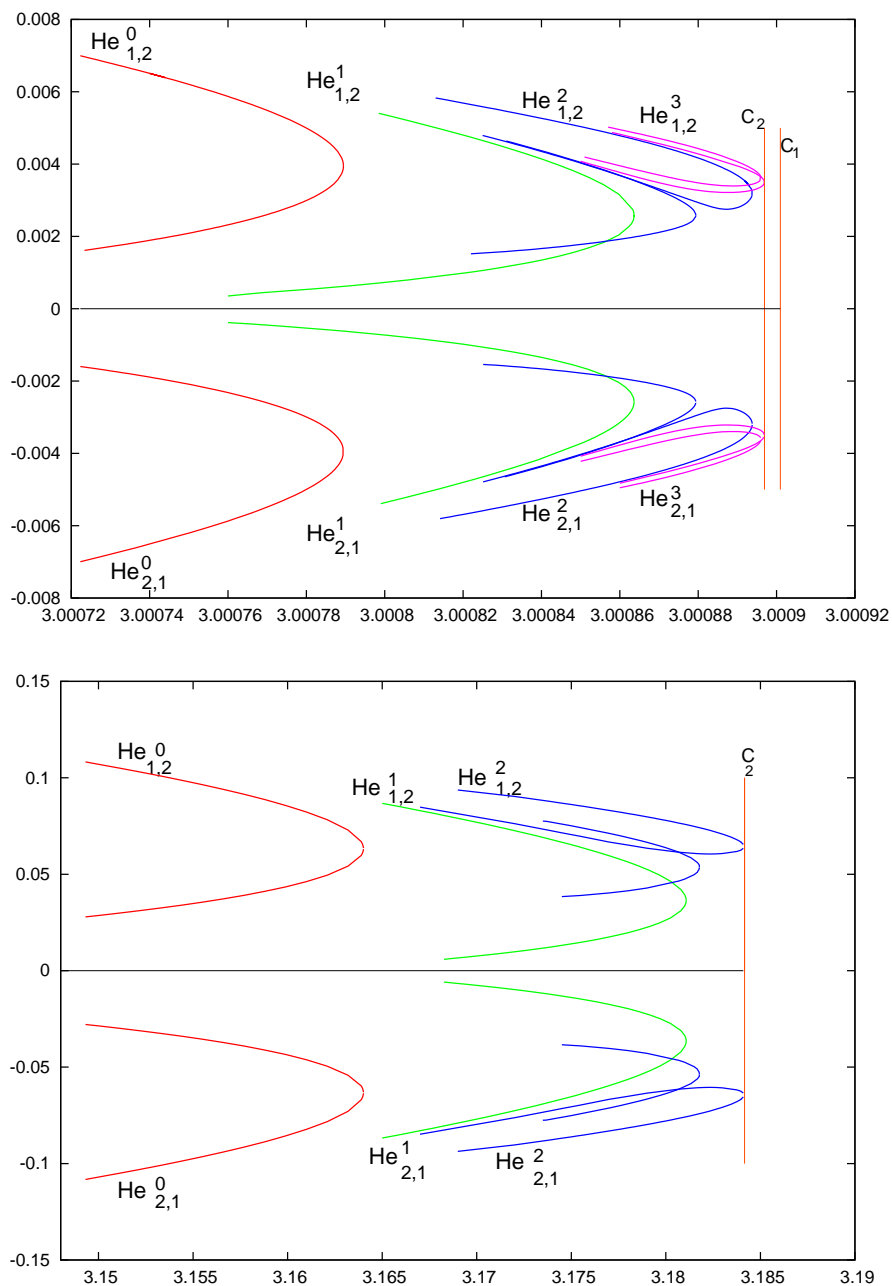
Figure 4.14: Families of heteroclinic connections. (top) Sun-Earth mass parameter. (bottom) Earth-Moon mass parameter. In this figures the x-axis contains the values of the Jacobi constant, while in the y axis the y coordinate of the central cut of the trajectory with $\mathcal{S}$ is shown. Note that connections with $y > 0$ correspond to heteroclinic orbits from L_1 to L_2, while their symmetric connections, from L_2 to L_1 are represented with $y < 0$.
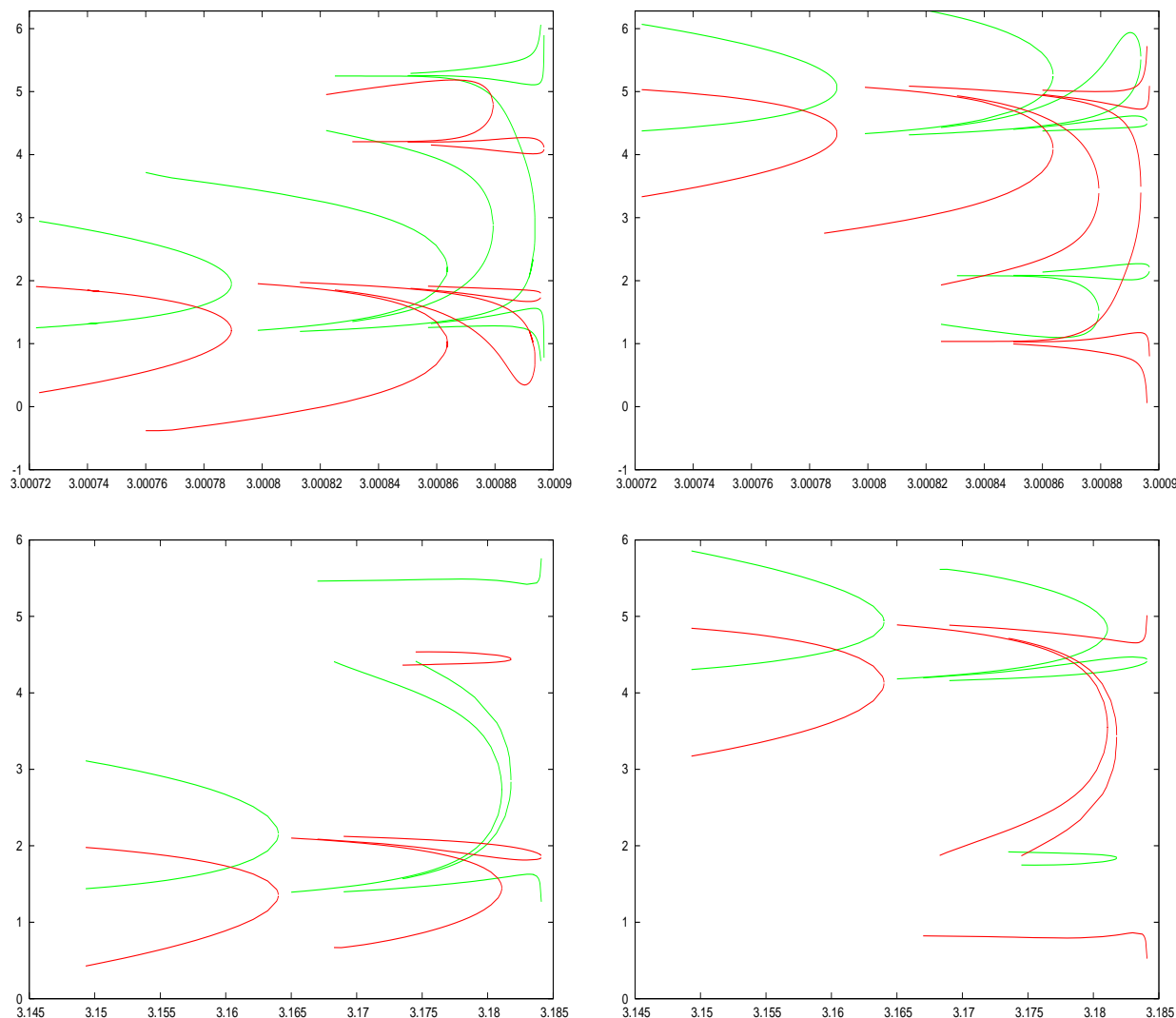
Figure 4.15: Families of heteroclinic connections. The x axis of the figures contains the values of the Jacobi constants for which the connections are found, and the y axis represents phases: Red curves represent the values of the departing phases on the unstable manifolds of the aforementioned connections, while green curves represent the values of the arriving phases on the stable manifolds. As the values of the Jacobi constant indicates, the pictures on the top correspond to heteroclinic connections in the Sun-Earth problem, while the pictures on the bottom, to heteroclinic connections in the Earth-Moon problem. Finally, figures on the left correspond to L1 to L2 connections, while figures on the right correspond to L2 to L1 connections. Note that the figures in each row are symmetric to each other with respect to $\theta = \pi$ and interchanging the roles of stable and unstable phases.

of a family of heteroclinic connections from L_1 to L_2 for the Sun-Earth problem, which has two branches that end at the bifurcation trajectory with $\mathcal{C} = 3.000863625$.
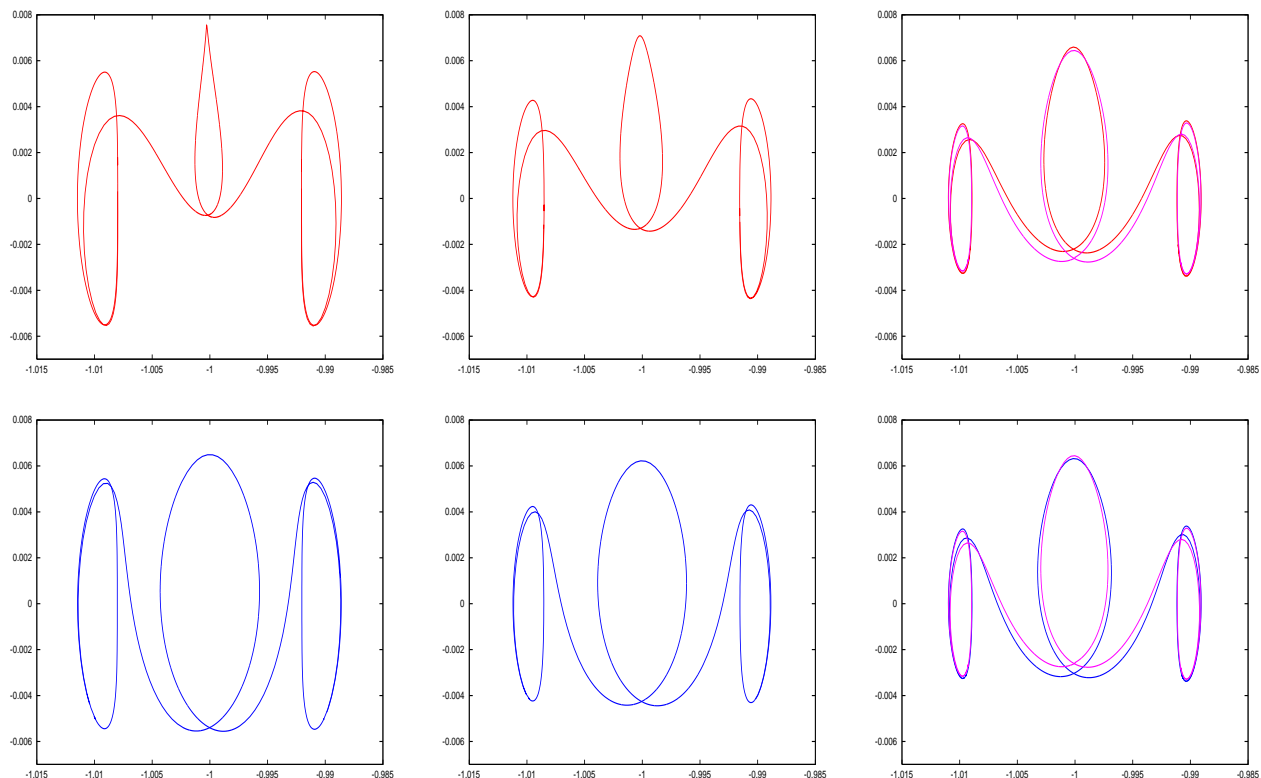
Figure 4.16: Heteroclinic connections belonging to different branches of the same family (from L1 to L2, 1 loop around the Earth). From left to right, the connections correspond to the values of $\mathcal{C}=$ 3.000799, 3.0008361 and 3.0008615. The two branches approach as $\mathcal{C}$ tends to 3.00086362, tending to the bifurcation trajectory represented in purple in the right column.

We say that a pair of heteroclinic orbits, one from L_1 to L_2 and the other from L_2 to L_1 is an heteroclinic channel. Figures 4.12 and 4.13 contain some representations of heteroclinic channels.

Symmetries in the heteroclinic families

The intrinsic symmetry property of the PRTBP is responsible for the existence of the so-called symmetric heteroclinic channels. If $(x(t), y(t), \dot{x}(t), \dot{y}(t), t)$ is a heteroclinic connection from L_1 to L_2, then $(\tilde{x}(t), \tilde{y}(t), \dot{\tilde{x}}(t), \dot{\tilde{y}}(t)) = (x(-t), -y(-t), -\dot{x}(-t), \dot{y}(-t))$, is a connection from L_2 to L_1 (see figure 4.14). That is,

$$\forall \gamma_1 \in He^n_{i_1,i_2} \quad \exists \, \gamma_2 \in He^n_{i_2,i_1} \quad \text{such that } (x, y, \dot{x}, \dot{y}, t) \in \gamma_1 \Leftrightarrow (x, -y, -\dot{x}, \dot{y}, -t) \in \gamma_2.$$

The vertical almost symmetry that exists for small values of μ does not give rise to return heteroclinic channels. That is to say that if γ_1 is a heteroclinic connection from L_{i_1} to L_{i_2}, and γ_2 is its vertical-almost-symmetric partner, then γ_2 also goes from L_{i_1} to L_{i_2}. In figure 4.12

some examples of symmetric heteroclinic channels, as well as vertical almost-symmetric pairs of connections are shown.

For the Earth-Moon case, the almost symmetry is lost as we have seen for homoclinic connections, especially for those values of the Jacobi constant which produce Lyapunov orbits of considerably different size in each equilibrium point. However, if Lyapunov orbits are similar (small values of the Jacobi constant), we can still find some almost vertical heteroclinic connections, as shown in figure 4.13.

Chapter 5

Transfer trajectories between the Sun-Earth and Earth-Moon L_2 regions

5.1   Introduction

The Sun-Earth L_2 libration point is becoming a very important location for deep space exploration (telemetry and observation missions such as Herschel, Planck, Darwin, TPF...). In addition, it is nowadays arising as a strategic point in the long-term human space exploration architecture ([13]). In this context, it is of the utmost importance not only to minimise the fuel expenditure, but also to reduce the risks to a level which is acceptable for manned missions. Therefore, it is very useful to study the natural dynamics of the bodies involved in the missions, starting by using simple models. The invariant manifolds of the Restricted Three Body Problem (RTBP) are a perfect example of how the natural dynamics can help in mission design. In fact, they have been used in the previous chapters to solve different problems such as the cheap transfer between libration point orbits or eclipse avoidance.

On the other hand, the Earth-Moon libration regions are also interesting locations for current and near-future space exploration. Not only are they close enough to the Earth to hold servicing facilities, but they are also convenient steps in the trip to the outer planets, such as Mars. One can think that it would be cheap to transfer to Earth-Moon libration points from the vicinity of the Earth by using the invariant manifolds of the libration orbits. Simple explorations show that this is not true, as the aforementioned manifolds never come to a close approach with the Earth. However, Sun-Earth libration orbits have bigger manifolds, which really approach the Earth in some cases. Therefore, the idea of coupling the Sun-Earth and Earth-Moon restricted three body problem manifolds in order to obtain low cost transfers to the lunar libration regions arose in a natural way ([52]).

In the present chapter, the idea of intersecting invariant hyperbolic manifolds will be exploited in a slightly different way than in chapter 4. Our goal is to join libration orbits belonging to Sun-Earth and Earth-Moon problems. That is, decoupling the problem in two restricted three body problems, computing the invariant manifolds of the chosen orbits and looking for intersections between them in convenient intermediate sections. In this way, initial working trajectories fulfilling the requirements of the missions can be obtained and, in a further step, they can be refined to more realistic models, resulting in real low cost motions which are close to

natural channels.

To sum up, this chapter is aimed at finding low cost connections between the solar libration regions and the lunar libration ones and it is divided in three parts. In the first part, asymptotic connecting trajectories are found between Lyapunov orbits of the planar Sun-Earth and Earth-Moon RTBPs. Secondly, this search for asymptotic transfers joining both RTBPs is performed in the three dimensional models and using Lissajous orbits. Finally, the last part of the chapter is devoted to refining the connecting trajectories that have been obtained between Lissajous orbits to realistic JPL ephemeris coordinates.

5.2   Connecting trajectories between planar Lyapunov orbits

As it is well known, models for the motion of n bodies are complex and the determination of particular solutions for them involves long computations. If we want to study the motion of a spacecraft under the influence of the Sun, the Earth and also the Moon, we need a four body model. However, in a first approach one can think of decoupling it in two restricted three body problems (RTBP). In this way, we can take advantage of our knowledge and experience with three body problems in order to find approximate solutions.

The Sun-Earth-Moon-spacecraft four body problem will be decoupled in:

- The Sun-Earth+Moon-spacecraft RTBP, which has the Sun and the Earth-Moon barycenter as primaries. We will refer to it as SE problem.

- The Earth-Moon-spacecraft RTBP, which has the Earth and the Moon as primaries. It will be referred as EM problem.

In the first studies, we will neglect the inclination of the plane of motion of the Moon with respect to the ecliptic plane (i.e. the plane of motion of the Earth around the Sun), which is approximately 5 degrees. Therefore, in our simplified model, the Sun, the Earth and the Moon are considered to be revolving in a single plane. In addition, we only consider positions of the spacecraft belonging to this plane of motion of the three bodies: Sun, Earth and Moon. Consequently, the restricted three body problems that we use in this part of the work are planar.

The small primary of the SE system is considered to have a mass which is the addition of Earth and Moon masses, and to be placed where the Earth-Moon barycenter lays. On the other hand, the origin of coordinates of the EM system coincides with the aforementioned barycenter. Consequently, the natural way of coupling these two problems is by deploying the EM system inside the SE one, as shown in figure 5.1. In this figure, the relative position between the Sun-Earth x axis and the Earth-Moon one is represented by angle β. The position of the Earth-Moon system with respect to the Sun-Earth+Moon one is time dependent.

5.2.1   Lyapunov orbits and their hyperbolic invariant manifolds

In the PRTBP, there exists only one planar periodic motion around L_2 (respectively L_1) for each value of the Jacobi constant: the so-called planar Lyapunov orbit. We aim at finding connections
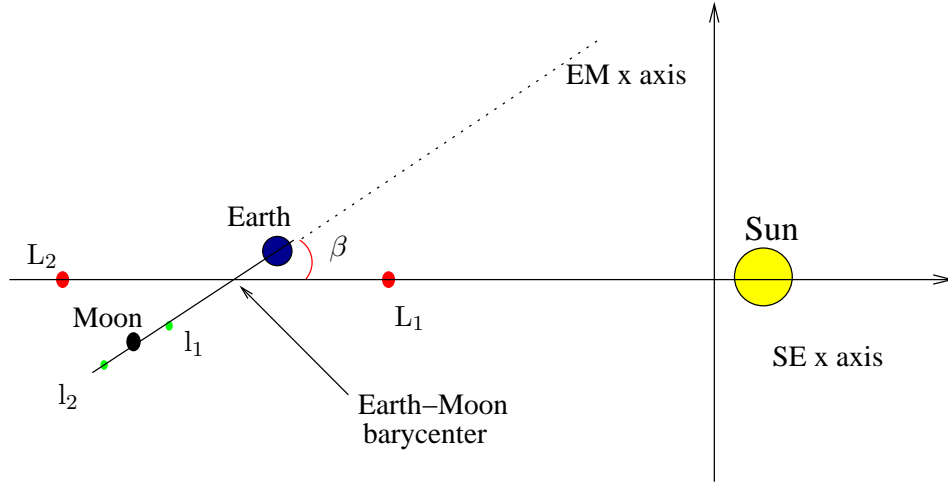
Figure 5.1: Coupling between the RTBPs.

between such orbits around L_2 of the EM problem and L_2 of the SE one. Before starting to describe how we look for these connections, some ideas on the computation of the planar Lyapunov orbits and their stable and unstable hyperbolic manifolds are given in this section.

Remember that the linear part of the solutions of the equations of motion of a RTBP is,

$$
\begin{aligned}
x(t) &= A_1 e^{\lambda t} + A_2 e^{-\lambda t} + A_x \cos(\omega t + \phi), \\
y(t) &= cA_1 e^{\lambda t} - cA_2 e^{-\lambda t} + \bar{\kappa} A_x \sin(\omega t + \phi)
\end{aligned}
\tag{5.1}
$$

where c, $\bar{\kappa}$, ω and λ are constants for a given model and libration point.

The A's are free amplitudes. A_1 and A_2 are the ones associated with the hyperbolic manifolds. If $A_1 = A_2 = 0$, expressions in (5.1) describe the linear part of the Lyapunov orbit, which is essentially a periodic oscillation in the xy plane with x amplitude equal to A_x and y-amplitude a quantity which is also depending on A_x. When $A_1 = 0$ and $A_2 \neq 0$ we have orbits tending to the Lyapunov orbit of amplitude A_x when time tends to infinity (stable manifold). On the contrary when $A_2 = 0$ and $A_1 \neq 0$, orbits leave the vicinity of the Lyapunov exponentially fast in forward time (unstable manifold).

When we consider also the non-linear terms, solutions are obtained by means of formal series in powers of the amplitudes of the form:

$$
\begin{aligned}
x(t) &= \sum e^{(i-j)\theta_2} [x_{ijk}^p \cos(p\theta_1) + \bar{x}_{ijk}^p \sin(p\theta_1)]\tilde{\alpha} \\
y(t) &= \sum e^{(i-j)\theta_2} [y_{ijk}^p \cos(p\theta_1) + \bar{y}_{ijk}^p \sin(p\theta_1)]\tilde{\alpha}
\end{aligned}
\tag{5.2}
$$

where $\tilde{\alpha} = A_1^i A_2^j A_x^k$, $\theta_1 = \omega t + \phi$, $\theta_2 = \lambda t$ and,

$$
\omega = \sum \omega_{ijk} A_1^i A_2^j A_x^k, \qquad \lambda = \sum \lambda_{ijk} A_1^i A_2^j A_x^k.
$$

Summation is extended over all i, j, k and $p \in \mathbb{N}$. However, due to symmetries, many of the coefficients x_{ijk}^p, $\bar{x}_{ijk}^p$, y_{ijk}^p, $\bar{y}_{ijk}^p$, ω_{ijk}, λ_{ijk} are zero. Moreover the series are truncated at a certain order, which is usually high. Nevertheless, we note that the meaning of the amplitudes in the

nonlinear expansions (5.2) is the same one as in the linear solutions (5.1). In particular, the analytical expression for the Lyapunov orbit is obtained by setting $A_1 = A_2 = 0$.

5.2.2   Poincaré section

The use of Poincaré sections is aimed at gaining a better understanding of the behaviour of the solutions of a dynamical system. On such sections, the flow is observed in a lower dimensional space, but relevant information can still be derived.

     The state space for the Planar Restricted three body problem is 4 dimensional, containing points of the form $(x, y, \dot{x}, \dot{y}) \in \mathbb{R}^4$. However, we work with solutions in fixed energy levels by fixing a value of the Jacobi constant $\mathcal{C}$. The set of points of the state space that belong to a given energy level is then 3 dimensional. That is, we only need to know 3 of the coordinates $(x, y, \dot{x}, \dot{y})$, and the fourth one yields from the value of the Jacobi constant. We will use $(x, y, \dot{y})$ when referring to a point belonging to, $\mathcal{M}(\mu, \mathcal{C})$, a given energy level,

$$\mathcal{M}(\mu, \mathcal{C}_*) = \{(x, y, \dot{x}, \dot{y}) \in \mathbb{R}^4 |\ \mathcal{C}(x, y, \dot{x}, \dot{y}) = \mathcal{C}_*\}.$$

Then, a Poincaré section of the form

$$\mathcal{S} = \{(x, y, \dot{x}, \dot{y}) \in \mathcal{M}(\mu, \mathcal{C}_*) | g(x, y, \dot{y}) = 0\},$$

and transversal to the tubes can be selected. If g is linear, $\mathcal{S}$ is a plane in $\mathcal{E}$.

     In this work, $\mathcal{S} = \{(x, y, \dot{x}, \dot{y}) \in \mathbb{R}^4 \mid x = -1 + \mu_{SE}\}$ is chosen (μ_{SE} stands for the mass parameter of the SE problem).

5.2.3   Intersections on the Poincaré section

Once a Jacobi constant for the SE problem is chosen, $\mathcal{C}_{SE}$, and another one for the EM problem, $\mathcal{C}_{EM}$, the amplitudes of the corresponding planar Lyapunov orbits around L_2 in each of the problems are determined. These amplitudes are represented by A_x in equations (5.1). Besides, A_1 and A_2 are the hyperbolic amplitudes in the same equations. In order to obtain initial conditions on the unstable manifold of the Lyapunov orbit, we take $A_2 = 0$ and $A_1 = \epsilon$. $\epsilon \ll 1$ is a small parameter representing the distance from the initial conditions on the manifold to the Lyapunov orbit. On the contrary, when we want to obtain initial conditions on the stable manifold, we take $A_1 = 0$ and $A_2 = \epsilon$.

     We integrate the unstable manifold of the planar Lyapunovs of the EM problem and the stable manifolds of the planar Lyapunovs of the SE one. These manifolds are two dimensional tubes which can be parametrised, for instance by the integration time and the initial phase on the corresponding Lyapunov orbit, θ, as schematically represented in figure 5.2.

     Therefore, the initial conditions (in Lindstedt-Poincaré coordinates) that we use in order to have a representation of the hyperbolic manifolds when looking for paths from the lunar L_2 Lyapunov orbits to the solar ones are:

- $(0, \epsilon, A_x^{SE}, \theta_i^{SE})$, with $i = 1, n$ and $\theta_i^{SE} \in [0, 2\pi)$ (for the stable manifold of the Sun-Earth+Moon Lyapunov).
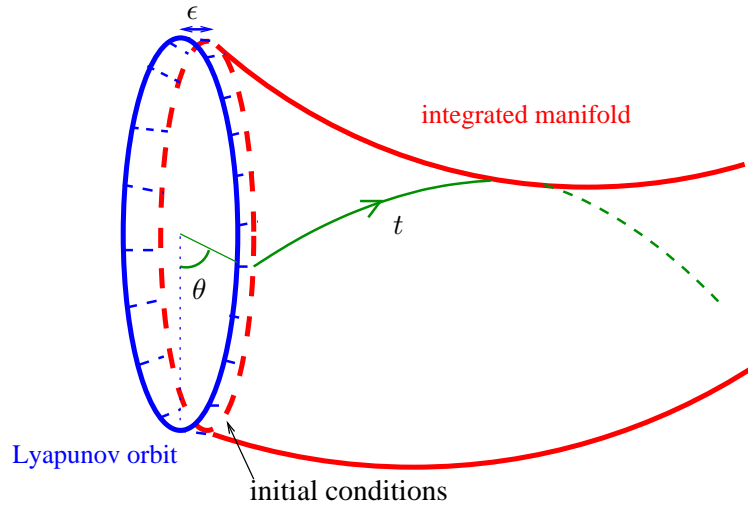
Figure 5.2: Schematic representation of a Lyapunov orbit and one of the hyperbolic manifolds associated to it.

- $(\epsilon, 0, A_x^{EM}, \theta_i^{EM})$, with $i = 1, m$ and $\theta_i^{EM} \in [0, 2\pi)$ (for the unstable manifold of the Earth-Moon Lyapunov).

These Lindstedt-Poincaré sets of initial conditions are transformed to position and velocity. Then, the corresponding state space points $(x, y, \dot{x}, \dot{y})$ are integrated forwards in time (for the unstable case) or backwards in time (for the stable case) until they intersect the section $\mathcal{S}$. What we get as a result of the intersection between a 2-dimensional tube and the plane $\mathcal{S}$ is generically a one dimensional object (curve) like the ones depicted in figure 5.5.

Assume that there exists a point belonging to two different curves on the section: one representing the intersection between $\mathcal{S}$ and the unstable manifold of a Lyapunov orbit and the other one between $\mathcal{S}$ and the stable manifold of another Lyapunov orbit. For all we know, this point belongs to a solution of the PRTBP which has asymptotically left a libration orbit at time $-\infty$ and which at the same time tends to another libration orbit as time tends to $+\infty$. Therefore, by integrating the aforementioned point forwards and backwards, we get a zero cost connecting trajectory joining both orbits.

A complete development of this idea and its application to finding zero cost connections between libration orbits around the points L_1 and L_2 of the Earth-Moon and Sun-Earth systems (separately) can be found in chapter 4. A new application of this methodology is done in the present section, aimed at finding low cost connecting trajectories between Lyapunov orbits belonging to different Restricted Three Body Problems. The main idea is to choose a Poincaré section common for both problems and integrate the EM and SE manifolds separately until they intersect this section. However, when dealing with different RTBPs and before looking for intersections between curves on $\mathcal{S}$, one has to make sure that they are in the same coordinate system and that the Poincaré section is in fact the same in both cases.

Let us describe the coupling in more detail, as represented in 5.4 including the Poincaré section. In each of the restricted three body problems section $\mathcal{S}$ is defined as a plane in the state
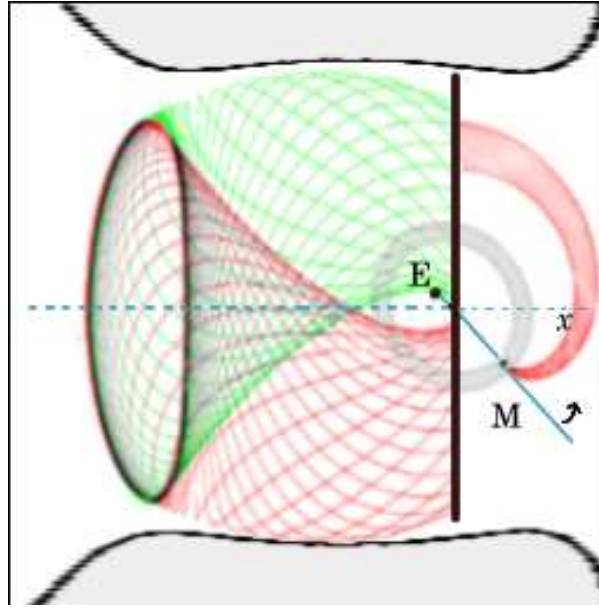
Figure 5.3: Representation of the hyperbolic manifolds of a Lyapunov orbit around L$_2$ in the SE problem until they intersect $\mathcal{S}$, and the unstable manifold of a Lyapunov orbit around L$_2$ in the EM problem, also until its first cut with $\mathcal{S}$.

space, perpendicular to the xy plane (of the adapted coordinate system) and forming a constant angle with the x-axis (i.e. line joining the primaries). To completely determine $\mathcal{S}$, however, it is still necessary to specify one point belonging to it. For the SE problem we make the section go through the point acting as small primary, which is the Earth-Moon barycenter. On the other hand, for the Earth-Moon case, we make the section contain the origin of coordinates of this adapted reference frame, which is no other than the Earth-Moon barycenter.

From now on, we will use the SE coordinate system as the global reference frame. The Poincaré section for the SE problem forms a constant angle with the SE x-axis, ϕ_{SE}. On the other hand, in the adapted coordinate system of the EM problem, the angle between the section and the EM x-axis is also fixed, ϕ_{EM}. The angle β (see figure 5.4) represents the position of the Earth-Moon x axis with respect to the axis joining the Sun and the Earth-Moon barycenter at a given moment of time. Actually, when looked in the SE coordinates, the Earth-Moon x-axis is revolving around the Earth-Moon barycenter at an angular speed we assume to be constant, $\dot{\beta} = \omega$. In order to determine this angular velocity, we have to take into account that β performs a complete revolution with respect to the Sun-Earth+Moon axis in a Moon synodic period (i.e. in the time that it takes for the Moon to go from full Moon to full Moon). Therefore, $\dot{\beta} = 2\pi/29.5309$ (rad/day). Consequently, ϕ_{EM} depends uniformly on the time in the SE frame in spite of being constant in the EM system.

Assume that at a given moment of time the relative position between the EM and the SE x-axis is such that both Poincaré sections are the same when looked in the SE reference frame. This is the adequate time for the coupling and the moment when the following relation is satisfied,

$$\phi_{SE} = \beta + \phi_{EM}. \tag{5.3}$$

Figure 5.4: Coupling between the RTBPs and Poincaré sections as seen in the coupled models. In the picture on the top we see the coupled models at a moment of time t when the section $\mathcal{S}'$ in the EM problem does not coincide with $\mathcal{S}$ in the SE coordinates. On the contrary, picture on the bottom shows the moment when both sections overlap, which we choose as initial time $t = 0$.

μ_{SE}	3.040423398444176e-06
μ_{EM}	0.01215058191870689
AU	149597870.691 km
Mean distance Earth-Moon	384400 km
Earth period	365.25 days
Moon period	29.53 days
τ time unit in E-M problem	$2\pi/29.53$
ω	11.366834171d0 rad/τ

Table 5.1: Values of some used constants (from [69]).

For the sake of simplicity, we choose the time for the coupling to be $t = 0$. As the PRTBP is autonomous, this choice does not represent a loss of generality. It is just a matter of waiting for the correct SE and EM relative configuration. However, once this origin of time has been chosen, changes of coordinates can be needed at different moments ($t \neq 0$). Then, ω will have to be used. When $t \neq 0$ we have that,

$$\phi_{SE} = \beta + \phi_{EM} + \omega t. \tag{5.4}$$

This is the key for coupling the restricted three body problems and serve our purpose of finding low energy transfers between them.

Let us summarise what we have said so far concerning the coupling of the problems:

- A couple of angles ϕ_{SE} and ϕ_{EM} are chosen. These are the angles between the x axis and the Poincaré section $\mathcal{S}$ in each of the problems.

- The integration of the manifolds from the vicinity of the Lyapunov orbits until they intersect $\mathcal{S}$ is performed independently in each RTBP (see figure 5.3).

- The time of the crossing of the Poincaré section is set to $t = 0$. This is also the time when the Poincaré section of the EM system, which is not a fixed plane when looked in SE coordinates, coincides with the Poincaré section of the SE system.

In order to find intersections between the curves we obtain on $\mathcal{S}$, both curves have to be in the same coordinate system. We have chosen the SE coordinates as the general frame in this work, therefore the cut of the manifold corresponding to the EM problem with the Poincaré section has to be transformed from EM coordinates to SE coordinates. There are two steps to be accomplished to this purpose: The conversion of the longitude and time units, and rotation from one system to the other one. The conversion of longitude and time units is easily derived from the mean values of the Earth-Moon distance and the astronomical unit (AU) in km, and the revolution periods of the Earth around the Sun and the Moon around the Earth. When it comes to the rotation angle, it yields from equation (5.3). We do the change of coordinates on the section, that is when $t = 0$, and thus the angle between both x-axis is,

$$\beta = \phi_{SE} - \phi_{EM}.$$

Note that this angle only depends on the constant angles we have fixed between the x-axis and the section $\mathcal{S}$ in each PRTBP.

5.2.4 Connecting trajectories

Given a couple of curves on the Poincaré section one being the intersection of a SE manifold with $\mathcal{S}$ and the other one the intersection of an EM manifold (with the corresponding change of coordinates), we look for intersections between them. See for instance figure 5.5, where the green curve represents the cut of the stable manifold of a Lyapunov orbit around L$_2$ in the SE system, and the red one the cut of a unstable manifold of a Lyapunov orbit around L$_2$ in the EM system.

If intersections are found in $y\dot{y}$ coordinates, the x coordinate can be obtained from them using the implicit definition of the Poincaré section, $g(x, y, \dot{y}) = 0$. In our case, it is straightforward to compute the x coordinate, as it is fixed to $-1 + \mu_{SE}$.
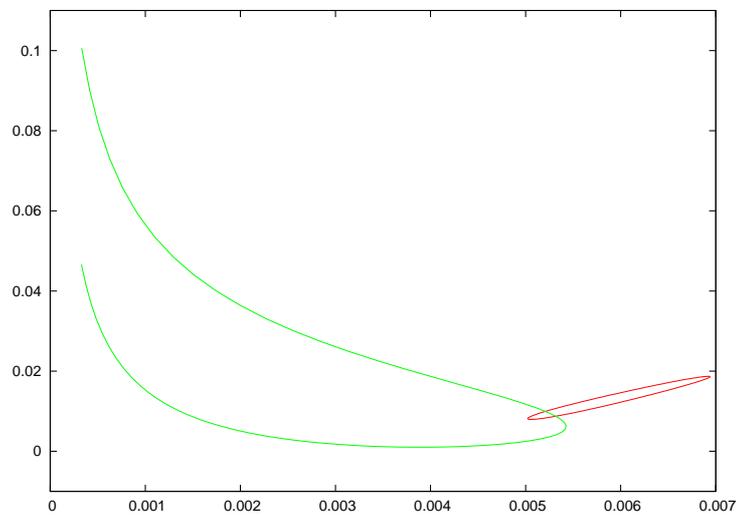
Figure 5.5: $y\dot{y}$ Representation of the first cut with the section of the stable manifold of the $\mathcal{C}=3.0008$ Lyapunov around L$_2$ in the SE system and the first cut with the section of the $\mathcal{C}=3.16$ Lyapunov around L$_2$ in the EM system. We see that the two curves intersect at two different points.

Therefore, we have intersecting points which coincide, so far, in 3 coordinates. The other coordinate, $\dot{x}$, is still unknown from the information that we have on the section and will be computed using the Jacobi constant. However, each one of the RTBP has its corresponding Jacobi constant. Consequently, what we usually get is a different $\dot{x}$ for each problem. So, a maneuver in the x direction of the velocity is necessary for the connecting trajectory to become a real transfer. This maneuver is computed in the following way:

- $\dot{x}$ is computed in the SE problem from $(x, y, \dot{y})$ and $\mathcal{C}_{SE}$.

- The same for $\dot{x}$ in the EM problem. Remember that the points we introduce in the expression of $\mathcal{C}_{EM}$ have to be in EM coordinates. However, once we have obtained $\dot{\bar{x}}_{EM}$ we can transform the complete point to SE coordinates again, obtaining $\dot{x}_{EM}$.

- Finally, the maneuver can be computed as,

$$\Delta v = \Delta \dot{x} = \dot{x}_{SE} - \dot{x}_{EM}. \tag{5.5}$$

In short, the intersection in the $y\dot{y}$ plane does not suffice to find a complete intersection in the phase space, as 2 Jacobi constants are involved and can lead to different $\dot{x}$. See for instance Figure 5.6, that shows the representation of a transfer trajectory obtained using this procedure. The first picture in the figure (top) represents the $xy\dot{x}$ projection, in which a jump is observed at the section crossing. On the other hand, the picture on the bottom represents the $xy\dot{y}$ projection which is continuous as these three coordinates coincide on the section.

For all we have said, there are four constants which play a role when trying to find a connecting trajectory like the ones we are describing. They are:

- The Jacobi constant of the SE problem, $\mathcal{C}_{SE}$.

- The Jacobi constant of the EM problem, $\mathcal{C}_{EM}$.

- The angle of the Poincaré section with the SE x-axis (ϕ_{SE}).

- The angle of the Poincaré section with the EM x-axis (ϕ_{EM}).

The natural thing to wonder now is which combination of values for these constants leads to connecting trajectories and, in a further step, which one minimises the Δv in equation (5.5).

5.2.5   Preliminary explorations

It is extremely difficult to organise all the resulting connections in a coherent way, if we have to take into account all possible values of the four aforementioned constants. In order to simplify the exposition of the results, some considerations have to be made:

- Results are presented for a fixed value of ϕ_{SE} equal to 90 degrees. Note that this angle could have been chosen to be any other angular value, as our method presents no restrictions for it.

- As stated in the previous subsection, all the trajectories that we are showing were obtained by propagating the unstable manifold of the Lyapunovs in the EM RTBP, and the stable manifold of the ones in the SE problem. Consequently, they represent paths from the lunar libration region to the solar one. Trajectories for the way back can be obtained analogously.

- Connections with a low number of cuts are usually preferred, as they provide more direct transfers. Therefore, we explore the first cuts of both manifolds with the Poincaré section.

- Finally, explorations have been made for values of the angle ϕ_{EM} in $[0, \pi)$. For values $\phi_{EM} > \pi$, no intersection between the manifolds has been found on the section (see figure 5.7).
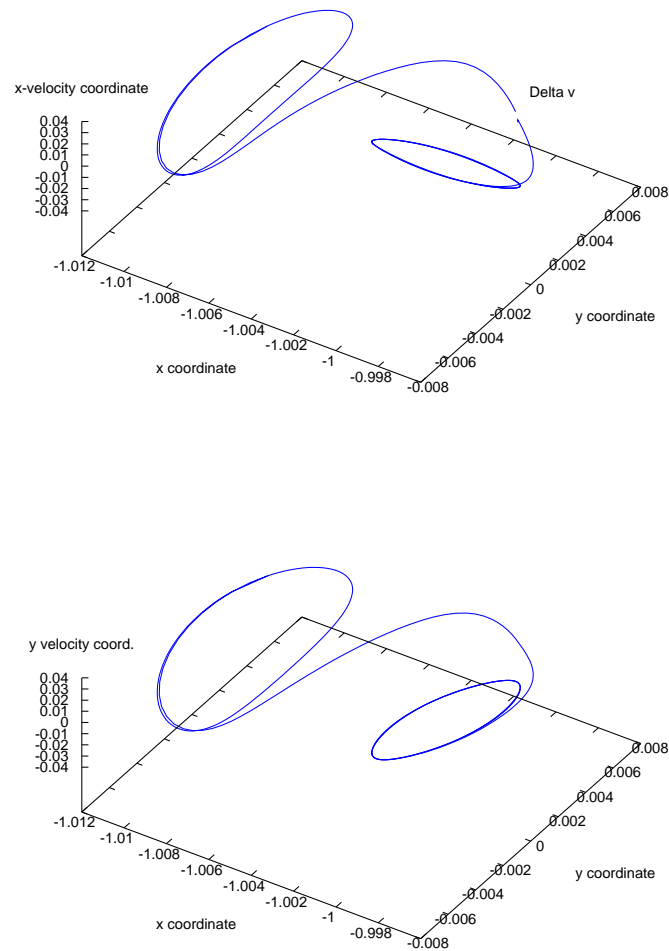
Figure 5.6: Trajectory connecting a L_2 planar Lyapunov orbit of the SE system ($\mathcal{C}_{SE}$=3.00077) with the L_2 Lyapunov of the EM system ($\mathcal{C}_{EM}$=3.18). The picture on the top shows the $xy\dot{x}$ representation, and the Δv can be clearly seen. The figure on the bottom contains the $xy\dot{y}$ representation of the same trajectory, with no jump in the $\dot{y}$ direction.
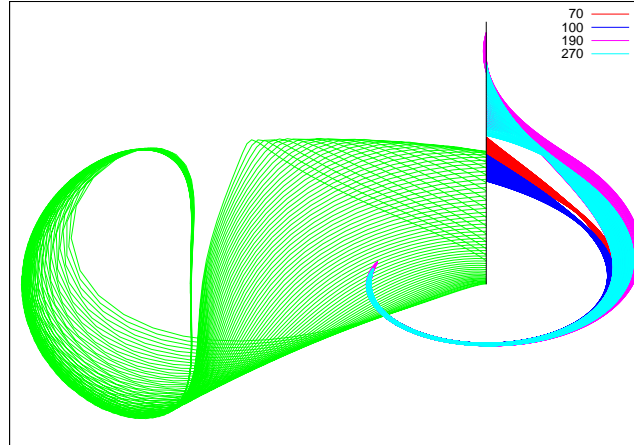
Figure 5.7: For values of ϕ_{EM} bigger than π (180 degrees), the unstable manifolds of Lyapunov orbits around L_2 in the EM problem do not intersect on the section with the stable manifolds of Lyapunov orbits around L_2 in the SE problem.

With these assumptions, explorations show that for each pair of Jacobi constants in $\mathcal{C}_{SE} \times \mathcal{C}_{EM} \in [3.000723, 3.0008622] \times [3.145, 3.184]$, there exists at least one $\phi_{EM} \in (0, \pi)$ for which an intersection in $(x, y, \dot{y})$ can be found between the first cut of the unstable manifold of the Lyapunov of the EM problem with $\mathcal{S}$ and the first cut of the stable manifold of the Lyapunov of the SE problem with the same section. This is a promising result, as a wide range of Jacobi constants is covered (remember that the ranges of $\mathcal{C}$ that allow us to work with the Linstedt-Poincaré expansions for Lyapunovs around L_2 are $[3.000721, 3.0008969]$ and $[3.14445, 3.184163]$ respectively).

Information of some example trajectories found using this method is presented in table 5.2. For each couple ϕ_{EM} and α_{SE}, the connection with lower $\Delta\dot{x}$ cost, the one with smaller α_{EM} in the corresponding family and, finally, the one with shorter transfer time (also belonging to the same family) are included in the table.

Note on the choice of ϕ_{SE} and the computation of connecting trajectories for $\phi_{SE} \neq 90$

The relative configuration is a key element when coupling two different models. In our case, this configuration is determined by two phases: ϕ_{EM} and ϕ_{SE}, which represent the angles between the x axis and the Poincaré section in each of the RTBPs. The aim of this part of our work is to show that connecting trajectories with small Δv exist between both models and to expose a complete methodology suitable for finding such trajectories. With this idea in mind, we chose a representative case ($\phi_{SE} = 90$ degrees) and we claim that the same technique is applicable for other values of ϕ_{SE}. The choice of this particular value as the angle of the Poincaré section in the SE problem is due to the fact that the manifolds we study cross the plane defined by this angle (perpendicular to the x axis) in a transversal way, which is good in terms of the shape and relative positions of the curves cutting the section, and therefore for the search of intersecting points. In addition, this particular plane has a fixed value of the x coordinate (in adapted SE

ϕ_{EM} (deg.)	α_{SE} (km)	α_{EM} (km)	$\Delta\dot{x}$ (m/s)	time (days)
30		17123.2	19.07	204.8
	355162.5	7390.3	37.67	201.9
		14414.6	23.65	201.2
		17123.3	11.88	199.4
	342740.1	8218.2	30.24	200.2
		14887.0	15.88	199.4
		17123.2	3.76	197.7
	330102.8	9123.9	21.69	198.5
		15804.2	6.29	197.7
		14556.0	0	196.1
	317215.5	10142.9	12.52	196.9
		15804.2	-2.73	195.9
		15086.8	-0.0002	195.3
	290520.0	12622.5	-11.5	193.8
		17123.2	-29.14	192.6
		17123.2	-24.26	194.1
	276603.8	14402.0	-30.48	192.1
		17123.2	-45.16	191.1
60		17123.2	46.81	200.6
	361302.0	5179.6	68.89	201.0
		12515.5	-55.29	200.4
		17123.2	43.63	199.7
	355162.5	5570.8	65.7	200.1
		12854.1	51.22	199.5
		17123.2	36.73	197.9
	342740.1	6385.7	58.97	198.4
		13436.4	43.59	197.8
		17123.2	29.06	196.1
	330102.8	7249.7	50.60	196.7
		14550.6	34.11	196.0
		17123.2	20.49	194.4
	317215.5	8223.8	42.49	195.1
		14001.2	27.01	194.3
		16627.7	0	191.1
	290520.0	10471.2	21.44	191.9
		17123.2	1.88	191.0
		12975.0	0	189.7
	276603.8	11855.8	6.6	190.3
		17123.2	-13.38	189.3

ϕ_{EM} (deg.)	α_{SE} (km)	α_{EM} (km)	$\Delta\dot{x}$ (m/s)	time (days)
90		17123.2	62.08	194.4
	330102.8	4457.6	89.80	194.8
		10971.2	74.77	194.2
		17123.2	53.72	192.7
	317215.5	5374.8	81.43	193.1
		12251.5	64.29	192.5
		17123.2	35.30	189.3
	290520.0	7500.9	60.08	189.9
		13436.4	43.14	189.2
		17123.2	22.30	187.6
	276603.8	8741.7	50.45	188.3
		14887.0	28.29	187.5
		17123.2	9.88	185.9
	262216.4	10166.5	35.24	186.6
		14887.0	15.43	185.9
		15048.1	0	184.3
	247265.9	11956.2	17.61	185.1
		17123.3	-8.06	184.2
120		17123.2	110.34	192.7
	330102.8	288.0	146.156	192.6
		8775.8	129.82	192.2
		17123.2	101.65	190.9
	317215.5	651.0	138.17	190.9
		8775.8	121.55	190.5
		17123.2	81.73	187.5
	290520.0	2692.0	119.42	187.6
		9555.3	101.09	187.2
		17123.2	57.07	184.0
	262216.4	5141.4	95.79	184.4
		11625.2	72.97	183.8
		16250.7	26.8	180.5
	231633.6	8431.5	62.48	181.1
		14887.0	31.82	180.4
		16897.2	0	178.6
	215161.1	10844.2	40.89	179.5
		17123.2	-1.15	178.6
		15707.5	0	178.0
	197627.8	15310.9	9.23	178.3
		17123.2	-18.18	177.6

Table 5.2: Connecting trajectories for ϕ_{SE}=90 deg. For each ϕ_{EM} and α_{SE} (first and second columns respectively) data corresponding to three different transfers is presented: the first one corresponds to the cheapest possible connection, the second one to the connection with the smallest possible Lyapunov around the EM L₂ point and finally, the third one to the connection with shortest transfer time.

ϕ_{EM} (deg.)	ϕ_{SE} (deg.)						
	60	70	80	90	100	110	120
30	89.16	58.91	22.67	3.76	55.84	119.27	191.36
	96.17	69.48	–	21.67	75.81	139.72	211.22
40	92.57	64.68	14.96	11.59	64.86	128.98	201.34
	84.33	52.71	–	30.80	86.03	150.59	222.36
50	78.74	45.74	6.47	19.99	74.48	139.37	212.08
	88.46	59.36	–	40.76	97.08	162.35	234.43
60	72.27	53.42	2.96	29.06	84.85	150.59	223.74
	83.78	37.84	16.50	51.62	109.12	175.13	247.57
70	64.74	28.84	8.23	38.97	96.13	162.81	236.48
	78.45	–	13.53	63.66	122.35	189.14	262.00
80	55.94	18.51	0.96	49.89	108.52	176.26	250.57
	72.36	–	25.46	77.11	137.01	204.64	277.96
90	45.58	6.55	11.31	62.08	122.30	191.23	266.31
	65.36	–	39.08	92.27	153.43	221.93	295.75
100	33.25	7.45	23.10	75.86	137.85	208.14	284.17
	57.27	20.92	54.80	109.57	172.03	241.43	315.78
110	18.42	9.49	36.73	91.71	155.69	227.58	304.80
	–	24.04	73.17	129.56	193.32	263.63	338.50
120	0.29	4.06	52.81	110.34	176.64	289.17	329.26
	–	44.03	94.97	152.99	218.03	250.49	–

Table 5.3: Maneuvers in m/s (in $\dot{r}$) corresponding to the intersecting points between the unstable manifold of the Lyapunov orbit around L$_2$ in the EM problem with $\alpha_{EM} = 17123.2$ km and the stable manifold of the Lyapunov orbit around L$_2$ in the SE problem with $\alpha_{SE} = 330102.8$ km, depending on different values of the initial configuration phases (ϕ_{SE} and ϕ_{EM}) (the $r\dot{r}$ projections on the Poincaré section of some of these intersections are shown in figure 5.8). This table shows that the results in terms of Δv are strongly dependent on the chosen values of ϕ_{SE} and ϕ_{EM}, and that the values of ϕ_{SE} between 70 and 90 degrees seem to be the most convenient ones.

coordinates), simplifying the methodology a little bit.

Furthermore, we must remark that the results are strongly dependent on the choice of the initial configuration, as we are not dealing with a single system of differential equations (and thus, the unicity of solutions with respect to initial conditions does not hold). That is to say that results shown in table 5.2, for instance, are only valid when the corresponding ϕ_{EM} and ϕ_{SE} are used. This fact is, actually, consequence of the obvious influence that the relative position of the Earth and the Moon have in the behaviour of the manifolds. Therefore, if this work was to be used for practical reasons in the future, studies on each particular initial configuration should be carried on, using the methodology that is presented here.

In figure 5.8 and table 5.3, an example proving that the methodology can be used for other values of ϕ_{SE} is presented. The variation of both the intersecting points on the section and the costs of the maneuvers depending on ϕ_{SE} can also be observed.

5.2.6   Families of connecting trajectories

If we find a connecting trajectory between the SE and the EM RTBPs, we can find another one, close to the former, by slightly varying either one of the Jacobi constants or ϕ_{EM}. This is due to the continuity of the solutions of each problem with respect to the initial conditions. So, instead of isolated connections we find a kind of manifold of connecting trajectories. Another way to explain it is by representing the connections grouped in families or bifurcation diagrams. In order to visualise these families we can fix the angle ϕ_{EM} (remember that ϕ_{SE} is already fixed to 90 deg) and vary the Jacobi constants for both problems. For instance, in the picture on the top of figure 5.9 some families of connections are depicted for the particular case $\phi_{EM} = 60$ deg. The x-axis corresponds to the Jacobi constant of the EM problem, while the y-axis corresponds to the y coordinate of the connecting point on the section. Each one of the curves is obtained for a particular value of the SE Jacobi constant. On the other hand, in the bottom of the same figure, the same families are represented, but now the y-axis shows the Δv that is needed in the $\dot{x}$ direction for the connecting trajectory to become a transfer path between both models. Similar plots can be obtained for any value of $\phi_{EM} < 180$ deg (see for example figure 5.10).

In order to better understand the way that each of the curves in figures 5.9 and 5.10 are obtained, see figure 5.11. The big green curve of the picture on the left qualitatively represents the first intersection of the stable manifold of a Lyapunov orbit around L_2 of the SE problem with the Poincaré section, for a given $\mathcal{C}_{SE}$. Besides, the small ellipse-like curves represent the first intersection of the unstable manifold of several Lyapunov orbits around L_2 of the EM problem with section $\mathcal{S}$, for four different values of $\mathcal{C}_{EM}$. Curves labelled with numbers from 2 to 4 intersect the SE curve in two points. The y coordinate of these intersecting points is represented in the picture on the right and varies slowly as $\mathcal{C}_{EM}$ increases. Finally, the number of intersections changes from two different values to only one for the curve labelled as number 1. This curve represents a tangency between the EM and the SE manifold curves in the picture on the left, which in turn is the final point for the curve on the right. That is to say that for values of $\mathcal{C}_{EM}$ bigger than the ones corresponding to curve number 1, the unstable manifold of the EM Lyapunov orbits does not intersect the stable manifold of the SE Lyapunov represented on the section.
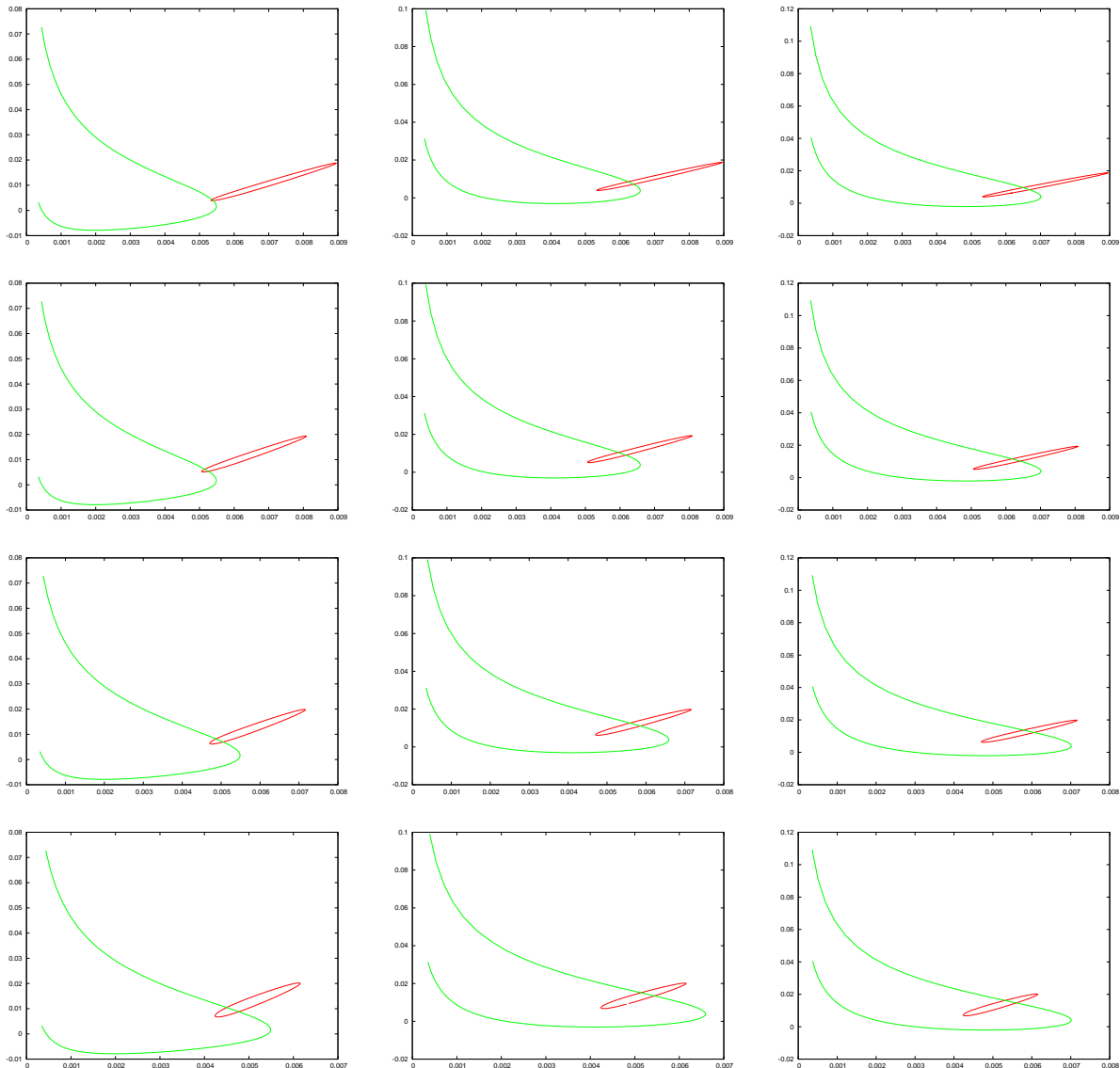
Figure 5.8: $r\dot{r}$ projection of several intersections between the stable manifold of the planar Lyapunov orbit around L$_2$ of the SE problem with $\alpha_{SE} = 330102.8$ km (in green) and the unstable manifold of the planar Lyapunov orbit around L$_2$ of the EM problem with $\alpha_{EM} = 17123.2$ km (in red). First row: $\phi_{EM} = 30$ deg. Second row: $\phi_{EM} = 60$ deg. Third row: $\phi_{EM} = 90$ deg. Last row: $\phi_{EM} = 120$ deg. The columns correspond to fixed values of the ϕ_{SE} equal to 80, 90 and 100 degrees respectively. The red curve is the same in the three pictures of each row, while the green curve is maintined in the columns. Note that if $r = \sqrt{(x+1-\mu)^2 + y^2}$, the $r\dot{r}$ projection corresponds to the $y\dot{y}$ projection when $\phi_{SE} = 90$ deg.
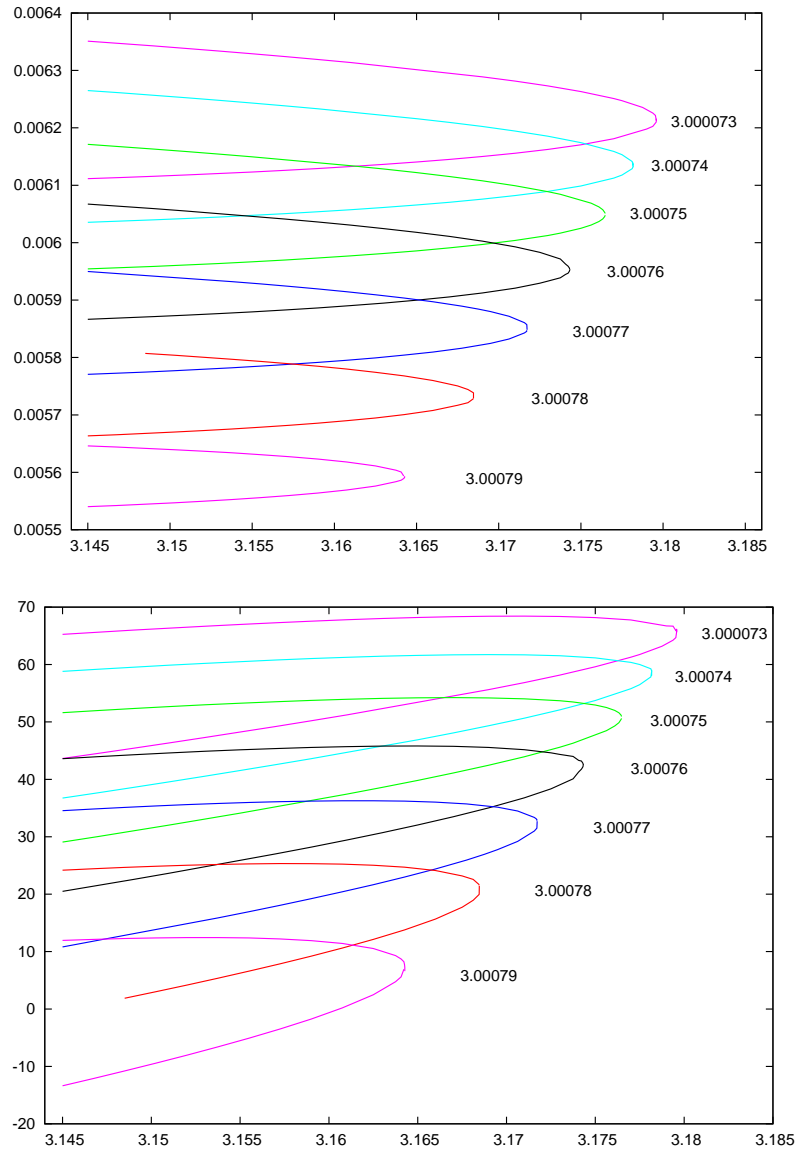
Figure 5.9: (top) Families of connecting trajectories. Angle ϕ_{SE} is fixed to 90 degrees, and ϕ_{EM} to 60 degrees. The x-axis corresponds to values $\mathcal{C}_{EM}$ and the y-axis to the y coordinate of the trajectories on $\mathcal{S}$. Each bifurcation curve corresponds to a particular value of $\mathcal{C}_{SE}$. (bottom) Same families of connections as in the figure above. Now the y-axis presents the cost in m/s of the Δv necessary in the $\dot{x}$ direction for jumping from the manifold of the SE problem to the manifold of the EM one.
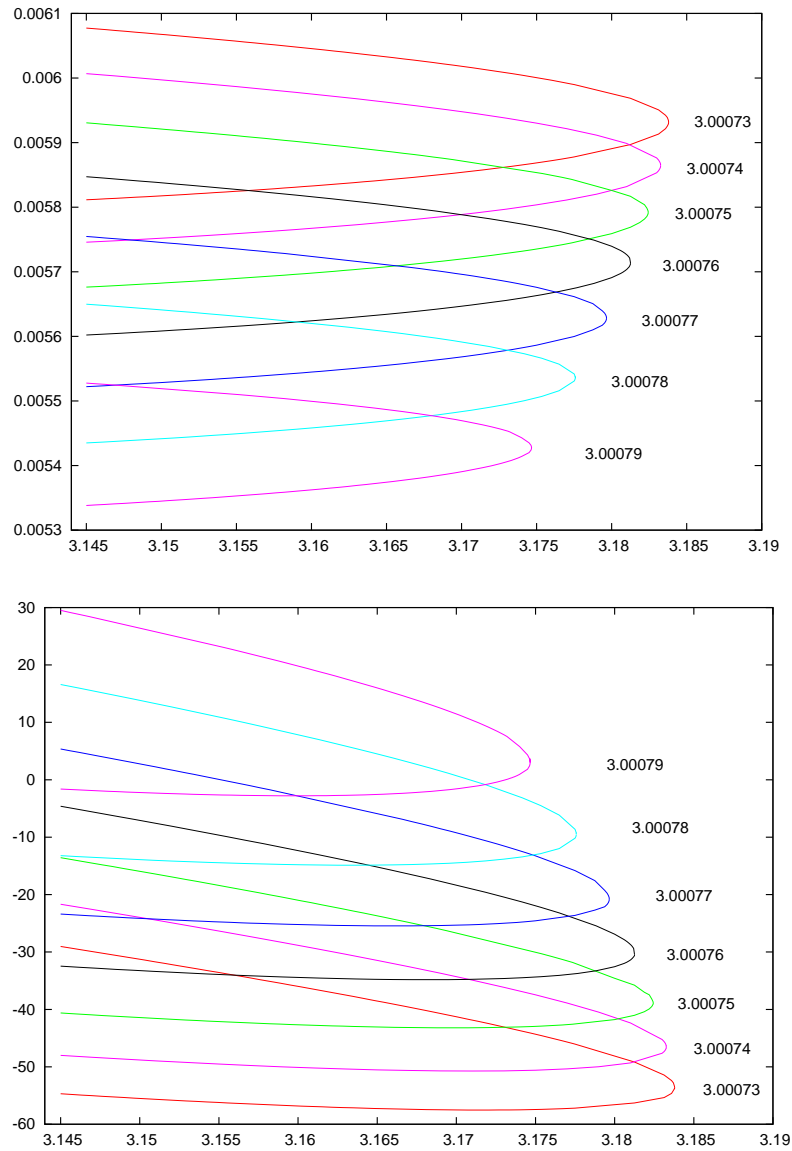
Figure 5.10: Another example of different families of transfer trajectories as in figure 5.9. This time ϕ_{SE} and ϕ_{EM} are fixed to 90 deg.
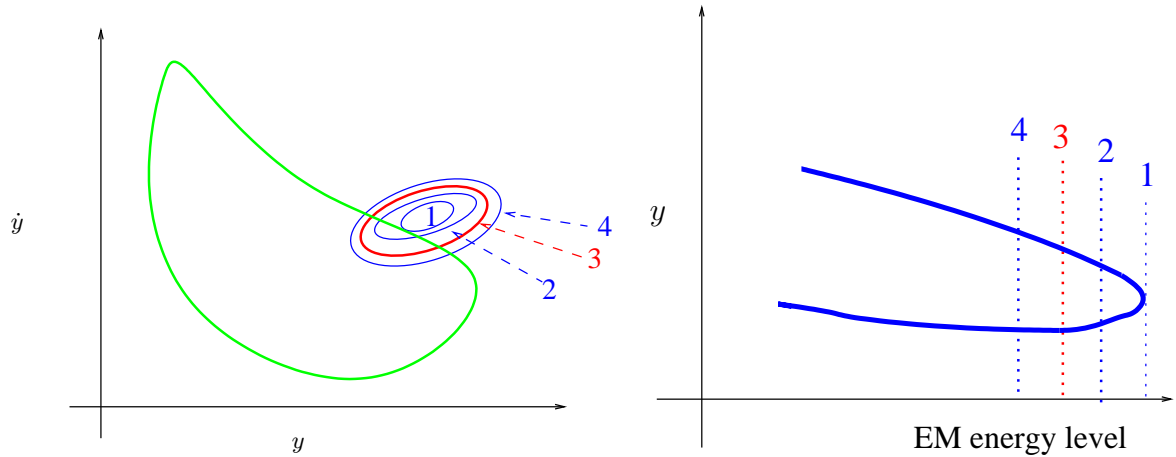
Figure 5.11: Section cut of the SE manifold for a fixed $\mathcal{C}_{SE}$ and cuts of the EM manifolds varying $\mathcal{C}_{EM}$ (see more explanations in the text).

5.2.7   Zero cost connecting trajectories

In addition to presenting important information about the families of connections in an organised way, another important fact can be observed in figures like 5.9 or 5.10. In the bottom part of these figures, the cost in m/s of the Δv necessary for the connecting trajectory to become a complete transfer is not depicted in absolute value but with its sign according to equation (5.5). This fact allows us to realize that in certain families, some of the connections need a positive Δv while some others need a negative one. Thus, the zero-cost line is crossed somehow. This means that for particular Jacobi constants and coupling angles, the manifolds of the coupled SE and EM RTBPs intersect both in position and velocity coordinates, with no need for a maneuver at all.

     If a single model had been used, a complete intersection in the state space for a given epoch would mean that the part of the trajectory coming from the lunar libration region and the part that approaches the solar libration one are indeed the same solution. Note, however, that in our case the complete intersection has a different meaning, as two different models (and their corresponding flows) are being used. Therefore, these zero cost connections do not represent real solutions of the 4 body problem, neither do they follow physical laws. Despite this fact, if the intersection between the manifolds is transversal enough, it may be robust with respect to perturbations. The real 4 body model for the Sun-Earth-Moon-spacecraft relative movements can be seen as a perturbation of our simplified model. Consequently, having a complete intersection in the phase space between the coupled RTBP models can result in very low cost connecting trajectories in more realistic models. Thus, it is worth studying the initial conditions which lead to these so-called zero cost transfers.

Determination of the initial conditions for a zero cost connecting trajectory.

Given ϕ_{SE} and ϕ_{EM}, we know how to compute connecting trajectories between planar Lyapunov orbits for each value of the Jacobi constants. In this way, we obtain pictures like the ones in

figures 5.9 and 5.10. We realized from these pictures that some of the curves representing the connecting trajectories cross the $\Delta v=0$ line. We now want to determine the initial conditions which lead to connecting trajectories with $\Delta v=0$. Let us concentrate on a particular example. For instance, $\phi_{SE} = 90$ deg., $\phi_{EM} = 60$ deg. and $\mathcal{C}_{SE} = 3.00079$ (see figure 5.9).
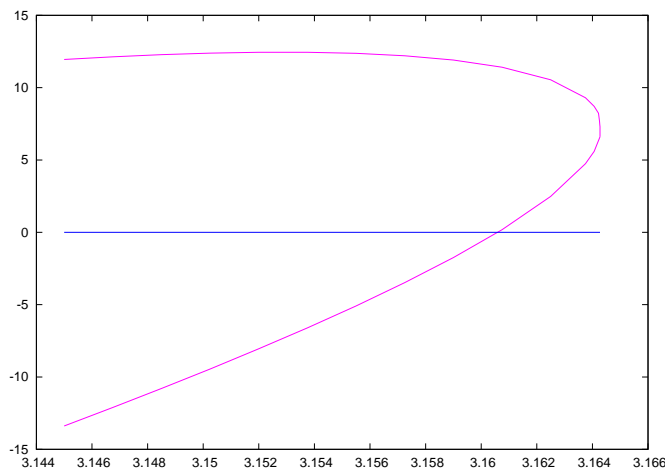
Figure 5.12: Detailed view of the cost curve corresponding to $\mathcal{C}_{SE} = 3.00079$ in figure 5.9.

In figure 5.12 one of the curves of figure 5.9 that crosses the zero cost line is represented in more detail. We can determine by observing this detailed figure the values of the Jacobi constant of the Earth-Moon problem between which the sign of $\Delta\dot{x}$ is changed (i.e. the $\Delta\dot{x} = 0$ line is crossed). In other words, we can find two values of $\mathcal{C}$, one corresponding to a positive Δv, which we note $\mathcal{C}_+$, and the other one to a negative Δv, $\mathcal{C}_-$. In our example, we can take for instance $\mathcal{C}_- = 3.158$ and $\mathcal{C}_+ = 3.162$. Using these values, $\mathcal{C}_+$ and $\mathcal{C}_-$, a zero finding procedure can be started.

Let ϕ_{SE} and ϕ_{EM} be fixed. Let F be,

$$F : [3.145, 3.185] \times [3.00073, 3.00089] \to \mathbb{R}^2, \quad F(\mathcal{C}_{SE}, \mathcal{C}_{EM}) = (\Delta\dot{x}_1, \Delta\dot{x}_2)$$

such that for each couple of Jacobi constants, it gives the $\Delta\dot{x}$ maneuvers corresponding to the intersections between the manifolds of the Lyapunov orbits defined by these $\mathcal{C}$, computed on the Poincaré section. Note that F takes values on $\mathbb{R}^2$ when two cuts occur between the aforementioned manifolds on the section (see figure 5.11). Remark also that applying F to a couple of Jacobi constants is equivalent to applying it to a couple of Lyapunov orbits, due to the unique existence of these orbits for each level of energy. Furthermore, each Lyapunov orbit is parametrised by a phase. Consequently, F is applied to a couple of Jacobi constants, but it implicitly depends on the phases that represent the connecting trajectories.

We restrict F to the chosen value of $\mathcal{C}_{SE}$. In our example, $\mathcal{C}_{SE} = 3.00079$. In addition, we select the correct branch of connecting trajectories, that is the one containing the intersection with $\Delta v = 0$. So, the restriction of F becomes,

$$F^* : [3.145, 3.185] \times \{3.00079\} \to \mathbb{R}.$$

Now a zero finding procedure applied to F^* allows us to compute a Jacobi constant for the EM problem, $\mathcal{C}_0$, such that $F^*(\mathcal{C}_0) = 0$. In fact, an iterative zero finding method does not provide the exact $\mathcal{C}_0$ but a good approximation to it for i big enough such that $|F^*(\mathcal{C}^{i+1})| < \delta_1$ or $|\mathcal{C}_-^{i+1} - \mathcal{C}_+^{i+1}| < \delta_2$ (with δ_1 and δ_2 given tolerances, which we take from 10^{-12} to 10^{-14})

Once the Jacobi constants that lead to the zero cost connection for each one of the problems are known, the corresponding manifolds are integrated to the section. Finally, the set of initial conditions that completely determine the zero cost connection is:

$$(\phi_{SE}, \phi_{EM}, \mathcal{C}_{SE}, \mathcal{C}_{EM}, \theta_{SE}, \theta_{EM})$$
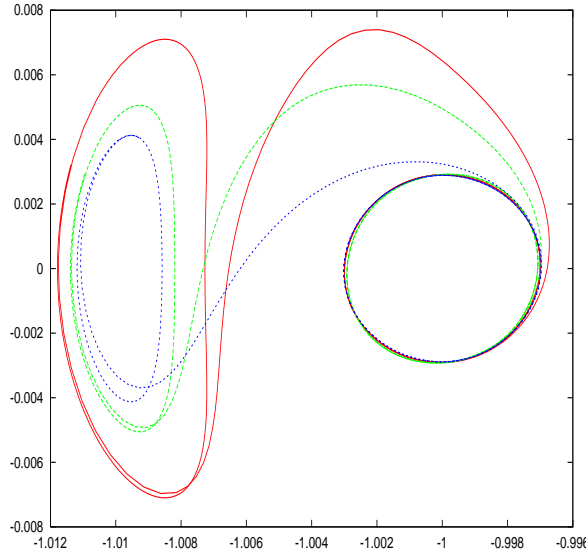
Figure 5.13: Zero cost transfers or connecting trajectories ($\phi_{SE} = 90$ deg). Red: $\mathcal{C}_{SE} = 3.00073263$, $\mathcal{C}_{EM} = 3.1703538$, $\phi_{EM} = 50$ deg. Green: $\mathcal{C}_{SE} = 3.00081225$, $\mathcal{C}_{EM} = 3.156907053$, $\phi_{EM} = 125$ deg. Blue: $\mathcal{C}_{SE} = 3.00084025$, $\mathcal{C}_{EM} = 3.166630339$, $\phi_{EM} = 170$ deg.

The procedure for finding zero cost transfers can be applied whenever a change in the sign of the Δv occurs for a particular family of connections. Some example zero cost connecting trajectories that were obtained in this way are represented in figure 5.13.

5.2.8   Families of zero cost connecting trajectories

To sum up, a method for exactly determining the initial conditions that represent a zero cost connecting trajectory, once a crossing of the Δv=0 line is detected, was presented in the previous section. An essential condition before starting the zero finding method that leads to the zero cost connection, however, is to perform a study of all connecting trajectories for a particular value of ϕ_{EM}, and hope that some of the curves we obtain will cross the Δv=0 line. Nevertheless, we are interested in obtaining families of zero cost connections, rather than isolated ones. Our experience in dealing with the restricted three body problem makes us think that this is possible,

as the continuous dependency of the solutions on the initial conditions makes all phenomena appear in families or manifolds.

Given ϕ_{SE} and ϕ_{EM}, let $(\mathcal{C}_{EM}, \mathcal{C}_{SE})$ be a couple of Jacobi constants for which a zero cost connecting trajectory exists. These Jacobi constants define the Lyapunov orbits, which are, in turn, parametrised by an angle, θ. Therefore, as we saw in the previous section, the complete set of initial conditions characterising a zero cost connection is,

$$(\phi_{SE}, \phi_{EM}, \mathcal{C}_{SE}, \mathcal{C}_{EM}, \theta_{SE}, \theta_{EM}).$$

We take a set of initial conditions for which a zero cost connection exists and we start a continuation method. That is, we want to find a new set $(\phi_{SE}, \phi_{EM}, \mathcal{C}'_{SE}, \mathcal{C}'_{EM}, \theta'_{SE}, \theta'_{EM})$, close to the original one and such that it also leads to a zero cost connection. At the moment, we keep the angles ϕ_{SE} and ϕ_{EM} fixed.

Before starting to explain the continuation method itself, let us describe in more detail the application which integrates the initial conditions until they reach the Poincaré section. As we said before, for each $\mathcal{C}$ there exists only one planar Lyapunov orbit, which in Lindstedt Poincaré coordinates is defined by its amplitude, α. Therefore, the set $(\mathcal{C}_{SE}, \mathcal{C}_{EM}, \theta_{SE}, \theta_{EM})$ is equivalent to $(\alpha_{SE}, \alpha_{EM}, \theta_{SE}, \theta_{EM})$. Now, the flow of the restricted three body problems is applied to each couple (α, θ) (i.e. to each initial point on the Lyapunov orbit) in the following way,

$$\Phi_{SE} : \mathbb{R}^+ \times [0, 2\pi] \to \mathcal{S}$$

$$\Phi_{SE}(\alpha_{SE}, \theta_{SE}) = (-1 + \mu_{SE}, \dot{x}_s, y_s, \dot{y}_s) \in \mathcal{S}.$$

$$\Psi \circ \Phi_{EM} : \mathbb{R}^+ \times [0, 2\pi] \to \mathcal{S}$$

$$\Psi \circ \Phi_{EM}(\alpha_{EM}, \theta_{EM}) = \Psi(\bar{x}, \dot{\bar{x}}, \bar{y}, \dot{\bar{y}}) = (-1 + \mu_{SE}, \dot{x}_l, y_l, \dot{y}_l) \in \mathcal{S}.$$

where Φ_{EM} and Φ_{SE} are the flows of the corresponding restricted three body problems, and Ψ is the change of coordinates from Earth-Moon to Sun-Earth+Moon reference frame. Obviously, Ψ depends on the angles ϕ_{EM} and ϕ_{SE}. Note that the time does not appear in the equation of the flow, as the RTBP is autonomous.

Now, the problem of finding a zero cost connection is reduced to finding a zero of the following function:

$$g(\alpha_{SE}, \alpha_{EM}, \theta_{SE}, \theta_{EM}) = (\dot{x}_l - \dot{x}_s, y_l - y_s, \dot{y}_l - \dot{y}_s). \tag{5.6}$$

We will apply a Newton-like method to g, as it is not difficult to compute all necessary information about the differentials of all the functions that are used. Actually, it is straightforward to compute the differential of Ψ, as it only consists of a rotation, a translation and a scaling of the magnitudes. Furthermore, the differential of the flow functions is essentially computed by using the first variational equations and slightly correcting them on the section. Thus, we can easily obtain the differential matrix of g. However, the dimension of this matrix is 3×4, as in (5.6) we have 3 equations but 4 variables. Therefore, the generalisation of the 1-dimensional Newton method cannot be used, as it applies to square matrices.

Let $x_z = (\alpha_{SE}, \alpha_{EM}, \theta_{SE}, \theta_{EM})$ represent a zero cost connection, $g(x_z) = (0\ 0\ 0)^t$. Remember that the Kernel of the linear application with matrix $Dg(x_z)$ is the set,

$$\mathrm{Ker}(Dg(x_z)) = \{w \in \mathbb{R}^4 \mid Dg(x_z)w = (0\ 0\ 0)^t\}.$$

The maximum range of the matrix $Dg(x_z)$ is 3. Therefore, the dimension of $\mathrm{Ker}(Dg(x_z))$ has to be greater or equal than one. This means that $\exists\ w \in \mathbb{R}^4$ such that $Dg(x_z)w = (0\ 0\ 0)^t$ and $w \neq (0,0,0,0)$. In other words, $\mathrm{Ker}(Dg(x_z)) \neq \{(0,0,0,0)\}$. Take $v \in \mathbb{R}^4$ such that $v \in \mathrm{Ker}(Dg(x_0))$, $v \neq (0,0,0,0)$. Now take $x \in \mathbb{R}^4$ close to x_z, $x = x_z + \epsilon v$ with $\epsilon \ll 1$.

For x we have that,

$$\begin{aligned} g(x) &= g(x_z) + \epsilon Dg(x_z)v + O(\epsilon^2) \\ g(x) &= 0 + 0 + O(\epsilon^2) \end{aligned} \qquad (5.7)$$

$g(x)$ is small. We want to correct x in order to obtain x^* such that $g(x^*) = (0\ 0\ 0)^t$ and x^* is close to x_z.

So, we set $x^0 = x$ and iteratively correct x in the following way,

$$x^{i+1} = x^i + \Delta x^i$$

with $\Delta x^i = (\Delta^i \alpha_{SE}, \Delta^i \alpha_{EM}, \Delta^i \theta_{SE}, \Delta^i \theta_{EM})$.

As we already explained, Δx^i cannot be directly computed by using a Newton method, as the corresponding differential matrix is not square. Therefore, we use the Lagrange multipliers method and consider minimum norm corrections at each step. That is to say that for each i we look for a Δx^i satisfying:

1. $Dg(x^i)\Delta x^i + g(x^i) = 0$ *(Newton like condition)*,

2. $\|\Delta x^i\|^2 = \min_{\Delta x \in W} \|\Delta x\|^2$, where $W \subset \mathbb{R}^4$ is the set of vectors satisfying the previous condition.

In this way, we need a vector multiplier $\lambda \in \mathbb{R}^3$. The Lagrange function that we have to minimise is:

$$G : \mathbb{R}^4 \times \mathbb{R}^3 \to \mathbb{R}$$
$$G(\Delta x^i, \lambda) = \|\Delta x^i\|^2 + \lambda(Dg(x^i)\Delta x + g(x^i)).$$

Equivalently, we have to solve the following system of linear equations,

$$\frac{\partial g}{\partial \Delta x_j}(x^i) = 0, \quad j = 1, 4, \qquad \frac{\partial g}{\partial \lambda_j}(x^i) = 0, \quad j = 1, 3.$$

$$\begin{pmatrix} 2Id_{4\times 4} & Dg^T \\ Dg & 0_{3\times 3} \end{pmatrix} \begin{pmatrix} \Delta\alpha_{SE} \\ \Delta\alpha_{EM} \\ \Delta\theta_{SE} \\ \Delta\theta_{EM} \\ \lambda_1 \\ \lambda_2 \\ \lambda_3 \end{pmatrix} + \begin{pmatrix} 0 \\ \vdots \\ \\ 0 \\ g_1(x_1^i) \\ g_2(x_1^i) \\ g_3(x_1^i) \end{pmatrix} = \begin{pmatrix} 0 \\ 0 \\ \\ \vdots \\ \\ \\ 0 \end{pmatrix}$$

This method quickly converges to $x = (\alpha'_{SE}, \alpha'_{EM}, \theta'_{SE}, \theta'_{EM})$ such that $g(x) = 0$. From this new zero cost connection represented by x, the continuation procedure can be started again, until the limiting values of the amplitudes related to the good convergence of the Lindstedt-Poincaré series are met. In this way, we obtain the curves represented in figure 5.14. Each curve represents the zero cost connections between Lyapunov orbits for $\phi_{SE} = 90$ degrees and the values of ϕ_{EM} indicated. Both pictures in this figure are equivalent, due to the aforementioned correspondence between $\mathcal{C}$ and α. In the picture on the top, the curves represent couples of Jacobi constants linked by zero cost connections, while in the picture on the bottom the same connections are represented in terms of the amplitudes α, in km, of the corresponding planar Lyapunov orbits.

So, we already know how to obtain a family of zero cost connections for fixed ϕ_{SE} and ϕ_{EM}, provided that a crossing of the zero-cost line has been detected when representing the connecting trajectories for the initial configuration represented by these phases. However, it would be interesting to be able to find zero cost connections more independently. That is, without having to perform all the previous explorations and computations leading to figures like 5.9 or 5.10.

For instance, given one of the curves of zero cost connecting trajectories containing either points of the type $(\mathcal{C}_{SE}, \mathcal{C}_{EM}, \theta_{SE}, \theta_{EM})$ or $(\alpha_{SE}, \alpha_{EM}, \theta_{SE}, \theta_{EM})$, for a particular value of ϕ_{EM}, one can think of changing this ϕ_{EM} and finding a new curve of zero velocity connections. A simple way of doing this is the following,

1. Choose a new value ϕ'_{EM}, close to ϕ_{EM} for which the curve of zero cost connections has already been found.

2. Take α'_{SE} (respectively $\mathcal{C}'_{SE}$) close to one of the α_{SE} of the aforementioned curve of zero cost connections and fix it.

3. Start a Newton method with $(\alpha'_{SE}, \alpha_{EM}, \theta_{SE}, \theta_{EM})$, in order to find a zero of $g(\alpha'_{SE}, \alpha_{EM}, \theta_{SE}, \theta_{EM})$. Note that if α'_{SE} is fixed, g depends on three variables. Therefore, the usual Newton method can be used in this case, as Dg becomes a square matrix.

If a zero cost connection exists for the values we have fixed of ϕ_{EM} and α'_{SE}, the Newton method will converge to it. Afterwards, the continuation method using Lagrange multipliers that we explained above can be used again to obtain the whole curve of zero cost connecting trajectories corresponding to the new ϕ_{EM}. However, we have blindly chosen α'_{SE} and ϕ'_{EM}. Therefore, it may happen that no zero cost connecting trajectory exists for these values. In this case, we change our choices and try again. This method is not as robust as the one starting by an already found zero cost connection. However, it has the advantage of allowing us to proceed without having to find all the connecting trajectories for each particular ϕ_{EM} and looking for intersections with the $\Delta v = 0$ line. It is the combination of these two strategies which allowed us to obtain figure 5.14.
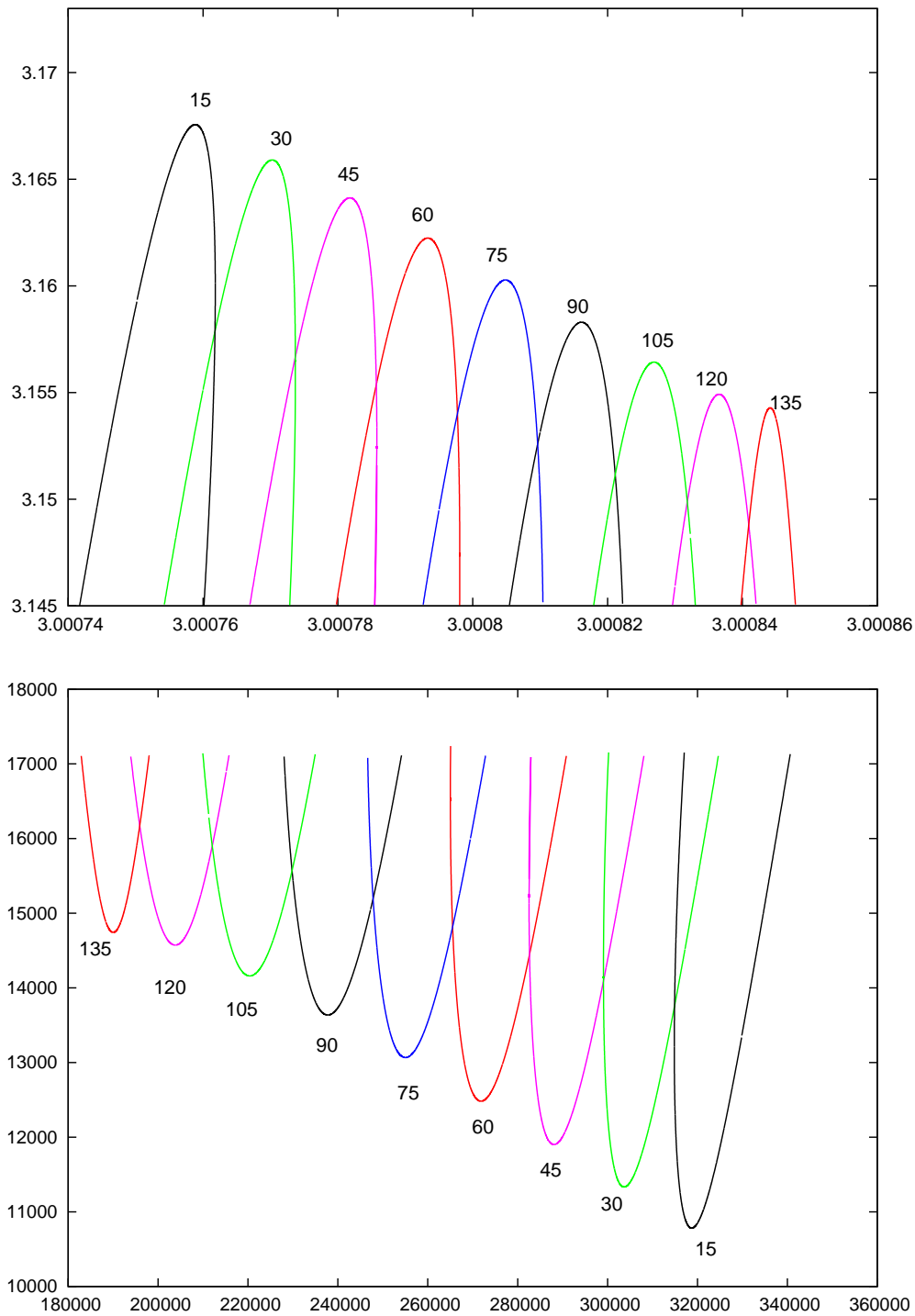
Figure 5.14: Families of zero cost connecting trajectories from planar Lyapunov orbits around the lunar L_2 and the same kind of orbits around the solar L_2 point. (top) pairs of Jacobi constants linked by zero cost transfers in the coupled RTBPs model. (bottom) same zero cost connections, but represented in terms of the amplitudes, in km, of the corresponding Lyapunov orbits. The x axis of the figures refers to the SE problem, while the y axis to the EM problem. The angle ϕ_{SE} is fixed to 90 degrees, while the number labelling each one of the curves corresponds to the value of ϕ_{EM} in degrees.

5.3   Connecting trajectories between Lissajous orbits

5.3.1   Introduction

In the previous section we studied connecting trajectories from planar Lyapunov orbits of the Earth-Moon L$_2$ to planar Lyapunov orbits of the Sun-Earth one. These trajectories mainly have a theoretic interest, confirming the existence of natural channels between both problems, and allowing us to better understand the behaviour of the transfer trajectories and to test some tools for their computation. However, our work is aimed at applications in mission design. Therefore, we need models which are more accurate than the planar approximations to the Sun-Earth and Earth-Moon systems. To start with, we will use three dimensional RTBPs. Concerning the orbits, we use 3-dimensional Lissajous orbits.

Once the connecting trajectories have been computed using two coupled RTBPs, another big step has to be taken, which is the refinement of the trajectories to a realistic ephemeris model. In this work, we have used a JPL ephemeris model. One of the most relevant differences between a RTBP model and an ephemeris model is that a realistic model is no longer autonomous. This implies that the results are dependent on the times chosen for the refinement.

5.3.2   Lissajous orbits and their hyperbolic manifolds

Lissajous orbits are quasi-periodic motions around the libration points. They are the composition of two oscillations: one in the plane of relative motion of the primaries (known as *in-plane* oscillation), and another oscillating movement perpendicular to this plane (known as *out-of- plane* oscillation). A more detailed description of these orbits can be found in chapter 3. Remember, however, that the linear approximation to these orbits and the manifolds arising from them provides us with useful information:

$$\left. \begin{array}{l} x(t) = A_1 e^{\lambda t} + A_2 e^{-\lambda t} + A_x \cos\left(\omega t + \phi\right) \\ y(t) = cA_1 e^{\lambda t} - cA_2 e^{-\lambda t} + \bar{k} A_x \sin\left(\omega t + \phi\right) \\ z(t) = A_z \cos\left(\nu t + \psi\right) \end{array} \right\} \tag{5.8}$$

$(\dot{x}, \dot{y}, \dot{z})$ are obtained from this expressions by differentiating with respect to t. $(A_1,\, A_2,\, A_x,\, A_z)$ are called amplitudes and characterise the orbit. On the other hand, phases ϕ and ψ represent the point on this orbit at $t = 0$. That is:

- A_1 and A_2 are called hyperbolic amplitudes. When both of them are zero, a point on the central manifold is obtained. In our case, a point on the Lissajous orbit, is obtained.

- A_x and A_z are the central amplitudes. They indicate the amplitude of the aforementioned in-plane and out-of-plane oscillations. Furthermore, these two amplitudes are independent from each other, in a range which depends on the Jacobi constant. That is to say that the in-plane and out-of-plane oscillations can be chosen to be similar in amplitude, or, on the contrary, one of them can be much more elongated than the other. Actually, this property implies an operational advantage of Lissajous orbits over the traditionally used Halo orbits. Remember that Halo orbits appear when a particular relationship between the frequencies of the oscillation is satisfied, and this results in a particular relationship

between the amplitudes, usually one of them being much bigger than the other one. For real missions, this fact implies long excursions of the satellite in one of the directions, which are not always desired.

- When $A_1 \neq 0$ and $A_2 = 0$, the part containing positive exponential terms in forward time in equations (5.8) survives. Therefore, the solution goes away exponentially fast from the central part. We say that a point on the unstable manifold of the Lissajous orbit defined by A_x and A_z is obtained in this case.

  Respectively, when $A_1 = 0$ and $A_2 \neq 0$, the solutions approach the Lissajous in forwards time, as they contain negative exponential terms, and we get a point on the stable manifold of the Lissajous orbit.

Therefore, A_x and A_z characterise the size of the Lissajous, while A_1 and A_2 tell us whether the points are on the central or the hyperbolic manifolds. Finally, ϕ and ψ represent each particular initial point on the solution defined by these four amplitudes.

5.3.3   Coupling between the two Restricted Three Body Problems

As we saw for the planar case, a convenient way of tackling the four body problem Sun-Earth-Moon-Spacecraft is to decouple it in two different restricted three body problems: the Sun-Earth+Moon RTBP (SE) and the Earth-Moon one (EM). Furthermore, we use the SE problem as general reference frame. Therefore, the natural thing to do is to deploy the Earth-Moon RTBP inside the Sun-Earth+Moon model.

Remember that the small primary of the SE somehow represents the Earth and the Moon together in the point (1-μ_{SE}, 0, 0). In fact, this point is the barycenter of the EM system. Then, this barycenter, which in the EM adapted coordinate frame acts as the origin of coordinates, circles the Sun at a constant angular rate on the ecliptic plane, completing a revolution every year. The Earth and the Moon, in turn, are assumed to circle around their common center of mass, in a plane with fixed small inclination with respect to the ecliptic. Finally, the position of the Moon with respect to the Sun-Earth axis is described by two angles (see figure 5.15):

- α: the angle from the axis joining the Sun and the Earth-Moon barycenter to the line of nodes of the Moon orbit, measured on the ecliptic plane.

- β: the angle from the line of nodes to the position of the Moon, measured on the plane of motion of the Moon around the Earth, or the plane of relative motion of the Earth and the Moon (mean longitude of the Moon).

Relation between (α, β) and the Sun-Earth-Moon angle, γ.

The relative configuration of the Sun, the Earth and the Moon at a given moment of time is usually described by a single angle, rather than the α and β that we defined. The Sun-Earth-Moon angle, γ, can be defined in the following way:

- Let P be the instantaneous plane of relative motion of the Earth and the Moon.

- Let r be the vector joining the Earth-Moon barycenter and the Sun.
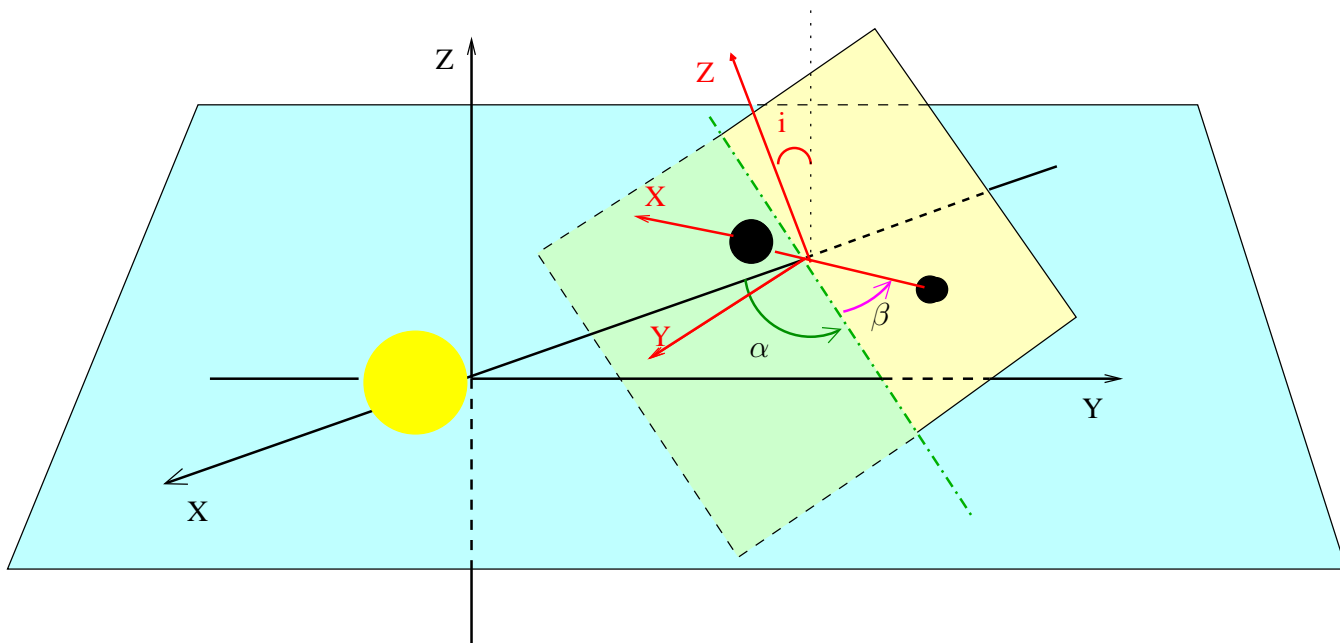
Figure 5.15: Coupling of the RTBPs. The figure shows the three angles which relate the SE coordinate frame with the EM one: i (inclination), α and β.

- r can be projected on P and r' is obtained.

- Let OX be the axis joining the Earth and the Moon.

- Now, define the Sun-Earth-Moon angle, γ, as the angle between OX and r', measured counterclockwise on P.

Simple geometrical considerations allow us to transform γ to (α, β) and the way back (see figure 5.15 and 5.16).

In spite of this geometrical simplicity, the transformation involves cumbersome algebra, which has been omitted in this dissertation.

5.3.4   Poincaré section

If we work with three dimensional RTBPs, the state space becomes 6 dimensional. In this case, a Poincaré section is a set of points of the form

$$\mathcal{S} = \{X = (x, y, z, \dot{x}, \dot{y}, \dot{z}) \in \mathbb{R}^6 \mid g(X) = 0\},$$

with $g : \mathbb{R}^6 \to \mathbb{R}$. Remember that Poincaré sections are used, in general, to study the flow of a system of differential equations in a lower dimensional space. The use of Poincaré sections is convenient again in this part of our study.

Our goal is to use the unstable manifold of a Lissajous orbit belonging to one of the models and integrate it until it meets the stable manifold of a Lissajous orbit of the other model. The Poincaré
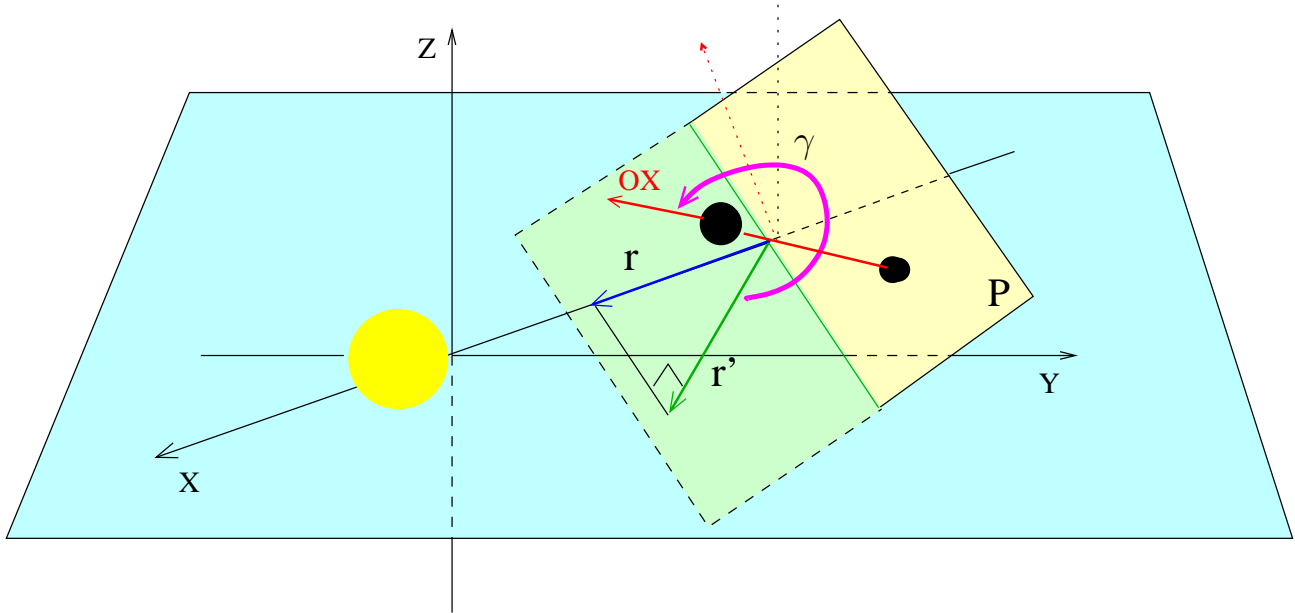
Figure 5.16: Coupling of the RTBPs. The figure shows the angle Earth-Moon-Sun (γ).

section will be used as the meeting point. Once $\mathcal{S}$ has been chosen, initial conditions on the stable (respectively unstable) invariant manifold of a particular Lissajous in the Sun-Earth+Moon system (respectively Earth-Moon) can be integrated backwards (respectively forwards) in time until they intersect $\mathcal{S}$.

As for the planar case, we take $\mathcal{S} = \{X \mid x = -1 + \mu_{SE}\}$ (in SE coordinates). This plane forms a fixed angle of 90 degrees with the SE x-axis and contains the Earth-Moon barycenter, which is the EM origin of coordinates.

Moreover, the RTBP model is autonomous. That is to say that time is not explicit in the equations of motion. Therefore, we can set $t = 0$ whenever we want. For the sake of simplicity, we choose $t = 0$ to be the moment when the manifolds intersect the section $\mathcal{S}$. As we explained above, each relative configuration between the SE and EM problems is defined by two angles: α and β. At time $t = 0$ is when the coupling between both problems is the one shown in figure 5.15. Let us discuss how this configuration changes with respect to time.

$\mathcal{S}$ is fixed in the SE coordinates. However, as it happened for the planar case, $\mathcal{S}$ is time dependent in EM coordinates. In fact, the EM x-axis rotates in the plane of motion of the Moon and the Earth, completing a revolution every month, and this modifies the angle β. Therefore $\dot{\beta} = \frac{2\pi}{27.3216}$ (rad/day), as 27.3216 days is the average time for the mean longitude of the Moon to increase 2π radians. In addition, the Earth-Moon line of nodes also rotates with respect to the Sun during the year, affecting angle α. In addition to the rotation of the Earth-Moon barycenter on the ecliptic, which makes the angle between the line of nodes and the SE x-axis vary in a clockwise direction (retrograde), the phenomenon known as regression of the nodes has to be taken into account, too. Consequently, the final average rate of variation of α is the addition of these two regressions: $\dot{\alpha} = -2\pi \left(\frac{1}{365.2536} + \frac{1}{18.5995 \times 365.2536} \right)$ (rad/day), as the cycle of regression of the lunar nodes has an average period of 18.5995 years.

The rates $\dot{\beta}$ and $\dot{\alpha}$ allow us to know the relative configuration of both problems at each moment of time. This knowledge is useful, for instance, when changes of coordinates at moments of time $t \neq 0$ are necessary.

5.3.5   Intersections on the Poincaré section

We aim at finding transfer trajectories between Lissajous orbits in the coupled model, given an initial configuration. We know that hyperbolic manifolds provide a way of quickly going away or, on the contrary, approaching a Lissajous orbit. Our intention, then, is to find intersections between the stable manifold of one of the Lissajous and the unstable manifold of the other one, as such intersections provide a natural way of leaving the vicinity of the first Lissajous and approaching the other one. For this purpose, there are two possible senses of motion: from the EM Lissajous to the SE one, and the other way round. In this work, the EM to SE sense has been chosen. This means that we will use the unstable manifold of the EM orbit (because it goes away from the vicinity of L_2), and the stable manifold of the SE orbit (as it approaches it). For the way back, that is from SE to EM libration regions, exactly the same methodology could be applied and similar results would be obtained.

Remember that a state on one of the hyperbolic manifolds of a Lissajous orbit is represented in Lindstedt Poincaré coordinates by four amplitudes and a couple of phases. Let $(A_x, A_z)_{\mathrm{SE}}$ be the central amplitudes defining the Lissajous around L_2 in the SEM system, and $(A'_x, A'_z)_{\mathrm{EM}}$ the amplitudes defining the Lissajous around L_2 in the EM system. The hyperbolic amplitudes, A_1 and A_2 are set to 0 or ϵ, depending on whether the manifold is stable (SE) or unstable (EM). Finally, in order to obtain a set of initial conditions representing the whole manifold of the Lissajous orbit in both RTBPs, we take a discrete set of $(\phi_i, \psi_j) \subset [0, 2\pi]\mathrm{x}[0, 2\pi]$, $i = 1.. \ n_1$, $j = 1.. \ n_2$.

Consequently, the sets of initial conditions that we have are:

- $(0, \epsilon, A_x, A_z, \phi_i, \psi_j)_{SE}$, $i = 1..n_1$, $j = 1..n_2$, for the stable manifold of the SE Lissajous orbit.

- $(\epsilon, 0, A'_x, A'_z, \phi'_i, \psi'_j)_{EM}$, $i = 1..n'_1, j = 1..n'_2$, for the unstable manifold of the EM Lissajous orbit.

where $\epsilon << 1$ represents the distance on the hyperbolic manifold, from the quasi-periodic Lissajous orbit to the point which is used as initial condition.

We integrate the SE initial conditions backwards in time, until they intersect $\mathcal{S}$. EM conditions are integrated forwards in time in the EM system, until they also intersect $\mathcal{S}$. However, the Poincaré section is given in SE coordinates and the integrated points coming from the lunar region are in EM coordinates. There are two possible ways of coping with this problem. The first is to find the expression of $\mathcal{S}$ in EM coordinates, according to the relative configuration at $t = 0$. Once the cut has been found in EM coordinates, the inverse change of coordinates is applied to the resulting intersecting points, in order to have them in the same coordinate frame as the SE ones. One could also think of not transforming the section, but transforming the integrated points at each step to SE coordinates until the cut with $\mathcal{S}$ in SE coordinates was found and refined. This second option requires many more changes of coordinates, with the consequent increase in

computational time that this implies. For this reason, the first approach has been used in the present work.

Now that we know which are the steps we have to follow to obtain the cuts of the manifolds with the Poincaré section, it is time to look for intersections between them. In the 3-dimensional models, intersections on $\mathcal{S}$ are not curves as it happened for the planar models. Any planar projection of the intersections we are dealing with is 2-dimensional. In addition, complete information about the state space cannot be derived from any of the possible planar projections. In a planar projection there is only information about two coordinates. Therefore, four coordinates are still free. Furthermore, the Jacobi constant provides another relation between these 4 coordinates. The function defining the section provides another one. All in all, always two degrees of freedom remain unsolved when looking at the aforementioned projections[1].

Therefore, one has to make some more considerations before knowing how to take advantage of a planar projection of the intersection of the manifolds with $\mathcal{S}$. As it is well known, differences in velocity can always be adjusted by an adequate Δv. However, deviations in position cannot be dealt with in the same way, as maneuvers do not produce a change in positions. Therefore, if connecting trajectories between the Lissajous exist, they have to be coincident in positions on the section. Nevertheless, on the Poincaré section x is fixed to $x = -1 + \mu_{SE}$. So, points that belong to the intersection of the manifolds in the yz projection of the cuts with $\mathcal{S}$ represent complete intersections in position between the SE manifold and the EM one. Consequently, connecting trajectories between the Sun-Earth L$_2$ region and the Earth-Moon L$_2$ region can be found by studying overlapping regions in yz coordinates on $\mathcal{S}$. A Δv will be associated with each of these connecting trajectories, as the overlapping occurs in positions, not in velocities.

For some values of the amplitudes in both sides, no intersecting region exists on the section. However, for some other values, we get an overlapping like the one depicted in Fig. 5.17. The red points represent the intersection of the EM unstable manifold with $\mathcal{S}$, while the green ones belong to the stable manifold form the SE Lissajous orbit. Note that in the picture the discreetisation performed on the phases can be observed. Points with the same ϕ and consecutive ψ have been joined by segments, forming the vertical curves that we observe in the figure, $\gamma_i = \{(\phi_i, \psi_j), j = 1, n_2\}$. On the other hand, as the in-plane phase moves from i to $i+1$, different curves are obtained ($\gamma_i, \gamma_{i+1} \ldots, i = 1, n_1$). The denser the grid we take, the closer the curves appear.

5.3.6   Computation of connecting trajectories between Lissajous orbits.

It seems clear from figure 5.17 that there exist connecting trajectories joining the pairs of Lissajous that result in a yz overlapping in the coupled RTBPs. That is to say there exist initial conditions both on the SE and the EM Lissajous that result in each point (y, z) of the aforementioned overlapping regions once integrated to the section. However, we have discreetised the initial conditions and probably a particular point in the region does not correspond to any of the points on the manifolds that we have integrated and stored. Therefore, we somehow have to find the

---

[1]Note that for the planar case, the study of a planar projection on $\mathcal{S}$ was enough to obtain complete information of the state space. If two coordinates, say y and $\dot{y}$ were coincident on $\mathcal{S}$, then x was obtained from the definition of this section and $\dot{x}$ from the Jacobi constant.
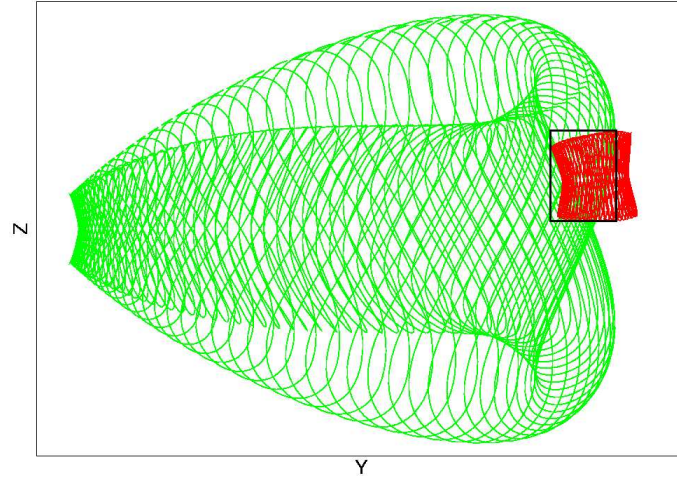
Figure 5.17: yz projection of the stable manifold of a Lissajous in the SE system (in green) with amplitudes $(A_x, A_z) = (184152.8, 301536.6)$ km and the unstable manifold of a Lissajous in the EM system (in red) with amplitudes $(A_x, A_z) = (6560, 20000)$ km, at the crossing with the Poincaré section. The intersecting region in position coordinates is contained in the black square.

exact phases that lead to (y, z), taking as a seed a couple of phases such that the point on the section associated with (ϕ, ψ) is close to (y, z) (the same for the EM case, (ϕ', ψ')). Note that only the phases play a role, whereas all the amplitudes remain fixed. The reason for this is that we want the Lissajous orbit on the torus defined by (A_x, A_z) to remain unaltered, and the same for the distance from the Lissajous to the initial conditions on the manifolds, represented by the hyperbolic amplitudes (A_1, A_2).

Let F_1 and F_2 be,

$$F_1 : [0, 2\pi] \text{ x } [0, 2\pi] \subset \mathbb{R}^2 \rightarrow \mathbb{R}^2, \quad F_1(\phi, \psi) = (y, z)_{SE},$$

$$F_2 : [0, 2\pi] \text{ x } [0, 2\pi] \subset \mathbb{R}^2 \rightarrow \mathbb{R}^2, \quad F_2(\phi', \psi') = (y, z)_{EM}.$$

F_1 is the restriction in (y, z) of the Poincaré map, which is the integrated flow from the initial point on the manifold defined by the phases (ϕ, ψ) to the Poincaré section in the SE case. F_2, in turn, is also the restriction in (y, z) of the Poincaré map for the EM case, but composed in addition with the change of coordinates from EM to SE on the Poincaré section. In more detail,

$$F_1(\phi, \psi) = \Phi_P^{SE} \circ \Psi^{SE}(\phi, \psi)|_{y,z}$$

$$F_2(\phi', \psi') = \xi \circ \Phi_P^{EM} \circ \Psi^{EM}(\phi', \psi')|_{y,z}$$

where,

$$\Psi : \mathbb{R}^6 \rightarrow \mathbb{R}^6, \quad \Psi(A_1, A_2, A_x, A_z, \phi, \psi) = (x, y, z, \dot{x}, \dot{y}, \dot{z}),$$

is the map which transforms amplitudes and phases into position-velocity points in the vicinity of L_2. As it has been said, we make the amplitudes remain fixed. Therefore we consider the restriction of Ψ that acts only on the phases.

$$\Phi_P : \mathbb{R}^6 \to \mathbb{R}^6, \quad \Phi_P(x, y, z, \dot{x}, \dot{y}, \dot{z}) = (-1 + \mu, y_f, z_f, \dot{x}_f, \dot{y}_f, \dot{z}_f),$$

is the integrated flow to the Poincaré section, obtained essentially by integrating the first variational equations of equations (2.1) and correcting them on the section.

And,

$$\xi : \mathbb{R}^6 \to \mathbb{R}^6, \quad \xi(x, y, z, \dot{x}, \dot{y}, \dot{z})_{EM} = (x, y, z, \dot{x}, \dot{y}, \dot{z})_{SE}.$$

is the change of coordinates from the EM coordinates to the SEM ones (a composition of rotation and a translation, together with a scaling factor).

Given (y, z) on the section and (ϕ, ψ) such that $F_1(\phi, \psi)$ and (y, z) are close to each other, we can use a 2-dimensional Newton method on F_1 and obtain (ϕ^*, ψ^*) such that $F_1(\phi^*, \psi^*) - (y, z) = (0, 0)$. We can do the same for F_2. It is clear from the definition of F_1 and F_2 that there are no differentiability problems. In addition, if we store enough overlapping points, that is a narrow grid of (ϕ, ψ) is used to obtain the cuts with the section, good seeds are available for any (y, z) in the intersecting region. Therefore, a Newton method is an adequate and fast way to solve the problem.

To sum up, the steps that we follow are:

1. Fix the relative Sun-Earth-Moon configuration at $t = 0$, by giving a value to the angles α and β in figure 5.15.

2. Choose $\mathcal{S}$, the Poincaré section.

3. Pick a Lissajous orbit around L_2 in the SE system, and a Lissajous orbit around L_2 in the EM system by choosing their central amplitudes $(A_x, A_z)_{SE}$ and $(A_x, A_z)_{SE}$.

4. Choose the direction in which we want to transfer from one orbit to the other.

5. Take a discrete set of points on the Lissajous orbits, given by a grid in (ϕ, ψ), and move along the unstable (respectively stable) manifold using A_1 and A_2 to obtain the initial conditions.

6. Integrate the initial conditions on the invariant manifolds until they intersect $\mathcal{S}$. For the EM case, transform the points on the section to SE coordinates.

7. In case the manifolds do not intersect on the section, change some of the parameters in 1, 2 or 3.

   On the contrary, if an overlapping exists, take a grid on the yz projection of the intersection of the manifolds on $\mathcal{S}$. For each point (y, z) on the grid, find the corresponding phases (ϕ, ψ) and (ϕ', ψ') such that $F_1(\phi, \psi) = F_2(\phi', \psi') = (y, z)$, using a Newton method applied to F_1 and F_2.

8. Finally, the connecting trajectory is obtained by integrating the correct initial conditions from both manifolds. Each connecting trajectory consists of two parts: the SE part, integrated with the SE RTBP equations, and the EM part, with the EM equations. Both trajectories intersect the Poincaré section at the same point, to which we assign $t = 0$.

Note once again that the velocity vectors of the SE point and the EM point at the moment when the manifolds intersect the section ($t = 0$) are not the same. The intersection, as we have computed it, occurs only in positions. A Δv is necessary if we want this intersection to take place in the full state space.

More than one connecting trajectories through a particular point on the section

Sometimes it may happen that more than one connecting trajectory exists through a particular point on the Poincaré section $(-1 + \mu_{SE}, y, z)$. This is because a couple (y, z) is not univoquely determined by a pair of initial phases (ϕ, ψ), neither in the EM problem nor in the SE.

The uniqueness of the solutions of a system of ODEs given an epoch applies to the complete state $X = (x, y, z, \dot{x}, \dot{y}, \dot{z})$. That is to say that given (t, X) there exists a unique couple (ϕ, ψ) such that the trajectory with these initial phases goes through the point X at time t (for fixed A_1, A_2, A_x and A_z). Actually, as the RTBP is autonomous, time does not play an important role in our case. Thus, given a point $X = (x, y, z, \dot{x}, \dot{y}, \dot{z})$ and four values of the amplitudes, there exists a unique couple of phases (ϕ, ψ) on the corresponding hyperbolic manifold that are the initial conditions for a trajectory containing X, but the time is not relevant and we can choose it to be any value.

However, in this work we look at a projection of the cut in the Poincaré section and there is some information that we are not aware of when picking (y, z): the velocity vectors. Therefore, the fact that there exist several couples of initial phases leading to a particular point (x, y, z) on the section does not contradict the uniqueness of solutions with respect to initial conditions, as long as these points on the section have different velocity vectors, $(\dot{x}, \dot{y}, \dot{z})$.

Remember functions F_1 and F_2 that we defined in subsection 5.3.6. An intersecting point of the (y, z) projection satisfies that there exist (ϕ, ψ) and (ϕ', ψ') such that $F_1(\phi, \psi) = (y, z)_{SE} = (y, z)_{EM} = F_2(\phi', \psi')$. However, F_1 and F_2 are restrictions of another application, $\mathcal{F}$, which takes each point on a hyperbolic manifold of a Lissajous orbit (described in Lindstedt-Poincaré coordinates) and integrates it until it reaches $\mathcal{S}$. Thus, $\mathcal{F}$ is the composition of the Poincaré map, Φ_P, with the application that transforms Lindstedt-Poincaré coordinates to RTBP points, Ψ,

$$\mathcal{F} : \mathbb{R}^6 \to \mathbb{R}^6, \quad \mathcal{F} = \Phi_P \circ \Psi$$

$$\mathcal{F}(A_1, A_2, A_x, A_z, \phi, \psi) = \Phi_P \circ \Psi(A_1, A_2, A_x, A_z, \phi, \psi) =$$
$$= \Phi_P(x_0, y_0, z_0, \dot{x}_0, \dot{y}_0, \dot{z}_0) = (-1 + \mu_{SE}, y, z, \dot{x}, \dot{y}, \dot{z}),$$

where $(x_0, y_0, z_0, \dot{x}_0, \dot{y}_0, \dot{z}_0)$ represents the initial point on the manifold in the adequate coordinate frame.

Once the amplitudes (hyperbolic and central) have been fixed, $\mathcal{F}$ is an injective application. This is a consequence of the aforementioned uniqueness of solutions in the complete state space,

as well as the fact that Lindstedt-Poincaré coordinates univoquely determine the points on the Lissajous orbit and manifolds.

Despite the injectivity of $\mathcal{F}$, F_1 and F_2 are not injective applications. There can exist pairs (ϕ_a, ψ_a) and (ϕ_b, ψ_b) such that $F_1(\phi_a, \psi_a) = F_1(\phi_b, \psi_b)$, and the same for F_2. It is important to bear in mind that the images of these pairs of phases coincide in position but not in velocity. Consequently, they lead to connecting trajectories which cross the section through the same point in position, but need different adjusting maneuvers to complete the transfer.

Qualitatively, it is not difficult to determine the regions with different number of connecting trajectories through each (y, z). For instance, see figure 5.18, which is a detailed view of the black rectangle shown in figure 5.17. Observing how the manifold is folded on the section, we can differentiate 3 different sectors in this figure, labelled as regions A, B and C.
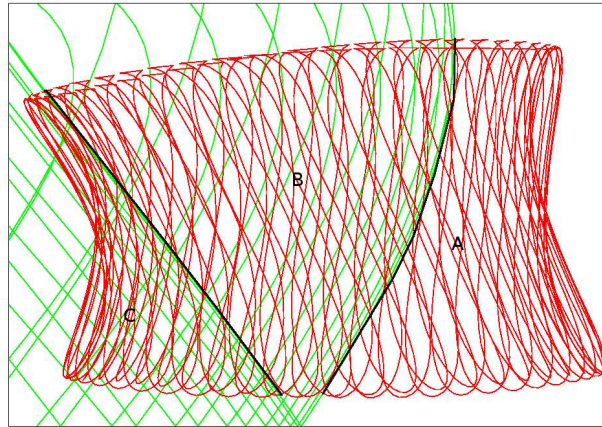
Figure 5.18: Detailed view of figure 5.17. The regions labelled with A, B and C are different in terms of number of connecting trajectories. A: no connecting trajectories, C: more connecting trajectories for each (y,z) than in region B, as another fold in the green (SE) manifold is overlapping the region.

In order to learn how to count the number of connecting trajectories that go through each (y, z), let us concentrate on the green curves we see in figure 5.17 that come from the discreetisation performed on the initial conditions of the stable manifold of the SE orbit, and which we called γ^i. Remember that for a given discreetisation on the in plane phase ϕ, $\{\phi_i, i = 1..n\}$, we obtain the corresponding curves

$$\gamma^i = \{(x, y, z, \dot{x}, \dot{y}, \dot{z}) = F_1(\phi_i, \psi), \psi \in [0, 2\pi]\}.$$

As a consequence of the aforementioned uniqueness of the solutions of a system of ODEs, $\gamma^i \cap \gamma^j = \emptyset$ in $\mathbb{R}^6$. However, curves γ^i appear as being folded on themselves in the yz projection. As a consequence of these foldings, it may happen that different curves γ^i intersect with each other in this projection. Therefore, we have that there $\exists (y, z) \in \gamma^{i_1} \cap \gamma^{i_2}$. That is to say that some points (y, z) are the result of integrating (ϕ_{i_1}, ψ_{j_1}) and also (ϕ_{i_2}, ψ_{j_2}), with $\psi_{j_1} \neq \psi_{j_2}$ and $\phi_{i_1} \approx \phi_{i_2}$. This is the case, for instance, of the points in region B of figure 5.18 or the points in the red zone of the picture on the right of figure 5.21. Consequently, we can say that given a point (y, z) in these regions, and for each couple of phases of the EM side such that $F_2(\phi', \psi') = (y, z)$, there

exist two different couples (ϕ, ψ) from the SE side such that $F_1(\phi, \psi) = (y, z)$. This means that there exist two different connecting trajectories starting at (ϕ', ψ'). So, when storing the set $\mathcal{B} = \{(\phi', \psi') \in [0, 2\pi] \times [0, 2\pi] \mid F_2(\phi', \psi') \in B\}$, we will label it with a number 2, meaning that there are two different ways of reaching the stable manifold of the SE Lissajous starting at the point represented by the couple of phases (ϕ', ψ') on the EM Lissajous unstable manifold.

For some other points, such as the ones in region C of figure 5.18 or the blue region in the picture on the right of figure 5.21, not only do the green curves fold on itself, but also another type of overlapping occurs. This second type of overlapping is easy to understand if we keep in mind that we are integrating the manifold associated with a torus. Naturally, a projection in positions of a torus-like object presents overlappings corresponding to the *front* and the *back* sides of the original torus (see figure 5.21). Therefore, each point in these regions is associated with 4 different pairs (ϕ, ψ) from the SE side: two of the front part (as a consequence of the foldings in frontal γ^i's) and two of the back part (respectively, due to the foldings of γ^i's from the back part).

Figure 5.19: Four different connecting trajectories between a Sun-Earth+Moon Lissajous around L_2 and an Earth-Moon one (in SE coordinates), which have a common crossing point on the Poincaré section (in position coordinates). As their velocity vectors are not the same on the section, the Δv that is needed to adjust the velocities of the trajectories coming from the SE side with the one coming from the EM side is computed for each case. In the xy projection (top right) we observe how two of the connecting trajectories have similar in-plane starting phases at the SE side, while the other two also have similar in-plane phase. In the xz projection (bottom right) we observe, however, that the out of plane arriving phases are different in all the connecting trajectories.

For instance, in figure 5.19, four different connecting trajectories which go through the same point on the section are represented. Two of them have the in-plane phase of the SE close to 0.75 rad, ϕ_{i_1}, while the other ones have it close to $\phi_{i_2}=1.49$ rad. So, two of them are due to the folding of γ^{i_1} with $\phi_{i_1} \approx 0.75$ (in the front part of the torus, remarked in violet in figure 5.21), while the
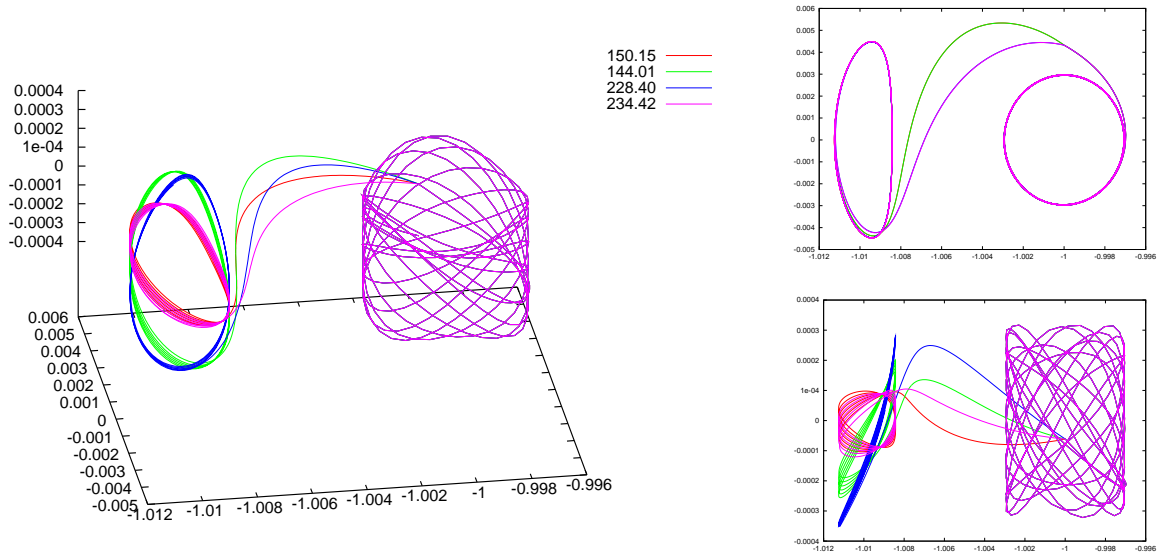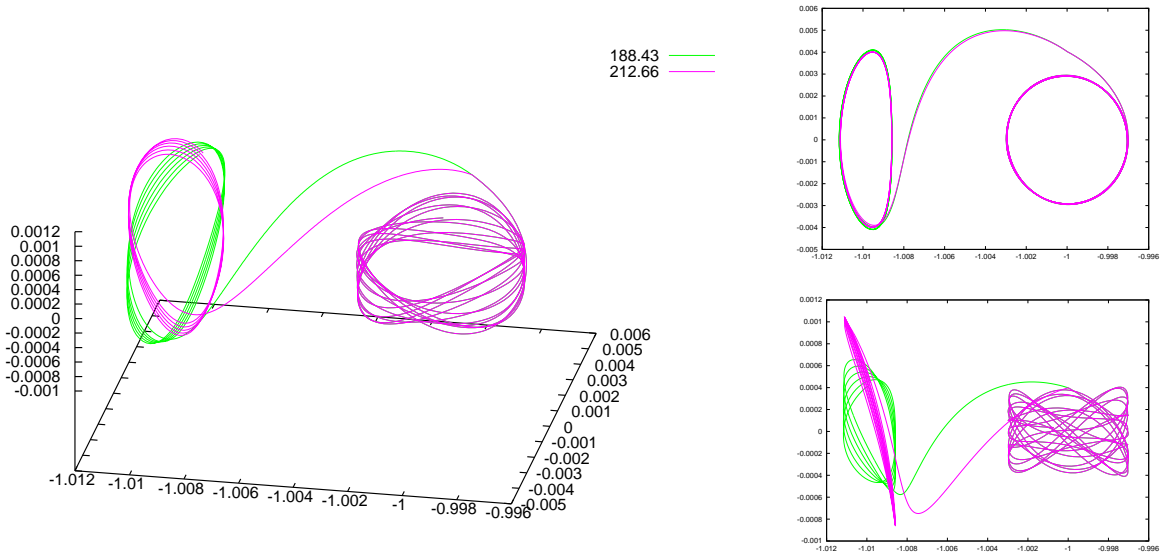
Figure 5.20: Two different connecting trajectories between a Sun-Earth+Moon Lissajous around L_2 and an Earth-Moon one (in SE coordinates), which have a common crossing point on the Poincaré section (in position coordinates). Top right picture shows that the in-plane arriving phase at the SE Lissajous is similar, while in the bottom right picture the fact that the out of plane phase is different can be observed.

other two come from the folding of γ^{i_2}, with $\phi_{i_2} \approx 1.49$, which in the yz projection lays close to γ^{i_1} but comes from the back part of the torus (in black in figure 5.21). We can observe in that these four connecting trajectories are quite different and are associated with a different Δv on the coupling point. Obviously, as they all act as connecting trajectories between the same pair of Lissajous orbits, we are usually interested in the cheapest one. In addition, it is also interesting to note that in the xy projection of the transfer trajectories, also in figure 5.19, one can clearly see that two of them have similar in-plane arriving phase to the SE Lissajous and the same for the other two. On the contrary, in figure 5.20 we observe how two different connecting trajectories with a common crossing point on the section look like. In this case, the fact that two connections exist through this point is due to a simple folding in the curves γ^i, so both connections have similar in-plane arriving phases and different out-of-plane ones. We will then label the phases from the EM side leading to a point in the section belonging to a region like C (figure 5.18) with number 4. In figures 5.22, 5.23 and 5.24 some examples of how the regions with different number of associated trajectories look like in the EM phase-space are shown.

Nevertheless, this does not mean that only two different connecting trajectories cross the section through each point in B, and 4 different connecting trajectories do so for each point in C. The total number of connecting trajectories now depends on the overlappings in the EM manifold projection. For the parts where the overlapping in the EM projection is simple (only curves γ^i folding on themselves), the total number of connecting trajectories will be doubled: combinations between the pairs of phases from the SE side and the two pairs from the EM side. That is, a total possible number of 4 or 8 connections. Besides, for the parts where the overlapping in EM manifold projection is double (γ^i folding and overlappings between *front* and *back* parts of
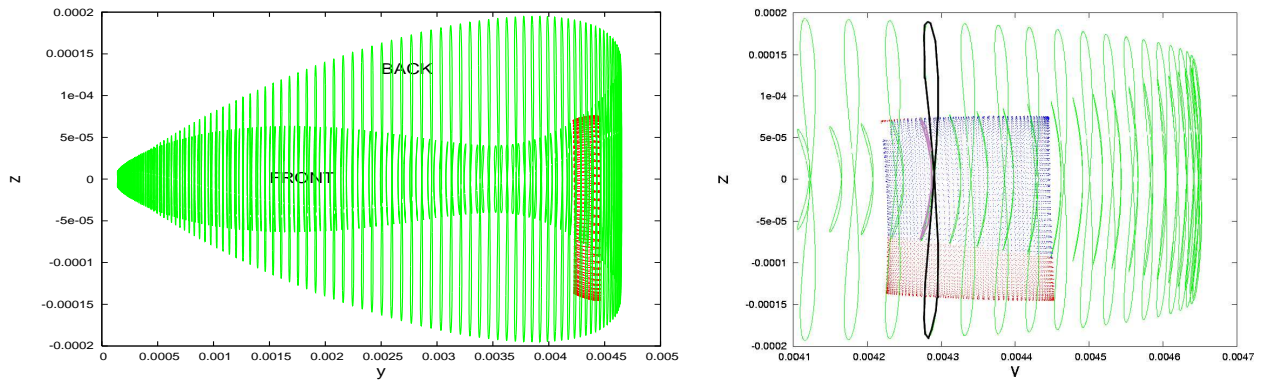
Figure 5.21: (left) In green the yz projection of the intersection of the stable manifold of a Lissajous orbit around L_2 in the SE problem, with $A_x = 214800$ km and $A_z = 30152.9$ km. In red we have the intersection of the unstable manifold of a Lissajous orbit around L_2 in the EM problem, with $A_x = 2623.7$ km and $A_z = 8000$ km. The coupling angles at $t = 0$ are $\alpha = 95$ deg. and $\beta = 25$ deg. The labels 'FRONT' and 'BACK' represent different zones on the Lissajous which are overlapped in the projection. (right) Detail of the picture on the left. The blue zone represents the points whose initial phases from the EM side are joined to the SE libration region by 4 different connecting trajectories, while the red zone represents the points whose initial phases lead to two different connecting trajectories. In black one of the green curves from the back part is remarked, while one of the curves from the front part is remarked in violet.

the Lissajous), we can either have 8 connecting trajectories or a maximum total number of 16 different connecting trajectories through a given point $(x, y, z) \in \mathcal{S}$. Consequently, one has to be careful when constructing the database which contains the information of the overlappings and the connecting points.

5.3.7   Preliminary explorations

Note that when applying the method explained in section 5.3.6, there are several things that have to be chosen. Different choices result in different intersections on the Poincaré section and therefore different connecting trajectories from one libration region to the other one.

Essentially, the free variables are:

- The Poincaré section, $\mathcal{S}$.

- The sense of the integration: from SE to EM or the other way round.

- The Sun-Earth-Moon configuration at $t = 0$, represented by the angles α and β.

- The size of the Lissajous orbits: amplitudes A_x and A_z for both RTBPs.

In this part of the work, the Poincaré section has been fixed to

$$\mathcal{S} = \{X = (x, y, z, \dot{x}, \dot{y}, \dot{z}) \in \mathbb{R}^6 \mid x = -1 + \mu_{SE}\} = \{X \in \mathbb{R}^6 \mid g(X) = 0\}$$

	SE (km)	EM (km)
A_x	80000 - 250000	1500 - 10000
A_z	15000 - 550000	5000 - 35000

Table 5.4: Amplitudes of the Lissajous orbits around L_2 in the SE and EM problems which have been explored in the search for asymptotic connecting trajectories.

with $g(x, y, z, \dot{x}, \dot{y}, \dot{z}) = 1 - \mu_{SE} + x$ (in SE coordinates). The same method could be applied if another section was chosen, with no further modification. Even if $\mathcal{S}$ does not correspond to a plane with x, y or z fixed, it still enough to make two of these coordinates match on the section by applying a Newton method on the phases (ϕ, ψ), and obtain the third one from the $g(X)$ which defines $\mathcal{S}$.

As for the direction of the integration, all results presented here go from the vicinity of L$_2$ in the EM problem to the vicinity of L$_2$ in the SE problem.

Concerning the configuration at $t = 0$, only relative positions of the Moon corresponding to $\alpha + \beta \in [80, 120]$ degrees lead to intersections in positions on $\mathcal{S}$ at the first cut. In the way we approximate the manifolds, no intersections were found for values of α and β outside of this range, at least without additional cuts with the section, which lead to longer trajectories than the ones in which we are interested in this work. Note that the range is given in terms of the sum of two angles: one in the ecliptic (α) and the other one in the plane containing the orbit of the Moon (β). Thus, strictly speaking, their sum has no physical meaning. However, the inclination of one plane with respect to the other (5 degrees approximately) is so small, that the angles can be added as if they laid in the same plane, in order to present the results in a simple way.

Finally, concerning the size of the Lissajous, table 5.4 shows the maximum and minimum sizes which have been successfully explored in both models. If a Lissajous orbit lays between these ranges of amplitudes, at least one connecting trajectory for one particular initial configuration has been found with a Lissajous orbit from the other model. It is very important to note that our study does not intend to be exhaustive in terms of Lissajous amplitudes, but to provide a contribution on how to effectively compute connections between particular pairs of Lissajous orbits. This is one of the reasons for using only square Lissajous orbits around the lunar L$_2$ point. These orbits are seen as a means to reach the lunar libration region and maintain the satellite there for a particular time span. Therefore, other studies should be performed when necessary including other types of orbits. Actually, we should also mention here that the amplitudes that have been explored (see table 5.4) are essentially limited by the convergence of Lindstedt-Poincaré expansions of the manifolds. Future work will be devoted to exploring a wider range of amplitudes, by using other ways of describing the Lissajous orbits and the manifolds (such as normal form expansions [49]).

5.3.8   Results.

A database, containing the overlapping points as well as the maneuvers which are necessary on the section to make the transfer possible, has been produced using the coupled SE and EM RTBPs. The amplitude ranges that have been studied, as well as the values of the phases α and β, which

represent the relative configuration of both restricted models at $t = 0$ (i.e. the moment of the section crossing), were stated in the previous section. Naturally, it is extremely difficult to present this huge amount of results in a simple way. Therefore, some tables are presented in this section, aimed at showing a sample of the type of results that must be expected when dealing with the intersections of manifolds belonging to Lissajous orbits. The cases presented in these tables will be used in the following sections for testing the refinement method. A much more exhaustive collection of results can be found in the attached DVD [2]. Moreover, figures 5.22, 5.23 and 5.24 show different possible kinds of overlappings that occur on the Poincaré section between the integrated manifolds. In these figures, the points in the phase space of the EM initial conditions which result in two different connecting trajectories with a common point on the Poincaré section are depicted in red, while the ones resulting in four different connecting trajectories are depicted in green. The tangency points (either resulting in 1 or 3 connecting trajectories) are not shown in the figure, as they do not introduce valuable information (they lay in the borders between red and green regions), but finding them implies using a very thick net with the corresponding increase in the computational time.

In table 5.5, results are presented for connecting trajectories starting at medium sized square Lissajous orbits around L$_2$ of the EM problem (A_z from 14000 to 23000 km) and arriving at square Lissajous orbits around L$_2$ of the SE problem. Intersections are rarely found under these conditions for square Lissajous orbits in the SE side having A_x smaller than 100000 km. For this reason, all examples in the table have big Lissajous motions in the solar region as arrival orbits. On the other hand, we have already proved that when an overlapping takes place in the Poincaré section between two integrated hyperbolic manifolds, infinitely many connecting trajectories can be found joining the corresponding orbits, with different Δv values in the coupling point (see section 5.3.6). Furthermore, initial conditions on the orbits are discreetised in order to integrate the manifolds. Therefore, among all possible connecting trajectories derived from the section overlapping between the hyperbolic manifolds of the two different Lissajous orbits, the table only displays the cheapest one obtained from the discreetised set of initial conditions. Thus, the cost values shown in the table are close to the minimum possible cost of a connecting trajectory joining the corresponding Lissajous orbits in the coupled RTBPs model, but they have not been obtained by means of any optimisation procedure. They range from 200 to 400 m/s, which implies that the maneuvers are quite big and seems to indicate that it is not easy to find low cost connecting trajectories from solar to lunar libration regions by means of square Lissajous orbits in both sides. Finally, the addition of the integration time on both manifolds is shown in the last column of the table. All transfer time are around half a year.

On the other hand, results are presented for non-square Lissajous orbits around the SE L$_2$ point in table 5.6. If the Lissajous motion in the solar side has big A_x amplitude and small A_z amplitude, the chances are that transfer trajectories to the lunar L$_2$ region are much cheaper than for the square SE Lissajous case: from slightly less than 100 m/s to 200 m/s in the vast majority of cases. As for the transfer time, it may take a little longer to complete these transfers than the ones shown in table 5.5, but the integration time in all the cases that have been explored never surpasses the 7 months upper bound.

---

[2]The database in the attached DVD contains transfer trajectories starting at square Lissajous in the EM side and having Lissajous orbits of the SE problem with big A_x amplitudes and small A_z amplitudes as arrival orbits. For other particular values of the amplitudes, the interested reader should contact the author.
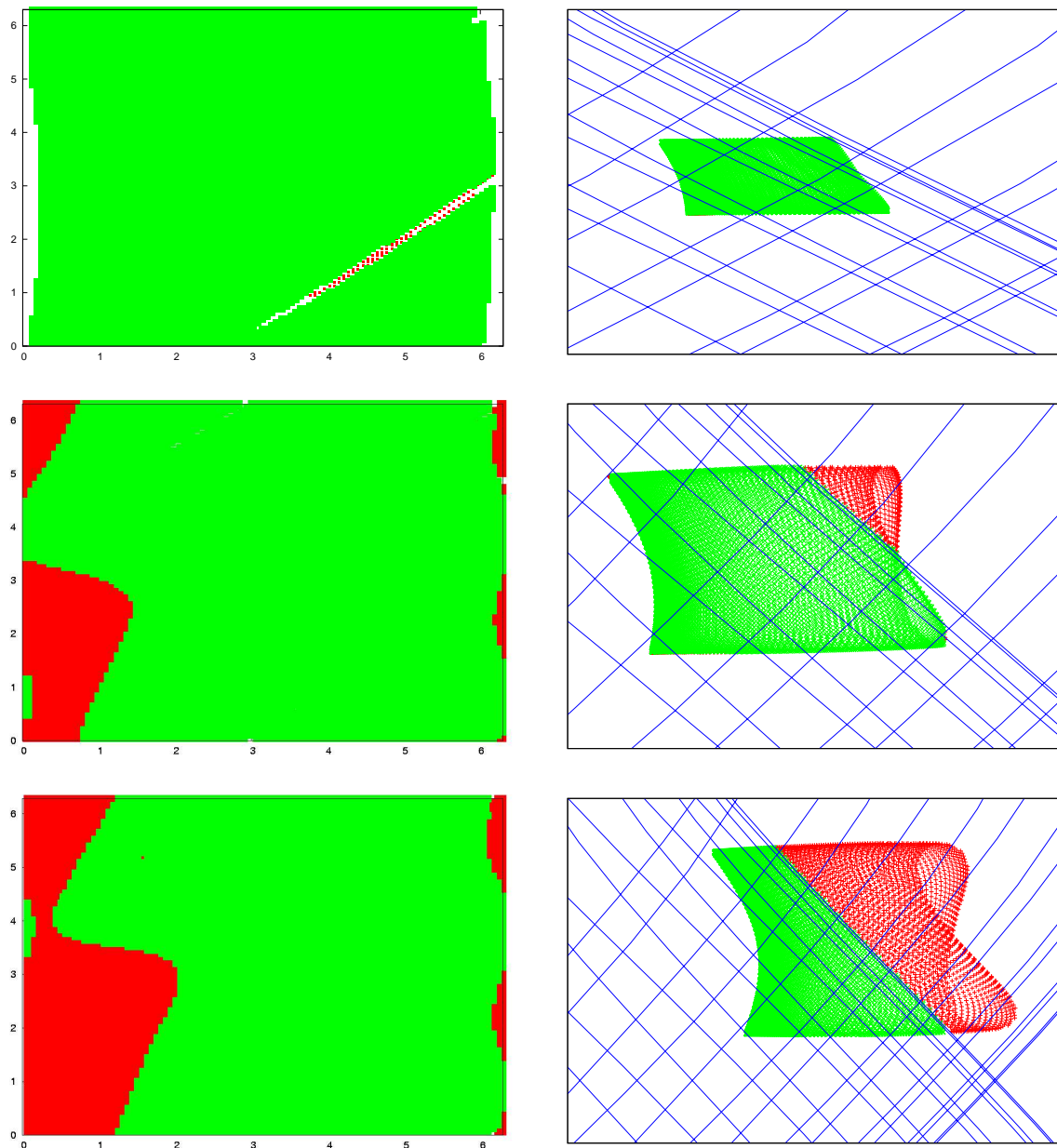
Figure 5.22: (left) x-axis: ϕ, y-axis: ψ. Couple of initial phases of the Earth-Moon L_2 Lissajous orbits unstable manifold. Red points represent couples of phases which lead to points on the Poincaré section that are joined to the Sun-Earth Lissajous orbit by two different points (i.e. the SE manifold reaches the section at this points with two different velocity vector). Green points are initial conditions with 4 different arriving points on the Sun-Earth Lissajous. (right) yz projection in the Poincaré section. Red and green points are the (y, z) coordinates associated with the corresponding phases on the left. Blue lines represent the cut with the section of the stable manifold of the Lissajous orbit of the SE manifold. The pictures in these figure, as well as the ones in figures 5.23 and 5.24 are intended to provide examples of different overlapping situations.
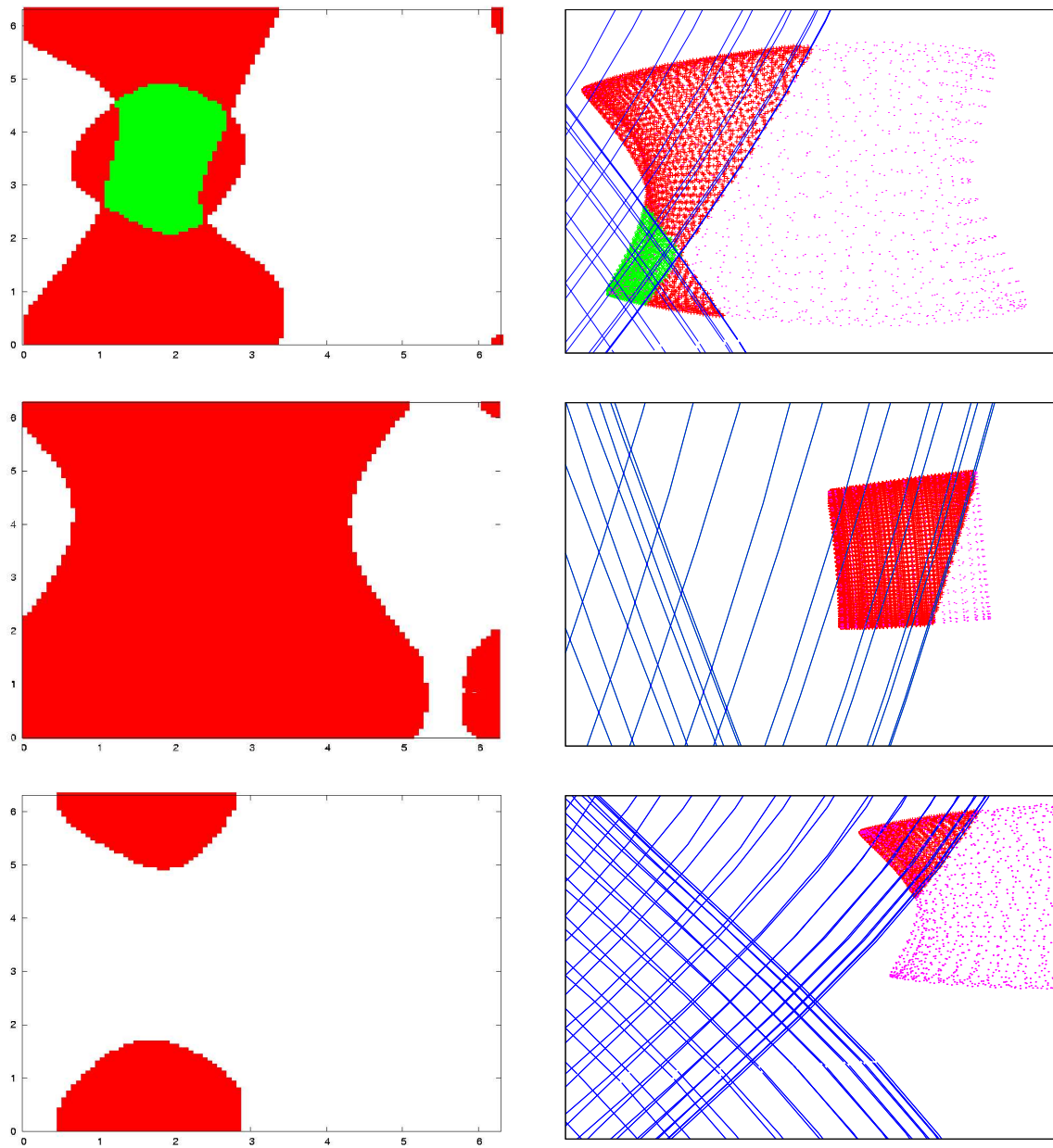
Figure 5.23: Same comments as in figure 5.22 apply. In addition, violet dots represent the part of the Earth-Moon Lissajous manifold which does not intersect the Sun-Earth one.

Figure 5.24: Same comments as in figure 5.22 apply. In particular, the pictures in this figure correspond to cases in which the Lissajous orbit from the Sun-Earth side has small z amplitude (less than 10^5 km).

	SE amplitudes (km)		EM amplitudes (km)		phases (deg)		cost	time
	A_x	A_z	A_x	A_z	α	β	(m/s)	(days)
1	100072.0	320000	6560.7	20000	50	40	419.19	166.05
2	103200.0	330000	5576.6	17000	45	50	394.49	166.84
3	106327.0	340000	7544.8	23000	80	10	377.00	167.27
4	112581.4	360000	6560.7	20000	50	50	347.84	170.33
5	115708.7	370000	6560.7	20000	35	60	303.18	169.51
6	121963.2	390000	5904.6	18000	65	30	295.20	169.48
7	125090.3	400000	6232.6	19000	55	45	284.60	170.71
8	134472.2	430000	4592.5	14000	30	75	287.24	171.96
9	137600.0	440000	5576.0	17000	65	40	268.67	174.98
10	137600.0	440000	7216.7	22000	80	20	249.16	169.51

Table 5.5: Sample cases of square Lissajous orbits around the L_2 point of the Sun-Earth and the Earth-Moon problems whose manifolds have an overlapping region in yz coordinates on the Poincaré section with $x = -1 + \mu_{SE}$. The table shows the amplitudes of the Lissajous, the relative configuration phases at $t = 0$, as well as the costs of the necessary maneuvers in the point where the RTBPs are coupled and the total integration times (from the point where the trajectory leaves the EM Lissajous vicinity until it reaches the SE Lissajous). When two manifols associated with Lissajous orbits intersect in the aforementioned Poincaré section, an infinite number of connecting trajectories with the corresponding Δv can be found. The table only shows the cost of the connecting trajectory which is fairly close to the optimal one (the cheapest of all trajectories obtained by taking a discreet set of 100×100 phases in the initial conditions defining the unstable manifold of the EM Lissajous).

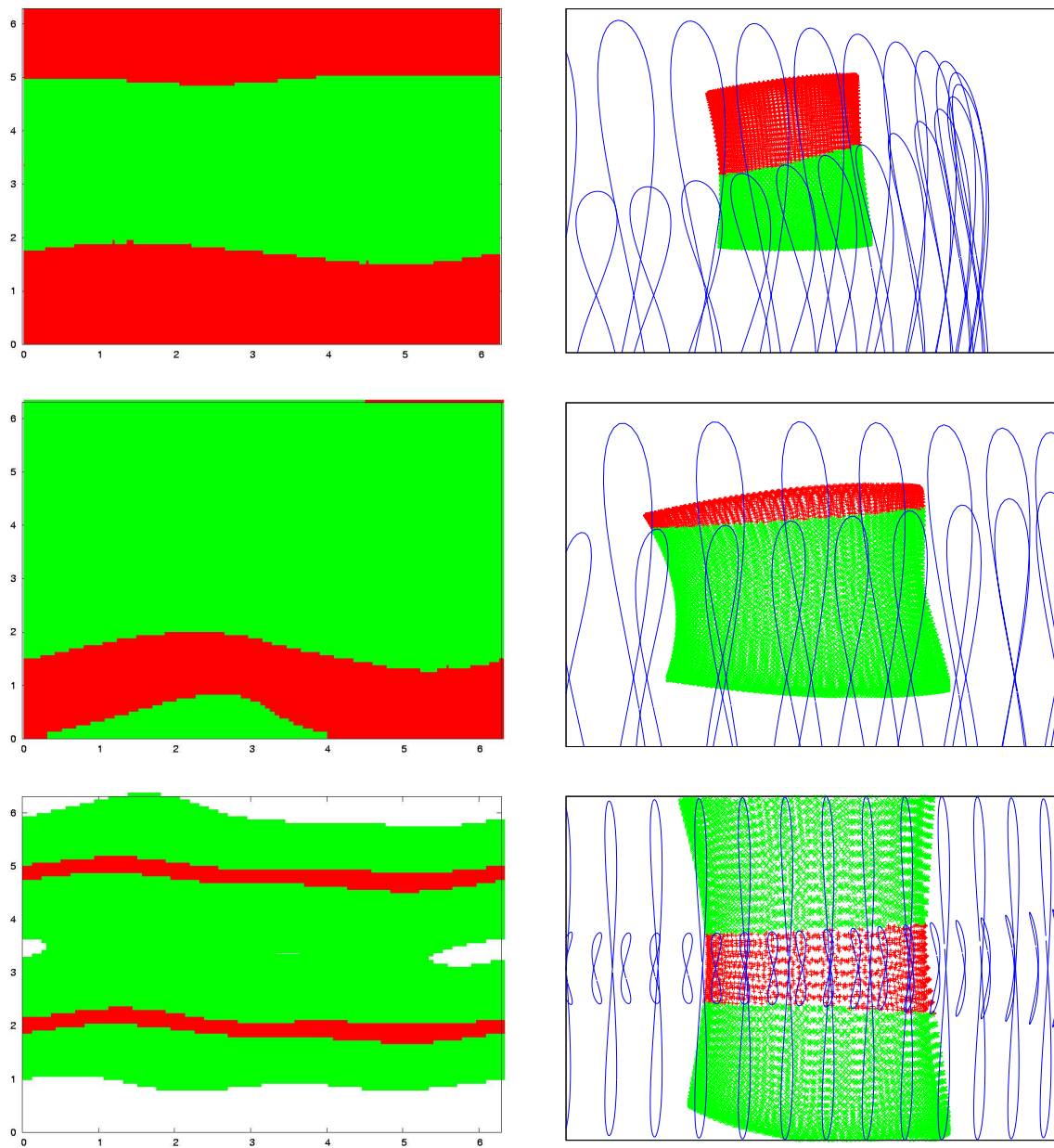|	SE amplitudes (km)		EM amplitudes (km)		phases (deg)		cost	time
	A_x	A_z	A_x	A_z	α	β	(m/s)	(days)
11	244088.3	75382.4	5248.5	16000	15	105	163.08	183.92
12	244088.3	75382.4	4592.5	14000	20	100	167.55	204.89
13	244088.3	75382.4	6560.7	20000	0	120	155.71	201.98
14	212964.4	75382.4	5248.5	16000	10	100	209.59	179.18
15	212964.4	75382.4	2952.3	9000	60	45	243.53	169.33
16	194619.3	90458.9	4920.5	15000	25	95	102.99	177.71
17	177341.7	60305.9	4920.5	15000	35	70	173.87	172.57
18	175638.0	90458.9	6560.7	20000	30	85	72.23	173.94
19	177341.7	60305.9	6888.7	21000	75	35	52.74	169.98
20	157075.8	45229.4	6888.7	21000	5	100	87.69	169.02

Table 5.6: Same comments as for table 5.5, but in this case the Lissajous in the SE side are not square Lissajous orbits. They have big A_x and small A_z amplitudes. It is clear from these tables that in terms of cost in the coupled RTBPs, it is much better to use big and flattened Lissajous orbits in the SE side than square ones.

Therefore, some conclusions can be drawn from the results contained in the present section. Firstly, that big in-plane amplitudes together with small out-of-plane amplitudes for the SE Lissajous seem to be the most adequate for this type of transfer trajectories using the coupled SE and EM RTBPs model. Secondly, that we must expect a transfer time of rawly half a year. And, finally, that the Δv maneuvers in the Poincaré section or the coupling point are big, ranging from slightly less than 100 m/s in the best cases to even 400 m/s when big square Lissajous in the SE side are used.

5.4   Refinement to JPL coordinates

A complete methodology for the search of connecting trajectories between Lissajous orbits of the SE and the EM systems has been developed in the previous sections. However, these trajectories do not correspond to a realistic model, but to the coupling of two restricted three body problems. Consequently, further refinements are necessary in order to use them as real paths from the libration regions of one of the systems to the libration region of the other one. Using a simple model to obtain the first approximation to the motion and then refining it to a more realistic path is a common technique in trajectory design ([44]). In this section, a procedure aimed at getting solutions close to the ones previously obtained for the coupled RTBPs, but of more realistic equations of motion by using JPL ephemeris is presented ([76]). It is important to note that the results that will be obtained in the present section have to be regarded as good initial seeds for a further optimisation procedure more than final realistic solutions, as they contain big Δv's in the coupling point, which are inherited from the already commented maneuvers in the coupled RTBPs.

Unfortunately, for these more realistic models of motion of the bodies of the Solar System, a complete study of the phase space around the libration points (or their dynamical substitutes) like the one that already exists for the RTBP has not yet been carried out, as it is much more complicated to perform. Furthermore, one of the fundamental differences between the RTBP and an ephemeris model is that the equations of motion are no longer autonomous. That is, an initial epoch has to be fixed, which determines the behaviour of the solution. Remember that for the coupled RTBPs we made the time on the section be $t = 0$. This is a delicate point in the method, as it is the place where the problems are coupled. The crossing of the section is also the point that we use for setting an initial epoch when refining a particular trajectory to JPL coordinates. Given a connecting trajectory in the coupled RTBP's, as well as the initial configuration associated with it (angles α and β at $t = 0$), the choice of the JPL date that corresponds to the moment of the coupling, $t = 0$, can be made in the following way:

1. Choose an initial future date (day, month, year).

2. Find a date, as close as possible to the chosen one, such that the configuration of the Sun, Earth and Moon bodies in JPL ephemeris corresponds to the angles α and β of the original trajectory.

3. Use this date as initial epoch t_0, corresponding to $t = 0$ in the coupled RTBPs. That is to say that the chosen date corresponds to the section crossing time.

Now the points on the manifold approaching the SE Lissajous will be associated with times $t > t_0$, while the points on the unstable manifold of the EM Lissajous with times $t < t_0$.

It may happen that another time reference or requirement exists for a particular mission. For instance, if the date at which the spacecraft should arrive to a Lissajous around the SE L$_2$ is known instead of the time for the section crossing. We can adapt our refinement to this kind of restriction by using the approximation of the flight time provided by the RTBP. For example, let the required arrival date at the SE Lissajous be equal to t_L (in dynamic Julian days). Compute the flight time from section $\mathcal{S}$ to the Lissajous around L$_2$ in the SE RTBP for the connecting trajectory that is being refined to JPL coordinates, t_{fl} (in days). Then we can approximate the Julian date for the section crossing, $t_{\mathcal{S}}$, by $t_{\mathcal{S}} = t_L - t_{fl}$ and use this date as the future date mentioned in step 1.

5.4.1   Multiple shooting method

The method that we use for transforming the connecting trajectories to JPL coordinates is a multiple shooting procedure, similar to the one used for the numerical solution of boundary-value problems ([79]).

As in the standard multiple shooting method, the total time span is splitted into a number of shorter subintervals, $t_0, t_1, t_2, ..., t_N$, with t_0 the initial epoch and $t_N - t_0$ the length of the time interval. Let us denote by

$$Q_i = (t_i, x_i, y_i, z_i, \dot{x}_i, \dot{y}_i, \dot{z}_i,)^T, \quad i = 0, 1, ..., N$$

the points on the RTBP connecting trajectory, and by $\Delta t_i = t_{i+1} - t_i$, i=0,...,N-1. Let $\Phi(t, Q_i)$ be the image of the point Q_i under the flow associated with the realistic equations of motion in the solar system after an amount of time t.

If all the points Q_i were on the same orbit of the new JPL equations, then $\Phi(\Delta t_i, Q_i) = Q_{i+1}$ for $i = 0, ..., N - 1$. As this is not the case, a change in the Q_i is needed in order to fulfil the matching conditions. Consequently, one must solve a set of N nonlinear equations, which can be written as

$$F \begin{pmatrix} Q_0 \\ Q_1 \\ \vdots \\ Q_N \end{pmatrix} = \begin{pmatrix} \phi(Q_0) \\ \phi(Q_1) \\ \vdots \\ \phi(Q_{N-1}) \end{pmatrix} - \begin{pmatrix} Q_1 \\ Q_2 \\ \vdots \\ Q_N \end{pmatrix} = \Phi \begin{pmatrix} Q_0 \\ Q_2 \\ \vdots \\ Q_{N-1} \end{pmatrix} - \begin{pmatrix} Q_1 \\ Q_2 \\ \vdots \\ Q_N \end{pmatrix} = 0.$$

A Newton's method is used to solve the system above. If $Q^{(j)} = \left(Q_0^{(j)}, Q_2^{(j)}, ..., Q_N^{(j)} \right)^T$, denotes the j-th iterate of the procedure, Newton's equations can be written as

$$DF(Q^{(j)}) \cdot (Q^{(j+1)} - Q^{(j)}) = -F(Q^{(j)}),$$

where the differential of the function F has the following structure

$$DF = \begin{pmatrix} A_0 & -I & & & \\ & A_2 & -I & & \\ & & \ddots & \ddots & \\ & & & A_{N-1} & -I \end{pmatrix},$$

with $D\Phi = \mathrm{diag}(A_0, A_2, ..., A_{N-1})$. As each of the transition matrices, A_i, that appear in $D\Phi$ are 6×6, at each step of the method we have to solve a system of $(N-1) \times 6$ equations with $6 \times N$ unknowns, so some additional conditions must be added. This is the only difference with the standard multiple shooting method and is due to the fact that our problem is not a real boundary-value one. As additional equations, initial or final conditions at times $t = t_0$ or $t = t_N$ can be fixed. From the numerical point of view, one has to be careful with the choice because the problem can be ill conditioned from a numerical point of view. This is because the matrix $DF(Q)$ can have a very large condition number. To avoid this bad conditioning, we can choose smaller values for Δt_i, but in this case the number of points Q_i increases and the instability is transferred to the procedure for solving the linear system. In addition, another important disadvantage of the extra boundary conditions is that they can force the solution in a non natural way giving either convergence problems for long time spans, or solutions in JPL coordinates which are far from the original RTBP ones.

To avoid this, we can apply Newton's method directly. As the system has more unknowns than equations, we have (in general) an hyper-plane of solutions. From this set of solutions we try to select the one closer to the initial connecting trajectory used to start the procedure. This is done by requiring the correction to be minimum with respect to the Euclidean norm, for instance. Denoting by $\Delta Q^{(j)}$

$$\Delta Q^{(j)} = Q^{(j+1)} - Q^{(j)},$$

and requiring $\|\Delta Q^{(j)}\|_2$ to be minimum, one gets the Lagrange function $\mathrm{L}(\Delta Q, \Lambda)$ with (vector) multiplier Λ,

$$L(\Delta Q, \Lambda) = \Delta Q^T \cdot \Delta Q + \Lambda^T \cdot (F(Q) + DF(Q) \cdot \Delta Q),$$

we get

$$\Delta Q^{(j)} = -DF(Q^{(j)})^T \cdot \left[DF(Q^{(j)}) \cdot DF(Q^{(j)})^T \right]^{-1} \cdot F(Q^{(j)}), \tag{5.9}$$

which gives the value of $\Delta Q^{(j)}$ explicitly.

5.4.2   First approximation to real ephemeris connecting trajectories

To start with, one can think of trying to refine the whole connecting trajectories using a multiple shooting method, after properly setting the initial epoch. However, this will rarely provide satisfying results, as the parallel shooting cannot generally couple the two different RTPBs with no additional help. That is to say that the connecting trajectory obtained from coupling two RTBPs may be too far from a real JPL ephemeris trajectory at some points for the parallel shooting to smooth it at the first try.

On the contrary, each one of the legs (SE and EM) can be easily refined from RTBP to JPL coordinates, if these transformations are done separately. The problem is, naturally, that the point corresponding to the initial epoch, which in RTBP coordinates was coincident on the section for both sides, is no longer the same. Consequently, some kind of forcing in the conditions corresponding to the point on the section, in order to obtain connecting trajectories which are continuous in position in JPL coordinates, cannot be avoided. We have used a forcing that consists of refining the EM leg with no restrictions, and then using the final (x, y, z) coordinates that have been obtained as the position coordinates of the first point of the SE leg. In other words, we force the initial point of the SE leg to be the final one of the EM leg, which we have

obtained by freely refining the part of the connecting trajectory coming from the lunar region. We can call this method the *section-forced refinement to JPL coordinates.*
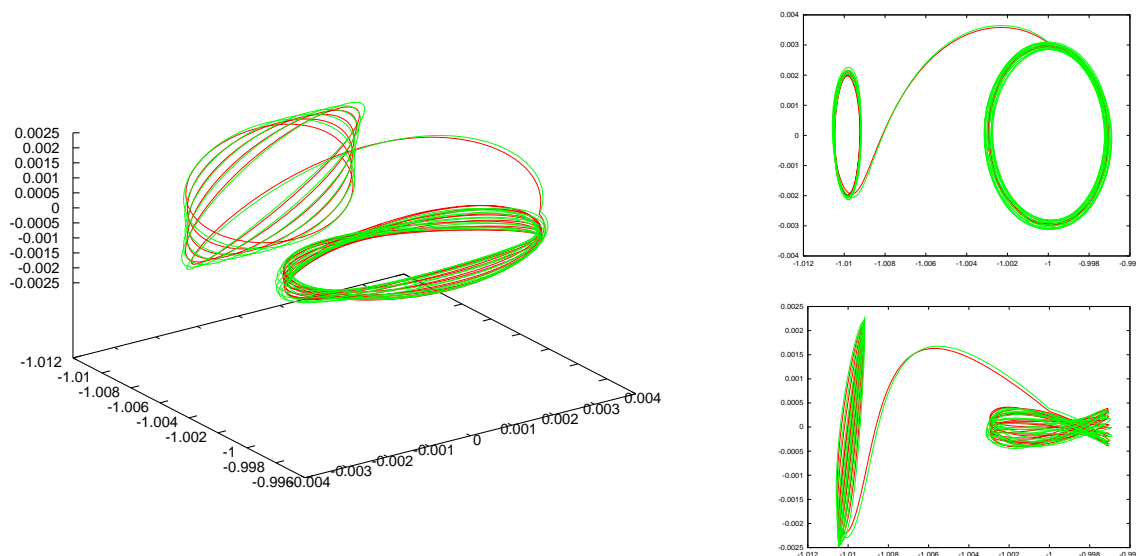
Figure 5.25: (left) 3D representation of the connecting trajectory labelled as 1 in table 5.5. In red, the trajectory as it was obtained in the coupled RTBPs. In green, the result of applying the section forced refinement to the RTBP one and setting the date for the section crossing to August the 24th 2015. (right) xy and yz projections of both the RTBP and the JPL refined trajectory. These projections show that the section forced refinement provides a JPL position continuous trajectory which is very similar to the one obtained in the coupled RTBP model.

The section-forced refinement to JPL coordinates can be applied to any of the connecting trajectories that we obtain by coupling the two RTBPs. As a result, we get trajectories in JPL coordinates, which are continuous in position but need a Δv in the coupling point. Some trajectories that were obtained using this method are shown in figures 5.25 and 5.26, and correspond to connecting trajectories contained in table 5.5 and 5.6 (as detailed in the caption of the figures).

Actually, we can apply this refinement method to the whole set of connections that we learnt how to find in section 5.3.6 between two particular Lissajous orbits. We ought to bear in mind, however, that the refinement depends on the date that is chosen for coupling point (i.e. the section crossing). Therefore, different results are obtained both in terms of the maneuver point (i.e. the *forced* point on the section) as well as the costs for different section crossing epochs (see table 5.7). For instance, if the real relative configuration between the Sun, the Earth and the Moon at the chosen epoch is very different from the one required by the RTBP connecting trajectory, the parallel shooting method will obviously modify this original RTBP trajectory in order to obtain a position continuous one in JPL coordinates. This means that some of the obtained JPL connecting trajectories may be different from the original RTBP ones in terms of the departure and arrival phase on the Lissajous orbits, but always maintain the values of the amplitudes of the Lissajous in both sides. Some examples of how the cost and the coupling point change are depicted in figure 5.27.

	RTBP cost (m/s)	JPL cost (m/s)			
		28-Dec-2009	19-Apr-2013	24-Aug-2015	15-Nov-2018
1	419.19	516.55	489.58	523.34	523.38
2	394.49	491.29	464.80	496.22	502.17
3	377.00	484.13	456.73	491.20	488.16
4	347.84	430.68	410.05	432.47	453.49
5	303.18	362.52	348.21	362.80	400.04
6	295.20	376.61	368.18	374.95	420.76
7	284.60	351.09	344.45	348.88	397.91
8	287.24	323.10	324.91	316.74	381.60
9	268.67	332.53	335.35	327.02	389.66
10	249.16	315.88	320.75	310.41	374.53
11	163.08	214.65	186.09	227.30	199.64
12	167.55	219.24	188.94	232.40	202.53
13	155.71	173.06	143.12	187.83	157.39
14	209.59	255.45	220.99	271.59	226.60
15	243.53	170.58	233.48	155.16	265.90
16	102.99	128.47	116.09	137.01	154.73
17	173.87	187.99	167.38	199.09	192.33
18	72.23	87.46	93.27	95.88	141.10
19	52.74	79.43	124.64	80.92	166.49
20	87.69	128.81	103.13	144.96	134.73

Table 5.7: Maneuvers at the coupling point which are necessary when the coupled RTBP connecting trajectories of table 5.5 and 5.6 have been refined to JPL ephemeris using the section forced refinement, for several epochs of section crossing. Note that we cannot assure that the chosen section crossing epoch is exactly the moment when the coupling takes place. The refinement method uses the closest epoch to the chosen one for which the real relative configuration of the Sun, Earth and Moon positions corresponds to the initial configuration phases (α and β) of the coupled RTBPs. Thus, the maximum difference between the chosen epoch shown in the table and the real maneuvering point is of two weeks in the worst case.
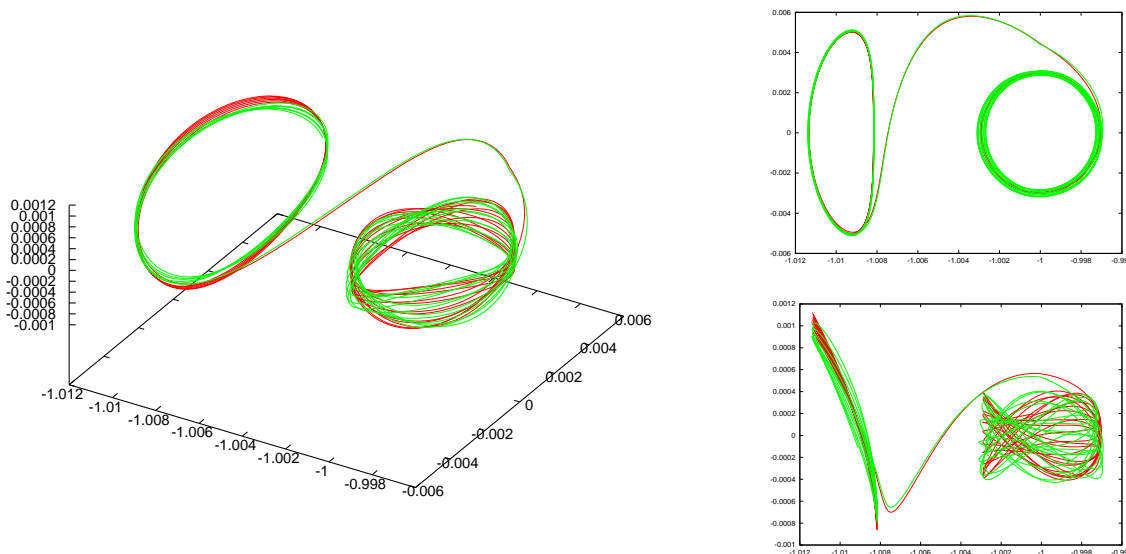
Figure 5.26: Same comments as for figure 5.25. In this case the connecting trajectory which is represented is labelled as 13 in table 5.6.

Moreover, the cost of the maneuver in JPL coordinates is of the same order of magnitude as the original one in the coupled RTBPs, as observed in table 5.7. However, the cost of JPL maneuvers is usually higher than the cost of the original ones in RTBPs, being this fact a natural consequence of the higher complexity of the JPL model. Despite this general increase in the cost, sometimes the JPL trajectory has a lower cost than the original one in RTBPs (see for instance some of the values for trajectories 15 and 17). These examples support the claim that the increase in the costs after the refinement procedure is not an intrinsic characteristic of the section forced refinement method that we use, but of the JPL ephemeris themselves. Furthermore, the dates displayed in the aforementioned table have been randomly chosen in order to prove that the section forced refinement provides JPL position continuous trajectories, no matter which refinement date we pick. Therefore, if no strict requirement exists for the time of section crossing, a study can be performed in order to determine the most convenient intersecting date on the section for a given pair of Lissajous orbits (both the position at the moment of the maneuver and the magnitude of this maneuver should be taken into account when deciding which is the most convenient time).

It must be remarked that the connecting trajectories in JPL coordinates which are obtained from the coupled RTBPs ones by using the section forced refinement have to be regarded just as a good initial seed for obtaining cheaper realistic trajectories and not as final usable trajectories themselves. For instance, trajectory optimisation procedures could be applied to them and low cost transfers are bound to be obtained. No optimiser has been used in the present doctoral work and this issue is left as part of the future work. On the contrary, a search for free connecting trajectories in JPL coordinates has been successfully performed by modifying the multiple shooting algorithm, as shown in the following sections.
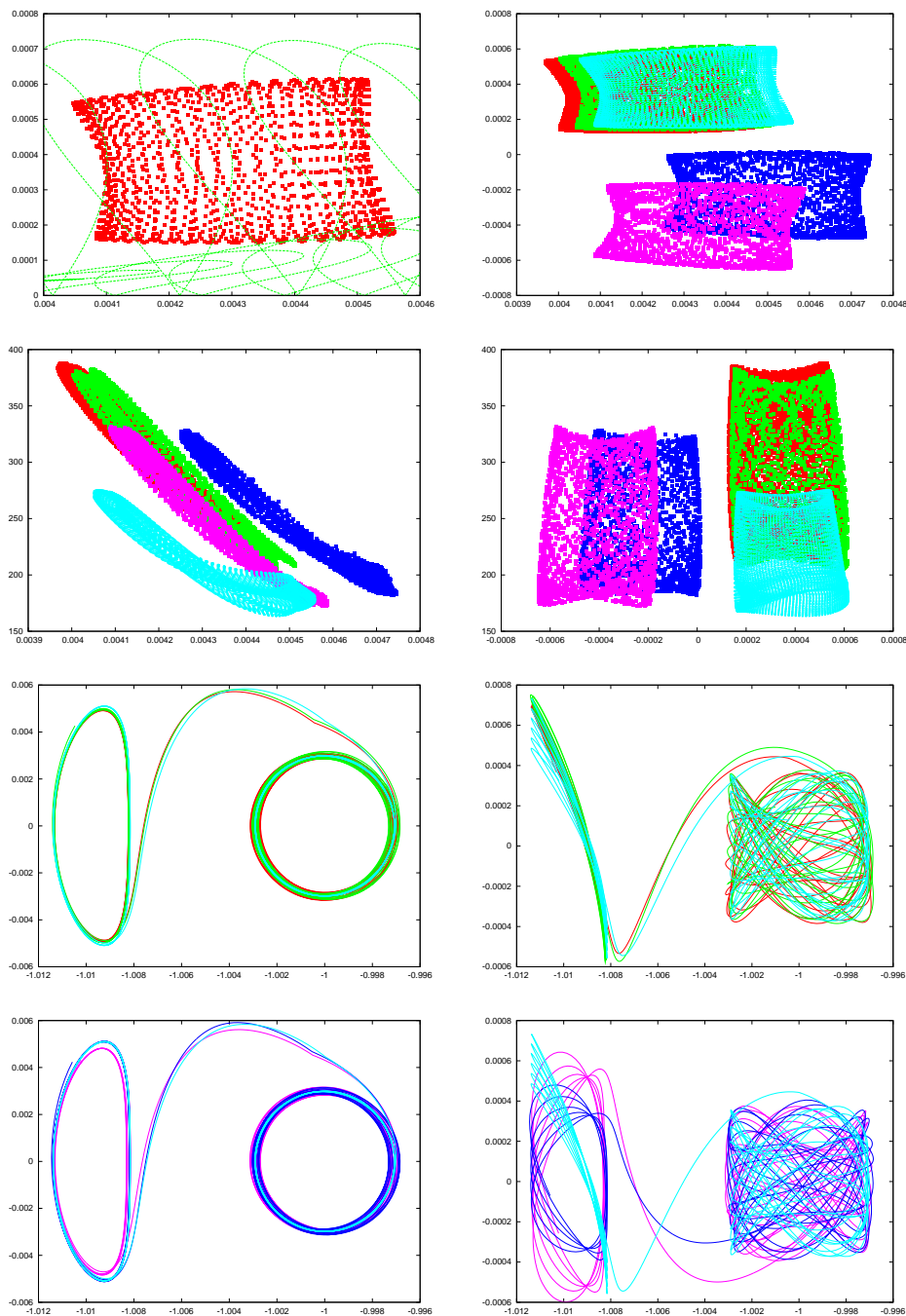
Figure 5.27: These pictures are aimed at showing the effect of different section crossing epochs used in the section forced refinement to JPL (corresponding to the connecting trajectory labelled with number 11 in table 5.6). In the first row on the left, the yz projection of the overlapping region between the manifolds in RTBP coordinates is shown. The picture in this row on the right, as well as the ones in the second row correspond to planar projections (yz, $y\Delta v$ and $z\Delta v$ respectively, coordinates in SE RTBP units and Δv in m/s) of the points of the aforementioned overlapping region when the section forced refinement has been applied to them. Finally, in the last two rows, the xy (left) and xz (right) projections of the JPL connecting trajectories corresponding to different crossing dates (as shown in table 5.7, line 11) are represented. [Colour code: Light blue: RTBP coordinates. Green: JPL with section crossing on December, 28th 2009. Violet: JPL with section crossing on April, 19th 2013. Red: JPL with section crossing on August, 8th 2015. Blue: JPL with section crossing on November, 15th 2018.]

5.4.3   Zero cost connecting trajectories in JPL coordinates

It has been shown in section 5.4.2 that it is not difficult to obtain JPL ephemeris trajectories starting from the ones obtained in the RTBPs, as long as the SE and the EM parts are treated separately (i.e. two different runs of the multiple shooting procedure: from the EM Lissajous orbit to the Poincaré section and, on the other hand, from the Poincaré section to the SE Lissajous orbit).

Let $\{Q_0^l, \ldots, Q_N^l\}$ be the points in JPL coordinates which are the result of applying the parallel shooting method to the EM part of the trajectory. The subindices are ordered according to the direction of the integration, as the parallel shooting works in forward time. That is, Q_0^l corresponds to the initial point on the unstable manifold of the EM Lissajous and Q_N^l corresponds to the point on the section. Respectively, $\{Q_0^s, \ldots, Q_M^s\}$ are the points obtained by using the parallel shooting method on the SE part of the trajectory: Q_0^s is the point on the section, while Q_M^s on the stable manifold. With this notation and assuming that the section forced refinement explained in the previous sections has been used, Q_N^l and Q_0^s have the same position coordinates. Therefore, we have that $Q_N^l - Q_0^s = \Delta v$, with

$$\Delta v = (x, y, z, \dot{x}, \dot{y}, \dot{z})_N^l - (x, y, z, \dot{x}, \dot{y}, \dot{z})_0^s = (0, 0, 0, \Delta\dot{x}, \Delta\dot{y}, \Delta\dot{z}). \tag{5.10}$$

The magnitude of these changes of velocity $\Delta\dot{x}$, $\Delta\dot{y}$ and $\Delta\dot{z}$, that are needed for the connecting trajectory to be used as a transfer are sometimes of hundreds of meters per second. For this reason, there is little chance that the introduction of the complete trajectory in a parallel shooting algorithm leads to a zero cost connection. However, a slight modification of the multiple shooting method can be used in order to iteratively reduce the maneuvers, Δv, and obtain zero cost connecting trajectories in real ephemeris when possible.

It is convenient to use the following notation in order to introduce the trajectory in a multiple shooting algorithm aimed at reducing the section Δv,

$$Q_i = Q_i^l, \ i = 0, .., N - 1 \ \text{ and } \ Q_i = Q_{i-N}^s, \ i = N, .., N + M.$$

Note that this implies that the point corresponding to the SE part, Q_0^s, is used on the section instead of the last point of the EM leg, Q_N^l. Moreover, if ϕ represents the flow of the equations of motion in JPL ephemeris, the following equality is satisfied after the section forced refinement:

$$F\begin{pmatrix} Q_0 \\ Q_1 \\ \vdots \\ Q_{N-1} \\ Q_N \\ \vdots \\ Q_{N+M-1} \end{pmatrix} = \begin{pmatrix} \phi(Q_0) \\ \phi(Q_1) \\ \vdots \\ \phi(Q_{N-1}) \\ \phi(Q_N) \\ \vdots \\ \phi(Q_{N+M-1}) \end{pmatrix} - \begin{pmatrix} Q_1 \\ Q_2 \\ \vdots \\ Q_N + \Delta v \\ Q_{N+1} \\ \vdots \\ Q_{N+M} \end{pmatrix} = \begin{pmatrix} 0 \\ 0 \\ \vdots \\ 0 \\ 0 \\ \vdots \\ 0 \end{pmatrix}$$

which essentially implies that points Q_i belong to a natural trajectory in JPL coordinates, but a maneuver Δv is needed in order to jump from Q_{N-1} to Q_N (i.e. from the EM part to the SE

part). We can use the following simplification of the notation,

$$
\Phi \begin{pmatrix} Q_0 \\ Q_1 \\ \vdots \\ Q_{N+M-1} \end{pmatrix} = \begin{pmatrix} \phi(Q_0) \\ \phi(Q_1) \\ \vdots \\ \phi(Q_{N+M-1}) \end{pmatrix}
$$

Now, the modification of the parallel shooting consists of introducing the maneuver vector Δv in the equations which we want to make zero, and iteratively reducing it. Therefore, at each step we use the parallel shooting method in order to find the new trajectory $\{Q_0^j, ...Q_{N+M}^j\}$ which satisfies,

$$
F \begin{pmatrix} Q_0^j \\ Q_1^j \\ \vdots \\ Q_{N-1}^j \\ Q_N^j \\ \vdots \\ Q_{N+M-1}^j \end{pmatrix} = \Phi \begin{pmatrix} Q_0^j \\ Q_1^j \\ \vdots \\ Q_{N-1}^j \\ Q_N^j \\ \vdots \\ Q_{N+M-1}^j \end{pmatrix} - \begin{pmatrix} Q_1^j \\ Q_2^j \\ \vdots \\ Q_N^j \\ Q_{N+1}^j \\ \vdots \\ Q_{N+M}^j \end{pmatrix} - \begin{pmatrix} 0 \\ 0 \\ \vdots \\ \Delta^j \\ 0 \\ \vdots \\ 0 \end{pmatrix} = \begin{pmatrix} 0 \\ 0 \\ \vdots \\ 0 \\ 0 \\ \vdots \\ 0 \end{pmatrix} \tag{5.11}
$$

where Δ^j represents the maneuver vector at iteration j, which is reduced as j increases. For instance, we can choose $n \in \mathbb{N}$ and let $\Delta^j = \Delta^{j-1}(1 - \|\Delta v\|\|\Delta^{j-1}\|^{-1}/n)$. With this definition of Δ^j, equations (5.11) are trivially satisfied for $j = 0$, as the trajectory is continuous in position under the flow of the JPL equations at each of the nodes and Δ^0 corresponds to the transfer maneuver after the section forced refinement [3]. At each iteration $\|\Delta^j\| < \|\Delta^{j-1}\|$, until a final trajectory is obtained with $\|\Delta^m\| < \delta$, with δ the required tolerance (we usually use 10^{-6}). Note that by choosing n we are choosing the maximum number of iterations that would be necessary to obtain $\|\Delta^j\| = 0$. Therefore, if n is too small, maybe we are trying to smooth the maneuver too fast and the parallel shooting method may not converge. On the other hand, if n is too big, the computational time is significantly increased, due to the amount of multiple shooting systems that have to be solved.

5.4.4   Results

When applying the method to reduce the maneuver at the coupling point, results can be classified in three groups:

1. Some trajectories are easily refined to $\Delta v = 0$ and the arrival Lissajous orbits around the SE L_2 point do not change in a significant way (see figures 5.28 and 5.29). These are the most interesting cases for mission prototyping, as one can design the trajectory in the well known equations of the RTBP and then transform it to a realistic transfer trajectory by using the JPL ephemeris.

---

[3] Other definitions for Δ^j are also possible, as long as they satisfy $\|\Delta^j\| < \|\Delta^{j-1}\|$ $\forall j \geq 1$ and they maintain the computational time within reasonable bounds.

Figure 5.28: Trajectory joining a Lissajous around L_2 in the EM system and a Lissajous around the L_2 point of the SE system. (see details in table 5.6, where this connection is labelled as 15). In the first row on the left a 3D representations of the starting JPL coordinates trajectory is shown (i.e. the result of applying the section forced refinement to coupled RTBPs original seed), with a cost of 155.16 m/s. On the same row but on the right side the refined JPL connecting trajectory with zero cost is depicted. In both cases, the section crossing takes place on August the 24th 2018. On the second row, the xy and xz projections of the connecting trajectories are shown. It can be observed that for these particular amplitudes and section crossing date, the effects of the maneuver smoothing do not affect the characteristics of the connecting trajectory in a significant way.
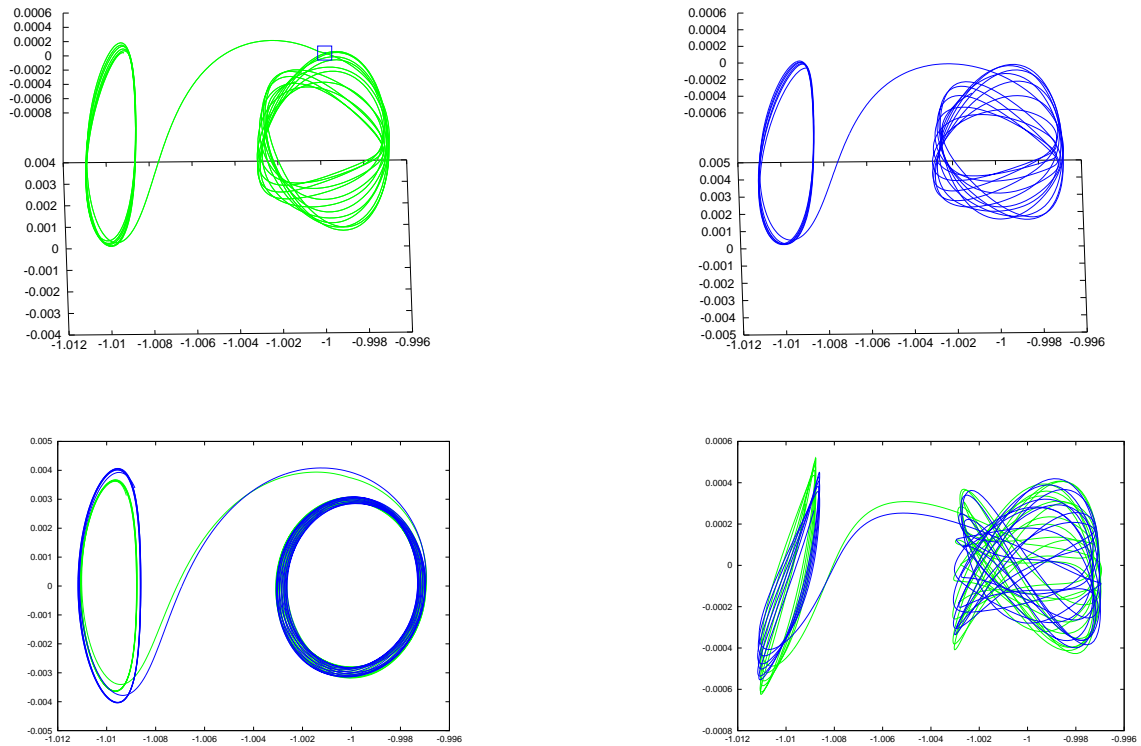
Figure 5.29: Trajectory joining a Lissajous around L$_2$ in the EM system and a Lissajous around the L$_2$ point of the SE system. (see details in table 5.6, where this connection is labelled as 19). In the first row on the left a 3D representations of the starting JPL coordinates trajectory is shown (i.e. the result of applying the section forced refinement to coupled RTBPs original seed), with a cost of 80.92 m/s. On the same row but on the right side the refined JPL connecting trajectory with zero cost is depicted. In both cases, the section crossing takes place on August the 24th 2018.
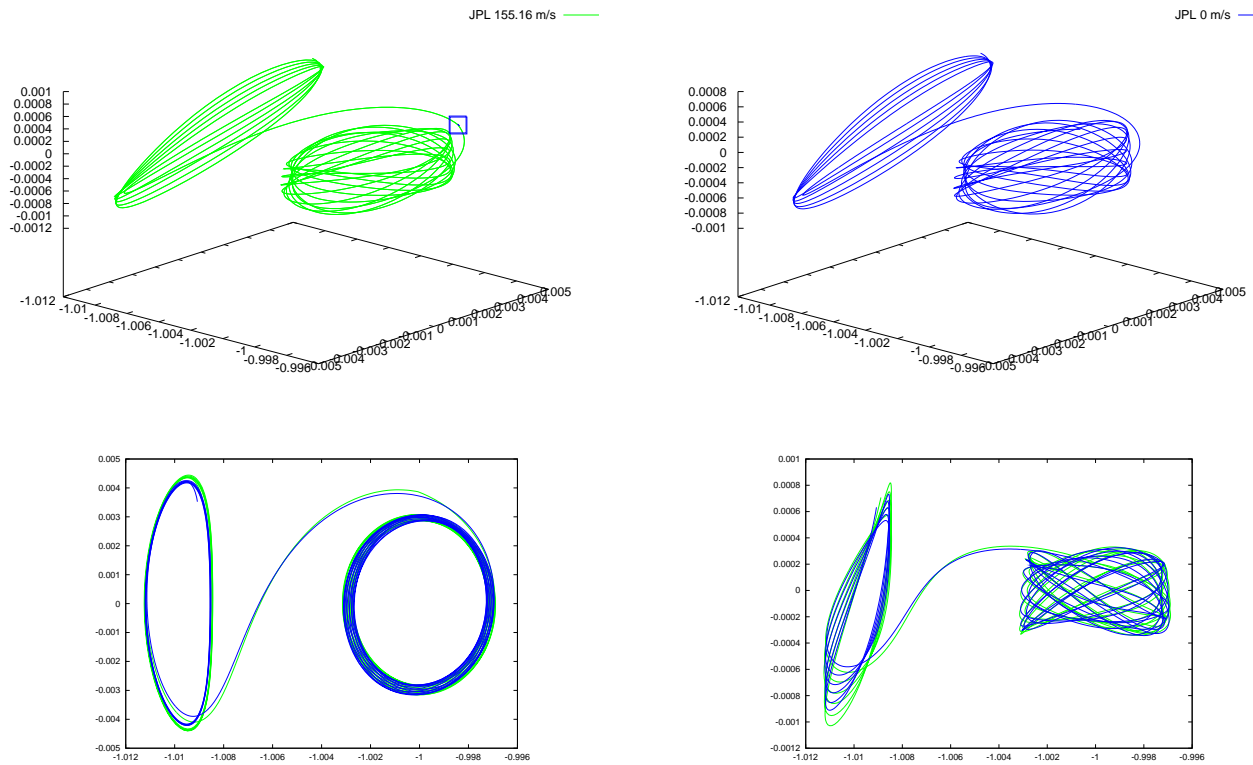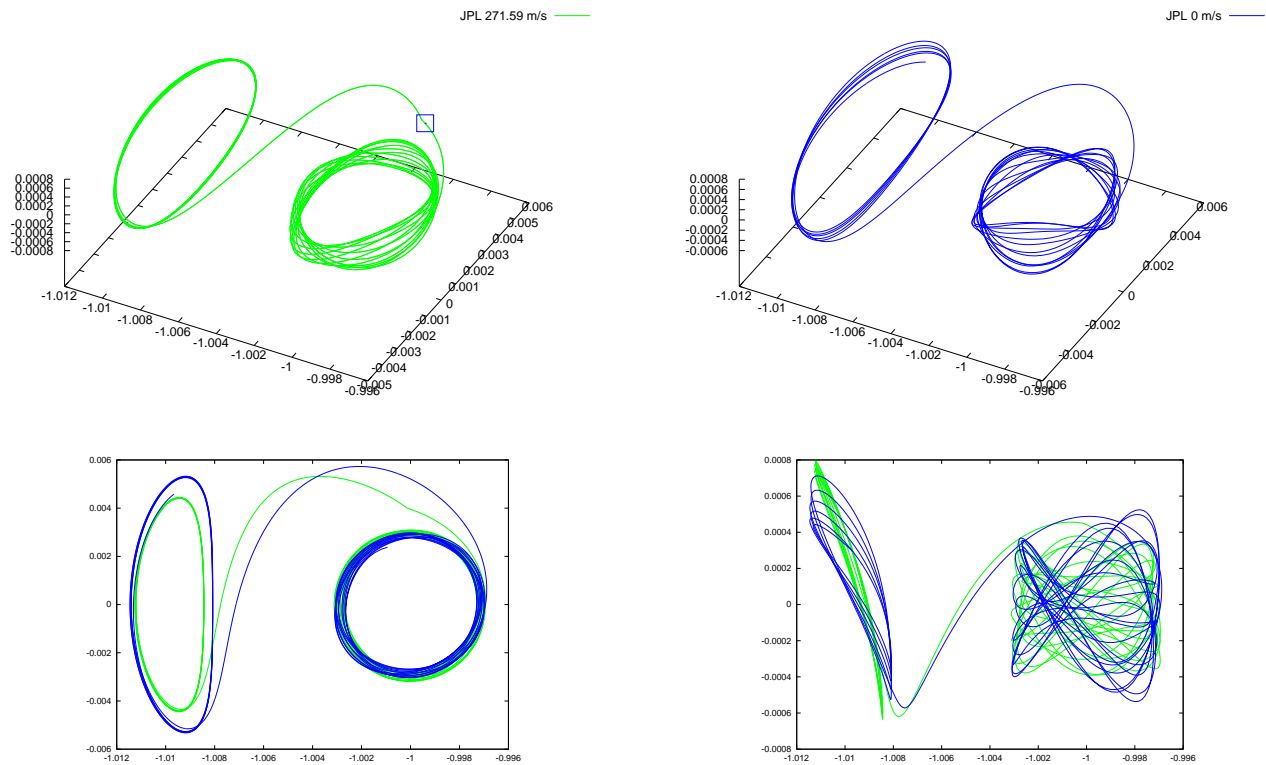
Figure 5.30: Trajectory joining a Lissajous around L_2 in the EM system and a Lissajous around the L_2 point of the SE system. (see details in table 5.6, where this connection is labelled as 14). In the first row on the left a 3D representations of the starting JPL coordinates trajectory is shown (i.e. the result of applying the section forced refinement to coupled RTBPs original seed), with a cost of 271.6 m/s. On the same row but on the right side the refined JPL connecting trajectory to zero cost is depicted. In both cases, the section crossing takes place on August the 24th 2018. The effects of the maneuver reduction can be observed in the projections shown in the second row. The in-plane amplitude has been slightly enlarged (picture on the left containing the xy projection), while the out of plane amplitude has been reduced a little (picture on the right, xz projection). These are the effects which can be expected when applying the procedure for reducing the maneuver on the section.

Trajectories associated with big and flattened Lissajous orbits in the solar regions are prone to exhibiting this good behaviour in the refinement process. In fact, Lissajous like the ones we have just described are close to planar Lyapunov orbits, for which zero cost connecting trajectories have already been found (in the coupled RTBPs models). Furthermore, even z oscillations that may seem big in the EM system are seen as close to planar motions when looked in the SE reference frame. Therefore, no big z oscillation can be expected in the SE Lissajous coming from a natural trajectory which is born as a small z oscillating motion in the EM side. Despite this a priori considerations on the shape of the SE Lissajous, studies should be performed in each particular case, as other kinds of Lissajous orbits can also lead to zero cost JPL trajectories with no significant modifications.

2. In other cases, the refinement of the transfer trajectory to a zero cost JPL trajectory results in important changes in the original orbits (see figures 5.30 and 5.31). When this happens one can choose whether to use the new orbits as nominal trajectories or to apply amplitude correcting maneuvers once in the arrival orbit, in order to transfer to the desired Lissajous.

   Another option in these cases would be to stop the procedure before the zero cost transfer is obtained. It is then a matter of finding the balance between cost and deviation from the original orbits (see figure 5.32).

3. Some other trajectories cannot be refined to zero cost transfers, as all attempts to reduce the coupling maneuver to zero fail due to a divergence in the maneuver reduction algorithm. This is the case for instance of many of the trajectories having as arrival orbit a square SE Lissajous around L_2 or the non-square arrival SE Lissajous with A_z amplitudes bigger than 150000 km (see figure 5.31). In the vast majority of cases, however, the coupling maneuver can be reduced to less than 100 m/s.

   If it is not possible or operationally convenient for the transfer to perform such big maneuvers, the designer should consider other means to reach the desired Lissajous around the solar L_2. For instance, using a Lissajous orbit which can be reached by a zero (or low enough) cost connecting trajectory and performing amplitude change maneuvers afterwards.

The three different possibilities commented above correspond to the convergence and divergence behaviour that one must expect when dealing with these kinds of refinements, for several reasons. Firstly, the initial seeds were found in a model which does not correspond to the physical reality. In addition, these initial seeds which have been introduced into the section-forced refinement and further manevuer reduction are not even required to have a small Δv in the original coupled RTBPs model (sometimes this Δv reaches 400 m/s). Furthermore, trajectories have to be associated with a refining epoch in the JPL ephemeris, while the coupled RTBPs model is autonomous. Taking all this into account, different degrees of convergence of the refinement procedure have to be expected:

• When the trajectory in the coupled RTBPs model is close to a natural transfer and the chosen epoch for the refinement is apropriate, zero cost trajectories are obtained in real ephemeris which are similar to the initial seed (case number 1, which we can call convergence case of the refinement procedure).
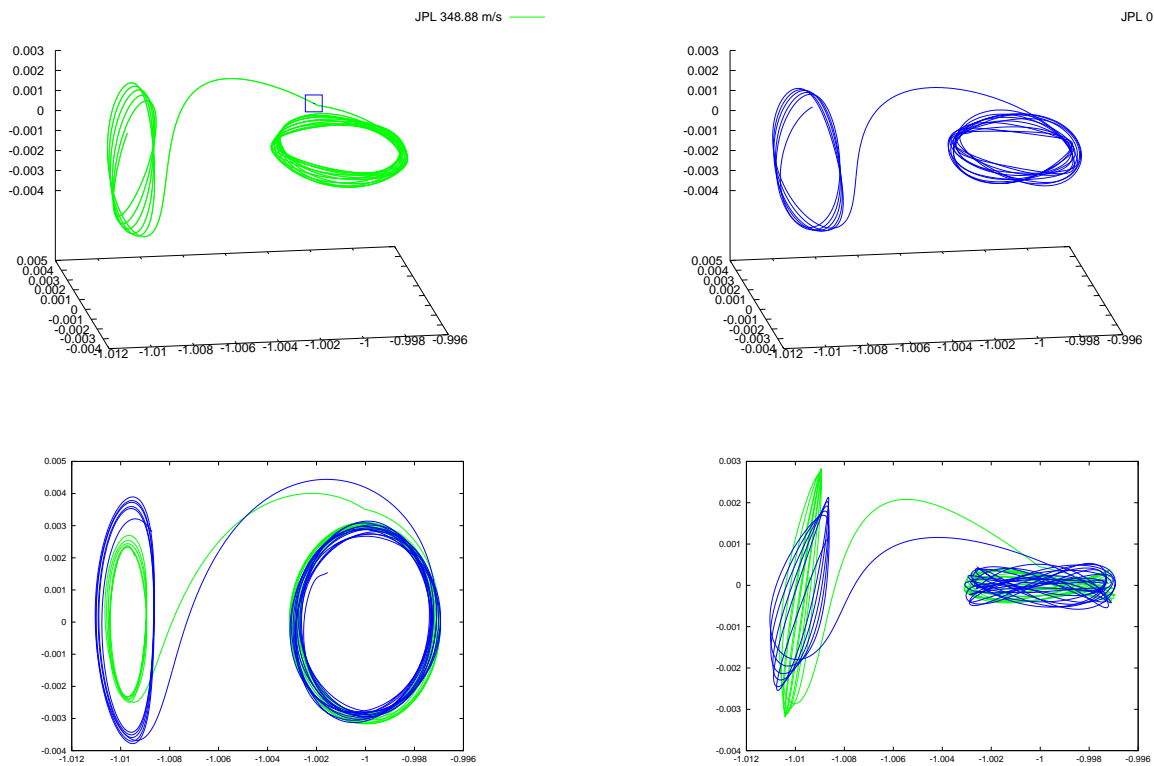
Figure 5.31: 3D representation of the real ephemeris transfer corresponding to the amplitudes and initial configuration labelled as 7 in table 5.5. Same comments as for figures 5.30 and 5.28 apply, in terms of the meaning of each of the figures as well as epoch of section crossing, but in this case the modification of the in-plane and out of plane amplitudes in order to achieve a zero cost transfer is significant. If one is interested in maintaining the original characteristics of the connecting trajectory, the refinement procedure can be stopped before the 0 cost is reached, as shown in figure 5.32.
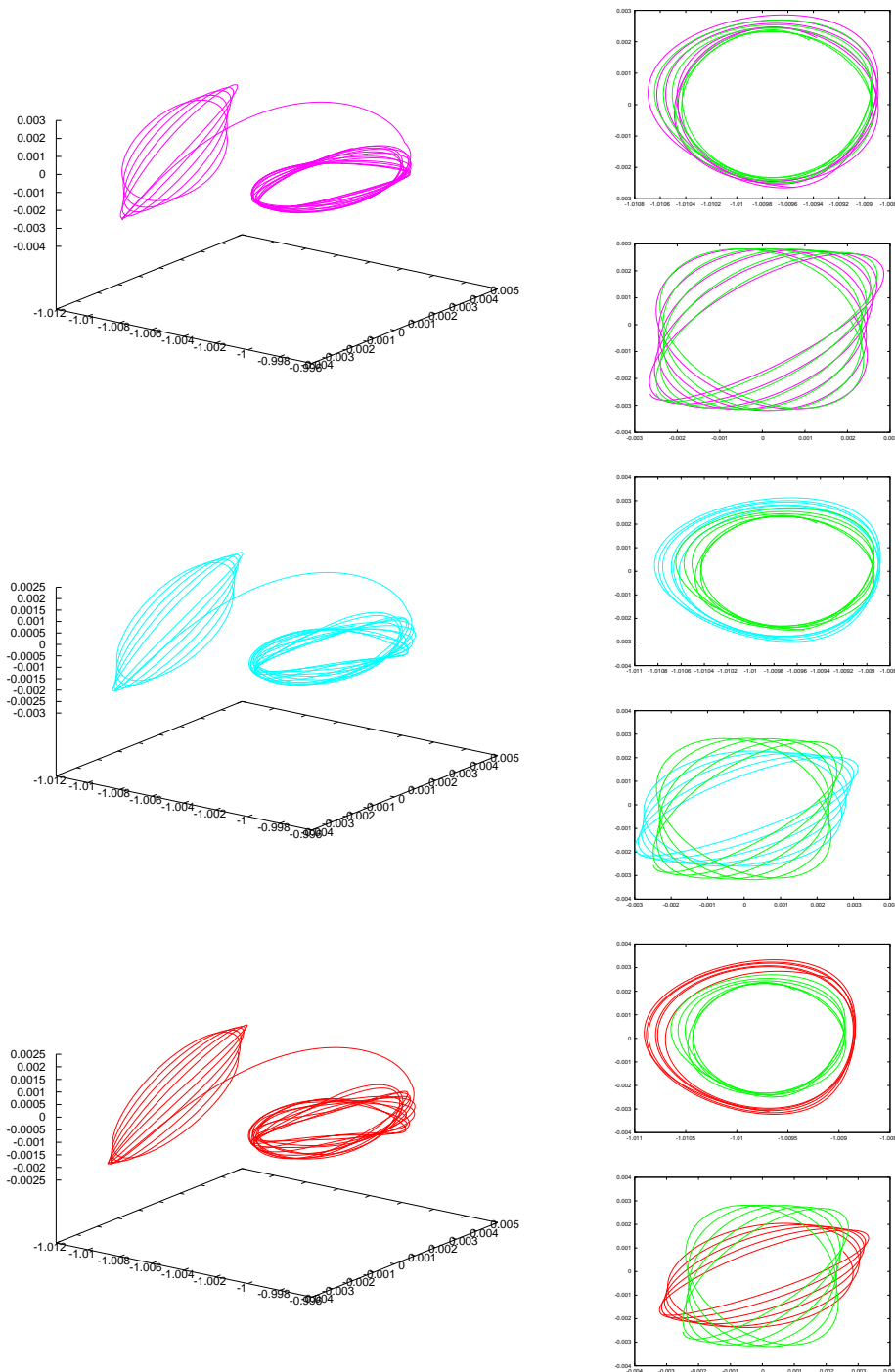
Figure 5.32: Same example trajectory as in figure 5.31. In these pictures some steps of the refinement to zero cost are shown. The column on the left shows the 3D representation of the refined JPL trajectory for a Δv of 247 m/s (first row), 141 m/s (second row) and 98 m/s (third row). Besides, the column on the right contains the xy and yz projections of the SE Lissajous orbit for the aforementioned refined trajectories compared to the original JPL one (always in green, obtained in the first refinement of the RTBPs using the section forced refinement for the date of section crossing August the 24th 2015), which costed around 350 m/s. One can choose to stop reducing the maneuver whenever the adequate deal between cost and resemblance to the initial trajectory has been met.
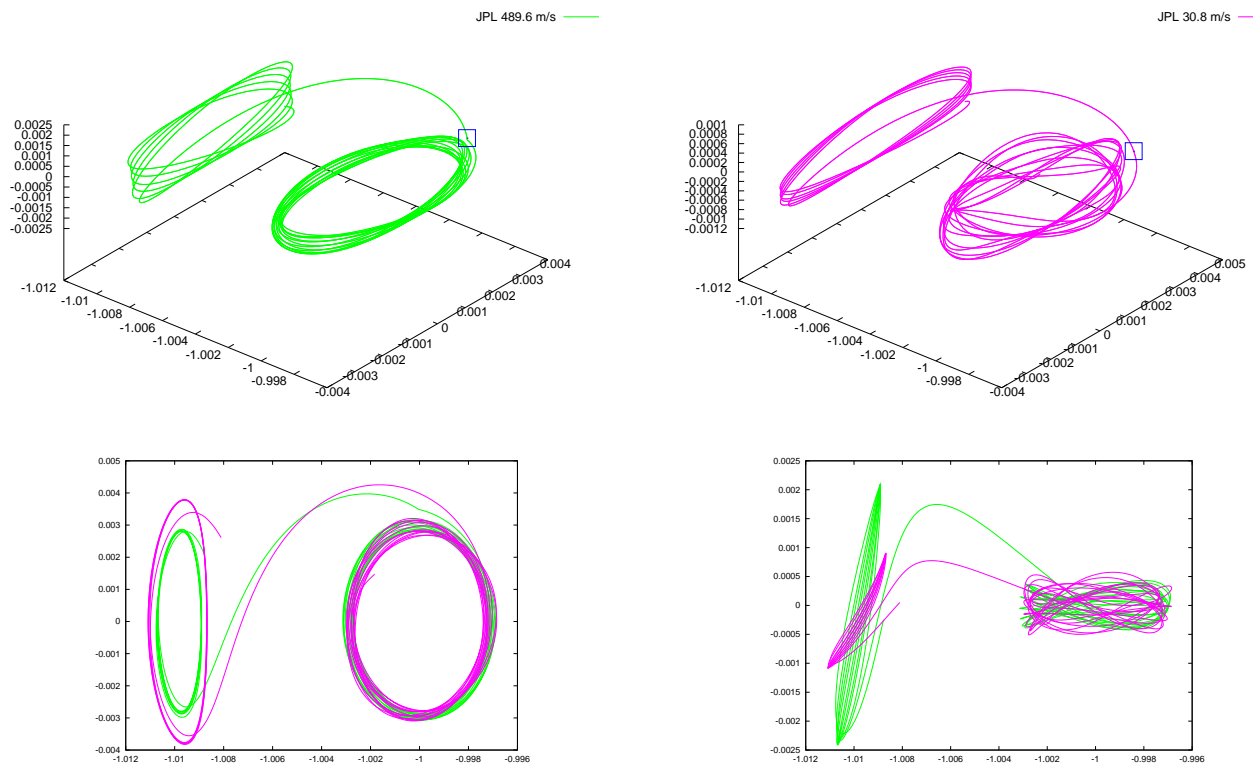
Figure 5.33: Trajectory joining a Lissajous around L_2 in the EM system and a Lissajous around the L_2 point of the SE system. (see details in table 5.5, where this connection is labelled as 5). In this case, the refinement to JPL coordinates had to be stopped before the zero cost transfer trajectory had been obtained. In the first row on the left a 3D representations of the starting JPL coordinates trajectory is shown (i.e. the result of applying the section forced refinement to coupled RTBPs original seed), with a cost of 489.6 m/s. On the same row but on the right side the refined JPL trajectory to 30.8 m/s cost is depicted. In both cases, the section crossing takes place on April the 19th 2013. The out of plane amplitude of the arriving Lissajous orbit on the SE side is too big for a cheap connecting trajectory to exist to the lunar libration region. In the refinement procedure, the out of plane amplitude is reduced and the in plane amplitude enlarged as shown in the xy and xz projections in the second row. In spite of these modifications to the arriving Lissajous side, a zero cost transfer trajectory could not be obtained joining the solar and lunar libration regions in this case.

- On the contrary, when no real ephemeris connecting trajectories exist for the given values of the Lissajous amplitudes the refinement procedure is obviously unable to find them. This corresponds to the above cases 2 and 3.

  For case number 2, even if no real connecting trajectory exists for the given amplitudes of the coupled RTBP trajectory, this initial trajectory is close enough to a natural transfer between Lissajous orbits of different amplitudes for the iterative refinement procedure to converge to it. This fact proves that our method is a good search method, despite the fact that it may not be interesting for mission prototyping in this case.

  Finally, when the original trajectory in the coupled RTBPs lies in a region which is too far from any zero cost connecting trajectory in real ephemeris, the refinement methods performs in the best possible way, which is reducing the maneuver until a point is reached when any further modification in the vicinity of the trajectory would increase its cost. That is to say, when a positive minimum of the Δv is found (case number 3).

Therefore, the divergences of the refinement should be regarded as a lack of real zero cost connections, rather than as weak points of our methodology.

All comments on the Lissajous amplitudes with respect to the behaviour of the refinement procedure mainly refer, so far, to the SE Lissajous orbit. As for the EM side, the Lissajous orbits undergo in all cases a significant increase in size when compared to the original ones in RTBP (see figure 5.34). Lindstedt-Poincaré expansions used to describe the Lissajous and their hyperbolic manifolds are valid for a range of amplitudes which may be too small for transferring purposes.
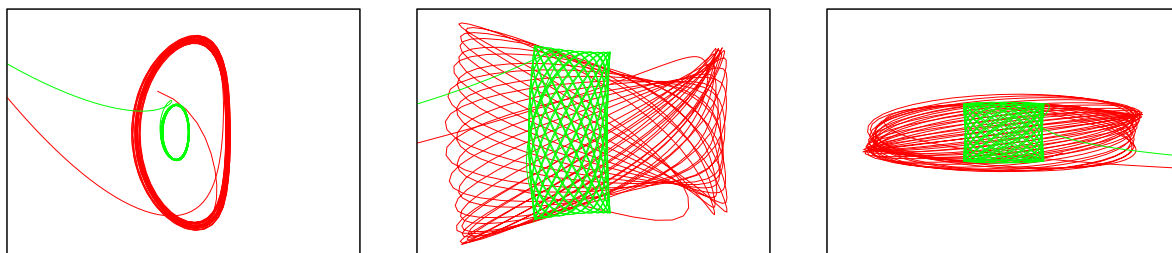
Figure 5.34: Final refined trajectory around the lunar L$_2$ libration point (in red), corresponding to original amplitude values A$_x$=2952.3 km and A$_z$=9000 km in the EM RTBP (square Lissajous, depicted in green). The pictures show, from left to right, the xy, xz and yz projections of the ephemeris trajectory in the lunar libration region in lunar adapted coordinates (EM RTBP system adapted coordinates centred in L$_2$.). The complete connecting trajectory corresponds to the initial angles $\alpha = 60$ deg. and $\beta = 45$ deg. and the arrival orbit is a Lissajous orbit around the solar L$_2$ libration point with A$_x$=212964.4 km and A$_z$=75384.4 km (this transfer is labelled as number 15 in table 5.6 and the section is crossed on August the 24th 2015. Figure 5.28 shows the 3D representation of this trajectory in the SE system adapted coordinates.). The y amplitude changes from 9000 km to almost 30000 km, and the x amplitude from around 3000 km to 10000 km. This changes are significant when depicted in Earth Moon coordinates, but they are not that important if one takes into account that we are dealing with amplitudes of hundreds of thousands of km in the Sun-Earth side. Consequently, the most important thing is to obtain an orbit in the EM libration region which is naturally maintained around the L$_2$ point and follows a Lissajous-like pattern.

Nevertheless, this increase is not seen as a big problem for the present work, as we were interested in proving that a way of finding transfer trajectories from the lunar libration regions to solar libration orbits, based on the coupled RTBPs, exists and that it is also usable for transforming the approximated coupled solutions to real ephemeris ones. Therefore, any orbit which is naturally maintained in the L_2 libration region for more than 2 years (as the ones we obtain in JPL coordinates) is considered an acceptable starting orbit, even if it is quite big. Note also that differences in size which may seem big in EM coordinates (of the order of thousands of km) are relatively small in the frame of the general problem, involving solar libration motions with amplitudes of a few hundreds of thousands of km. If other types of orbits around the Moon were desired, a particular study focused on lunar libration regions should be carried on.

Furthermore, it can be observed in all refined JPL trajectories with either zero or low cost maneuvers that the relative configuration of the Earth and the Moon at the moment when the trajectory leaves the vicinity of the EM Lissajous orbit is always similar, and close to the full moon configuration (Moon aligned with the Sun-Earth axis). Actually, the angle between the Sun-Earth axis and the Earth-Moon vector at the moment when the transfer trajectory leaves the vicinity of the Earth-Moon Lissajous can be computed and it ranges between 5 and 20 degrees. That is to say that we have to look for transfer windows from lunar to solar libration regions from 0.5 to 1.6 days after a full moon, in early waning lunar phase (see figure 5.35).
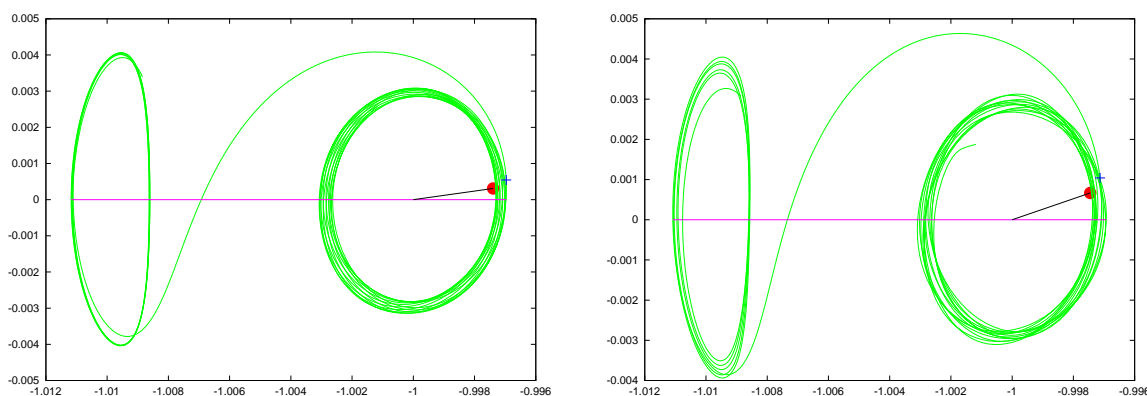
Figure 5.35: Representation of the Earth-Moon vector with respect to the Sun-Earth axis at the moment when the trajectory leaves the vicinity of the Earth Moon Lissajous (point on the trajectory represented by a cross). (left) xy representation of the zero cost JPL ephemeris connecting trajectory corresponding to 19 in table 5.6. The angle between the Earth-Moon vector and the Sun-Earth axis is approximately 5 degrees in this case. (right) xy representation of the zero cost JPL ephemeris connecting trajectory corresponding to 8 in table 5.5. This case corresponds to a big angle between the Earth-Moon vector and the Sun-Earth axis of around 19 degrees. Both trajectories have a section crossing date close to August the 24th, 2015.

Furthermore, we would also like to comment the fact that a trajectory between two given Lissajous orbits exhibits one of the three aforementioned behaviours in the refinement procedure is always dependent on the dates that are chosen for the refinement. It is true that when a trajectory turns out to be refinable to zero cost for a particular chosen epoch, it usually is whenever the starting date (see figure 5.36 and 5.37). However, different dates can lead, for instance, to

greater deviations from the original orbits or even to cases for which zero cost trajectories cannot be reached.
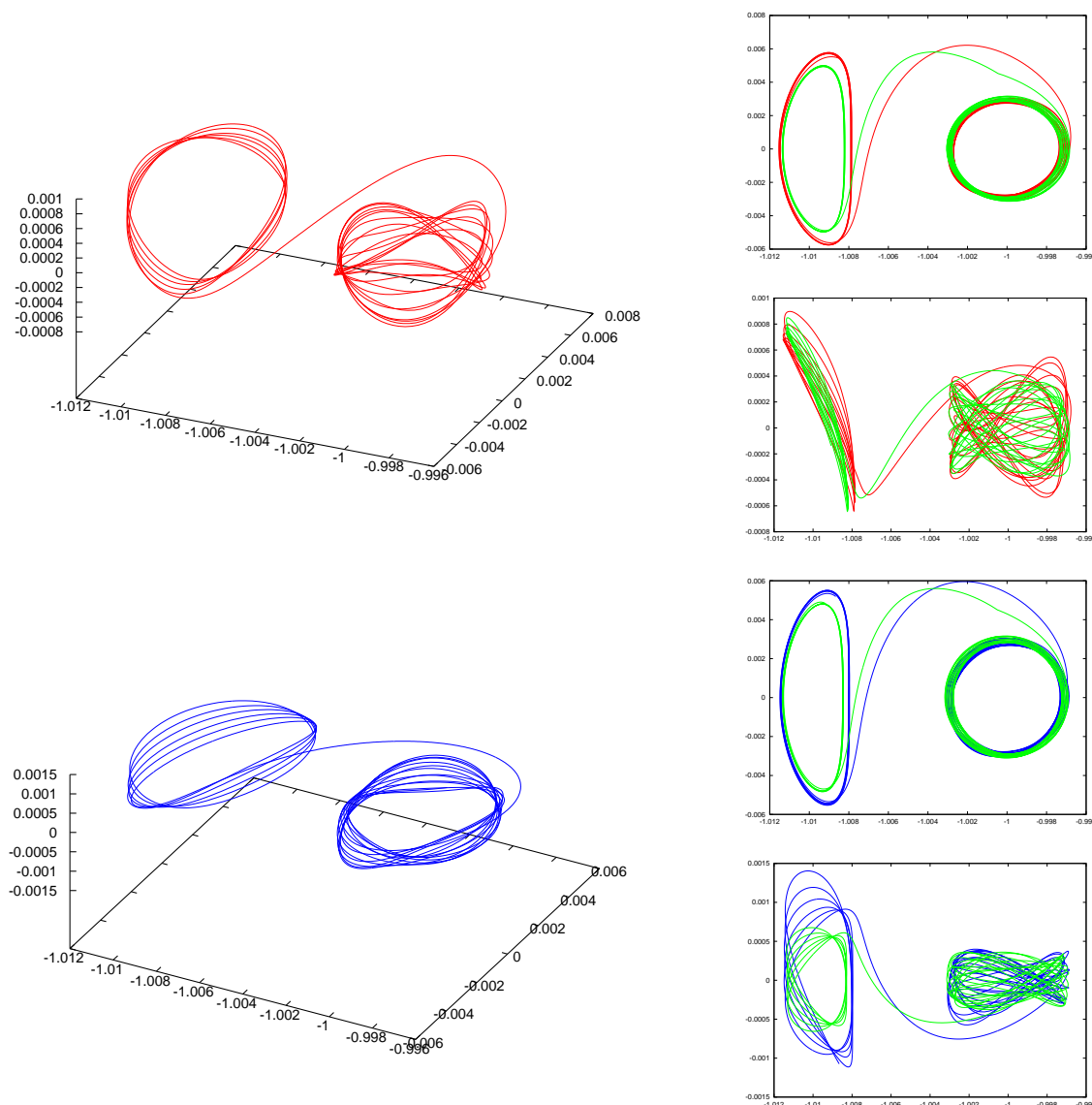
Figure 5.36: See comments in figure 5.37.

We have developed a method to refine coupled RTBP trajectories to real ephemeris coordinates. For initial trajectories in these coupled RTBPs which are close to the natural dynamics of the real system, zero cost transfers are easily obtained and they are as well kept similar to the original seeds in the coupled models.

When the initial seed in the restricted problems represents a trajectory which is far from a natural transfer, it will be changed in the process of Δv reduction and sometimes, completely free connecting trajectories cannot be obtained (as they may not exist in the real model). In
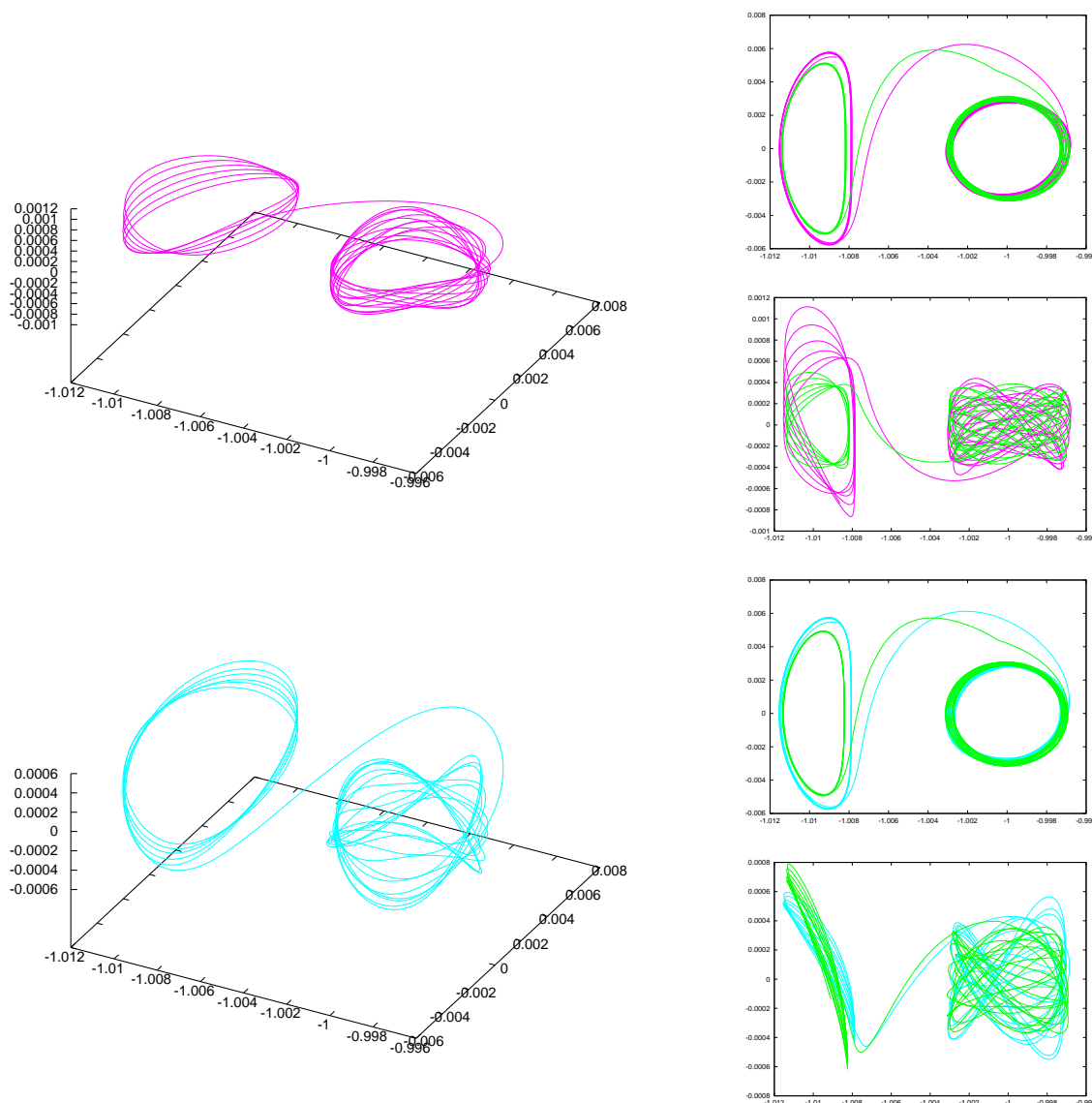
Figure 5.37: Three different ways of refining the connecting trajectory labelled as 12 in table 5.6 to a zero cost JPL trajectory, depending on the date of the section crossing. In figure 5.36 the chosen date is April the 19th 2013. In the first row of the present figure (in purple) the section crossing takes place on November the 15th 2018. Finally, the last representation (in light blue) corresponds to the section crossing on August the 24th 2015. All connecting trajectories are compared in the right column to the original JPL trajectory that was obtained by applying the section forced refinement to the RTBP transfers at the different section crossing epochs, by means of the xy projection (top) and xz projection (bottom). The original JPL trajectory is always depicted in green.

the worst case, however, our method allows for a reduction of the coupling maneuver to values around 100 m/s, when no shape and size requirements are imposed.

In terms of the characteristics of the solar Lissajous orbits, natural transfers which resemble the ones that can be computed in the coupled RTBPs can be expected for Lissajous orbits with big in-plane amplitudes (bigger than 200000 km) and the smaller out-of-plane amplitudes the better (smaller than 100000 km). Solar Lissajous orbits which do not satisfy these criteria (for instance, square Lissajous orbits) usually lead to expensive connecting trajectories in the coupled restricted three body problems, which have to be significantly modified in the refinement procedure in order to reduce the Δv associated with them. Finally, one has to bear in mind that in all cases the results are dependent on the epoch that is chosen for the coupling of the models.

Conclusions and Future work

All topics covered in this doctoral thesis are aimed at taking advantage of dynamical systems theory in the restricted three body problem (RTBP) for applications to mission design. Some questions arose during this work which are still open and may be the topic of further research. A brief summary and conclusions of the results achieved, as well as hints on the possible directions for future work are presented in what follows.

The eclipse avoidance problem in the so-called Lissajous-type orbits around L_1 and L_2 motivated the work presented in chapter 3. The linear approximation to the analytical description of these orbits has been used to tackle the problem. As Lissajous-type motion essentially takes place on a torus, it is described by a couple of angles if the amplitudes are fixed. Then, Lissajous orbits are seen in the phase plane as straight lines of constant slope. This fact allows for a simple geometric solution not only of the eclipse avoidance problem, but also the rendez-vous and the transfer between different Lissajous orbits using non-escape maneuvers. Consequently, the effective phases plane, or EPP, proves to be a useful tool in mission design.

A strategy for eclipse avoidance, based on similar ideas to the ones developed in the aforementioned chapter, has been successfully implemented in the preliminary design of the Herschel-Plank mission of the European Space Agency. This adaptability to real missions shows that the linear approximation to Lissajous orbits allows us to obtain results which are accurate enough for our purposes. In fact, the effect of the nonlinearities in the effective phase plane is just a slight perturbation of the exclusion zones representation. Thus, if the radius of the exclusion zones is taken a little bigger than strictly necessary, eclipse avoidance maneuvers computed in the linear problem are usable in more realistic models. However, for the sake of completeness, some future work will be devoted to adapting the eclipse avoidance and rendez-vous strategies to a more complete model, using the nonlinear terms in the description of the motion.

Furthermore, the hyperbolic manifolds associated with libration point orbits can be regarded as tubes which go away (unstable manifolds) or approach (stable manifolds) the aforementioned orbits in a natural way as time goes by. Therefore, an intersection between the stable manifold of an orbit and the unstable manifold of another one results in a natural asymptotic path joining them. Homoclinic connections are found by intersecting stable and unstable manifolds associated with a single orbit (i.e. they provide a way to asymptotically leave an orbit and return to it). On the other hand, heteroclinic connections are found by intersecting a stable manifold associated with an orbit and an unstable manifold associated with a different one. A method for numerically computing homoclinic and heteroclinic trajectories between planar Lyapunov orbits for any given Jacobi constant and RTBP mass parameter has been developed and results are presented in

chapter 4. The aforementioned methodology has been applied to the Sun-Earth and Earth-Moon cases, for which a description of the possible asymptotic connections up to a given number of loops around the small mass, which are grouped in families, is presented.

This part of the work was mainly aimed at developing tools for finding intersections between manifolds and setting the basis for a more applied research. Its natural future continuation would be to look for intersections between other periodic or quasi-periodic libration point orbits in the 3-dimensional RTBP (such as Halo or Lissajous orbits) and other more general invariant objects in a given energy level of the RTBP.

Finally, the idea of intersecting manifolds is exploited in a different way in chapter 5. The Sun-Earth-Moon-spacecraft four body problem can be modelled, in a first approximation, as two coupled RTBPs: the Sun-Earth one and the Earth-Moon one. In this way, the first part of chapter 5 deals with the coupling of two planar RTBPs in order to approximate the Sun-Earth-Moon problem and find transfer trajectories from lunar to solar planar Lyapunov orbits belonging to both L_2 libration regions. This work uses the ideas introduced in chapter 4 in order to compute intersections between hyperbolic manifolds. In addition, it provides and insight into the techniques and tools that are necessary for the coupling of different RTBPs, as well as the problems that arise when trying to approximate a four body problem in this way. Actually, low cost transfers between Lyapunov orbits belonging to the aforementioned libration regions have been found and they are presented in groups or families. In particular, even complete intersections between manifolds belonging to planar Lyapunov orbits of the two problems are presented (that is, intersections in position and velocity coordinates), which result in zero cost transfers in the coupled RTBPs model. Nevertheless, all results obtained by coupling two different models are strongly dependent on the relative configuration of these models. In our work, this relative configuration is represented by a couple of angles at time $t = 0$. The methodology we present is valid for any given value of these angles, but results are presented only for particular cases. It would be interesting, as a topic for future work, to find a complete topological description of the aforementioned families as a function of the coupling angles.

Moreover, transfer trajectories joining Lissajous orbits around L_2 points in the Sun-Earth and Earth-Moon problems are computed in the second part of chapter 5. The coupling between 3-dimensional RTBPs is more complicated than between planar ones, resulting in a harder search for intersections between manifolds. In this case, trajectories which are continuous in position in the coupled RTBPs are found. Then, the maneuvers that are needed in the coupling point for these trajectories to become transfers are computed. Furthermore, with the aim of providing realistic trajectories for mission design, a method for refining the coupled RTBPs trajectories between Lissajous type orbits to JPL realistic ephemeris is presented in the last part of the chapter. In a first step, the Sun-Earth and the Earth-Moon parts of the trajectory are independently refined to JPL. This provides a first approximation to position continuous trajectories in JPL coordinates with a Δv. Such trajectories could be used as initial seeds for a trajectory optimisation algorithm in order to obtain real low cost transfers in JPL coordinates for a given initial epoch. The use of optimisation techniques on these trajectories is actually left as part of the future work. On the contrary, this chapter finishes by presenting a method for slowly reducing the maneuver at the coupling point in the JPL refined trajectories, which leads to satisfying results and even to free trajectories joining Lissajous-type motions from the solar and lunar libration regions.

Appendix A

Guide to the attached DVD

A database containing information on intersections between unstable manifolds of square Lissajous orbits of the EM problem and stable manifolds of Lissajous orbits in the SE problem, with small A_z amplitude is attached to this PhD. thesis dissertation in the form of a DVD. This appendix is aimed at providing the information which is needed in order to use the aforementioned database.

Files `SE.dat` and `EM.dat`

The files `SE.dat` and `EM.dat` contain data defining the Lissajous orbits from each of the problems which have been used in the search for connecting trajectories.

Information concerning solar Lissajous orbits is stored in the file `SE.dat`. Each line in this file contains:

$$\texttt{i}, \mathcal{C}_{SE}, A_x, A_z$$

- `i`: an integer from 1 to 33, representing the line number in the file. This integer value is used as a label for the orbit.

- $\mathcal{C}_{SE}$: The Jacobi constant, representing the energy level to which the orbit and its manifolds belong.

- A_x and A_z: The values of the in-plane and out-of-plane amplitudes of the Lissajous orbit in SE RTBP coordinates normalised around L$_2$. In order to convert these amplitudes to km, they have to be multiplied by AU $\gamma_2^{SE} \approx 1.50768455 \ 10^6$.

The angle of the Poincaré section with the Sun-Earth x axis, ϕ_{SE} is fixed to 90 degrees.

Information concerning lunar Lissajous orbits is stored in the file `EM.dat`. Each line in this file contains:

$$\texttt{j}, \alpha, \beta, A_x, A_z$$

- `j`: an integer from 1 to 3591, representing the line number in the file and which is also used as a label characterising the corresponding orbit.

- α, β: Angular values in degrees which define the relative configuration of the EM and the SE x axis at the moment of the coupling between the RTBPs. Remember that only values of these phases such that $\alpha + \beta \in [80,120]$ are used.

- A_x, A_z: the values of the in-plane and out-of-plane amplitudes of the Lissajous orbit in EM adapted coordinates around L_2. In order to convert these amplitudes to km, they have to be multiplied by $3.844 \ 10^5 \gamma_2^{EM} \approx 6.451462 \ 10^4$.

Intersections on the Poincaré section, file `inters.dat`

The file `inters.dat` contains information on the overlapping regions on the Poincaré section between the manifolds of the Lissajous orbits defined in `SE.dat` and `EM.dat`.

The unstable manifold of each of the orbits in `EM.dat` has been integrated forwards in time, until the Poincaré section has been reached. A change of coordinates on this section (from EM to SE) using the phases α and β has been performed and the cuts in SE coordinates have been stored. On the other hand, the stable manifold of each of the orbits in the file `SE.dat` has been integrated backwards in time, and its cut with the Poincaré section has been compared to each of the stored cuts belonging to manifolds from the EM side.

Every time that an overlapping in yz coordinates on the Poincaré section between the cuts coming from the SE and the EM sides has been detected, a new line has been added to the file `inters.dat`, containing:

$$\texttt{i, j}, \ \mathcal{C}_{SE}, \ A_x^{SE}, \ A_z^{SE}, \ \alpha, \ \beta, \ A_x^{EM}, \ A_z^{EM}, \ y_m, \ y_M, \ z_m, \ z_M$$

- `i, j`: integers which indicate which are the orbits from the `SE.dat` and `EM.dat` files, respectively, whose associated manifolds have been found to intersect on the Poincaré section.

- $\mathcal{C}_{SE}$, A_x^{SE}, A_z^{SE}: Jacobi constant and amplitudes of the SE Lissajous orbit labelled with integer `i` in `EM.dat` (amplitudes in km).

- α, β: relative configuration phases used for coupling the RTBPs.

- A_x^{EM}, A_z^{EM}: amplitudes of the EM Lissajous orbit labelled with integer `j` in the file `EM.dat` (amplitudes in km).

- y_m, y_M, z_m, z_M: the overlapping between the cuts of the manifolds takes places inside the rectangle $[y_m, \ y_M] \times [z_m, \ z_M] \subset \mathbb{R}^2$. This rectangle is a raw approximation of the intersecting region on the section, obtained by comparing the minimum and maximum values of the y and z coordinates in each of the cuts (SE and EM manifolds) and choosing the most restrictive ones (greatest of the minimums and smallest of the maximums).

Connecting trajectories

Each line of the file `inters.dat` contains the necessary information for starting the search for connecting trajectories between the manifolds associated to two particular Lissajous orbits.

First of all, the in-plane, ϕ, and out-of-plane, ψ, initial phases on the unstable manifold of the EM Lissajous are discreetised. In particular, 100 equidistant phases are taken in $[0,2\pi]$ (both for ϕ and for ψ). Then, the initial conditions on the unstable manifold of the EM Lissajous defined by these phases and the corresponding amplitudes are integrated to the Poincaré section. Only the couples of phases whose integrated state falls inside the rectangle $[y_m, \ y_M] \times [z_m, \ z_M]$ are selected. A Newton method is then applied to the starting phases on the corresponding SE Lissajous, in order to match the points on the section with the ones from the SE Lissajous as explained in section 5.3.6. Note that for the sake of simplicity in building this database, the Newton method has only been applied to the SE side[4].

The connecting trajectories through each point of the overlapping region are associated to a Δv, which stands for the difference in velocities between the SE and EM branches that have been integrated independently to the section. Remember also from chapter 5 that more than one connecting trajectory can exist for a given point of the overlapping region. That is to say that more than one couple of phases from the SE side can be associated to each of the initial phases in the EM side.

Therefore, a large amount of information has to be stored concerning the intersections defined by each line in `inters.dat`. This information is organised in two files: `sistem`n`.dat` and `colors`n`.dat`.

Files `sistem`n`.dat` and `colors`n`.dat`

Let n be the number of a line contained in the file `inters.dat`. This information contained in this line is used as an input in our algorithm for the search of connecting trajectories. Once the trajectories associated to the input line n have been computed, two files are generated: `sistem`n`.dat` and `colors`n`.dib`.

`sistem`n`.dat`

This file contains information on which couples of phases from the EM and SE manifolds are joined by connecting trajectories. Furthermore, the points through which the connecting trajectories cross the section, as well as the necessary Δv and the integration times are also contained in it.

Each file `sistem`n`.dat` has a header like the one that has been copied here as an example (corresponding to $n{=}54015$):

```
# Amplituds TL   0.100000E-02   0.000000E+00   0.661003E-01   0.201504E+00
# Amplituds ST   0.000000E+00  -0.100000E-02   0.117628E+00   0.400000E-01
# Angle seccio, alfa i beta   0.900000E+02   0.950000E+02   0.150000E+02
# I1,I2,F1S,F2S,X,Y,Z,XP,YP,ZP,DV1,DV2,DV3,T1,T2
# I1,I2 fases TL, X,Y,Z,XP,YP,ZP punt corresponent
```

---

[4]That is to say that the points on the overlapping region defined by each of the couple of phases $(\phi_i, \psi_j) = (2\pi\frac{i}{100}, 2\pi\frac{j}{100})$ are the ones which define the net on the overlapping region to which the aforementioned section of chapter 5 refers. In other words, there is no need for applying a Newton method on the EM side of the integration, because each point on the net is already associated with a couple of phases on the manifold of the lunar Lissajous orbit.

```
# F1S,F2S fases ST
# T1,T2 temps de liss a seccio.(1:TL, 2:ST)
# DV=XST-XTL --> (XP,YP,ZP) + DV = V_ST
# Finestra fases TL    0.000000E+00    0.628319E+01    0.000000E+00    0.628319E+01
# Finestra fases ST    0.109956E+01    0.163363E+01    0.355000E+01    0.603186E+01
# Num.fases TL, ST  100  100    53  200
```

- The first two lines contain the values of the amplitudes A_1, A_2, A_x, A_z as explained in section 5.3.5 (A_1 and A_2 are the hyperbolic amplitudes, which are either 0 or ϵ, depending on whether we want to approximate the stable or the unstable manifold. A_x and A_z are the usual in-plane and out-of-plane amplitudes in RTBP normalised coordinates around L_2). The amplitudes in the first line correspond to the EM problem, while the ones in the second line to the SE problem.

- Three angular values are contained in the third line (in degrees):

  - ϕ_{SE}: the angle between the Sun-Earth x axis and the Poincaré section.
  - α and β: the phases representing the relative configuration of the SE and EM RTBPs at the moment of the coupling (see figure 5.15).

- From the 4th to the 8th line of the header, a short explanation of the meaning of each of the columns of the file is given:

  - First two columns: integer values I1 and I2. These values define the initial phases on the EM manifold in a net of 100 equidistant phases ($\phi = 2\pi\frac{I1}{100}$, $\psi = 2\pi\frac{I2}{100}$).
  - Third and fourth column: F1S, F2S $\in \mathbb{R}$, in radians. In-plane and out-of-plane phases on the SE Lissajous manifold which represent the arriving phases of the connecting trajectory.
  - From the 5th to 10th column: position and velocity coordinates of the state on the Poincaré section which is the result of integrating the EM initial condition represented by phases I1 and I2 and the corresponding amplitudes (state given in SE barycentric RTBP coordinates).
  - From the 11th to the 13th column: Δv vector in SE barycentric RTBP coordinates which has to be added to the integrated point coming from the EM manifold in order to jump to the SE manifold (i.e. to convert the velocity vector to the one on the SE manifold defined by phases F1S and F2S).
  - Last two columns: T1S, T2S$\in \mathbb{R}$. Integration times from the initial conditions on the manifolds to the Poincaré section (T1S refers to the EM side and so it represents a forwards integration time, while T2S to the SE side and therefore represents a backwards integration time). Both time values are expressed in SE RTBP time units (365.25 days $= 2\pi$ SE RTBP time units).

- Finally, additional information on the windows (*Finestra*) and number of phases which have been used on both manifolds is contained in the last three lines of the header. This is related

to the fact that not all initial phases on the manifolds lead to points that belong to the overlapping region on the section. Actually, the subset of $[0, 2\pi] \times [0, 2\pi]$ which contains initial phases leading to the overlapping region $[y_m,\ y_M] \times [z_m,\ z_M]$ is not usually a connected set. Thus, a study has to be performed for each of the connected components of the subset of phases. This is why the three lines of information about the windows and number of phases appear not only in the header but in some other parts of the file `sistemn.dat`.

colors$n$.dib

The other file associated with line n of `inters.dat` is called `colorsn.dat` The information contained in this file is used for drawing pictures like the ones in figures 5.22, 5.23 and 5.24. Essentially, once the file `sistemn.dat` has been obtained, one can count the number of connecting trajectories starting at each particular couple of phases on the EM Lissajous. Then, the cheapest one can be chosen and this information, together with the y and z coordinates of the point through which the connecting trajectory crosses the Poincaré section is stored in file `colorsn.dib`.

The files `colorsn.dib` also have a header, similar to the one in `sistemn.dat` but shorter. A sample header has been reproduced here (also corresponding to n=54015):

```
# Amplituds TL    0.100000E-02    0.000000E+00    0.661003E-01    0.201504E+00
# Amplituds ST    0.000000E+00   -0.100000E-02    0.117628E+00    0.400000E-01
# Angle seccio, alfa i beta    0.900000E+02    0.950000E+02    0.150000E+02
# Finestra fases TL    0.000000E+00    0.628319E+01    0.000000E+00    0.628319E+01
# I1,I2,Y,Z,N--I1,I2:fases TL; Y,Z:coord.seccio
# N: numero de connexions ST per aquestes fases TL
```

- The first two lines are exactly the same as in the file `sistemn.dat` containing the values of the hyperbolic and central amplitudes of the integrated manifolds.

- The third line is also the same as in sistem$n$.dat, containing the angular values of the ϕ_{SE}, α and β phases in degrees.

- In the fourth line, the intervals of in-plane and out-of-plane phases which have been integrated on the EM Lissajous (always discreetised in 100 equidistant values) are shown.

- Finally, the last lines explain the meaning of each one of the columns of the data stored in the file:

  - I1, I2: integers (from 1 to 100) defining the starting phases of the connecting trajectories on the EM manifold ($\phi = 2\pi \frac{I1}{100}$, $\psi = 2\pi \frac{I2}{100}$).
  - Y, Z: y and z coordinates of the state on the section associated with phases I1 and I2 (in SE barycentric RTBP coordinates).
  - N: number of connecting trajectories starting at the initial conditions defined by phases I1, I2 on the EM manifold and reaching the SE Lissajous stable manifold.
  - The last column in each line shows the cost in meters per second of the cheapest connecting trajectory, among the N possibilities.

How to find information on particular connecting trajectories

If one is interested in the connecting trajectories between a given pair of Lissajous orbits contained in the database, the first thing to do is to find out which are the values `i` and `j` which characterise the orbits in the files `EM.dat` and `SE.dat` respectively. Tables 1, 2 and 3 provide indications in this direction.

	A_z SE RTBP normalised around L$_2$							
$\mathcal{C}_{SE}$	0.01	0.02	0.03	0.04	0.05	0.06	0.07	0.08
3.00083	12	13	14	15	16	17	18	19
3.00084	20	21	22	23	24	25	26	27
3.00085	28	29	30	31	32	33	–	–

Table 1: Line number in file `SE.dat` associated with the SE Lissajous orbit depending on the Jacobi constant and A_z amplitude. The values of the out-of-plane amplitudes contained in the table range from 15000 to 120000 km. Small out-of-plane amplitudes in the SE side are prone to provide cheap connecting trajectories in the coupled RTBPs model, and this is why these orbits have been included in the database.

Secondly, one has to check whether the line starting by "i,j" exists in the file `inters.dat`. If no line in `inters.dat` starts by "i,j" it means that no overlapping region has been detected between the manifolds using this Poincaré section. Otherwise, if the intersection is stored in `inters.dat`, the number of the line, n, leads to the associated files `sistem`n`.dat` and `colors`n`.dat`. These data files have been grouped in directories and compressed in order to simplify its storage. Table 4 indicates which is the compressed directory `DN.tar.gz` associated with each range of lines of the file `inters.dat`.

Finally, due to the huge amount of data that we are dealing with, only some lines in `inters.dat` were selected and the corresponding files stored in the DVD. Despite this fact, the present database contains a big sample of results, which can be used as initial seeds for a wide range of trajectory design studies and provides a complete qualitative idea of the behaviour of the intersections. Our method can be used on any given Lissajous orbits and initial relative configuration, and therefore, any particular intersection between manifolds can be computed when necessary, even if it is not contained in the database.

$\alpha\backslash\beta$	75	80	85	90	95	100	105	110	115	120
0		1–16	17–32	33–48	49–64	65–80	81–96	97–112	113–128	129–144
5	145–160	161–176	177–192	193–208	209–224	225–240	241–256	257–272	273–288	

$\alpha\backslash\beta$	65	70	75	80	85	90	95	100	105	110
10		289–304	305–320	321–336	337 –352	353–368	369–384	385–400	401–416	417–432
15	433–448	449–464	465–480	481–496	497–512	513–528	529–544	545–560	561–576	

$\alpha\backslash\beta$	55	60	65	70	75	80	85	90	95	100
20		577–592	593–608	609–624	625–640	641–656	657–672	673–688	689–704	705–720
25	721–736	737–752	753–768	769–784	785–800	801–816	817–832	833–848	849–864	

$\alpha\backslash\beta$	45	50	55	60	65	70	75	80	85	90
30		865–880	881–896	897–912	913–928	929–944	945–960	961–976	977–992	993–1008
35	1009-1024	1025-1040	1041-1056	1057-1072	1073-1088	1089-1104	1105-1120	1121-1136	1137-1152	

$\alpha\backslash\beta$	35	40	45	50	55	60	65	70	75	80
40		1153-1168	1169-1184	1185-1200	1201-1216	1217-1232	1233-1248	1249-1264	1265-1280	1281-1296
45	1297-1312	1313-1328	1329-1344	1345-1360	1361-1376	1377-1392	1393-1408	1409-1424	1425-1440	

$\alpha\backslash\beta$	25	30	35	40	45	50	55	60	65	70
50		1441-1456	1457-1472	1473-1488	1489-1504	1505-1520	1521-1536	1537-1552	1553-1568	1569-1584
55	1585-1600	1601-1616	1617-1632	1633-1648	1649-1664	1665-1680	1681-1696	1697-1712	1713-1728	

$\alpha\backslash\beta$	15	20	25	30	35	40	45	50	55	60
60		1729-1744	1745-1760	1761-1776	1777-1792	1793-1808	1809-1824	1825-1840	1841-1856	1857-1872
65	1873-1888	1889-1904	1905-1920	1921-1936	1937-1952	1953-1968	1969-1984	1985-2000	2001-2016	

$\alpha\backslash\beta$	5	10	15	20	25	30	35	40	45	50
70		2017-2032	2033-2048	2049-2064	2065-2080	2081-2096	2097-2112	2113-2128	2129-2144	2145 -2160
75	2161-2176	2177-2192	2193-2208	2209-2224	2225-2240	2241-2256	2257-2272	2273-2288	2289-2304	

$\alpha\backslash\beta$	0	5	10	15	20	25	30	35	40	45
80	2305-2320	2321-2336	2337-2352	2353-2368	2369-2384	2385-2400	2401-2416	2417-2432	2433-2448	
85	2449-2464	2465-2480	2481-2496	2497-2512	2513-2528	2529-2544	2545-2560	2561-2576		
90	2577-2592	2593-2608	2609-2624	2625-2640	2641-2656	2657-2672	2673-2688			
95	2689-2704	2705-2720	2721-2736	2737-2752	2753-2768	2769-2784				
100	2785-2800	2801-2816	2817-2832	2833-2848	2849-2864					
105	2865-2880	2881-2896	2897-2912	2913-2928						
110	2929-2944	2945-2960	2961-2976							
115	2977-2992	2993-3008								
120	3009-3024									

Table 2: Line numbers in file `EM.dat` associated with the EM Lissajous orbits, depending on the values of α and β. For each couple (α, β), a range of lines is indicated in the table, as several square Lissajous orbits around L_2 point have been considered. In particular, 15 different square EM Lissajous orbits with A_z from 5000 to 20000 km (the corresponding A_x in these EM square Lissajous orbits satisfies $A_z = 3.048 A_x$).

$\alpha\backslash\beta$	75	80	85	90	95	100	105	110	115	120
0		3025-3027	3028-3030	3031-3033	3034-3036	3037-3039	3040-3042	3043-3045	3046-3048	3049-3051
5	3052-3054	3055-3057	3058-3060	3061-3063	3064-3066	3067-3069	3070-3072	3073-3075	3076-3078	

$\alpha\backslash\beta$	65	70	75	80	85	90	95	100	105	110
10		3079-3081	3082-3084	3085-3087	3088-3090	3091-3093	3094-3096	3097-3099	3100-3102	3103-3105
15	3106-3108	3109-3111	3112-3114	3115-3117	3118-3120	3121-3123	3124-3126	3127-3129	3130-3132	

$\alpha\backslash\beta$	55	60	65	70	75	80	85	90	95	100
20		3133-3135	3136-3138	3139-3141	3142-3144	3145-3147	3148-3150	3151-3153	3154-3156	3157-3159
25	3160-3162	3163-3165	3166-3168	3169-3171	3172-3174	3175-3177	3178-3180	3181-3183	3184-3186	

$\alpha\backslash\beta$	45	50	55	60	65	70	75	80	85	90
30		3187-3189	3190-3192	3193-3195	3196-3198	3199-3201	3202-3204	3205-3207	3208-3210	3211-3213
35	3214-3216	3217-3219	3220-3222	3223-3225	3226-3228	3229-3231	3232-3234	3235-3237	3238-3240	

$\alpha\backslash\beta$	35	40	45	50	55	60	65	70	75	80
40		3241-3243	3244-3246	3247-3249	3250-3252	3253-3255	3256-3257	3258-3260	3261-3263	3264-3266
45	3267-3269	3270-3272	3273-3275	3276-3278	3279-3281	3283-3285	3286-3288	3289-3291	3292-3294	

$\alpha\backslash\beta$	25	30	35	40	45	50	55	60	65	70
50		3295-3297	3298-3300	3301-3303	3304-3306	3307-3309	3310-3312	3313-3315	3316-3318	3319-3321
55	3322-3324	3325-3327	3328-3330	3331-3333	3334-3336	3337-3339	3340-3342	3343-3345	3346-3348	

$\alpha\backslash\beta$	15	20	25	30	35	40	45	50	55	60
60		3349-3351	3352-3354	3355-3357	3358-3360	3361-3363	3364-3366	3367-3369	3370-3372	3373-3375
65	3376-3378	3379-3381	3382-3384	3385-3387	3388-3390	3391-3393	3394-3396	3397-3399	3400-3402	

$\alpha\backslash\beta$	5	10	15	20	25	30	35	40	45	50
70		3403-3405	3406-3408	3409-3411	3412-3414	3415-3417	3418-3420	3421-3423	3424-3426	3427-3429
75	3430-3432	3433-3435	3436-3438	3439-3441	3442-3444	3445-3447	3448-3450	3451-3453	3454-3456	

$\alpha\backslash\beta$	0	5	10	15	20	25	30	35	40	45
80	3457-3459	3460-3462	3463-3465	3466-3468	3469-3471	3472-3474	3475-3477	3478-3480	3481-3483	
85	3484-3486	3487-3489	3490-3492	3493-3495	3496-3498	3499-3501	3502-3504	3505-3507		
90	3508-3510	3511-3513	3514-3516	3517-3519	3520-3522	3523-3525	3526-3528			
95	3529-3531	3532-3534	3535-3537	3538-3540	3541-3543	3544-3546				
100	3547-3549	3550-3552	3553-3555	3556-3558	3559-3561					
105	3562-3564	3565-3567	3568-3570	3571-3573						
110	3574-3576	3577-3579	3580-3582							
115	3583-3585	3586-3588								
120	3589-3591									

Table 3: Line numbers in file `EM.dat` associated with the EM Lissajous orbits, depending on the values of α and β. For each couple (α, β), a range of lines is indicated in the table, as several square Lissajous orbits around L$_2$ point have been considered. In particular, 3 different square EM Lissajous orbits with A_z equal to 21000, 22000 and 23000 km (the corresponding A_x in these EM square Lissajous orbits satisfies $A_z = 3.048 A_x$).

directory	lines	directory	lines	directory	lines
D01	90– 1735	D12	19270–21079	D23	38580–40295
D02	1770– 3485	D13	21080–22025	D24	40330–42045
D03	3520– 5235	D14	23250–24545	D25	42080–43795
D04	5270– 6985	D15	24580–26295	D26	43830–44880
D05	7020– 8735	D16	26330–28045	D27	46035–47295
D06	8770–10485	D17	28080–29795	D28	47400–48310
D07	10520–12235	D18	29830–31595	D29	49080–50795
D08	12270–13985	D19	31580–33295	D30	52580–54260
D09	14020–15735	D20	33330–35045	D31	54295–56045
D10	15770–17485	D21	35080–36795	D32	56080–57795
D11	17520–19235	D22	36830–38545	D33	57830–59825

Table 4: Ranges of lines of the file `inters.dat` whose associated files `sistem`n`.dat` and `colors`n`.dat` are contained in each one of the compressed directories of the database.

Appendix B

Resum

Aquesta tesi doctoral està emmarcada en el camp de l'astrodinàmica. Concretament, tracta el disseny de missió en òrbites de libració. El punt de partida de tots els estudis continguts en la present memòria és la teoria de sistemes dinàmics, que proporciona una descripció acurada de la dinàmica en les regions de libració. No obstant això, aquest treball és aplicat. Per tant, fa ús d'aquesta descripció teòrica amb l'objectiu de donar solucions a problemes que s'han detectat en el disseny de missions reals.

El problema restringit de tres cossos, o RTBP, és un model ben conegut que serveix per estudiar el moviment d'un cos de massa infinitesimal sota l'atracció gravitatòria de dos cossos molt massius. Els 5 punts d'equilibri d'aquest model han estat motiu de nombrosos estudis des del segle passat. Els resultats continguts en aquesta memòria fan referència a dos d'aquests punts d'equilibri: L_1 i L_2, que es troben un a cada banda del més petit dels mencionats cossos massius, i són els que han centrat més interès per aplicacions pràctiques en les últimes dècades (per missions com SOHO, Genesis, Herschel-Planck...). La inestabilitat és una propietat bàsica d'aquests punts d'equilibri, que és heredada per les òrbites que els envolten i és la responsable de l'existència de direccions estables i inestables en cada punt de les òrbites de libració. La unió d'aquestes direccions, o més precisament, de totes les trajectòries asimptòtiques que emanen de les òrbites periòdiques i quasi-periòdiques al voltant de L_1 i L_2, formen un objecte invariant que o bé s'apropa (en el cas de les direccions estables) o bé s'allunya (en el cas de les inestables) de l'entorn dels punts de libració. Aquests objectes invariants s'anomenen varietats hiperbòliques de les òrbites de libració. Un coneixement i descripció adequats de les esmentades varietats pot ser extremadament útil pel disseny de missions, ja que són la clau per a entendre la dinàmica del sistema.

El primer problema tractat en el nostre treball són les estratègies per evitar eclipsis en òrbites de Lissajous. Genèricament, qualsevol missió en òrbita al voltant del punt L_2 del sistema Terra-Sol es veu afectat per ocultacions degudes a l'ombra de la Terra, a no ser que se li apliquin maniobres per evitar eclipsis. Si l'òrbita és al voltant de L_1, els eclipsis són deguts a la forta influència electromagnètica del Sol en aquestes regions. Per altra banda, les òrbites de Lissajous són un tipus d'òrbites de libració que resulten de la combinació de dues oscil.lacions perpendiculars. El seu principal avantatge sobre altres tipus d'òrbites, com ara les Halo, és que les amplitudes d'una òrbita de Lissajous poden ser escollides independentment una de l'altra i això les fa més adaptables als requeriments de cada missió. En aquest treball utilitzem l'aproximació lineal a la descripció anal.lítica de les òrbites de Lissajous per tal de calcular l'anomenada direcció de

179

no-escapament, que permet fer transferències entre diferents òrbites canviant les amplituds o les fases (o tot a la vegada) i al mateix temps evitar la part inestable del moviment.

A més, un altre problema que també és interessant pel disseny de missió és el *rendez-vous*, entès com la manera de fer que dos satèl.lits diferents es trobin en una òrbita o s'apropin fins a una distància donada. Les eines desenvolupades per les estratègies de prevenció d'eclipsis ens permeten també planificar maniobres senzilles de *rendez-vous*, ja sigui per incloure-les en l'anàl.lisi i disseny preliminar de la missió, o bé quan aquesta ja s'està portant a terme, com a pla d'emergència.

Per altra banda, existeixen canals de baix cost que uneixen els punts L_1 i L_2 d'un sistema donat, com els que va utilitzar la missió Genesis. Aquest canals representen una manera natural de transferir d'una regió de libració a l'altra i es poden trobar intersecant varietats estables i inestables d'òrbites al voltant de L_1 i L_2. Si tenim present que les varietats estables tendeixen cap a l'objecte que les genera quan el temps avança, i que les varietats inestables fan el mateix però si fem anar el temps enrera, una intersecció entre una varietat estable i una d'inestable proporciona un camí asimptòtic entre els objectes invariants corresponents. Connexions d'aquest tipus entre òrbites de Lyapunov planes, que són òrbites periòdiques entorn L_1 i L_2, són estudiades en aquesta tesi i específicament calculades pels casos dels problemes restringits Sol-Terra i Terra-Lluna.

A més, la idea d'intersecar varietats estables i inestables per tal de trobar connexions entre òrbites es pot aplicar també per trobar camins de baix cost entre les regions de libració del sistema Terra-Lluna i les del sistema Terra-Sol. Se sap que les varietats estables de les òrbites entorn els punts de libració lunars no s'apropen prou a la Terra com per proporcionar una transferència de baix cost des de l'entorn de la Terra fins a la Lluna. En canvi, les varietats estables i inestables d'algunes òrbites de libració del sistema Sol-Terra sí que s'acosten a la Terra. Per tant, si es pogués trobar un camí natural entre les òrbites de libració solars i les lunars, s'obtindria una manera barata d'anar a la Lluna fent servir varietats invariants. I al revés, un camí de les regions de libració lunars cap a les regions de libració solars permetria, per exemple, que una estació de servei fos col.locada en òrbita en un punt de libració de la Lluna i servís com a base per donar servei a les missions que operen en òrbites de libració del sistema Sol-Terra. Aquesta és bàsicament la idea de l'última part de la tesi. Amb l'objectiu d'unir les regions de libració dels dos problemes esmentats, el problema de quatre cossos Sol-Terra-Lluna-nau es pot descomposar en dos problemes restringits de 3 cossos. Així, podem buscar interseccions entre les varietats pertanyents a òrbites de cada un dels problemes. Per començar, busquem trajectòries que connectin les òrbites planes de Lyapunov dels sistemes Terra-Sol i Terra-Lluna. Més endavant, la búsqueda es porta cap al problema tridimensional, amb el conseqüent augment de la dificultat per descriure els objectes i trobar-ne interseccions. No obstant, un mètode per trobar trajectòries que connectin òrbites de Lissajous dels dos models s'ha pogut trobar i s'exposa en el capítol final. I finalment, es presenta també un mètode per refinar aquestes trajectòries trobades acoblant dos problemes restringits de tres cossos cap a efemèrides reals JPL. En alguns casos, és possible anar reduint la maniobra necessària en el punt d'acoblament fins a valors molt petits o zero, cosa que proporciona trajectòries realistes de cost zero a punt per ser utilitzades en el disseny de missions.

Bibliography

[1] E. Belbruno and J.K. Miler. *A Ballistic Lunar Capture Trajectory for the Japanese Spacecraft Hiten.* JPL, IOM 312/90.4–1371, 1990.

[2] E. Belbruno. *Capture Dynamics and Chaotic Motions in Celestial Mechanics.* Princeton University Press, 2004.

[3] J. L. Bell et al. *Genesis Trajectory Design.* Advances in the Astronautical Sciences, 103:1525–1537, 2000.

[4] T. A. Bray and C. L. Goudas. *Three Dimensional Periodic Oscillations About L_1, L_2, L_3.* Advances in Astronomy and Astrophysics, 5:71–130, 1967.

[5] J. V. Breakwell and J. Brown. *The Halo Family of Three Dimensional Periodic Orbits in the Earth–Moon Restricted Three Body Problem.* Celestial Mechancis, 20(4):389–404, 1979.

[6] J. V. Breakwell, A. A. Kamel, and M. J. Ratner. *Station-Keeping for a Translunar Communications Station.* Celestial Mechanics, 10(3):357–373, 1974.

[7] J. Cobos and M. Hechler. *FIRST Mission Analysis: Transfer to Small Lissajous Orbits around L_2.* Technical Report MAS Working Paper No. 398, ESOC, 1997.

[8] J. Cobos, J. J. Masdemont, *Astrodynamical Applications of Invariant Manifolds Associated with Collinear Libration Orbits.* Proceedings of the Conference Libration Point Orbits and Applications, pages 253–268, World Scientific, 2003.

[9] A. Delshams, P. Gutiérrez. *Effective stability and KAM theory.* J. Differential Equations, 128:415-490, 1996

[10] D. W. Dunham. *Utilization of Libration–Point Orbits.* In Problemi di Astronautica e di Meccanica Celeste a Ricordo del Prof. G. Colombo., pages 239–274. Atti della Accademia delle Science di Torino, Suppl. al Vol 122, 1988.

[11] D. W. Dunham, S. J. Jen, C. E. Roberts, A. W. Seacord, P. J. Sharer, D. C. Folta, and D. P. Muhonen. *Transfer Trajectory Design for the SOHO Libration-Point Mission.* 43rd Congress of the International Astronautical Federation, IAF Paper 92–0066, 1992.

[12] R. W. Farquhar. *The Role of the Sun–Earth Collinear Libration Points in Future Space Explorations.* Space Times, 39(6):9–12, 2000.

[13] R. W. Farquhar. *IAC-03-IAA.13.2.03 The Utilization of Libration Points for Human Exploration in the Sun-Earth-Moon System and Beyond.* 54th International Astronautical Congress of the International Astronautical Federation, Bremen (Germany) Sep.29-Oct.3, 2003.

[14] R. W. Farquhar and D. W. Dunham. *Use of Libration–Point Orbits for Space Observatories.* Observatories in Earth Orbits and Beyond, Ed by Y. Kondo, Kluwer Academic Publishers, pages 391–395, 1990.

[15] R. W. Farquhar. *Station–Keeping in the Vicinity of Collinear Libration Points with an Application to a Lunar Communications Problem.* Space Flight Mechanics, Science and Technology Series 11:519–535. American Astronautical Society, New York, 1967.

[16] R. W. Farquhar. *Comments on Optimal Controls for Out of Plane Motion About the Translunar Libration Point.* Journal Spacecraft and Rockets, 8(7):815–816, 1971.

[17] R. W. Farquhar. *Utilization of Multi-Body Trajectories in the Sun–Earth–Moon System.* Technical Report 80740, NASA Technical Memorandum, 1980.

[18] R. W. Farquhar and D. W. Dunham. *A New Trajectory Concept for Exploring the Earth's Geomagnetic Tail.* AIAA Aerospace Sciences Meeting, 1980.

[19] R. W. Farquhar and D. W. Dunham. *Libration–Point Staging Concepts for Earth–Mars Transportation.* Technical Report M002, NASA, 1986.

[20] R. W. Farquhar, D. P. Muhonen, and D. L. Richardson. *Mission Design for a Halo Orbiter of the Earth.* Journal Spacecraft and Rockets, 14(3):170–177, 1977.

[21] D. Folta and M. Beckman. *Libration Orbit Mission Design: Applications of Numerical and Dynamical Methods.* Libration Point Orbits and Applications, World Scientific, 2003.

[22] F. Gabern and À. Jorba. *A Restricted Four-Body Model for the Dynamics near the Lagrangian Points of the Sun-Jupier System.* Discrete and Continuous Dynamical Systems. Series B, 1(2):143–182, 2001.

[23] G. Gómez, A. Jorba, J. Masdemont, and C. Simó. *Study of the Transfer from the Earth to a Halo Orbit Around the Equilibrium Point L_1.* Celestial Mechanics, 56(4):541–562, 1993.

[24] G. Gómez, A. Jorba, J. J. Masdemont, and C. Simó. *Study of the Transfer Between Halo Orbits.* Acta Astronautica, 43(9–10):493–520, 1998.
5 Orbit.

[25] G. Gómez, W. S. Koon, M. W. Lo, J. E. Marsden, J. J. Masdemont and S. D. Ross. *Connecting Orbits and Invariant Manifolds in the Spatial Restricted Three-Body Problem.* Nonlinearity, 17:1571–1606, 2004.

[26] G. Gómez, W. S. Koon, M. W. Lo, J. E. Marsden, J. J. Masdemont, and S. D. Ross. *Invariant Manifolds, the Spatial Three-Body Problem and Space Mission Design.* Advances in The Astronautical Sciences, 109, 1:3–22, 2001.

[27] G. Gómez, J. Llibre, and J. J. Masdemont. *Homoclinic and Heteroclinic Solutions in the Restricted Three-Body Problem.* Celestial Mechanics, 44:239–259, 1988.

[28] G. Gómez and J. J. Masdemont. *Some Zero Cost Transfers Between Halo Orbits.* Advances in the Astronautical Sciences, 105(2):1199–1216, 2000.

[29] G. Gómez, J. J. Masdemont and M. Marcote. *Trajectory correction maneuvers in the transfer to libration point orbits.* Libration Point Orbits and Applications. World Scientic Publishing Company, 2003.

[30] G. Gómez and J. M. Mondelo. *The Phase Space Around the Lagrange Points of the RTBP.* Physica D, 157(4):283–321, 2001.

[31] G. Gómez, K. C. Howell, J. J. Masdemont, and C. Simó. *Station-Keeping Strategies for Translunar Libration Point Orbits.* Advances in the Astronautical Sciences, 99:949–967, 1998.

[32] G. Gómez, J. Llibre, R. Martínez, and C. Simó. *Dynamics and Mission Design Near Libration Point Orbits – Volume 1: Fundamentals: The Case of Collinear Libration Points.* World Scientific, 2000.

[33] G. Gómez, J. Llibre, R. Martínez and C. Simó. *Dynamics and Mission Design Near Libration Point Orbits – Volume 2: Fundamentals: The Case of Triangular Libration Points.* World Scientific, 2000.

[34] G. Gómez, À. Jorba, J. J. Masdemont and C. Simó. *Dynamics and Mission Design Near Libration Point Orbits – Volume 3: Advanced Methods for Collinear Points.* World Scientific, 2000.

[35] G. Gómez, J. J. Masdemont and C. Simó. *Lissajous Orbits Around Halo Orbits.* Advances in the Astronautical Sciences, 95:117–134, 1997.

[36] G. Gómez, J.J. Masdemont, and C. Simó. *Quasihalo Orbits Associated with Libration Points.* Journal of The Astronautical Sciences, 46(2):1–42, 1999.

[37] M. Hechler. *SOHO Mission Analysis L_1 Transfer Trajectory.* Technical Report MAO Working Paper No. 202, ESA, 1984.

[38] M. Hénon. *Vertical Stability of Periodic Orbits in the Restricted Problem I. Equal Masses.* Astronomy & Astrophysics, 28:415–426, 1973.

[39] T. A. Heppenheimer. *Optimal Controls for Out of Plane Motion About the Translunar Libration Point.* Journal of Spacecraft and Rockets, 7:1088–1092, 1970.

[40] L. A. Hiday and K. C. Howell. *Impulsive Time–Free transfers Between Halo Orbits.* School of Aeronautics and Astronautics. Purdue University, 1992.

[41] K. C. Howell, B. T. Barden, and M. W. Lo. *Application of Dynamical Systems Theory to Trajectory Design for a Libration Point Mission.* Journal of the Astronautical Sciences, 45(2):161–178, 1997.

[42] K.C. Howell, B.T. Barden, R.S. Wilson, and M.W. Lo. *Trajectory Design Using a Dynamical Systems Approach with Application to Genesis.* AAS/AIAA Astrodynamics Specialist Conference, AAS Paper 97-709., 1997.

[43] K.C. Howell, D.L. Mains, and B.T. Barden. *Transfer Trajectories from Earth Parking Orbits to Sun–Earth Halo Orbits.* AAS/AIAA Spaceflight Mechanics Meeting, AAS Paper 94-160, 1994.

[44] K.C. Howell and H.J. Pernicka. *Numerical Determination of Lissajous Trajectories in the Restricted Three-Body Problem.* Celestial Mechanics, 41(1–4):107–124, 1988.

[45] K.C. Howell and H.J. Pernicka. *Stationkeeping Method for Libration Point Trajectories.* Journal of Guidance, Control and Dynamics, 16(1):151–159, 1993.

[46] B.L. Jones and R.H. Bishop. *Rendezvous Targeting and Navigation for a Translunar Halo Orbit.* Journal of Guidance, Control and Dynamics, 17(5):1109–1114, 1994.

[47] À. Jorba and J. Villanueva. *On the Persistence of Lower Dimensional Invariant Tori Under Quasiperiodic Perturbations.* J. Nonlinear Science, 7:427–473, 1997.

[48] À. Jorba and J.J. Masdemont. *Dynamics in the Center Manifold of the Restricted Three–Body Problem.* Physica D, 132:189–213, 1999.

[49] À. Jorba and J. Villanueva. *Numerical Computation of Normal Forms Around Some Periodic Orbits of the Restricted Three Body Problem.* Physica D, 114:197–229, 1998.

[50] J. A. Kechichian *The Efficient Computation of Transfer Trajectories between Earth Orbit and L_1 Halo Orbit within the Framework of the Sun-Earth Restricted Circular Three Body Problem* AAS/AIAA Space Flight mechanics meeting, Paper AAS 00-174. Clearwater, Florida, 2000.

[51] W. S. Koon, M. W. Lo, J. E. Marsden, and S. D. Ross. *Resonance and capture of jupiter comets.* Celestial Mechanics and Dynamical Astronomy, 81(1):27–38, 2001.

[52] W. S. Koon, M. W. Lo, J. E. Marsden, and S. D. Ross. *Shoot the Moon.* AAS/AIAA Space Flight Mechanics Meeting, Paper AAS 00-166. Clearwater, Florida, 2000.

[53] W. S. Koon, M. W. Lo, J. E. Marsden and S. D. Ross. *The Genesis Trajectory and Heteroclinic Connections.* AAS Paper 99-451, AAS/AIAA Astrodynamics Specialist Conference, Girdwood, Alaska, 1999.

[54] W. S. Koon, M. W. Lo, J. E. Marsden and S. D. Ross. *Low Energy Transfer to the Moon.* Celestial Mechanics and Dynamical Astronomy, 81(1):63–73, 2001.

[55] W. S. Koon, M. W. Lo, J. E. Marsden and S. D. Ross. *Constructing a Low Energy Transfer between Jovian Moons.* Contemporary Mathematics, American Mathematical Society 292:129–145, 2002.

[56] W. S. Koon, M. W. Lo, J. E. Marsden, and S. D. Ross. *Heteroclinic Connections Between Periodic Orbits and Resonance Transitions in Celestial Mechanics.* Chaos, 10(2):427–469, 2000.

[57] M. W. Lo and S. Ross. *SURFing the Solar Sytem: Invariant Manifolds and the Dynamics of the Solar System.* Technical Report 312/97, 2-4, JPL IOM, 1997.

[58] A. Marinescu, A. Nicolae and M. Dumitrache *Optimal low-thrust libration points rendezvous in Earth-moon system .* AIAA Guidance, Navigation, and Control Conference and Exhibit, Portland, OR, Aug. 9-11, 1999, Collection of Technical Papers. Vol. 1 (A99-36576 09-63)

[59] H. Matsuo et al. *Optimization of Low Thrust Trajectories for Collinear Lagrange Point Mission.* Proceedings of the Symposium on Mechanics for Space Flight, Tokyo, pages 87–102, 1983.

[60] J. J. Masdemont. *High Order Expansions of Invariant Manifolds of Libration Point Orbits with Applications to Mission Design.* Dynamical Systems: An International Journal, 20(1):59 - 113, (2005).

[61] F. R. Moulton. *An introduction to Celestial Mechanics* 2nd revised edition New York, Dover (1970).

[62] H. J. Pernicka and K. C. Howell. *Sun–Earth Libration Point Trajectories that Avoid the Solar Exclusion Zone.* Journal of the Astronautical Sciences, 38(3):269–288, 1990.

[63] H. Poincaré. *Les Méthodes Nouvelles de la Mécanique Céleste.* Gauthier–Villars, 1892, 1893, 1899.

[64] D. L. Richardson. *Analytical Construction of Periodic Orbits About the Collinear Points.* Celestial Mechanics, 22(3):241–253, 1980.

[65] D. L. Richardson. *A note on the Lagrangian Formulation for Motion About the Collinear Points.* Celestial Mechanics, 22(3):231–235, 1980.

[66] J. Rodríguez-Canabal. *Operational Halo Orbit Maintenance Technique for SOHO.* European Space Agency, (Darmstadt, Germany, editor). Second International Symposium on Spacecraft Flight Dynamics, ESA SP–255, pages 71–78, 1986.

[67] F. L. Scarf, E. J. Smith and R. W. Farquhar. *Science return from ISEE-3 at comet Giacobini-Zinner.* TRW Space and Technology Labs. Plasma Wave Expt. for the ISEE-3 Mission 12 p (SEE N83-35851 23-75), 1983.

[68] D. J. Scheeres. *The Restricted Hill Four–Body Problem with Applications to the Earth–Moon–Sun System.* Celestial Mechanics and Dynamical Astronomy, 70(2):75–98, 1998.

[69] K. P. Seidelmann *Explanatory supplement to the astronomical almanac: a revision to the Explanatory Supplement to the Astronomical Ephemers and the American Ephemeris and Nautical Almanac; prepared by the Nautical Almanac Office, U.S. Naval Observatory ... [et al.]* University Science Books (Mill Valley, California), 1992.

[70] P. Sharer, J. Zsoldos and D. Folta. *Control of Libration Point Orbits Using Lunar Gravity–Assisted Transfer.* Advances in the Astronautical Sciences, 64:651–663, 1993.

[71] C. L. Siegel and J. K. Moser. *Lectures on Celestial Mechanics.* Springer–Verlag, 1971.

[72] C. Simó. *Analytical and Numerical Computation of Invariant Manifolds.* Modern Methods in Celestial Mechanics, pages 285–330. D. Benest and C. Froeschlé, editors. Editions Frontières, 1990.

[73] C. Simó. *Dynamical Systems Methods for Space Missions on a Vicinity of Collinear Libration Points.* Hamiltonian Systems with Three or More Degrees of Freedom, pages 223–241. C. Simó (editor), Kluwer Academic Publishers, 1999.

[74] S. J. Sponaugle et al. *Optimal Cycling Between Cislunar and Cismartian Libration Points with Reussable Nuclear Electric Transfer Vehicles.* Advances in the Astronautical Sciences, 75:141–161, 1991.

[75] S. Stalos, D. Folta, B. Short, J. Jen and A. Seacord. *Optimum Transfer to a Large–Amplitude Halo Orbit for the Solar and Heliospheric Observatory (SOHO) Spacecraft.* Advances in the Astronautical Sciences, 84:639–650, 1993.

[76] E. M. Standish, X. X. Newhall, J. G. Williams and W. F. Folkner. *JPL Planetary and Lunar Ephemerides, DE403/LE403.* Technical Report JPL IOM 314.10–127, NASA–Jet Propulsion Laboratory, 1998.

[77] T.F. Starchville and R.G. Melton. *Optimal Low–Thrust Transfers to Halo Orbits About the L_2 Libration Point in the Earth–Moon System (Elliptical Problem).* Advances in the Astronautical Sciences, 99:1489–1505, 1998.

[78] E. L. Stiefel, G. Scheifele. *Linear and Regular Celestial Mechanics.* Springer-Verlag, NY, 1971.

[79] J. Stoer and R. Bulirsch. *Introduction to Numerical Analysis.* Springer Verlag, 1983.

[80] A. A. Sukhanov, N. A. Eismont and A. V. Prudloglyad. *Trajectory Design for Experimental Mission to Sun–Earth L_1 and L_2 Points Using SEP.* Journal of the Brazilian Society Mechanical Sciences, 21:313–321, 1999.

[81] V. Szebehely. *Theory of Orbits.* Academic Press, 1967.

[82] F. C. Vandenbussche, P. Temporelli. *The Trip to the L1 Halo Orbit.* ESA Bulletin 88, 1996.

[83] W. Wiesel. *The Restricted Earth–Moon–Sun Problem I: Dynamics and Libration Point Orbits.* Technical report, Air Force Institute of Technology Wright-Patterson AFB, Ohio, 45433, 1984.

[84] R. S. Wilson, K. C. Howell and M. W. Lo. *Optimization of Insertion Cost Transfer Trajectories to Libration Point Orbits.* Advances in the Astronautical Sciences, 103:1569–1586, 2000.

[85] C. G. Zagouras and P. G. Kazantzis. *Three-Dimensional Periodic Oscillations Generating From Plane Periodic Ones Around the Collinear Lagrangian Points.* Astrophysics Space Science, 61(4):389–409, 1979.